Effects of strontium malonate (NB S101) on the compositional, structural and biomechanical properties of calcified tissues in rats and dogs

Raffalt, Anders Christer; Andersen, Jens Enevold Thaulov

Publication date:
2011

Document Version
Publisher's PDF, also known as Version of record

Effects of strontium malonate (NB S101) on the compositional, structural and biomechanical properties of calcified tissues in rats and dogs

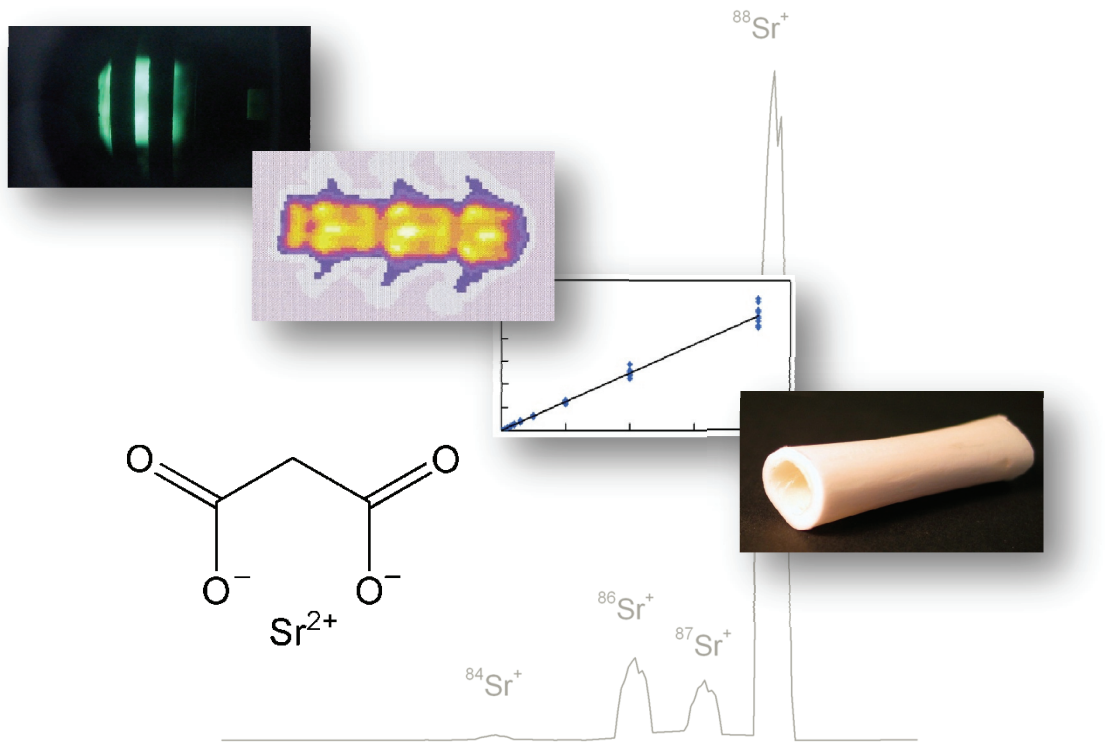

PhD Thesis

Anders C. Raffalt

2011

DTU

Department of Chemistry

Technical University of Denmark

Effects of strontium malonate (NB S101) on the compositional, structural and biomechanical properties of calcified tissues in rats and dogs

PhD Thesis

Anders C. Raffalt

The Analytical Chemistry Group

Department of Chemistry

Technical University of Denmark

Supervisor

Associate Professor, dr.techn. Jens E.T. Andersen

January 2011

Preface and acknowledgements

The present dissertation is submitted to the Technical University of Denmark in partial fulfilment of the requirements for the degree of PhD. The scholarship was funded by the Technical University of Denmark (DTU) and the work was carried out in the Analytical Chemistry Group (ACG) at the Department of Chemistry, DTU, with Associate Professor, dr.techn. Jens E.T. Andersen as supervisor.

It is a great pleasure to be able to thank those who have contributed to the work that is presented in this thesis. Without their help, advice and support, I would not have been able to complete my PhD study.

First and foremost I owe my deep and sincere gratitude to my supervisor, Associate Professor Jens E.T. Andersen, for his encouragement and guidance throughout my PhD study and for always being available for questions and discussions. I shall miss our debates about the appropriate amount of beans needed for a proper cup of coffee.

From the Analytical Chemistry Group, I would like to thank Søren R. Sørensen for his companionship, help and hard work on the strontium malonate project – he stood by my side when there were still 160 rat femurs and 160 skull biopsies left to clean and digest. I would also like to thank Betina M.F. Roesdahl for always providing practical assistance when it was needed the most.

I owe a great debt of gratitude to Dr. Jens-Erik B. Jensen, MD, at Hvidovre Hospital for his interest in the project and for his invaluable help with the densitometric and mechanical measurements. I am also very grateful to Rudien Kold for preparing the dog vertebra biopsies. I am much indebted to Professor Henrik Spliid at DTU Informatics for giving advice on statistical data analysis and to Christian G. Frankær at DTU Chemistry for collecting and analysing the EXAFS data.

I was lucky enough to get to spend six months in the BEACh group at the University of Plymouth, UK, under the supervision of Professor Paul Worsfold. I tremendously enjoyed my time there and I am deeply grateful to Paul Worsfold and all the wonderful people in the BEACh group who made my stay so rewarding, both personally and scientifically. In particular, I would like to thank Dr. Jin Bo Zhao for all the time he spent helping me with nutrient measurements.

I am very grateful to Associate Professor Ian McKelvie, now University of Melbourne, for inviting me to his group at Monash University, Melboune, Australia, and for his enormous hospitality during my stay. Also thanks to Peter Ellis for helping me with the SIA equipment and for teaching me a thing or two about LabVIEW programming.

I would like to thank Osteologix Inc. for amending the animal study protocols for my benefit and for placing the samples at my disposal. I am much indebted to Dr. Stephan Christgau, former COO at Osteologix A/S, for valuable advice and a very productive collaboration.

Many thanks are due to Peter Pritzl for careful and kind proofreading during the writing up period. I also owe a special thanks to my fellow conspirator Jytte Kristensen for sharing ups and downs and for keeping me company on those long days.

I gratefully acknowledge the financial support from the Danish Ministry of Science, Technology and Innovation through an *EliteForsk* travel scholarship, as well as the financial support from Director Ib Henriksen's Foundation, the Idella Foundation and Fabrikant P.A. Fisker's Foundation to acquire the Apex-Q sample introduction system and the ICP-MS apparatus.

Anders C. Raffalt
Kgs. Lyngby, January, 2011

Abstract

Strontium is known to have a positive effect on bone by concomitantly increasing bone formation and decreasing bone resorption, thereby providing a sustained skeletal benefit. Strontium ranelate (SrR) has been shown to reduce the risk of both vertebral and non-vertebral fractures in patients with postmenopausal osteoporosis. Strontium malonate (SrM) is currently being developed as a novel pharmaceutical for the treatment and prevention of osteoporosis. SrM potentially provides considerable advantages over SrR with respect to Sr content, bioavailability and ease of administration.

SrM was tested in three animal studies: 1) a 4-week study in dogs using SrM doses of 0 (control), 300, 1000 and 3000 mg kg^{-1} day^{-1}, 2) a 26-week study in rats, and 3) a 52-week study in dogs, both using SrM doses of 0 (control), 100, 300 and 1000 mg kg^{-1} day^{-1}. Femurs, vertebrae, skullcaps and teeth from the treated animals were examined for treatment-related changes in concentrations of Sr, Ca, Mg and P using inductively coupled mass spectrometry (ICP-MS). Bone mineral density (BMD) was determined using dual energy X-ray absorptiometry (DEXA), and the biomechanical properties of the bones were assessed using bending and compression tests. A procedure was developed for determination of Mg, P, Ca and Sr in diluted serum using ICP-MS in combination with an Apex-Q desolvation unit. The Apex inlet system reduced the generation of oxides in the ICP and improved the sensitivity for Sr by a factor of 14 compared with a conventional cross-flow nebuliser. Rh was found to be a suitable internal standard for all four analytes. Reliable estimates of the measurement uncertainties were achieved by pooling calibration data obtained on different days.

Treatment with SrM resulted in a dose-dependent increase in Sr contents in all analysed tissues. The highest concentrations were found in rat incisor, which contained an average of 45 ± 11 mg g^{-1} Sr in the highest dose group, corresponding to a 450-fold increase compared with placebo. The Sr/(Sr+Ca)mol% in the four groups were respectively 0.015, 1.2, 5.8 and 7.7 for incisors and 0.015, 0.6, 1.9 and 5.0 for femurs. Sr concentrations in rat incisor and rat femur were strongly correlated with approx. 30% less Sr found in the femurs. A strong correlation between serum Sr and incisor Sr was also observed. In dogs, the highest concentrations of Sr were found in skullcap after 52 weeks of treatment, with an average of 28 ± 12 mg g^{-1} Sr in the highest dose group, corresponding to a 350-fold increase compared with placebo. The Sr/(Sr+Ca)mol% in the four treatment groups were respectively 0.011, 2.5, 3.8 and 4.4 for femurs; 0.019, 3.3, 4.7 and 6.5 for calvaria and 0.013, 0.75, 1.1 and 1.6 for molar teeth. Sr concentrations in femur and molar were correlated. Sr concentrations in dog femur mid-shaft after 4 weeks were approx. 1/3 of the

concentrations after 52 weeks, suggesting that initial incorporation of Sr proceeded by a faster mechanism than the long-term incorporation. In both rats and dogs, long-term treatment with SrM was associated with decreased concentrations of Ca and P in the mineralised tissues. EXAFS measurements indicated that Sr had substituted Ca in the bone apatite structure, but that Sr also coordinated to other atoms, most likely oxygen in collagen and water. The incorporation of Sr into the HAp increased with increasing dose.

A simple stoichiometric model was proposed for incorporation of Sr into the hydroxyapatite (HAp) matrix of bones and teeth. The model showed excellent agreement with the analytical data and demonstrated that at least a part of the perceived loss of Ca and P was caused by the increased weight of HAp following adsorption and incorporation of Sr. It was found that respectively 70 – 72% of femur, 78% of rat incisor and 85% of dog molar was made up by HAp.

The maximum strength of the dog femurs (three-point bending) was significantly reduced (19%) in the highest dose group, indicating a weakening of the apatite structure. A non-significant increase (9%) in strength was seen in the low and medium dose groups. Measurements of bone mineral density (BMD) using DEXA was found to be heavily influenced by presence of Sr in the mineralised matrix, and linear correction of 9% was determined for a 1:10 molar ratio of Sr:HAp. The corrected BMD increased significantly in dog femur mid-shaft in the group treated with 300 mg kg^{-1} day^{-1} SrM. The corrected BMD was found to be strongly correlated with bone strength, indicating that the increase in corrected BMD following SrM treatment was associated with concomitant increase of bone strength.

Dansk resumé

Strontium har en positiv effekt på knoglevæv, idet Sr på samme tid øger knogledannelsen og mindsker knogleresorptionen. Herved opnås en vedvarende, gavnlig virkning på knoglerne. Behandling med strontiumranelat (SrR) har vist sig at nedbringe hyppigheden af både vertebrale og non-vertebrale knoglebrud hos patienter, der lider af osteoporose (knogleskørhed). Strontiummalonat (SrM) er under udvikling som et nyt lægemiddel til behandling og forebyggelse af knogleskørhed, og SrM har som medicinalprodukt en række potentielle fordele frem for SrR i form af bedre biotilgængelighed, højere strontiumindhold og lettere indtagelse.

SrM blev undersøgt i tre dyrestudier: 1) et 4-ugers studie i hunde med SrM doser på 0 (kontrol), 300, 1000 og 3000 mg kg^{-1} dag^{-1}, samt 2) et 26-ugers studie i rotter og 3) et 52-ugers studie i hunde, begge med SrM doser på 0, 100, 300 og 1000 mg kg^{-1} dag^{-1}. Lårbensknogler (femur), lændehvirvler (lumbar vertebra), hjerneskal (calvaria) og tænder fra de behandlede dyr blev undersøgt for behandlingsrelaterede ændringer med hensyn til indhold af Sr, Mg, P og Ca ved brug af ICP-MS (inductively coupled plasma-mass spectrometry). Knoglernes mineraldensitet (BMD, bone mineral density) blev målt ved brug af DEXA (dual energy X-ray absorptiometry), og knoglestyrken blev undersøgt ved hjælp af mekaniske bøjnings- og kompressionstests. Der blev udviklet en metode til måling af Sr, Mg, P og Ca i fortyndet serum baseret på ICP-MS koblet til et Apex-Q prøveintroduktionssystem. Apex-systemet reducerede dannelsen af oxider i ICP'en og forbedrede sensitiviteten for Sr med en faktor 14 i forhold til en konventionel forstøver. Rh var velegnet som intern standard for alle fire analytter. En realistisk vurdering af måleusikkerheden blev opnået ved at pulje kalibreringsdata fra flere forskellige måledage.

SrM-behandlingen førte til en dosisafhængig stigning i strontiumindhold i alle analyserede væv. De højeste koncentrationer blev fundet i rottefortænder, hvor den gennemsnitlige Sr-koncentration i den højeste dosisgruppe var 45 ± 11 mg g^{-1}, svarende til en stigning på 450 gange i forhold til kontrolgruppen. I rotterne var molforholdet Sr/(Sr+Ca)mol% i de fire behandlede grupper hhv. 0,015; 1,2; 5,8 og 7,7 i fortænder og 0,015; 0,6; 1,9 og 5,0 i lårben. Der var en stærk korrelation mellem Sr-koncentrationerne i serum og i fortænder. Sr-indholdet i fortænder og lårben var ligeledes korreleret, og lårbenene havde ca. 30 % lavere Sr-indhold end tænderne. I hundene blev de højeste Sr koncentrationer fundet i hjerneskal, hvor gennemsnittet i den højeste dosisgruppe var 28 ± 12 mg g^{-1} Sr, svarende til en stigning på 350 gange i forhold til kontrolgruppen. Sr/(Sr+Ca)mol% i de fire behandlede grupper var hhv. 0,011; 2,5; 3,8 og 4,4 for lårben, 0,019; 3,3; 4,7 og 6,5 for hjerneskal og 0,013; 0,75; 1,1 og 1,6 for kindtænder. Der var korrelation mellem Sr-koncentrationerne i lårben og tænder. Sr-koncentrationen i lårbensskaftet var efter

4 uger ca. 1/3 af koncentrationen efter 52 uger, hvilket tyder på at den indledende inkorporering af Sr finder sted via en hurtigere mekanisme end langtids-inkorporeringen. I både rotter og hunde var langtidsbehandling med SrM forbundet med fald i Ca- og P-koncentrationerne i de mineraliserede væv. Målinger med EXAFS (Extended X-ray Absorption Fine Structure) viste at Sr substituerede Ca i knoglehydroxyapatit, men at Sr også var bundet til andre atomer, sandsynligvis oxygen i kollagen og vand.

En enkel, støkiometrisk model for strontiums inkorporering i hydroxyapatit (HAp) i knogler og tænder blev foreslået. Modellen viste fremragende overensstemmelse med de analytiske resultater og demonstrerede at en del af det observerede tab af Ca og P skyldes, at inkorporering og adsorption af Sr øger vægten af HAp. Modellen viste at hhv. 70 – 72 % af lårbenene, 78 % af rottefortænderne og 85 % af hundekindtænderne bestod af HAp.

Styrken i hundelårbensknoglerne (tre-punkts bøjning) var signifikant reduceret (19%) i den højeste dosisgruppe, hvilket indikerer en svækkelse af HAp-strukturen. Der blev desuden set en ikke-signifikant (9 %) stigning i knoglestyrken i lav- og mellem-dosisgrupperne. Måling af BMD ved brug af DEXA blev påvirket meget af tilstedeværelse af Sr i den mineraliserede matrix, og en lineær korrektion på 9 % for et molforhold for Sr:HAp på 1:10 blev fundet. Den korrigerede BMD var signifikant forøget i lårbensskaftet i hunde behandlet med 300 mg kg^{-1} dag^{-1} SrM. Korrigeret BMD var stærkt korreleret med knoglestyrke, hvilket indikerer at stigningen i korrigeret BMD efter behandling med SrM var forbundet med en stigning i knoglestyrke.

List of words and abbreviations

Anterior	Front, frontal
BMC	Bone Mineral Content
BMD	Bone Mineral Density
Calvaria	Skullcap
Caudal	Back, towards the rear
Cortical bone	Same as compact bone
cps	Counts per second
Cranial	Towards the head
CRM	Certified Reference Material
DEXA	Dual Energy X-ray Absorptiometry
Diaphysis	The shaft (mid-section) of a long bone
DPA	Dual-Photon Absorptiometry
ETAAS	Electrothermal Atomic Absorption Spectrometry
EXAFS	Extended X-ray Absorption Fine Structure
FAAS	Flame Atomic Absorption Spectrometry
FAES	Flame Atomic Emission Spectrometry
Femur	Thighbone
FSP	Fundamental Sampling Principle
GUM	Guide to the expression of Uncertainty in Measurement
Hypocalcaemia	A condition characterised by abnormally low concentrations of calcium in the blood.
ICP-AES	Inductively Coupled Plasma Atomic Emission Spectrometry
ICP-MS	Inductively Coupled Plasma Mass Spectrometry
IRMM	Institute for Reference Materials and Measurements
IS	Internal Standard
NIST	National Institute for Standards And Technology
NNA	Neutron Activation Analysis
OLSR	Ordinary Least-Squares Regression
Osteomalacia	A bone condition in adults characterised by softening of the bone due to inadequate mineralisation. Similar to *rickets* in children.
Pixi	Proton Induced X-Ray Emission
Posterior	Back, towards the rear

QUAM	Quantifying Uncertainty in Analytical Measurement
Rachitis	Same as rickets
Rickets	A softening of bone in children, usually as a result of vitamin D or calcium deficiency. Similar to *osteomalacia* in adults.
RM	Reference Material
SRM	Standard Reference Material
Tibia	Shinbone
TOS	Theory Of Sampling
Trabecular bone	Same as cancellous or spongy bone.
UV/Vis	Ultraviolet-visible light
WLSR	Weighted Least-Squares Regression
XRF	X-ray Fluorescence

Specific remarks

For brevity, the term "serum Sr" is often used in this thesis as an abbreviated form of "the concentration Sr in serum". Likewise, "femur BMD" reads "the bone mineral density in femur. Similar abbreviations are "femur Ca", "tooth Sr", etc. Animal studies are referred to as e.g. "4-week dog" for a study in dogs with a treatment time of 4 weeks.

Throughout the report, "Sr" and "Sr^{2+}" as well as "strontium" and "strontium ions" are used interchangeably. It is implied that strontium always exists in oxidation state +II in aqueous solutions and biological systems.

CHAPTER ONE

Introduction

This chapter gives a brief introduction to the background, aims and methodology of the present project. It also presents the outline of the dissertation.

1.1 Project background

Strontium is widely distributed throughout the biosphere due to the widespread geochemical occurrence and high bioavailability of the element. Although not considered an essential nutrient, strontium has been known to have an effect on calcified tissue since the beginning of the last century [1]. The first clinical trials with strontium were performed in 1952 by Shorr and Carter [2], who found that the element improved remineralisation of bone in humans. In recent years, strontium's positive effect on bone has been documented by numerous *in vitro* and *in vivo* studies. As a result, strontium ranelate (SrR) (Figure 1.1) was approved in the EU in 2004 as a drug for treatment of osteoporosis, a bone disease that affects millions of people worldwide. Strontium ranelate is produced by the French company Servier under the commercial names Protelos®, Protos®, Protaxos®, Bivalos® and Osseor®, and it is the only strontium-based prescription drug currently available.

The present work is a continuation of a collaboration started in 2003 between the then Danish company Nordic Bone A/S and the Analytical Chemistry Group (ACG) at the Department of Chemistry, Technical University of Denmark. Nordic Bone contacted Dr. Andersen of the ACG in search of a suitable strontium compound to be developed as a novel and competitive antiosteoporotic drug. The ACG initiated investigations of a range of potential candidate compounds, of which strontium malonate (SrM) (Figure 1.1) was chosen for further testing and designated the compound code *NB S101*. A high-yield synthesis of anhydrous strontium malonate was developed by Christgau *et al.* [3] and the compound was characterised by its crystal structure [4].

Following the initial toxicological tests of strontium malonate, Nordic Bone A/S changed its name to Osteologix A/S (now Osteologix, Inc.), and the company commenced the extensive statutory, preclinical trials in animals. Upon completion of these toxicological studies, the clinical phase 1-3 trials were initiated. The phase 1 and phase 2 trials have now been successfully completed, and phase 3 trials are currently in progress. In August 2010, Osteologix announced that it had granted Servier an exclusive license to develop and commercialise strontium malonate outside the U.S.

As a pharmaceutical, strontium malonate has several advantages over strontium ranelate. SrM provides better strontium bioavailability [5, 6], a higher strontium content (SrM: 46% Sr (w/w) vs. SrR: 34% Sr (w/w)), and the anion is more readily synthesised. Perhaps most importantly, SrM can be formulated in a tablet, which eases the administration as compared to the existing SrR treatment. SrR is purchased as granules wrapped in single-dose sachets containing 2 grams of strontium ranelate, and the drug is taken orally once daily as a suspension in a glass of water.

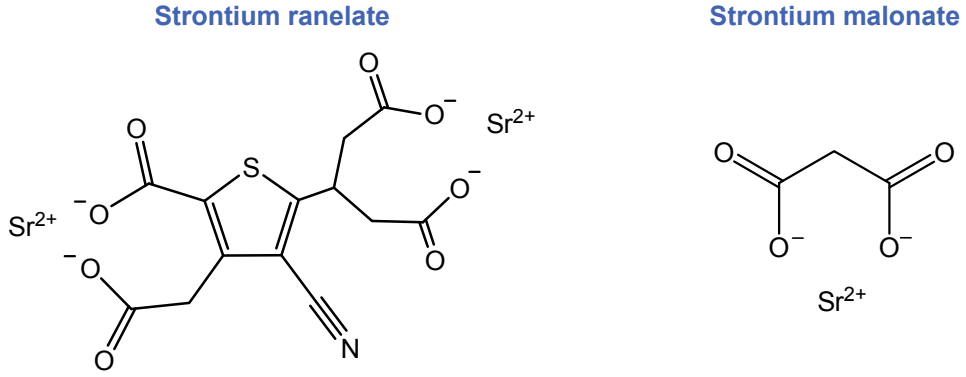

Figure 1.1 Structures of strontium ranelate [7] and strontium malonate [4].

1.2 Project objectives

The discovery of strontium's potency as an antiosteoporotic pharmaceutical agent generated much interest and research in the field, but the exact mechanism by which strontium exerts its effect on bone remains unclear. The objective of the present work was firstly to test the potential of strontium malonate as a new strontium-based pharmaceutical by evaluation of its bioavailability and toxicity. Secondly, the aim was to gain insights into the incorporation of strontium in bone and to examine the effect of strontium treatment on the properties of serum, teeth and bones in animals.

Using a range of different analytical techniques, we studied the structure, elemental composition and the mechanical properties of bone and teeth in animals treated with high doses of strontium. In order to ensure correct, well-founded clinical conclusions, the measurement uncertainties associated with the analytical results were evaluated, and quality control schemes were applied throughout the study.

1.3 Methodology

As explained above, the initial tests of strontium malonate included several preclinical trials in animals (rats and dogs). These toxicological studies presented a unique opportunity to examine the *in vivo* effect of strontium treatment on the elemental composition and mechanical properties of bone. Upon request of the ACG, Osteologix kindly agreed to amend the study protocol to include removal of selected tissue samples at necropsy. Thus, after completion of each animal study, skeletal parts such as femur, skull, tibia, vertebrae and incisors were removed, wrapped in cotton gauze soaked with isotonic water and shipped to the ACG for analysis. The samples were examined for strontium-induced changes in inorganic tissue composition and mechanical properties, using various analytical techniques such as mass spectrometry and bone densitometry. Procedures for sample preparation and analysis were established and optimised, and the validity of the obtained results was ensured via measurement uncertainty budgets and continuous quality control (QC). A thorough knowledge of the performance of the applied analytical methods was considered to be a fundamental prerequisite for a correct clinical interpretation of the data. Therefore, the concepts of metrology and QC were regarded as essential, integrated parts of the project. Also, it was important to process the analytical results using appropriate statistical methods.

By these means, the impact of treatment factors (strontium dose, duration of treatment and gender) on measured values (i.e. bone Sr content, bone mineral density, bone cell activity and bone strength) could be investigated. In order to obtain a correct evaluation of strontium's effect on the mineral density of bone, it was necessary to establish a correction factor for densitometric measurements of strontium-rich bones. Furthermore, correlations between incorporation of Sr in different skeletal sites were studied. Finally, a model for ion exchange in the inorganic bone phase was developed and tested on the available data.

1.4 Dissertation outline

The first part of this dissertation consists of 4 introductory chapters, presenting overviews of strontium's biological role, analytical methods for determination of strontium as well as an introduction to some of the apparatus that was applied in the project. Then follows detailed discussions of the optimisation and uncertainty evaluation of ICP-MS measurements, after which the results from two animal studies are presented. The final chapter contains some concluding remarks and an outlook.

1.4.1 Introduction to analysis and biological effect of strontium

Chapter 2 is a review of the biological role of strontium, including its geological and biological prevalence, the mechanism of uptake and effect in the organism, as well as its incorporation into calcified tissues. The chapter also includes sections on bone physiology and osteoporosis, and the results of clinical trials with strontium malonate are briefly described.

Chapter 3 presents an overview of analytical procedures for determination of strontium in biological tissues found in the literature. The focus is on spectrometric methods as well as the procedures necessary for sample preparation. Applications of metrology and reference materials in clinical studies are also discussed.

Chapter 4 provides an introduction to three experimental techniques that have been used extensively through this study: inductively coupled plasma mass spectrometry, dual energy X-ray densitometry and mechanical strength measurements.

1.4.2 Instrumental optimisation, metrology and quality assurance

Chapter 5 deals mainly with the instrument optimisation and protocol development for ICP-MS determination of Mg, P, Ca and Sr in serum samples from rats treated with strontium ranelate. The serum samples were analysed as a part of two studies on strontium's effect on fracture healing and bone regeneration, both coordinated by Dr. Annemarie Brüel at Aarhus University [8].

Chapter 6 presents discussions of sampling procedures, measurement uncertainty and quality control related to the ICP-MS analyses.

1.4.3 Animal studies

Three animal studies were conducted on strontium malonate. The first of these investigations was a short-term study in which 24 dogs were treated with high doses of strontium malonate for 4 weeks [9]. Femur bones, teeth and bone marrow were

analysed for strontium and calcium, and the results of the analysis are reprinted in Appendix II. For brevity, this study is referred to as "4-week dog" in this report.

Chapter 7 describes a long-term study in rats ("26-week rat"). 160 rats were treated with Sr for 26 weeks. The study includes ICP-MS and densitometric analyses of femur bones and incisors, as well as a model for incorporation of Sr in the inorganic bone phase. The study was planned and executed in collaboration with Søren R. Sørensen [10].

Chapter 8 describes a long-term study in dogs ("52-week dog"). 40 dogs were treated with Sr for 52 weeks. The study includes ICP-MS and densitometric analyses as well as biomechanical measurements. A correction factor is presented for calculation of true densitometric results in the presence of high concentrations of Sr.

1.4.4 Concluding remarks

Chapter 9 summarises the results that have been presented in the previous chapters and outlines suggestions for future work.

1.4.5 Appendix

Appendix I considers analysis of phosphate in fresh-waters using stopped-flow analysis. The work was carried out during two complementary visits respectively to University of Plymouth, UK, (six months duration) and Monash University, Melbourne, Australia (three weeks duration).

Appendix II is a reprint of the published results from the short-term study in dogs [11].

Appendix III presents equations used for regression calculations.

CHAPTER TWO

Strontium in biological systems

2.1 Introduction

Compared with the two lighter group II elements calcium and magnesium, strontium has attracted relatively little attention in the fields of clinical chemistry and human biology. In recent years, however, the development of the drug strontium ranelate (Protelos™) has stimulated an increasing interest in the biological significance of the element. The purpose of this chapter is to provide an overview of the biological and clinical role of strontium, including uptake, distribution, excretion, toxicology and clinical effect. Emphasis is put on the element's impact on bone remodelling and role as an antiosteoporotic drug. The chapter also provides background information on bone physiology and osteoporosis, and the final section presents an overview of clinical studies on strontium ranelate.

2.2 Chemistry

Strontium is a member of the alkaline earth elements (Group 2 in the periodic table). The atomic number is 38 and the atomic weight is 87.62. In many chemical aspects (size, oxidation potential, solubility of salts), the properties of Sr occupy an intermediate position between Ca and Ba. Sr has a high oxidation potential, and the Sr atom easily looses the two electrons in the 5s orbital, producing the Sr^{2+} ion ($Sr \rightarrow Sr^{2+} + 2e^-$, E=2.89 V). Like the other alkali earth metals, Mg, Ca and Ba, Sr exists solely in oxidation state +II in aqueous chemistry and biological systems. Freshly cut elemental Sr has a silvery-white colour, but on exposure to air the colour changes to a dark yellow, due to formation of strontium oxide (SrO). Naturally occurring strontium consists exclusively of the four stable isotopes ^{84}Sr, ^{86}Sr, ^{87}Sr and ^{88}Sr, but a large number of radioactive isotopes are known [12, 13].

Inorganic Sr compounds have several commercial uses as components in ceramics, magnets and television faceplate glass. When heated, strontium burns with a crimson colour, a property that has been exploited by the application of strontium salts in pyrotechnics [14]. The most important of the radioactive Sr isotopes are the beta-emitters ^{89}Sr and ^{90}Sr, which both have commercial uses (Table 2.1). The amount of reported applications of organic Sr compounds is limited, but the introduction of strontium ranelate as an antiosteoporotic drug has led to a growing interest in synthesis and crystal structures of strontium(II) salts [4, 15].

Table 2.1 Commercial uses of radioactive Sr isotopes.

Isotope	Physical half-life [16]	Use
^{85}Sr	64.85 days	Calcium tracer for studies of bone formation [17, 18]
^{89}Sr	50.52 days	Palliation of pain from metastatic bone cancer [19]
^{90}Sr	29.1 years	Present in nuclear fall-out and spent fuel-rods from nuclear reactors [20]

2.3 Occurrence

Discovered in a mine near the Scottish town of Strontian in 1790, strontium was isolated for the first time in 1808. Strontium is widely distributed throughout the environment. It constitutes about 0.02-0.03% of the earth's crust, placing it among the 20 most common elements on earth. Owing to its high oxidation potential, elemental Sr does not exist in nature. The most important Sr minerals are the white or blue-white celestite ($SrSO_4$) and the white strontianite ($SrCO_3$), both shown in Figure 2.1. Sr is also found in isomorphs with aragonite ($CaCO_3$) and witherite ($BaCO_3$), and all Ca minerals usually contain small amounts of Sr [14]. The average Sr/Ca ratio in the earth's crust was estimated to 8 mg Sr per 1000 mg Ca, albeit with large regional differences [13]. In 1955, Bowen and Dymond [21] found Sr/Ca ratios in the range of 1.2-500 mg Sr per 1000 mg Ca in English soils, with the higher values found in sandy, acid soil with low Ca content and in soils rich in celestite. Sr is the most abundant trace metal in seawater, reaching concentrations of up to 8 mg L^{-1}, while fresh waters such as rivers and springs contain lower concentrations (1-800 µg L^{-1}) [22, 23]. Groundwater can contain considerably higher Sr concentrations. One drilling in the Copenhagen area was reported to contain 53 mg L^{-1} [24].

Figure 2.1 Photographs of the naturally occurring strontium minerals celestite (a) [25] and strontianite (b) [26]. (a) is released into the public domain and (b) is copyright © 2006 by Amethyst Galleries, Inc., reprinted with permission.

The radioactive isotope, ^{90}Sr, is a major environmental contaminant after atomic bomb tests and in cleanup of decommissioned nuclear facilities [27]. Together with ^{131}Cs, ^{90}Sr was the major contributor to radioactive contamination of the environment after the Chernobyl nuclear power plant accident [28]. With a half-life of 29 years, the isotope may cause long-term internal irradiation damages if it is accumulated in the body [29], and it is linked to bone cancer, cancer of the soft tissue near the bone and leukaemia [20]. Because of its deleterious effects, ^{90}Sr has been studied extensively, but the radioactive Sr isotopes will not be discussed further in this report. It is merely imperative to note that the radiation hazards related to these isotopes are not present in the medical application of stable Sr.

2.4 Sources

The wide environmental distribution makes Sr a natural constituent of food and beverages. High amounts of Sr are found in seafood (up to 25 mg kg^{-1}), grains and cereals (up to 18 mg kg^{-1}), whereas meat, poultry, vegetables, milk, fruit and various beverages contain lower amounts (0.05-3.5 mg kg^{-1}) [23, 30, 31]. The intake of Sr depends on the diet and geographical region. Strontium is a plant growth stimulant, but full replacement of Ca by Sr results in reduced growth. The Sr/Ca ratio in plants usually correlates with that of their corresponding soil or nutrient solution [32]. In the Western countries, a normal diet contains 2-4 mg Sr per day [13], while the exposure from the air is in the order of 400 ng per day [20]. Thus, the daily Sr intake is negligible compared to the intake of Ca, which normally is about 1 g per day [33]. Clearly, if the Sr concentration in the drinking water exceeds a few mg L^{-1}, the water becomes the main source of Sr exposure.

2.5 Limit values

There is no limit value stated for the amount of Sr in drinking water either in the EU directive on drinking water [34] or in WHO guidelines on water quality [35]. The Danish Environmental Protection Agency stated a limit of 10 mg L^{-1} for drinking water for human consumption [36]. The United States Environmental Protection Agency (USEPA) set a federal limit of 4 mg L^{-1} and the states of Maine and Florida have thresholds of 2.4 and 4.2 mg L^{-1}, respectively. Additionally, USEPA has derived a *chronic reference dose* (RfD), which is an estimate of the daily exposure that is likely to be without risk of deleterious effects during a lifetime. RfD for Sr is 0.6 mg kg^{-1} day^{-1}, corresponding to an average daily intake of 42 mg Sr for a human with a body weight of 70 kg [20].

2.6 Strontium metabolism

Several reviews have been published on the biological activity of Sr [13, 37-39]. As can be seen from Table 2.2, Sr is a trace metal in the human body. A detailed list of Sr concentrations in various organs and tissues can be found in reference [23]. Unlike Mg and Ca that are both essential for a number of enzymatic and cellular processes, Sr is not considered to be an essential element in human nutrition, as absence of Sr in the diet does not cause death. Ca is a major component of bone and dentine and kept under strict homeostatic control, i.e. the concentration of Ca in the blood is strictly maintained within a very narrow range through accurate feedback mechanisms [33]. A similar control of the levels of Sr in the body has not been identified.

Table 2.2 Atomic weight, ionic radii and abundance of Mg, Ca and Sr in the human body [16].

Element	Atomic weight	M^{2+} ion radius (Å) [40]	Amount (g)*	% of body weight*
Mg	24.31	0.72	19	0.027
Ca	40.08	1.00	1000	1.4
Sr	87.62	1.18	0.32	$4.6 \cdot 10^{-4}$
Ba	137.33	1.35	0.022	$3 \cdot 10^{-5}$

*Composition of a 70-kg "standard man".

Many studies, including both whole-body investigations and studies on isolated organs, have shown that Sr often acts similarly to Ca, albeit with lower biological activity. Hormones whose secretion is elevated or inhibited by presence of Ca are also affected by Sr, and Sr can substitute Ca in a number of physiological processes, such as muscular contraction and blood clotting. Apparently, any active process that transports Ca across biological membranes also transport Sr, but to a lesser degree.

These processes, where Sr is in competition with Ca, include intestinal absorption, renal excretion, lactation and placental passage.

Ingested Sr is distributed in plasma, extracellular fluids, soft tissues and the skeleton. Because of strontium's chemical and physical resemblance with Ca, it is a natural bone-seeking element, and, like Ca, it accumulates in the skeleton [37]. In animals kept on a normal diet, approximately 99% of the absorbed Ca and Sr is deposited in bone.

2.6.1 Uptake and excretion of strontium

Sr enters the body primarily via the gastrointestinal tract, while a lesser amount may be absorbed through the lungs and skin [38]. Absorption has been shown to decrease with age in rats, but whether this is also the case with humans is disagreed upon between reviewers [13, 38]. Absorption is promoted by fasting and vitamin D [37], and inhibited by presence of phosphate, Ca [41, 42] and chelating agents such as sodium alginates [43]. Sr uses the same pathways as Ca for uptake and transport across the intestinal wall, but the carrier system has greater affinity for Ca [44, 45]. Combined with the much lower content of Sr in the diet, this means that Sr absorption is inhibited competitively by Ca. It has been suggested that the absorption of Sr happens entirely by passive diffusion [46, 47], but carrier-mediated mechanisms has also been proposed [45, 48]. Sr can be transferred across the intestinal wall against a concentration gradient, albeit with much lower efficiency than Ca [44]. It has been suggested that transport of Sr from the intestinal lumen to the blood may be entirely passive, while active transport may play a role in transferring Sr from the blood into the intestinal lumen. Such an arrangement might constitute a sort of homeostatic regulation of blood Sr concentrations at high levels [13]. When administered alone, about 25-30% of a Sr dose is absorbed in humans [38]. In the presence of Ca, Sr is absorbed to a lesser degree than Ca, with reported Sr/Ca absorption ratios of 0.5-0.7 [49, 50]. The discrimination of Sr in favour of Ca by the ion channels and calcium carriers may be due to the larger ion radius of Sr [13].

Strontium is excreted primarily through urine, but also thought faeces and sweat [38]. Strontium taken orally is primarily excreted in stool, whereas intravenously infused Sr is excreted mostly in the urine [51]. Sr excreted in faeces is either non-absorbed, orally administered Sr, or Sr that has been excreted from the blood to the intestine [38]. The renal clearance of Sr is about 3 times higher than for Ca, perhaps due to a lower degree of tubular reabsorption in the kidneys [13].

2.7 Strontium deficiency

As mentioned above Sr does not seem to be essential to the human organism, but it has been shown to prevent caries in humans [52, 53]. Sr concentrations in water, tooth enamel and plaque were inversely related to prevalence of caries, and Sr increased dental thickness in rats [54, 55]. Nielsen [13] tentatively hypothesised that the therapeutic effect of Sr on osteoporosis could indicate that one feature of osteoporosis might be a certain degree of Sr deficiency, but little data is available on levels of bone Sr in normal, non-osteoporotic humans. Observations have been reported of low levels of Sr in the femur head, which is a frequent site of fractures in the elderly [56].

2.8 Strontium toxicity

According to the Unite States Department of Health and Human Services [20], no cases of acute toxic effects from Sr overdosing have been reported in man. The only Sr compound that is considered harmful to humans is strontium chromate, but the toxicity is due to the carcinogenic chromium. However, increased bone Sr content has been associated with the presence of osteomalacia (softening of adult bone caused by defective mineralisation) in patients undergoing hemodialysis [57]. This may be accelerated by Sr contamination of dialysis fluids, which has been seen in some developing countries [58, 59]. More than 5% of patients in dialysis experience osteomalacia [13]. Additionally, some investigators found that intravenous administration of high doses of Sr was associated with an increased renal excretion of Ca [51, 60], which may lead to hypocalcaemia (low levels of Ca in the blood) [13].

2.9 Early studies of Sr as an antiosteoporotic agent

Although the discovery that strontium interacts with bone was done a least a century ago, the development of strontium ranelate as a drug against osteoporosis has been accompanied by a rather recent clinical interest in the element. The studies reported by Lehnerdt [1] in 1910 may be the first to deal with the influence of strontium on bone tissue. The first observations indicating that strontium may be useful in the treatment of osteoporosis were published in 1952 by Shorr and Carter [2]. They found that moderate doses of strontium lactate (1.75 g Sr per day) administered to osteoporotic patients improved the remineralisation of bone as observed by an increased deposition of calcium. As a result of this report, McCaslin and Janes [61, 62] at the Mayo Clinic (Rochester, MN, U.S) initiated treatment with

strontium lactate of a series of osteoporotic patients in the years 1953-1957. A total of 72 patients were treated for periods of 3 months to 3 years. Of these 72 patients, 32 were available for a follow-up study, showing in all treated patients a subjective clinical improvement in terms of functionality and relieved pain. Though unable to explain the underlying mechanism of action, the observation moved the authors to conclude that "the therapeutic value of the drug appears to be established".

Despite these promising observations, it was to take almost three decades before the potentially beneficial effects of Sr on bone conditions were further investigated. Starting in 1981, Skoryna *et al.* [60, 63, 64] studied the effect of strontium administration on serum and tissue concentrations of Sr and Ca, discovering that Sr could help remineralise bone lesions originating from metastatic bone cancer. Later followed a small-scale clinical study, where administration of small doses of strontium carbonate (600-700 mg Sr per day) for six months was found to stimulate trabecular bone formation, evaluated by taking biopsies of the iliac crest [65]. These studies rekindled the clinical interest in strontium, ultimately leading to the release of strontium ranelate.

It remains a question why it should take almost 30 years before the observations reported in the 1950's received the attention they disserved, but it has been speculated that it may in part be due to the reports of rachitogenic effects of high doses of strontium. Also, the presence of the radioactive ^{90}Sr in nuclear fallout and waste may for many years have associated stable strontium with the radiation damages and contamination caused by radiostrontium [13].

2.10 Bone physiology

This section is intended to provide some basic information on the function, composition and structure of bone tissue. More detailed information on bone biology and disease can be found in references [66-71].

The skeleton has two primary functions:

1) a biomechanical, supporting, carrying and protecting the body,

2) a metabolic, serving as a reservoir for many ions, e.g. Ca and P.

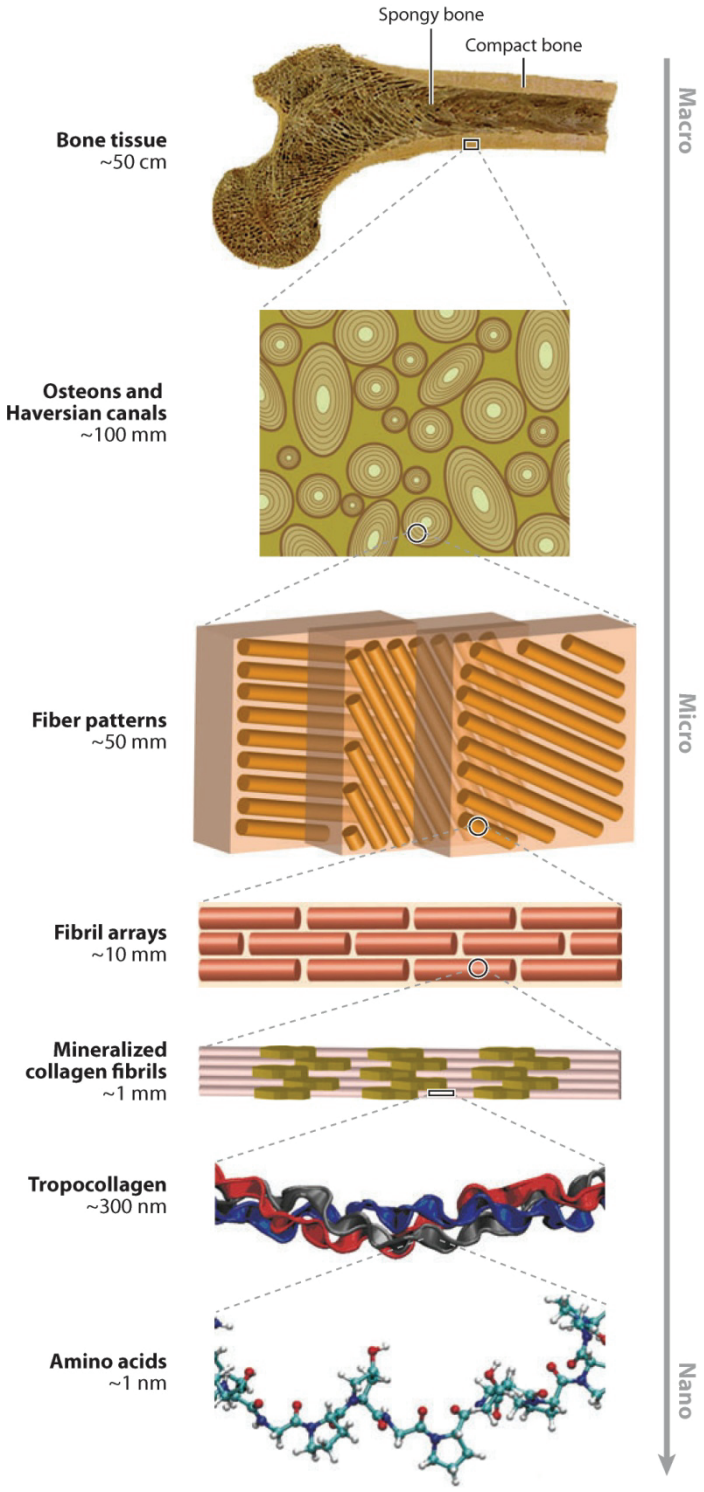

Figure 2.2 Hierarchical structure of bone, showing the seven levels of hierarchy. The two main categories of bone are 1) cortical (compact) bone that is found on the surface of all bones and 2) trabecular (spongy) bone that fills the inside of many bones. Compact bone is composed of concentric, lamellar structures of bone tissue (*osteons*) that surround and protect blood vessels occupying the *Haversian canal*. Each lamella is composed of fibres arranged in geometrical patterns. Each of these fibres consists of several linked collagen fibrils, forming together a fibril array. The mineralised collagen fibrils are the basic building blocks of bone. They are composed of collagen protein molecules (tropocollagen) formed from three chains of amino acids [67]. Reproduced by permission of Massachusetts Medical Society.

Making up the supporting framework of the body, bone tissue must satisfy several contradictory needs. Carrying the weight of the body requires stiffness, i.e. the ability to resist loading without deforming. At the same time, the bones must

posses a certain amount of flexibility, so that they can absorb energy by deforming rather than cracking. If the bones are too brittle and inflexible, loading will lead to structural failure, initially by development of microcracks and later by complete fracture. On the other hand, too much flexibility will cause a bone to bend beyond its peak strain, also resulting in fracture. This demand for structural strength must be balanced by a requirement for the bones to be light, so that movement is not hampered. Different types of bones are fine-tuned to achieve specific functional properties. Long bones such as femur and tibia are resistant against bending, short bones like vertebrae are resistant to compression but highly flexible, while plate-like bones like the skull provide protection for vital organs. The remarkable ability to accommodate the opposing demands of stiffness and flexibility, strength and lightness, is reflected in the ingenious biomechanical structure of bone tissue [67-69].

2.10.1 Composition and structure of bone

Bone tissue consists of bone cells imbedded in a matrix of organic material (primarily the fibrous protein type I collagen) stiffened by crystals of an inorganic calcium phosphate mineral very similar to hydroxyapatite (Figure 2.2). The crystals of bone are plate-shaped with average dimensions of 50 x 25 nm. Together with the third major component, water, the organic and inorganic constituents are associated in an ordered structure, sometimes referred to as the *mineralised collagen fibril* [69].

2.10.1.1 Hydroxyapatite

Wopenka and Pasteris [72] produced an in-depth mineralogical review on biological apatite. Pure hydroxyapatite (HAp) has a stoichiometric composition of $Ca_5(PO_4)_3OH$, often written as $Ca_{10}(PO_4)_6(OH)_2$ to denote that there are two formula units in one crystallographic unit cell. Using a somewhat simplified view, there a four different types of crystallographic positions in the apatite unit cell (Figure 2.3): (1) tetrahedral sites for six P^{5+}- ions, each in 4-fold coordination with oxygen, (2) Ca[I] sites for four of the Ca^{2+}-ions, (3) Ca[II] sites for the six other Ca^{2+}-ions, arranged in such a way that they form an anion channel, and (4) the channel site occupied by OH^-.

The apatite structure is highly accommodating to chemical substitutions. The body is able to fine-tune the composition of the crystal according to the different mechanical requirements of the structure (bone apatite, enamel apatite, dentine apatite). A large number of cations (e.g. Mg^{2+}, Fe^{2+}, Zn^{2+}, Sr^{2+}, and Pb^{2+}) can substitute Ca^{2+} in the apatite structure, but because insertion of any foreign ion will induce structural changes in the crystal, there is a limit to how much of a given ion that can be incorporated. According to Boivin *et al.* [73], a maximum of 1 out of 10

Ca ions can be replaced by Sr via heteroionic substitution in bone apatite. Sr^{2+} is mainly incorporated at the Ca[II] site [74].

In contrast, OH^- is readily replaced by F^-, because the F^- ion produces a better fit in the channel position than OH^-. This is exemplified by the fluoridation of tooth enamel via fluorinated dental products, which is advantageous because flourapatite is less soluble in acidic solutions than HAp. Carbonate ions can in principle substitute both at the OH-site and the PO_4-site, but it remains unclear exactly how CO_3^{2-} is incorporated. It seems to be generally accepted that, in biological apatite, CO_3^{2-} predominantly replaces PO_4^{3-}. Bone apatite contains approximately 7% (w/w) carbonate and tooth enamel about 3.5% (w/w).

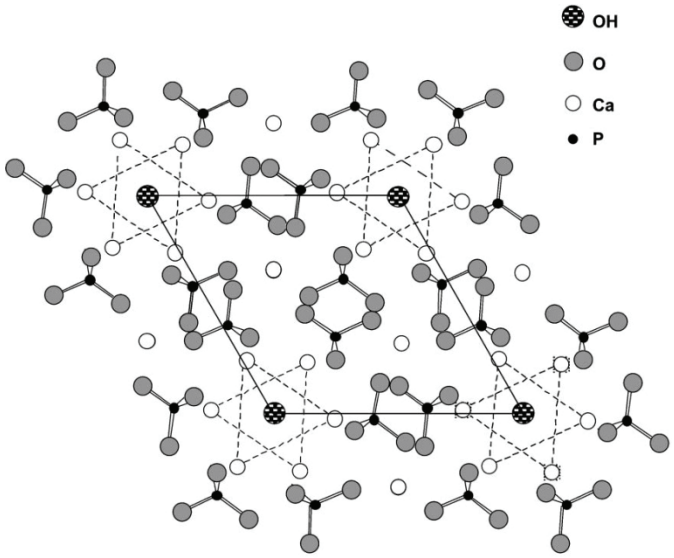

Figure 2.3 Projection of the (001) plane of the hydroxyapatite structure, showing the tetrahedral PO_4^{3-} ionic groups, Ca^{2+}-ions and OH^- channel ions. The parallelogram indicates outline of a unit cell. Six of the Ca^{2+} ions form a six-fold site in which the channel ions reside (OH^- in the case of hydroxyapatite) [72]. Sr is mainly incorporated at these Ca[II] sites. Reproduced from [75] by permission of The Royal Society of Chemistry.

Even though the mineral associated with bone and teeth is invariably denoted "hydroxyapatite" or "carbonated hydroxyapatite" in the medical literature, there is now some evidence for a lack of OH^-. In one study, Raman spectra of different apatites showed clear O-H stretching modes from hydroxyl groups for synthetic HAp and teeth enamel, while spectra for mammal cortical bone did not. Contrary to common statements, it therefore seems that bone apatites may not contain high concentrations of OH^- groups, and some may contain none at all [72].

Generally, the mechanic properties of the bone structure are largely determined by the mineral density [76]. A high mineral content increases the stiffness at the

expense of flexibility. By testing many different bones from different organisms, Currey [77] showed a clear correlation between stiffness and mineral density, bone stiffness increasing with increased mineral content.

2.10.1.2 Collagen

Whereas hydroxyapatite is the only mineral found in mature bone, more than 200 different proteins are present, collagen constituting about 90%. A collagen fibril is made up of three polypeptide chains of about 1000 amino acids wound together in a triple helix (Figure 2.2). Fibrils tend to merge with neighbouring fibrils, forming a larger structure called a fibre [69].

2.10.1.3 Water

The third component, water, is located in the gaps between the triple-helix molecules, within the fibril, between fibrils and between fibres. The presence of water is essential for the mechanical properties of the bone, and the results of mechanical measurements differ in dry and wet bone [69].

2.10.2 Bone types

Bone tissue is divided into two main categories: *cortical* bone and *trabecular* or *cancellous* bone. Cortical bone is dense and found in varying thickness on the outer surface of all bones, whereas trabecular bone is spongy and fills the insides of many bones [67]. The analogy to levers and springs formulated by Seeman *et al.* [68] is quite illustrative. Like a lever, long bones, e.g. the femur, must be able to resist bending and buckling, prioritising rigidity over flexibility. This property is provided by the compact cortical tissue, while lightness is achieved by the marrow cavity. In places where stress is mainly compressive, such as in the vertebrae or the femur neck, the porous structure of trabecular bone can act like a spring, absorbing energy by deformation at the expense of stiffness.

2.10.3 Modelling and remodelling

Though easily perceived as a rigid, inert material, bone is in fact a very adaptive organ, undergoing constant renewal. During childhood and adolescence, bones are formed by a modelling process which allows for concomitant formation of new bone at one site and resorption of old bone from another site, in effect allowing the bone tissue to shift position and grow in length and thickness. In modelling, osteoblast and osteoclast activity is uncoupled and the amount, shape and position of bone tissue can change rapidly [71].

The process of remodelling occurs throughout life and becomes the dominant process in adulthood. Unlike dentine, bones not only undergo remodelling on the surface but also internally [69]. In remodelling, a small amount of old bone is removed and then replaced with new bone at the same site. The remodelling has three main purposes: 1) to repair microcracks (or indeed fractures) in the skeleton caused by the stress of everyday activities, 2) to replace old bone which can loose its original elasticity and become brittle, 3) to enable the skeleton to act as a dynamic reservoir for calcium and phosphate by releasing and absorbing ions to and from the blood. In adults, most of the skeleton is replaced about every 10 years [71].

The resorption and formation processes are carried out by two types of specialised bone cells: *osteoclasts* and *osteoblasts* (Figure 2.1). Osteoclasts break down old bone tissue, carving long tunnels in the bone. These tunnels are then refilled by osteoblasts, leaving only a narrow tunnel and small capillaries to act as blood vessels. With time, the osteoblasts get surrounded by the bone tissue they have formed and then turn into a third type of cell, *osteocytes*, which are involved in the metabolism of the bone [68].

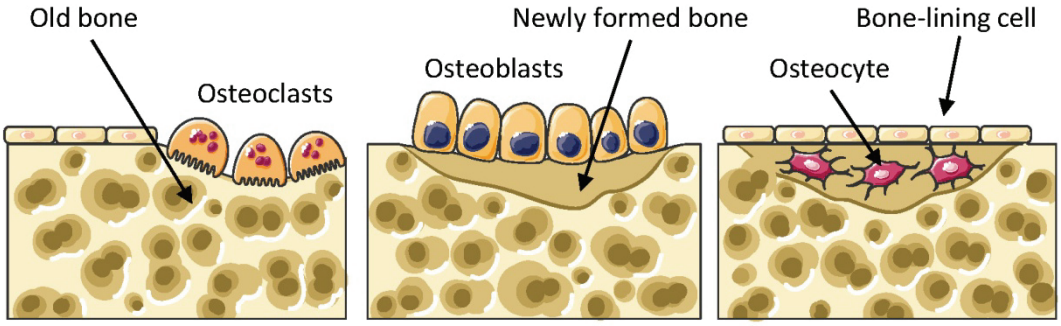

Figure 2.4 In bone remodelling, osteoblast activity is coupled to prior osteoclast activity. After bone resorption by osteoclasts, osteoblasts start laying down new bone. Some osteoclasts remain inside the newly formed bone and are converted to osteocytes, which are connected to each other. The resorption process takes place within a matter of weeks, while bone formation takes several months. Unless there is remodelling imbalance, net changes in the amount of bone are minimal. Figures were produced using Servier Medical Art [78].

In healthy adults there is a tight coordination between the activity of osteoblasts and osteoclasts, resulting in a fine balance between resorption of old bone and formation of new bone [79].

2.11 Osteoporosis

Osteoporosis (Gk. *osteon*, bone; *poros*: small hole or passage) is a major worldwide health problem, affecting an estimated 75 million people in Europe, USA

and Japan [80]. It is a severe, systemic skeletal disease characterised by an imbalance between the rates of bone resorption and bone formation, leading to a reduced bone mass and deteriorated microarchitecture of bone (Figure 2.5). The decrease in bone density and quality results in increased bone fragility and susceptibility to bone fractures.

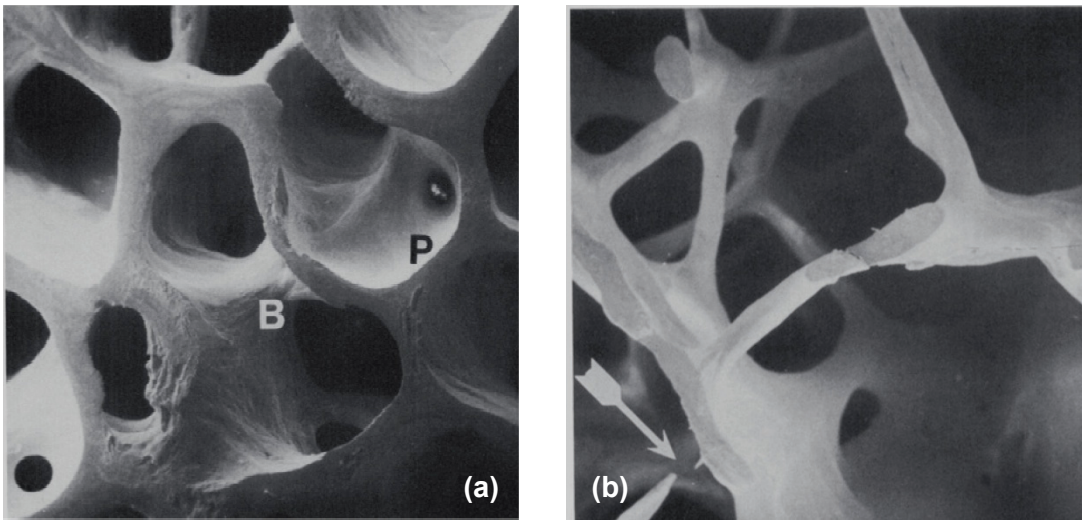

Figure 2.5 Scanning electron micrographs of iliac crest biopsies showing normal bone tissue (a) and osteoporotic bone tissue (b). P: Trabecular plate, B: Trabecular bar, Arrow: structural damage. Reproduced from [81] by permission of The American Society for Bone and Mineral Research.

The maximum amount of bone a person achieves in a lifetime, the *peak bone mass*, is normally reached around the age of 20-25 [82]. After the age of 30 the quantity of bone starts to decrease because the rate of resorption is no longer matched by the rate of formation. The loss of bone is about 0.5% per year in men and 1% in women. In the years just after the menopause, women may lose up to 6% bone mass per year, due to the reduced production of oestrogen [83]. The primary risk factors for osteoporosis are advanced age, female gender, family history (genetic factors), menopause, low body mass index, poor nutrition and insufficient exercise [82].

Because of the resulting bone fragility, osteoporosis is associated with an increased risk of low-energy fractures, especially in the forearm, vertebrae and the femur neck. Low-energy fractures originate from relatively minor trauma, resulting from normal activities or low falls, as opposed to high-energy fractures resulting from violent incidents such as traffic accidents or high falls. These fractures lead to pain, immobility, increased mortality, and loss of normal functioning and quality of life. Especially hip fractures contribute substantially to morbidity and mortality in the elderly [80]. On average 1 in 3 women over the age of 50 will experience

osteoporotic fractures, as will 1 in 5 men [84-86]. In Denmark, the estimated prevalence of osteoporosis in persons aged 50 years or more is 41% among women and 18% among men [87].

2.11.1 Diagnosis

Osteoporosis has no specific symptoms and cannot be diagnosed by a biochemical laboratory analysis. A diagnosis therefore depends on an assessment of skeletal mass, measured as *bone mineral density* (BMD) [88]. The standard method for determination of BMD is *dual energy X-ray absorptiometry* (DEXA) which is described in more detail in Chapter 4. The measured BMD is converted to a T-score, which is calculated by taking the difference between a patient's measured BMD and the mean BMD in healthy adults with peak bone mass, matched for gender and ethnic group, and expressing the difference relative to the young adult population standard deviation (SD) [89, 90]:

$$\text{T-score} = \frac{\text{Measured BMD-Young adult mean peak BMD}}{\text{SD of young adult population BMD}} \qquad (1\text{-}1)$$

A WHO study group has defined a T-score of < -2.5 as osteoporosis in postmenopausal women [91]. BMD measurements using DEXA were identified as strong predictors of osteoporotic fractures in clinical studies [92, 93], and, in practise, a patient with a low-energy fracture of the vertebra or hip is diagnosed with osteoporosis by definition [89].

Table 2.3 WHO definitions of Osteoporosis and Osteopenia based on BMD T-scores [91, 94].

Terminology	T-score
Normal	$T \geq -1.0$
Osteopenia (low bone mass)	$-1.0 > T > -2.5$
Osteoporosis	$T \leq -2.5$
Established (severe) osteoporosis	$T \leq -2.5$ in the presence of one or more low-energy fractures

2.11.2 Current treatment

The purpose of prevention and treatment of osteoporosis is to reduce the risk of fractures [89]. Prevention begins with ensuring an adequate intake of Ca and vitamin D, as well as participation in physical activity. Several medicines are approved for osteoporosis, traditionally divided into two categories: 1) anti-resorptive (or anti-catabolic) treatment, which inhibits osteoclastic activity and thereby reduces the rate of bone resorption, and 2) anabolic treatment that stimulates bone formation. Most

pharmaceuticals are considered to be mainly anti-resorptive. These include bisphosphonates (e.g. Alendronate®, Optinate®) and selective estrogen receptor modulators (SERM, Evista®). Parathyroid hormone (PTH) and PTH analogues (Preotract® and Forsteo®) have anabolic effects on bone. Clinically, strontium ranelate (Protelos®) is considered to be mainly anti-resorptive, with a weaker anabolic effect. Ca and vitamin D supplements are always recommended as co-therapy regardless of the primary medicine [82, 89, 95, 96].

2.12 Incorporation of strontium into bone

Strontium has a great affinity for bone and is readily incorporated into bone tissue. In an early study, MacDonald *et al.* [97] observed a rapid increase in bone Sr during the first day after oral administration of $SrCl_2$, followed by a much slower rate of increase the following 6-8 weeks. The authors suggested that this indicated two distinct deposition mechanisms: (1) An initial rapid mechanism, involving osteoblastic activity and formation of new bone, whereby Sr^{2+} is incorporated by surface adsorption, ion exchange with Ca^{2+} and protein binding of Sr^{2+}. This mechanism is eventually saturated. (2) A slower mechanism, incorporating Sr into the crystal lattice of existing bone mineral. X-ray diffraction studies by the same authors also confirmed that Sr is ultimately incorporated into the internal structure of the crystal lattice, causing distortions of the unit cell [98]. X-ray crystallographic [73] and radioisotope studies [99] later confirmed the idea of two mechanisms for Sr incorporation, i.e. a rapid uptake into newly formed bone and a slow ion-exchange process in old bone and it is now widely accepted [39]. In a more recent literature review, Dahl *et al.* [39] identified three essential mechanisms for uptake and release of bone-seeking elements:

1) Bone formation, leading to an increase in mineral density,
2) Resorption, releasing ions into the blood
3) Surface exchange of ions between the blood and bone can take place where bone surfaces are in contact with blood. Diffuse exchange is a slow process whereby ions can diffuse through the entire bone volume. These exchange processes are considered to be the main mechanisms of trace metal uptake in adults.

Even with large doses over a long period of time, the amount of Sr that is incorporated is always very low (a few percent) compared with Ca [39]. The discrimination against Sr in the incorporation into hydroxyapatite may be caused by

the larger ion radius, which produces a mild distortion of the crystal lattice of calcium hydroxyapatite. This may result in a weaker binding of Sr to the crystal [12].

After cessation of strontium treatment, the concentration of Sr in bone decreases substantially irrespective of the previously administered dose. Sr is eliminated by three processes: (1) clearance from the exchangeable bone pool, (2) displacement of Sr in hydroxyapatite, presumably by Ca and (3) removal through bone resorption by osteoclasts. Sr is better retained in new bone than in old, presumably because the heteroionic substitution during bone formation makes Sr more firmly linked to the structure than the surface exchange and adsorption processes occurring in old bone. Models suggest that the terminal half-life in humans is about 3 years [39].

2.12.1 Factors influencing the incorporation of strontium in bone

Dahl *et al.* also [39] summarised five main factors that influence the amount of Sr that is incorporated into bone: dose level (exposure), duration of treatment, gender, the concentration of Sr in the plasma and type of bone (Figure 2.6).

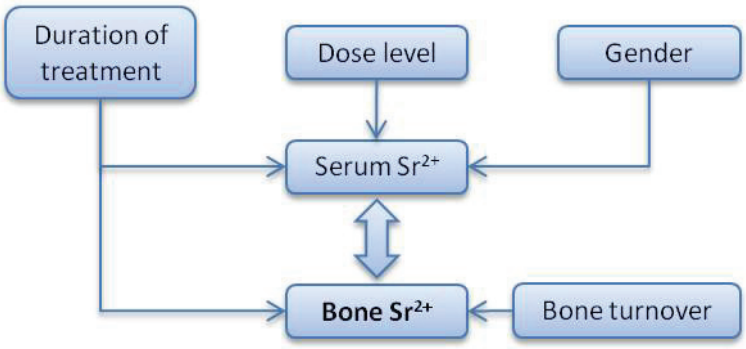

Figure 2.6 Factors influencing the incorporation of strontium into bone are dose level (level of exposure), duration of exposure, gender, serum Sr and bone remodelling rate. Redrawn from [39].

2.12.1.1 Dose level

It has been clearly demonstrated that bone Sr increases with the administered dose. Sr in rat femur increased proportionally with doses of 35-140 mg kg^{-1} day^{-1} Sr^{2+} after 4 and 8 weeks. At higher dose levels (up to 255 mg kg^{-1} day^{-1} Sr^{2+}) the dose-dependent relative increase was reduced until the bone Sr reached a plateau level. The explanation is most likely saturation of the gastrointestinal absorption combined with saturation of the incorporation mechanisms as discussed above [39].

2.12.1.2 Duration of treatment

Together with treatment dose, the duration of treatment plays an important role in determining the degree of Sr incorporation. In a 56-days study with rats, the bone Sr concentrations doubled from 10 to 25 days of treatment, even though a constant level of serum Sr had been reached after 10 days. Bone Sr continued to increase slightly from 28 to 56 days of treatment [39].

2.12.1.3 Serum strontium

In rats and monkeys serum Sr often reach a plateau level related to the administered dose within 4 weeks. As for bone Sr, the Sr concentration in serum increases relatively more at low doses than at high doses, due to saturation of the gastrointestinal absorption pathways. Such saturated Sr concentrations were seen to correlate positively with bone Sr in monkeys [39]. This relationship might mean that a reliable assessment of bone Sr in patients can be performed by taking a blood sample rather than a bone biopsy.

2.12.1.4 Gender

Rats kept on a normal laboratory chow (1% Ca, 0.02% Sr) showed no differences in femur or plasma Sr concentrations. However, oral administration of strontium ranelate to rats and monkeys resulted in higher bone and plasma Sr in males than in females. The difference may be caused by a gender difference in gastrointestinal absorption. A similar gender effect has not been reported in humans [39].

2.12.1.5 Bone type

Different skeletal sites incorporate different levels of Sr. The relative proportions of cortical and trabecular tissue in a given bone influences the Sr incorporation, because the bone turnover and thus the abundance of newly formed bone is higher in trabecular bone [39, 100]. Studies with radioisotopes have indicated that at least part of the variations in Sr bone uptake is related to the level of regional blood flow [101, 102]. Strontium concentrations in different skeletal sites (iliac crest and lumbar vertebra) were correlated in monkeys, independently of Sr dose [39]. It might therefore be possible to asses the Sr content of deeper skeletal sites by bone biopsies of the iliac crest in humans.

2.13 The effect of strontium on bone

The *in* vivo effects of Sr depend on the applied dose. High doses may disturb calcium metabolism and impair bone mineralisation, while low and moderate doses

have beneficial effects on bone. Quantitative limits between high and low doses are not completely established, but Marie *et al.* [37] considered a low dose to be less than 350 mg kg^{-1} day^{-1} Sr. Based on literature data, Cabrera *et al.* [38] found that a Sr concentration of more than 4 g L^{-1} in food or drinking water constitutes a high diary intake. Morohashi *et al*. [103] saw a need for a distinction between pharmacological and toxic doses of Sr. The authors found that a Sr dose of less than 15 mg per day had no adverse effects in rats, while a dose of 75 mg per day markedly suppressed Ca metabolism.

2.13.1 High doses

The first study indicating that Sr administered in high doses can induce defective bone mineralisation was published in 1935 [104]. Several animal studies have later shown that a high dietary intake of Sr can cause bone changes similar to those observed in rachitic bone, especially if the intake of Ca and vitamin D is low [38]. High doses of Sr can disturb Ca metabolism by reducing the intestinal absorption of Ca [105, 106] and by inducing hypocalcaemia and hypomineralised bone [48, 107, 108]. In pigs, a diet of 0.16% Ca and 0.47-0.67% Sr caused incoordination, weakness, reduced weight gain and leg paralysis [109].

One report of Sr related rickets in humans was published by Ozgur *et al.* [110], who investigated the prevalence of rickets in children aged 6-60 months in two regions with different soil Sr content in Turkey. Rickets (rachitis) is a bone disorder in children similar to osteomalacia in adults. It is characterised by a softening of the bones due to a decrease in bone mineralisation. In region I, which had a soil Sr concentration of >350 mg g^{-1}, the prevalence of rickets was 31.5%, while region II which had a soil Sr concentration of <350 mg g^{-1}, the prevalence was 19.5%. These findings are particularly important in areas where nutrition is mainly based on grain cereals. The prevalence of osteomalecia in dialysis patients with high serum and bone Sr were mentioned previously (section 2.8).

The mechanism behind these deleterious effects of high Sr doses seems to be a combination of competitive inhibition of intestinal Ca absorption and a reduced renal synthesis of 1,25-dihydroxy cholecalciferol, which is the hormonally active form of vitamin D responsible for increasing the concentration of Ca in the blood [13].

2.13.2 Low doses

Studies have shown that low doses of strontium administered (as chloride) to rats stimulated bone formation and increased trabecular bone volume [107, 111], as well as increased the volume of vertebral bone and the number of bone forming sites [112]. Later studies showed that strontium ranelate enhanced bone cell replication and bone formation *in vitro* [113]. Bonnelye *et al.* [114] reported that SrR treatment was followed by increased osteoblastic formation and function, as well as decreased osteoclastic activity in cultured bone cells.

Marie et al. [115] reported that SrR prevented trabecular bone loss in oestrogen-deficient rats by decreasing bone resorption. However, in a recent study, Fuchs *et al.* [116] observed that SrR treatment of oestrogen-deficient rats did neither increase bone formation nor inhibit bone resorption. Short-term studies showed that treatment with SrR reduced the loss of trabecular bone volume in hind-limb immobilized rats [117]. Using X-ray diffraction and Raman microspectrometry, Boivin *et al.* [73] studied the distribution of strontium in monkey bone after administration of strontium ranelate. It was found that Sr was dose-dependently incorporated into both cortical and trabecular bone, mainly into trabecular and new bone. The study also showed that the clearance of Sr is quite high. After withdrawal of SrR, bone Sr decreased rapidly and faster in old than in new bone. The authors suggested that this observation may be explained by the fact that Sr is mainly incorporated into old bone by adsorption and surface exchange, whereas new bone incorporates Sr deeper into the crystal lattice by ionic substitution, linking it more firmly to the structure. No changes in crystal structure were observed. As an antiosteoporotic drug, the rapid clearance distinguishes Sr from bisphosphonates, which, once incorporated, are irreversibly bound to bone [13]. Long-term studies in healthy rodents showed a dose-dependent increase in trabecular bone volume, mineralised bone volume and osteoblastic surface, accompanied by a reduction in osteoclastic surface and osteoclast number [118].

In recent studies, SrR has been shown to also have an effect on the biomechanical properties of bone. Long-term SrR treatment increased bone strength in both vertebra and femur in healthy rats [119], and prevented loss of bone strength in oestrogen-deficient rats [120]. In osteoporotic (oestrogen-deficient) rats, six weeks of SrR treatment produced an improved healing of bone fractures, measured by improved strength and stiffness of healed tibia bones [121]. However, short-term studies in chicken treated with $SrCO_3$ did not show any change in breaking strength of long bones [122].

2.13.3 Mechanism for strontium activity in bone

The exact mechanism by which Sr affects bone tissue is unclear at present, but it appears that Sr can act through activation of the calcium sensing receptor (CaSR). The CaSR is an extracellular receptor which helps maintaining Ca homeostasis in the body, making several cells and tissues able to sense and respond to small changes in extracellular concentrations of Ca^{2+}. The CaSR controls recruitment and survival of bone cells. Via the CaSR, elevations in blood Ca^{2+} concentrations are countered by increased osteoblastic activity and decreased osteoclastic activity, resulting in transfer of Ca from the blood to the skeleton [123, 124]. There is mounting evidence that Sr^{2+} acts as an agonist (activator) for the CaSR in bone cells [125-128]. However, recent studies have showed that SrR activated replication in osteoblasts deprived of the CaSR, indicating that another receptor mediates the effect of SrR on osteoblasts.

2.13.4 Clinical trials with strontium ranelate

In clinical trials, SrR has been shown to reduce the frequency of vertebral and non-vertebral (e.g. hip) fractures in women suffering from osteoporosis. In the first phase II trial [129], it was concluded that the minimum dose at which SrR is effective in preventing bone loss is 1 g per day (320 mg Sr^{2+} per day). In the second phase II trial [130], a significant and clinically relevant increase in lumbar bone BMD and a reduction in the number of patients experiencing vertebral deformities were observed after 12 and 24 months of SrR administration. A dose of 2 g day^{-1} was considered to be the best compromise between efficiency and safety. This was the first clinical study to demonstrate antiosteoporotic efficiency of SrR.

Two 5-year phase III trials [131] were conducted with postmenopausal women suffering from osteroporosis and with a medical history of at least one prevalent fracture. The treatment dose in both studies was 2 g SrR per day. In the first study called *Spinal osteoporosis therapeutic intervention* (SOTI) there was a significant reduction in the risk of vertebral fractures with 49% after the first year, 41% after three years and 36% after four years compared to placebo. Lumber BMD was increased 14% an average after 3 years [132, 133]. The second study, *Treatment of peripheral osteoporosis study* (TROPOS), showed a reduction in the risk of non-vertebral fractures of 16% after 3 years of treatment. In a subgroup with particularly high risk of fractures, a risk reduction of 36% was observed [134]. After 5 years, the TROPOS showed that the fracture risks in the treated group were reduced with 15% for nonvertebral fractures, 43% for hip fractures and 24% for vertebral fractures [135]. After 8 years of treatment the cumulative incidences of vertebral and non-

vertebral fractures were not significantly different from the incidences in the first 3 years, but lumber, femoral and hip BMD continued to increase throughout the 8-year period. SrR was reported to be safe and well tolerated over the 8-year treatment period [136].

Taken together, the clinical studies show that SrR treatment leads to a significant and sustained risk of vertebral and non-vertebral fractures in women suffering from osteoporosis.

2.14 Conclusion

Strontium is widely distributed in nature, and small amounts of the element are usually found whenever calcium is present. The dietary uptake of Sr is much lower than the uptake of Ca. In the body, Sr is in competition with Ca, as the two elements share the same routes and mechanisms for absorption and transportation. All transport processes has a higher affinity for Ca, and the biological activity of Sr is lower than that of Ca for all Ca-activated processes. Sr is not counted as an essential element, but at the same time the organism is able to tolerate quite high contents of Sr in the diet.

Sr has an effect on bone on both the molecular and cellular levels. It is a bone-seeking element and 99% of the Sr in the body is found in the skeleton. The amount of Sr incorporated in bone following Sr administration depends mainly on dose level, gender, type of bone and duration of treatment. Sr is incorporated into bone by ion exchange, both at the crystal surface and during formation of new bone. As a pharmaceutical agent, Sr has been shown to have a positive effect on bone tissue by concomitantly stimulating bone formation and reducing bone resorption, thereby providing a sustained skeletal benefit. Low and moderate doses of Sr have been shown to increase bone volume and osteoblastic activity while reducing osteoclastic activity. In rats, Sr prevented osteoporotic bone loss, increased mineralised bone volume and improved the biomechanical properties of bone. Conversely, high doses of Sr cause rachitis and hypocalcaemia due to competitive inhibition of Ca uptake. The mechanism behind strontium's effect on bone tissue is not fully understood, but it may involve activation of the calcium sensing receptor.

Phase III clinical trials have shown that treatment with strontium ranelate significantly reduces the risk of vertebral and hip fractures in osteoporotic women.

CHAPTER THREE

Analytical methods for the determination of strontium in biological matrices

3.1 Introduction

Sr measurements in biological fluids have long been used for assessment of Ca metabolism and pharmacokinetics [137]. The interest for determination of Sr in calcified tissues increased with the discovery of strontium's potential as an antiosteoporotic agent, and Sr isotope analysis of prehistoric bone can provide information about the migration patterns of ancient populations [138]. In forensic science, the fact that sea water contains much higher Sr concentrations than human blood has been used to establish sea drowning. When drowning occurs, Sr enters the body via the alveolocapillary membrane in the lungs, resulting in an increase of blood Sr [139, 140].

Earlier, atomic absorption spectrometry was the technique of choice for elemental analysis in clinical laboratories, but today, inductively coupled plasma atomic emission spectrometry and mass spectrometry are becoming increasingly popular because of their lower detection limits, wider dynamic ranges and multi-element capabilities [141]. This chapter provides an overview of the most common – as well as few less common – analytical techniques for determination of Sr in biological matrices. Sample preparation and the applications of metrology and reference materials for Sr quantification are discussed, and applied techniques and sample preparation procedures for analysis of bone, teeth, hair, whole blood, serum, plasma, marrow and urine are summarised in Table 3.1, p 37.

3.2 FAAS

Flame atomic absorption spectrometry (FAAS) has been used for determination of Sr in foodstuffs [142], teeth [143] and bone [56, 144-146]. Sr has its most sensitive resonance line at 460.7 nm. Air-acetylene and N_2O-acetylene flames provide similar sensitivities and detection limits, though the latter is usually recommended due to better accuracy. An air-acetylene flame is subject to strong interferences from Al, Fe, Mg, Si, Ca, PO_3^{4-}, SO_4^{2-}, NaCl and various acids (H_3PO_4 > H_2SO_4 > HCl > HNO_3), but the extent of interference is strongly dependent on flame stoichiometry, burner position and presence of releasing agents. Addition of 0.2-1% lanthanum, e.g. as $LaCl_3$, may reduce interference, but matrix matching with respect to acid concentration is strongly recommended. Even in the high-temperature N_2O-acetylene flame, interference from Ca and PO_3^{4-} remains a problem and a complete matrix-matching may be necessary [143]. Ionisation interference is observed in both flames; in a N_2O-acetylene flame Sr is approx. 80% ionised, while approx. 10% is ionised in the cooler air-acetylene flame. In both cases the ionisation can be suppressed by adding 0.1-0.2% K^+ as KCl [147-149]. Sanz-Medel *et al.* [150] found that the observed sensitivity using flame atomic emission spectrometry (FAES) was about four times higher than the sensitivity found using FAAS.

3.3 ETAAS

Electrothermal atomic absorption spectrometry (ETAAS) was used for quantification of Sr in bone [151], teeth [152], whole blood [145], plasma [137, 153], serum [151], urine [145, 151, 153], brain tissue [154] and saliva [155]. Following acidic sample digestion, typical analytical electrothermal protocols include drying at 90-250°C, pyrolysis at 1200-1500°C and atomisation at 2400-2700°C. The atomisation efficiency is relatively low due to formation of carbides, cyanides and halides [148]. Halide interference can be countered by using diluted HNO_3 as a matrix modifier [156] or by masking Sr with EDTA [157]. H_2SO_4, H_3PO_4 and $HClO_3$ cause interference and should be avoided in the sample preparation [148]. D'haese *et al.* [151] reported that addition of the surfactant Triton X-100® to dissolved bone samples improved the reproducibility, perhaps due to a more uniform sample deposition into the graphite furnace.

3.4 ICP-AES

Inductively coupled plasma atomic emission spectrometry (ICP-AES) is a very popular technique for determination of Sr and has been used for analysis of bone

[158, 159], lung [160], soft human tissues [161], urine, plasma, serum and dialysis fluids [162, 163]. Sanz-Medel *et al.* [150] compared FAAS, FAES and ICP-AES for determination of Sr in biological samples. The authors concluded that ICP-AES was the more suitable technique, owing to a better limit of detection (two orders of magnitude lower than N_2O-acetylene FAES), a linear range spanning five orders of magnitude, good precision (0.3%) and virtual absence of spectral interferences. The presence of 200 mg L^{-1} Ca and P had no significant influence on the emission of 2 mg L^{-1} Sr. In contrast, Shiraishi *et al.* [159] reported that accurate determination of Sr in bone (sample concentrations approx. 0.1 mg L^{-1} Sr) required matrix-matching of the standards due to significant spectral interferences, primarily from calcium and, to a minor extent, phosphate.

3.5 ICP-MS

Inductively coupled plasma mass spectrometry (ICP-MS) has been applied for quantification of Sr in bone and teeth [164-166], bone marrow [167] and serum [168-170], and for measuring isotope ratios in archaeological bone [171, 172]. The fundamental difference between ICP-AES and ICP-MS is that the ICP is used to generate photons in ICP-AES as opposed to positively charged ions in ICP-MS. For both techniques, plasma effects of 1000-1300 W are most frequently applied. In most ICP-MS studies, an internal standard (IS) is added to the calibration standards and samples in order to correct for non-spectroscopic interferences and instrumental drift. ^{89}Y, ^{103}Rh and ^{115}In have been used with success for determination of Sr [164, 167, 169, 170].

Determining Sr and other trace metals in teeth and bone, Outridge *et al.* [165] reported that a hydroxyapatite matrix gave rise to significant signal suppression of several isotopes and that Sr determination without an IS suffered from very poor precision (about 40%) and poor accuracy. Roberts *et al.* [164] used ^{115}In for Sr determination in bone but did not report any observations of interference on the Sr signal. Analysing serum and saline matrices, Gerotto *et al.* [173] found no significant spectral interferences affecting the Sr measurements in serum. Using cluster-analysis to evaluate ^{103}Rh, ^{89}Y and ^{128}Te as IS, the authors concluded that ^{89}Y provided the best correction for signal suppression induced by 0.5% NaCl. Prohaska *et al*. [138] used ICP-MS and laser ablation (LA) ICP-MS for measurement of $^{87}Sr/^{86}Sr$ ratios in prehistoric human teeth and bones. The LA-ICP-MS method was used for isotope measurements of transversal bone cross sections, resulting in a precision of 0.1-0.2%. The authors found that interference from ^{87}Rb necessitated an effective separation of Rb and Sr, either by a Sr specific resin or by a mathematical correction.

In a recent study, De Muynck and Vanheacke [166] used ICP-MS in combination with a dynamic reaction/collision cell (DRC) for determination of P, Ca and Sr in bone. NH_3 was used as a reactant gas and the flow rate was optimised based on the ratio between signals from the analytes and interfering ions. Addition of NH_3 improved the signal-to-noise ratios with a factor of about 200 for ^{42}Ca and a factor of 10 for ^{86}Sr and ^{88}Sr. The reactant gas reduces interferences via charge transfer between the neutral NH_3 and interfering ions (e.g. Ar^+, $ArCa^+$ and Ca_2^+). For instance, a positively charged Ar^+ ion formed in the plasma will react with (more precisely, accept an electron from) NH_3, forming Ar and NH_3^+. P has a slightly higher first ionisation energy than does NH_3, making it thermodynamically favourable to form NH_3^+ and P, which would be expected to remove P^+ from the reaction cell. However, it was demonstrated that P could be determined under the same conditions as for Ca and Sr. ^{103}Rh was used as IS for Sr and ^{51}V for Ca and P.

3.6 Other analytical techniques for determination of Sr

Neutron activation analysis (NAA) has been used for Sr determination in bone [174-176], serum and packed blood cells [177, 178]. NNA is well suited for analysis of bone samples, as it can be performed directly on solid samples, which reduces the sample preparation. However, the additional production of radioactivity in the samples, the relatively slow sample throughput and the limited availability of reactor facilities constitute considerable drawbacks of the technique [179]. X-ray fluorescence (XRF) has been used for analysis of bone and teeth [180-183]. In the context of clinical analysis, the major advantage of XRF is that measurements can be carried out *in vivo*, saving the patient the discomfort and pain of undergoing a bone biopsy. The main disadvantage is a relatively large uncertainty [183]. Other non-invasive methods for determination of trace elements in bone include proton induced X-ray emission (PIXI) [184] and dual-photon absorptiometry (DPA) [185].

3.7 Sample preparation

Table 3.1 presents an overview of different sample preparation procedures for biological samples found in the literature. The table is not exhaustive but shows the variety of procedures available. Generally, for techniques requiring liquid samples, solid tissues such as hair, teeth, bone and soft tissues are dissolved in concentrated mineral acids at high temperatures. HNO_3 or HNO_3/HCl is often used for calcified tissues, though in one case HF was recommended for total digestion of a bone reference material [186]. To decrease preparation time, the digestion mixture is heated, either at atmospheric pressure by means of a hot plate or a microwave oven,

or at elevated pressures in an autoclave or a closed-vessel microwave oven. The high pressure raises the boiling point of the acids and therefore substantially increases the dissolution rate of the organic matrix components [187]. Some investigators evaporated the digests to dryness on a hot plate, followed by redissolution in diluted nitric acid.

Bone samples are frequently cleaned of adhering blood, lean tissue and fat in order to avoid analyte contributions from these tissues. Typically, the cleaning is carried out mechanically with a scalpel and chemically by means of oxidants and solvents, e.g. hydrogen peroxide, ether, ethanol, formic acid or water. The clean samples are dried before weighing, in order to eliminate a mass contribution from water. Some investigators avoided these preparation steps by using dry ashing for removal of organic material and moisture. The bone and adhering tissue were ashed at temperatures of 450-800°C for up to 10 hours, and the inorganic bone ash was subsequently dissolved by acid digestion (cf. Table 3.1).

Microwave assisted or autoclave acid digestion has also been applied for preparation of whole blood, urine, plasma and serum. In ICP-MS, the major reasons to digest liquid samples are to avoid matrix-induced signal suppression and deteriorated, unstable performance caused by deposition of organic material on the nebuliser, injector tubes and cones. Digestion reduces the content of organic material and total dissolved solids, thereby reducing or eliminating the tendency to clogging [168, 188]. A major drawback of this approach is the high acid concentration in the digested sample. To avoid problems with nebulisation and corrosion inside the instrument, the digests must be diluted with about a factor of 10 before analysis. One alternative is to use UV photolysis to break down organic material, thus avoiding the use of concentrated mineral acids. UV digestion has been used for urine, serum and whole blood, and has been found to be preferable to conventional acid digestion [189, 190].

Several investigators have reported that satisfactory results could be obtained merely by diluting the liquid sample with water, dilute HNO_3 and/or Triton X-100® [191, 192], or an alkaline solution with EDTA for stabilisation [193]. Direct sample dilution of course reduces the time required for sample preparation compared to any digestion procedure. The advantage of diluting with an acid is that preparation of matching standards (i.e. standards made with the same acid) is more straightforward and that the standard solutions prepared are more stable [194]. Indeed, in most studies external standard solutions were made up in diluted HNO_3, but quantification

by standard addition [193] and matrix-matched standards have also been reported [166, 173].

3.8 Metrology

3.8.1 Uncertainty budgets

Few clinical studies, and indeed few studies on Sr, using spectrometric equipment for quantification refer to the metrological guidelines presented in the *Guide to the expression of uncertainty in measurement* (GUM) [195] or the Eurachem/CITAC guide *Quantifying Uncertainty in Analytical Measurement* (QUAM) [196]. The evaluation of analytical performance is almost invariably given as reproducibility/repeatability rather than a metrological uncertainty. We applied and discussed the concepts of GUM and QUAM in the 4-week dog study presented in Appendix II. One of the few other examples was published by Prohaska *et al.* who determined Sr isotope ratios in archaeological bones [138]. The authors stated that all uncertainty calculations were performed according to the Eurachem guidelines and explicitly declared that no outlier rejection was performed on the data. Bettinelli *et al.* [197] and Breda *et al.* [198] included measurement uncertainty in the validation of ICP-MS methods for determination of Pt in plasma, serum and urine. Bettinelli *et al.* found an instrumental limit of detection (LOD) of 2 ng L^{-1}, while the minimum quantifiable concentration in urine based on the calibration uncertainty was set to be three orders of magnitude higher at 2 µg L^{-1}.

Patriarca *et al.* [199] presented a worked example of an uncertainty budget for determination of Pb in blood using ETAAS. Combining contributions from calibration, repeatability and sampling, the authors arrived at a concentration-dependent combined uncertainty of up to 10%. The paper gave rise to some correspondence [200, 201] and an erratum [202] concerning the inclusion of bias data into the uncertainty calculations. As noted by Taylor *et al.* [203], the dispute as well as the low number of reported applications illustrate that more than a decade after the publication of the first edition of the Eurachem guide, the practical preparation and application of uncertainty budgets are far from well established for clinical analysis.

3.8.2 Reference materials

Reference material (RM) is a generic term for materials that can be used for calibration, validation and quality control of analytical methods. In particular the accuracy of an analytical procedure is generally demonstrated by the quantification

of relevant analytes in a reference material with a matrix and analyte concentrations matching those of the samples. The term certified reference material (CRM) is reserved for materials for which an unbroken chain of traceability has been established, and for which certified values are expressed with accompanying uncertainties at a stated confidence level. Many CRMs are produced by national metrological laboratories, following guidelines established by ISO. Major suppliers of commercial reference materials include IRMM (Belgium), LGC (United Kingdom), Biorad (CA, United States), NIST (MD, United States) and Sero (Norway). The United States National Institute for Standards and Technology (NIST) has registered the trademark SRM® (Standard Reference Material) for its CRMs, while the European Institute for Reference Materials and Measurements (IRMM) uses the trademark ERM® (European Reference Material) for CRMs produced in partnership with European organisations [141].

3.8.3 Applied reference materials in this project

During this project, three different reference materials were applied: NIST 1400 Bone Ash, NIST 1486 Bone Meal and Sero Seronorm Trace Elements Serum. The SRMs obtained from NIST were regarded as very suitable for the project, as they provided certified values for all the elements of interest (Sr, Ca, Mg and P) in matrices matching real samples. It was assumed that bone and dentine are so comparatively close in composition that a bone CRM could be used for validation of analysis of teeth as well.

In contrast, serum CRMs containing all the relevant analytes were not commercially available. In fluid reference materials such as blood, urine and serum, usually only a few elements are certified (e.g. Ca, Mg and Li in IRMM's BCR-304). Three of the most widely used reference materials, Sero's Seronorm Trace Elements Whole Blood, Serum and Urine, provide concentrations of more than 70 elements, but none of these values are certified. The conventional procedure for establishing certified analyte concentrations is to allow several laboratories to analyse the material, using different techniques, in order to obtain reliable consensus values. Conversely, most of the analytes in the Sero materials have been determined by a single laboratory only. In the documents accompanying the sample vials, the manufacturer states element concentrations as "analytical data", but the concentration of each analyte is listed by the analytical technique that was applied, resulting in up to three different reference concentrations for each element. Following the example set by Krachler *et al.* [191] the values provided by Sero are therefore referred to as "reported" rather than "certified" in this report.

3.9 Choice of technique

Three of the described techniques, FAAS, ETAAS and ICP-MS were available for this project. The primary aim was to quantify trace-level concentrations of Sr in bone, teeth and body fluids, and the secondary aim was to determine the macronutrients Mg, Ca and P, which are found in much higher concentrations (medium – high mg g^{-1} and mg L^{-1}). Keeping in mind that biological Sr concentrations are of the orders of 10-100 μg $L^{-1}$for serum and 50-200 μg g^{-1} for bone, it is clear from Table 3.1 that of the available techniques, only ETAAS and ICP-MS provide adequate limits of detection. FAAS has LODs in the low-medium μg L^{-1} range [204], whereas, with ETAAS, LODs are typically below 1 μg L^{-1}, corresponding to the low-medium ng g^{-1} range in solid tissues. ICP-MS provides the lowest LODs, with values ranging from about 1 μg L^{-1} to below 10 ng L^{-1}, corresponding to values below 1 ng g^{-1} in solids. Though Ca and Mg do exist in concentrations high enough to be measured by FAAS, these elements suffer from phosphate interferences [149]. Even though ETAAS provides an adequate LOD for Sr quantification, the technique has the major drawback of only being able to determine one element per analysis. Thus, as the large number of samples made analysis time an important factor, ICP-MS was chosen primarily for its multi-element capability and wide dynamic range.

It is worth noting here that the LODs given in Table 3.1 are not necessarily directly comparable, as the methods, by which they were obtained, are not explained in all cases. LODs are customarily given as three times the standard deviation (3σ) of a series of blank measurements, but whether this blank was made from ultrapure water, a diluted acid, a digested blank sample or a matrix matched blank is often not stated. LODs given on a mass basis (e.g. g $μg^{-1}$) for solids may either be based on 3σ of a sample with a very low analyte concentration compared with the LOD, or on 3σ of a blank, whilst taking into account the maximum amount of solid sample that can be conveniently weighed and transferred to the digestion vessel.

Table 3.1 Selected sample preparation procedures and analytical techniques for determination of Sr in biological matrices.

Sample	Sample preparation	Analytical technique	Limit of detection/ (limit of quantification)	Recovery (%)	Ref.
Bone	The bones were rinsed with a scalpel, H_2O_2 and water, placed in an ultrasonic bath with ether and dried at 105°C for 1 h. The dried bones were immersed in liquid nitrogen, put in a plastic bag, fractured with a hammer and freeze dried. The bone pieces were homogenised in an analytical mill, about 500 mg was dissolved with HNO_3 overnight and diluted with 0.016 M HNO_3. La was added as modifier.	ETAAS	0.13 µg L^{-1}	96.5-102.9	[145]
Bone	Up to 0.5 g bone was digested with 1 mL conc. HNO_3/HCl (3:1) over gentle heat. Rh was used as internal standard.	ICP-MS	1.3 µg L^{-1} 6 µg g^{-1} dry bone	108 ± 5*	[165]
Bone	The bones were dry ashed at 550°C. 400 mg bone ash was dissolved with 2 mL conc. HNO_3 and evaporated to dryness. The residual was dissolved with 5 mL 1 M HCl and diluted to 0.1 M HCl.	ICP-AES	0.3 µg L^{-1}	98-101	[159]
Bone and bone ash	Bone pieces were rinsed for adhering soft tissue with warm H_2O_2 for 4 h, placed in an ultrasonic bath for 5-10 min and washed with ethanol and water. The bones were dried to constant weight at 85°C and a minimum of 100 mg was digested with 5 mL HNO_3/HCl (1:1) at 90°C for 1 h and then diluted. Omitting the cleaning steps, bone with adhering soft tissue was dry ashed at 450°C for 4 h and digested as above. ^{115}In was used as internal standard.	ICP-MS	0.1 µg g^{-1} dry bone	-	[164]
Bone and dental tissue	Prior to digestion, the samples were ground to a fine powder and approx. 0.2 g was digested in a three-step procedure: 1) Microwave assisted acid digestion with HNO_3/HCl (4:1) for 15 min, followed by 2) further digestion and evaporation to dryness on a hot plate, and finally 3) redissolution of the digests in 10 ml 0.14 M HNO_3. The samples were diluted 1000 times with 0.14 M HNO_3 before analysis. ^{103}Rh was used as internal standard.	DRC-ICP-MS	0.2 µg L^{-1} (tissue digests)	99.6 ± 2.8* (bone) 99.0 ± 3.9* (bone ash)	[166, 205]
Bone and bone ash	Adhering tissue was removed using a Ti knife. The bone was cut into small pieces and freeze dried. For bone ash, the whole bones were calcinated at 800°C for 10 h and ground to a powder.	NNA	-	102.3 ± 5.2*	[175]

Table 3.1 (cont.)

Sample	Sample preparation	Analytical technique	Limit of detection/ (limit of quantification)	Recovery (%)	Ref.
In vivo bone	Non-invasive. Correct positioning of the subject is critical and may be very difficult depending on the skeletal site of interest.	XRF	0.25 mg Sr g^{-1} Ca	-	[183]
In vivo bone	Non-invasive. Correct positioning and immobility of the subject during measurement is critical.	DPA	-	-	[185]
Archaeological bone (isotope ratio)	The bone was rinsed with ether for 4 h, etched ultrasonically with 99% formic acid for 3 h, washed with water and dried at 50°C. The dried bone was ground and 50-100 mg was dissolved in 2 mL 65% HNO_3 at 160°C for 6 h.	ICP-MS	-	100.0±0.02 †	[171]
Archaeological bone	The bone was rinsed with ultrasonically in water, dried at 105°C and ashed at 725°C for 7 h. The bone ash was digested with 3 mL HNO_3 in a microwave oven at maximum temperature and pressure of 220°C and 35-40 bar.	ICP-MS	-	108 ± 9*	[172]
Tooth	0.2 g powdered sample was covered with 10 mL conc. HNO_3 and the slurry was introduced into a microwave oven (1100 W) through a closed flow system at a flow rate of 1.25 mL min^{-1}.	FAAS	61 µg L^{-1}	-	[206]
Tooth enamel	The enamel was separated from the tooth and dried at 105°C for 48 h. 0.1 g enamel was digested with 1 mL 62% $HClO_4$, 1 mL 0.02 g mL^{-1} NaCl was added, and the sample was diluted to a volume of 10 mL with water.	FAAS	(1% abs. for 0.36 and 0.25 mg L^{-1} with air-C_2H_2 and N_2O-C_2H_2, respectively)	98.3-98.8	[143]
Bone marrow	Approx. 4 g bone marrow was diluted with 1 mL 0.1 M Tris-HCl (pH 7.4) and centrifuged to exclude bone pieces. 0.3 g supernatant was digested with 0.5 mL conc. HNO_3 at approx. 100°C on a hot plate almost to dryness and then dissolved with 5 mL 0.1 M HNO_3. ^{103}Rh was used as internal standard.	ICP-MS	-	-	[167]
Brain tissue	The samples were freeze dried and lyophilised for 5-6 days, or dried at 105°C. Two procedures were applied: 1) 25 mg was digested with conc. HNO_3/H_2O_2 (2+0.5 mL) at 250-500 W. 2) 50 mg was digested in Parr-bombs with 2.5 mL conc. HNO_3 at 150°C for 3 h. $La(NO_3)_3$ was used as modifier.	ETAAS	0.057 µg L^{-1}	94-105	[154]
Urine	The samples were diluted 1:20 with dil. HNO_3 and 0.1% (v/v) Triton X-100.	ETAAS	0.13 µg L^{-1}	98.8-101.5	[145]

Table 3.1 (cont.)

Sample	Sample preparation	Analytical technique	Limit of detection/ (limit of quantification)	Recovery (%)	Ref.
Whole blood	The samples were homogenised on a vortex mixer and diluted 1:10 with 0.1% (v/v) Triton X-100.	ETAAS	0.13 µg L^{-1} (blank)	94.3-102.5	[145]
Blood	To 10 mL sample was added 100 µL 3% (w/v) Na_2-EDTA and 10 mL conc. HNO_3. The mixture was heated to 80-90°C for 8 h, 1 mL $HClO_4$ was added and the sample was digested in a microwave oven. The digested sample was diluted to a final acid concentration of 0.14 M HNO_3.	ICP-AES	0.3 µg L^{-1} (blank) (1 µg L^{-1})	-	[140]
Blood and tissue	To 10 mL blood or 1 g tissue was added 10 ml of 3:1:1 (v/v/v) conc. HNO_3/$HClO_4$/H_2SO_4 and the mixture was heated on a hotplate to 110°C for 2 h and 250°C for 2-3 h, respectively.	ICP-AES	0.01 µg g^{-1} blood 0.2 µg L^{-1} tissue	113	[207]
Whole blood (wb), plasma (p), urine (u), hair (h)	2.7-3.6 mL of 0.65% HNO_3 (w/v) and 0.1% (v/v) Triton X-100 (for blood) was added to 0.3-0.4 mL liquid sample. Hair samples were rinsed with acetone and water. 25 mg was dissolved with 0.25 mL conc. HNO_3 at 70°C for 1 h and diluted with 0.65% (w/v) HNO_3, 0.01% (v/v) Triton X-100 and 0.5% (v/v) butanol. ^{103}Rh was used as internal standard for all samples.	DRC- ICP-MS	b:0.007 µg L^{-1} (0.02 µg L^{-1}) p: 0.016 µg L^{-1} (0.05 µg L^{-1}) u: 0.004 µg L^{-1} (0.01 µg L^{-1}) h: 0.2 ng g^{-1} (0.7 ng g^{-1})	-	[139]
Serum	About 1 mL of serum was diluted (1+4) with water. ^{89}Y was used as IS.	ICP-MS	0.006 ng g^{-1} serum	99	[169, 170]
Serum	0.5 mL serum was mixed with 1 mL HNO_3, 0.5 mL H_2O_2 and 0.2 mL HF, and digested under high pressure in a microwave oven. The digested samples were diluted with water.	ICP-MS	0.014 µg L^{-1} serum	98-105	[168]
	To 0.5 mL serum was added 0.5 ml 25% TMA/0.2% EDTA, and the mixture was diluted with water. ^{103}Rh was used as internal standard.		0.012 µg L^{-1} serum		
Serum (s), urine (u), soft tissue (t)	s: diluted a factor of 4 with 0.5 mL L^{-1} Triton X-100/1 mL L^{-1} HNO_3. u: diluted a factor of 20 with 2 mL L^{-1} HNO_3. t: 100-300 mg was digested with 1-3 mL 100 g L^{-1} TMAH at 60°C for 12 h. The digested samples were diluted with 20 g L^{-1} TMAH/2 g L^{-1} EDTA.	ETAAS	s: 1.2 µg L^{-1} (9.0 µg L^{-1}) u: 0.3 µg L^{-1} (1.3 µg L^{-1}) t: 2.2 ng g^{-1} (8.3 ng g^{-1})	101 ± 5.3 102 ± 3.5 99 ± 4.2	[151]

TMA: trimethyl amine, TMAH: tetramethylammonium hydroxide, EDTA: ethylenediaminetetraacetate, Tris-HCl: tris(hydroxymethyl)aminomethane buffer, *calculated by propagation of reported uncertainties, †compared to a certified isotope ratio

CHAPTER FOUR

Introduction to experimental techniques: ICP-MS, DEXA and biomechanical testing

4.1 Introduction

This chapter gives an introduction to three of the analytical techniques that have been used during this study: inductively coupled mass spectrometry (ICP-MS), dual energy X-ray absorptiometry (DEXA), and mechanical testing. The ICP-MS apparatus was available at our laboratory, whereas the DEXA scanner and the mechanical testing machine was located at the Department of Endocrinology at Hvidovre Hospital and kindly put at our disposal by Dr. Jens-Erik B. Jensen.

4.2 Inductively coupled mass spectrometry

Since the first paper on ICP-MS was published by Houk *et al.* in 1980 [208], the technique has been applied for elemental and isotopic analysis at the trace and ultra-trace level in a variety of fields such as chemistry, geology, pharmacology as well as the clinical, forensic, nuclear, environmental and food sciences. The number of papers published each year on ICP-MS continues to grow, and the amount of available literature still merits regular publications of review papers, summarising recent fundamental studies, method developments and applications [192, 209-213].

In this project, ICP-MS was used for determination of Sr and other key bone elements in bone, teeth, bone marrow and serum. This section aims at giving a reader unfamiliar with the technique some background knowledge of the instrumental components and parameters. Emphasis is put on matters with a direct relevance for the following chapters. Further information can be obtained from the literature

updates mentioned above or some of the several comprehensive reviews that have been published on the technique, including introductory tutorials [204, 214-216] and extensive treatises on the fundamentals, applications and theory [217-219].

The basic instrumental design of the applied ELAN 6000 ICP-MS is shown in Figure 4.1. Briefly explained, an aqueous sample is pumped into a nebuliser, where it is converted to an aerosol and transported to the argon plasma. The plasma is generated by ionised argon coupled to a radio-frequency (RF) electromagnetic field, and it is used to atomise and ionise the sample components. Via the interface and the ion optics, the ions are then directed into the quadrupole mass filter, which separates the ions of interest from the ion beam and allow them to reach the detector.

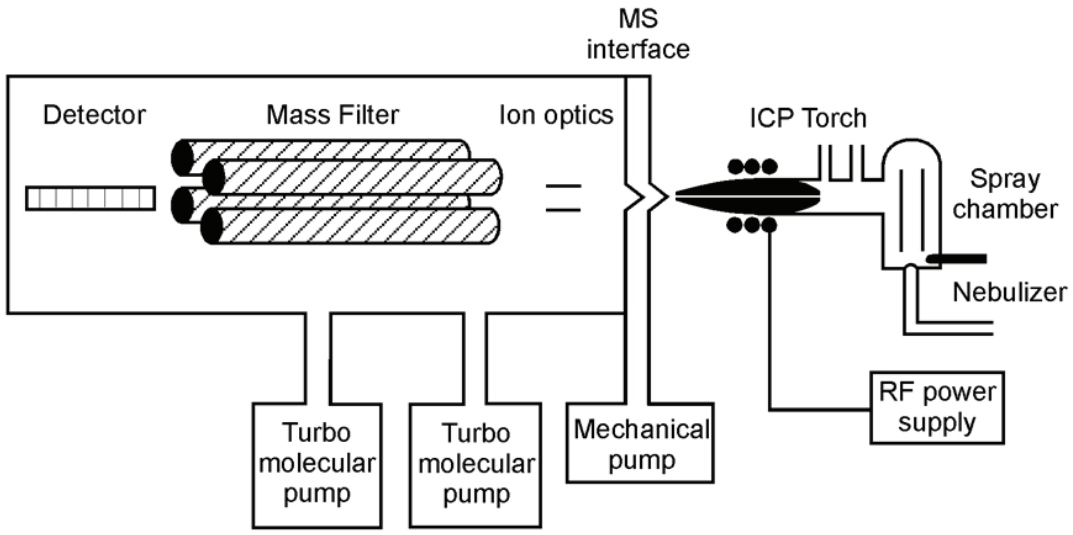

Figure 4.1 Basic instrumental components of an ELAN 6000 ICP-MS. See text for details.

4.2.1 Sample introduction

The main function of the sample introduction system is to convert the liquid sample into an aerosol. In the current project, two types of pneumatic nebulisers were applied: cross-flow and concentric microflow (Figure 4.2). Both designs use the mechanical forces of a gas flow to break up the liquid sample into a fine mist of droplets. In the cross-flow design, the argon gas is directed perpendicularly to the sample flow, while, in the concentric nebuliser, the gas is running in parallel to the sample capillary. Generally, the concentric design is more stable and produces an aerosol with smaller droplets than the cross-flow design. As the name suggests, the microflow nebuliser is able to handle very low sample flow rates. A useable aerosol can be produced at sample flows down to 20 μL min^{-1}, where a cross-flow type of

nebuliser typically requires a flow in the range of 0.4-1.0 mL min^{-1}. The main disadvantage of the microflow nebuliser is that it is more prone to clogging because of the narrower liquid capillary and shorter distance between liquid and gas injectors. The cross-flow nebuliser requires a peristaltic pump to propel the sample, whereas the concentric nebuliser is self-aspirating, relying on the fast flow of argon gas to suck up the sample (the venturi effect).

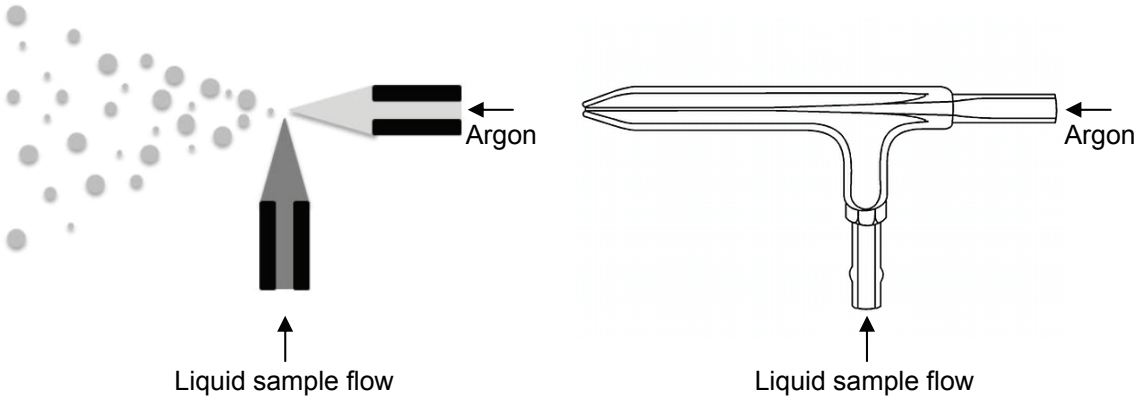

Figure 4.2 Schematics of a cross-flow nebuliser (left) and a concentric nebuliser (right).

The ICP is not very efficient at dissociating large droplets and therefore the aerosol cannot be injected directly into the plasma. Instead, the aerosol is introduced into a spray chamber, which has two purposes: 1) to smooth out pulses from the peristaltic pump, if one is used, and 2) to only allow the smaller droplets (< 10 µm) to pass through. In this work, the two most common types of spray chambers were applied: a Scott double-pass and a cyclonic spray chamber (Figure 4.3).

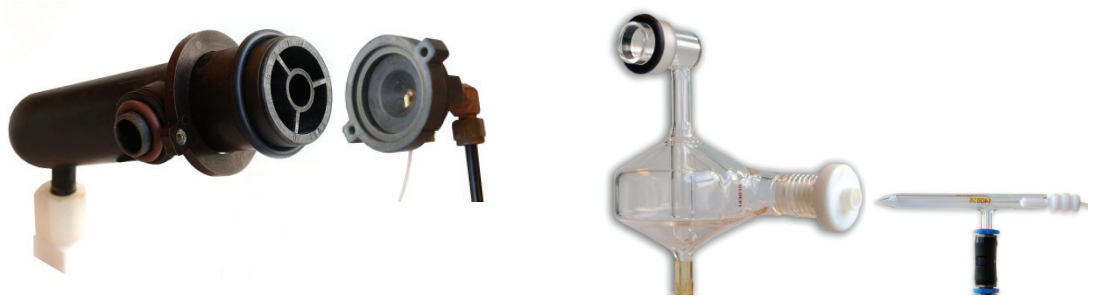

Figure 4.3 A double-pass spray chamber with a cross-flow nebuliser (left) and a cyclonic spray chamber with a concentric nebuliser (right).

Designed with two concentric tubes, the double-pass spray chamber discriminates the droplets by directing the spray into the central tube, where the larger droplets impinge on the inner wall and exit by gravity through a drain tube. The smaller droplets are forced back to the outer tube and on to the sample injector. In the

cyclonic spray chamber, the sample aerosol is introduced tangentially into the circular chamber, causing the larger droplets to collide with the wall and fall out the drain, while the smaller droplets are carried with the gas into the plasma. Cyclonic spray chambers are generally considered more efficient at separating the smaller droplets, while double-pass chambers are regarded as being more rugged for routine analysis [204, 219].

4.2.2 The plasma

The plasma torch consists of three concentric tubes, respectively carrying the plasma gas (15 L min^{-1}), auxiliary gas (0.8 L min^{-1}) and nebuliser gas (0.9-1.2 L min^{-1}) together with the sample aerosol. The torch is surrounded by a copper load coil connected to a radio frequency (RF) generator (Figure 4.4), which is used to create an intense electromagnetic field at the top end of the torch. The plasma is formed by the plasma gas, which flows tangentially into the torch through the outermost tube. The middle tube carries an auxiliary gas, which pushes the plasma away from the sample injector to prevent it from melting. The plasma is ignited by generating a high-voltage spark, which produces free electrons in the argon gas. The electrons are accelerated by the RF field at a power of 700-1600 W, causing collisions and further ionisation of the argon gas, sustaining the plasma at a temperature of 6.000-10.000 K. The sample injector introduces the sample aerosol into the plasma, where it is dried, vaporised, atomised and ionised as it passes through to the interface [204].

Beside the singly charged M^+ ions that are used for quantification of the sample components, many other ion species are formed in the plasma. Oxides of atomic ions are the most significant, but, depending on the plasma/nebuliser gas and the matrix components, also argides, nitrides, chlorides, hydrides and sulphides can be produced [220]. Additionally, elements with low second ionisation potentials, such as Ba and Sr, may form significant levels of doubly charged atomic ions, M^{2+}. Oxides form mainly due to the presence of water in the sample aerosol and oxygen in the ambient air and will therefore be produced regardless of the nature of the sample. They are a result of incomplete oxide dissociation in the plasma and recombination in the plasma-vacuum interface. Interferences caused by oxides are typically found at 16, 36 and 48 amu above the parent ion, corresponding to MO^+, MO_2^+ or MO_3^+ [221].

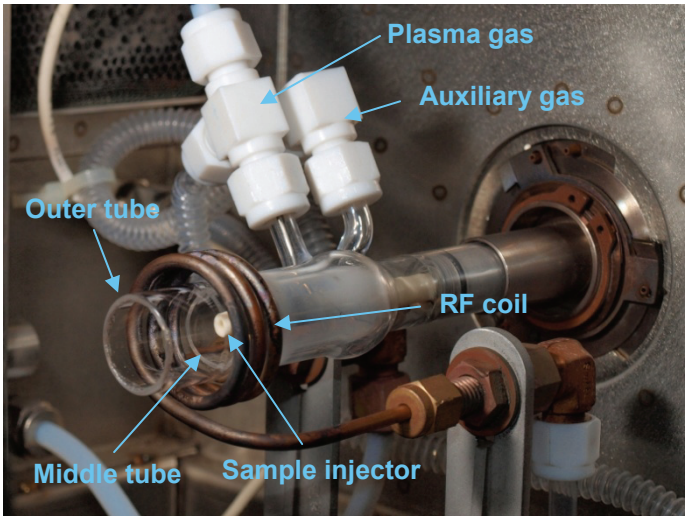

Figure 4.4 Photograph of a plasma torch, RF coil and sample injector mounted in an ICP-MS instrument. The sample aerosol is introduced into the plasma through the sample injector.

In one of the early, fundamental studies on operational ICP variables and signal optimisation, Horlick *et al*. [222] indentified RF power and nebuliser gas flow as key parameters, while Vaughan *et al.* [223] also found the sampling depth – the position of the RF coil and torch relative to the tip of the sampling cone (see section 4.2.3) – to play a significant role. The three parameters interact extensively, which means that any one sampling depth and RF power setting has a corresponding optimum nebuliser gas flow. If the RF power is changed, the gas flow must also be altered in order to achieve maximum signal.

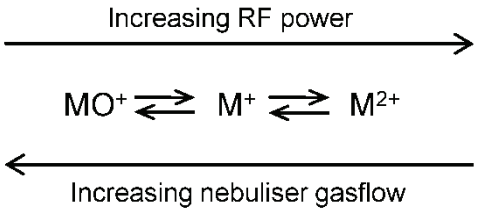

Figure 4.5 Effect on levels of oxides and doubly charged ions when changing RF power and nebuliser gas flow.

Generally, a high RF power causes a high degree of oxide dissociation, resulting in low levels of oxide species. The high plasma temperature, however, also causes an increase in formation of doubly charged ions. Conversely, if the flow of argon through the nebuliser is increased, the plasma gets relatively cooler, causing the level of oxides to increase, while the level of doubly charged ions decreases (Figure 4.5) [224]. However, opposite trends have also been observed [225], emphasising that the exact effects of the RF power and gas flow on ion intensities depend on the particular

instrument, sample matrix and analyte. In any case, optimising the ICP parameters is a matter of finding the best compromise between these three effects.

4.2.3 Interface and ion optics

The role of the interface region is to bring the ions from atmospheric pressure in the plasma to the high vacuum (< 0.01 Pa) in the mass spectrometer. The interface consists of two metallic (nickel or platinum) cones kept at 200-400 Pa. From the plasma, the ions pass into the first cone, called the sampler cone, which has an orifice of 0.8-1.2 mm i.d. After the sampler cone, the ions travel a short distance and pass through the second cone, called the skimmer cone, which is pointier than the sampler cone and has a smaller orifice of 0.4-0.8 mm i.d. When they emerge from the skimmer cone, the ions are directed towards the mass spectrometer by an electrostatically controlled cylinder lens, called the ion optics. To reduce background noise and keep the mass spectrometer clean, non-ionic species, such as photons, particulates and neutral sample components, are prevented to reach the detector by a stop disk placed behind the skimmer cone [204]. The applied lens voltage can be adjusted and optimised, primarily depending on the mass of the desired analyte, but also on the condition of the lens. During operation, neutral sample components may slowly collect on the lens, reducing its ability to deflect the ion beam [214].

4.2.4 Quadrupole mass filter

The mass filter is the heart of the ICP-MS system. It separates the ions arriving from the ion optics according to their mass/charge (m/z) ratio. A photograph of a quadrupole system from an ELAN 5000 ICP-MS is shown in Figure 4.6. The quadrupole consists of four metal rods on which can be placed both a direct current (DC) field and an alternating current of radio frequency. By appropriate selection of the RF/DC-ratio, ions with a specific m/z ratio can be steered through the middle of the rods and on to the detector, while ions with different m/z ratios will pass through the spaces between the rods and be ejected from the quadrupole.

The mass discrimination can basically be conducted in two different ways, depending on the objective of the analysis. One approach is performing a continuous scan across the mass range of interest, a method well suited for obtaining peak shape information and complete mass spectrums. Figure 4.7 presents an example of a mass spectrum of dissolved dog bone.

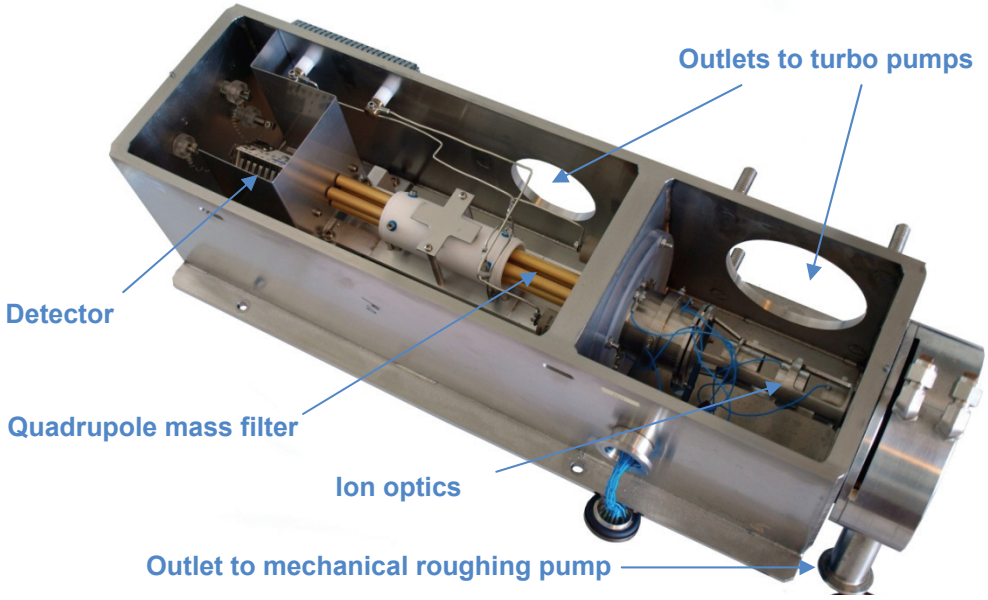

Figure 4.6 Photograph of the quadrupole system of a Perkin-Elmer ELAN 5000 ICP-MS showing the ion lenses, the rods of the quadrupole mass filter and the dynode detector.

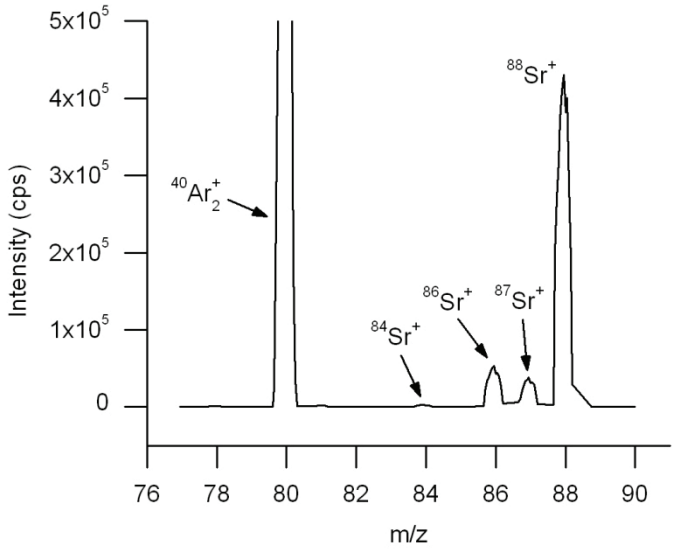

Figure 4.7 Section of a mass spectrum of dissolved dog bone, showing mass/charge (m/z) peaks of the four stable strontium isotopes.

The other approach is *peak hopping*, where the quadrupole is driven to discrete RF/DC-settings matching the m/z values of the analytes. At each mass peak, the electronics are allowed to settle and dwell for a certain period of time while the measurements are recorded (Figure 4.8). This approach has been used exclusively throughout this work, as it results in lower detection limits and faster analysis times.

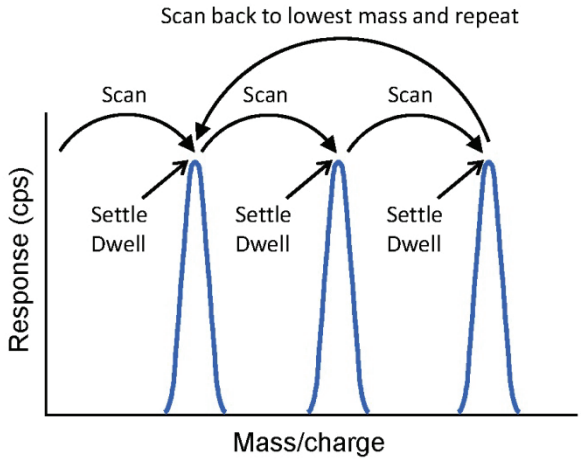

Figure 4.8 Illustration of the measurement protocol for the quadrupole in peak-hopping mode. Modified from reference [204].

While the scan and settling times depend on the instrument, the dwell time can be chosen for each mass as a compromise between precision and sensitivity on the one side and sample frequency on the other. A longer dwell time increases the total amount of ions registered by the detector, which improves the sensitivity and reliability at the expense of increased analysis time and higher sample consumption.

4.2.5 Detection

The ELAN 6000 ICP-MS is equipped with a dual stage dynode electron multiplier with 22 discrete dynodes (partly visible in Figure 4.6). The detector is placed off-axis to the quadrupole in order to minimise noise from stray radiation and neutral species. When the ions emerge from the quadrupole they are attracted to the first, negatively charged dynode, causing secondary electrons to be liberated. These electrons are accelerated to the second dynode where they generate more free electrons. This process is repeated at each dynode, until the final pulse of electrons is captured at the multiplier collector (anode) and registered by a counting circuitry [204]. The total gain of the electron multiplier can be defined as the average number of electrons arriving at the collector for each incoming ion [218].

In the samples analysed in this work, Sr was found in concentrations varying from the low μg L^{-1} range to more than 10 mg L^{-1}, and macronutrients such as Mg and Ca exist in even higher concentrations (10-100 mg L^{-1}). This difference of more than four orders of magnitude either requires several dilutions of each sample in order to bring each analyte to an appropriate concentration, or, more conveniently, a correspondingly wide dynamic range of the analytical method. With the dynode

detector, an extended dynamic range can be achieved by taking advantage of the detector's ability to provide two types of signals simultaneously [214, 218, 226]:

1) Conventional pulse signal suitable for detection of ion counts at ultra trace to trace concentrations. The gain is typically in the range of 10^6-10^8. A protection circuit cuts off pulse responses above $2 \cdot 10^6$ counts per second (cps).

2) Analogue current signal for determination of higher concentrations with responses in the range of 10^5-10^9cps. The analogue signal is measured at the midpoint dynode and the sensitivity is much lower than that of the pulse mode. The gain can be defined as the ratio between the output and the input ion current, and it is in the range of 10^4-10^6. The detector is completely cut off at signals exceeding $2 \cdot 10^9$ cps.

In the response range where the two stages overlap, the output current of the analogue detector stage can be normalised to the response of the pulse stage, providing a conversion factor that can be used to express all responses as pulse counts pr. second (Figure 4.9). In theory, this cross-calibration produces a linear response with a constant slope throughout both response regions. However, evidence for a significant nonlinearity between the two stages has been reported [227, 228].

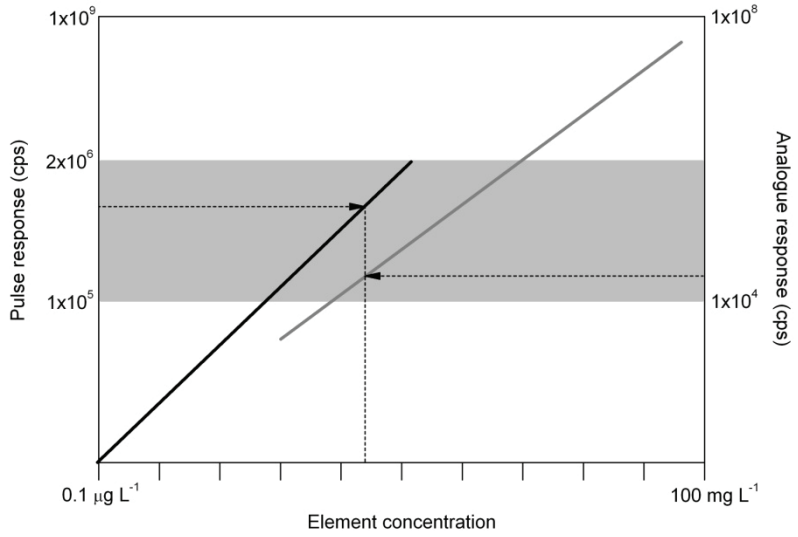

Figure 4.9 Cross calibration of the two detector stages by measuring concentrations that give both a pulse count and an analogue response. The resulting conversion factor is used to express all signals as ion counts pr. second.

When operating in dual-detector mode, ion intensities exceeding $2 \cdot 10^6$ cps are processed through the analogue circuitry at the midpoint dynode. Signals with fewer ions are amplified through all 22 dynodes and measured as a pulse signal.

4.3 Dual energy X-ray absorptiometry

DEXA scanners were introduced in 1987, and since then DEXA has become the method of choice for non-invasive evaluation of bone mineral status in clinical practise [90]. It is recommended by several guidelines for diagnosing postmenopausal osteoporosis [229-231], and, as described in Chapter 2, BMD T-scores obtained from DEXA scans of spine, femur and hip are recommended by WHO to classify normal, osteopenic and osteoporotic bone.

4.3.1 Principle of operation

As the name suggests, DEXA scanners evaluate BMD by measuring the transmission of two X-ray beams with different, known photon energies through the subject of interest. Across a broad range of photon energies, the X-ray transmission can be decomposed into the equivalent areal densities of any two reference materials. In the case of bone densitometry, the two materials are bone mineral (hydroxyapatite) and soft tissue, as the analysed bone will normally be surrounded by tissues such as skin, fat, muscles, tendons and bone marrow. The decomposition is limited to two materials because there are only two types of attenuation processes involved: Compton scattering and the photoelectric effect. The magnitude of these processes depend on photon energy and atomic mass, and because the Ca and P atoms in bone have higher masses (40 and 31) than the C, N and O atoms (masses 12, 14 and 16) in the soft tissue, DEXA can be used to distinguish between bone and soft tissue [90]. By using the mass attenuation coefficients for bone and soft tissue at the given photon energies, the attenuated intensities can be written as [232, 233]

$$I = I_0 \exp\left(-\mu_{soft} m_{soft} - \mu_{bone} m_{bone}\right) \tag{4-1}$$

$$I' = I'_0 \exp\left(-\mu'_{soft} m_{soft} - \mu'_{bone} m_{bone}\right) \tag{4-2}$$

where I and I_0 are the unattenuated and attenuated photon intensities, μ [$cm^2\ g^{-1}$] the mass attenuation coefficients and m the masses of the two types of tissue [$g\ cm^{-2}$]. $'$ denotes the same quantities at the second photon energy. The intensities and attenuation coefficients can be measured directly, leaving only m_{soft} *and* m_{bone}, which can be determined by solving the above equations. As each data point represents a

fixed area, a scan is processed by using the attenuation measurements to create a pixel-by-pixel map of BMD over the entire scanned region. The reported BMD value of the region is calculated as the mean BMD over all the pixels identified as bone. The total projected bone area is determined by first using a detection algorithm to find the bone edges and then summing the pixels within the edges [233]. The bone mineral content (BMC) in grams is found by multiplying the mean BMD by the projected bone area:

$$BMC = BMD \cdot Area \tag{4-3}$$

Examples of DEXA scan images are shown in Chapter 8.

4.3.2 Calibration and quality control

A DEXA scanner performs self-calibration at start-up. In addition, it is necessary to carry out an independent quality control in order to monitor instrumental drift. This is usually done by a daily scan of a so-called *phantom*, typically a known amount of mineral shaped as vertebrae, imbedded in a plastic material with an X-ray transmittance matching that of soft tissue. This does not only provide a daily check of the self-calibration, but, by recording a large number of phantom scans, it also allows for monitoring the long-term performance of the instrument [233, 234].

4.3.3 Precision and accuracy

The precision of a given DEXA scanner affects the ability to monitor a patient's response to treatment, while the accuracy affects the diagnosis of osteoporosis through the calculated T-score [235]. Usually, the precision of the DEXA measurement itself is approximately 1.5%. A poorer precision may be observed if the subject is placed incorrectly or is moving slightly during the scan. A precision of <2% for the spine and <4% for the hip is accepted in clinical practise. Bearing in mind that the expected age-related bone loss is about 1% per year, and the effect of anti-resorptive treatment is 1-3% per year, it is clear that, for the purpose of monitoring bone status, there is no point in repeating scans with less than 2-3 year intervals [234].

The accuracy of DEXA is challenged primarily by two issues. Firstly, the obtained scan is a 2 dimensional projection image of a 3 dimensional subject, leading to a result expressed as an areal density (g cm^{-2}) rather than a volumetric density (g cm^{-3}). In other words, BMD is a measure of the average thickness of bone tissue measured along the direction of the X-ray flux [236]. Because of the missing depth value in the calculation of the mineral density, the resulting BMD value is affected

by bone size as well as the true 3D volumetric density and orientation of the bone tissue.

The second issue is the two-component limitation. As can be seen from Equations (4-3) and (4-2) above, accurate density determinations depend on correct estimates of the attenuation coefficients of the two reference materials, μ_{soft} and μ_{bone}. Soft tissue, however, is not a well-defined homogeneous material. For the purpose of X-ray transmission, soft tissue consists of at least two types of tissue: lean muscle tissue and fat. Fat is largely composed of methylene units, $(CH_2)_n$, while lean tissue attenuates X-rays similarly to water (H_2O). The difference of the X-ray attenuation of the two types of tissue is therefore equivalent to the mass difference between C and O. Since adipose tissue is heterogeneously distributed in the body, the composition of the soft tissue overlaying a given bone may not be known exactly, and this introduces a potential error in the BMD estimate. Adding further to the soft tissue complexity, the marrow inside the bone is a mixture of red and yellow marrow, each with different attenuation coefficients. Thus, soft tissues may be constituted of three or four absorptiometrically different components, all influencing the magnitude of the X-ray attenuation. In clinical practise, this effect means that the result of e.g. a spine scan may suffer from significant error because of the large thickness of soft tissue in the abdomen [90, 236].

The composition of *extraosseous* soft tissue can be estimated by measuring the attenuation of the beams at sample sites that do not contain any significant bone tissue [237]. Tissue regions that are adjacent to bone provide a reference area of comparable thickness and composition, from which a line-by-line correction is applied to the bone region BMD [233]. A DEXA scan will therefore not only provide information about the bone mass but also an estimate of the soft tissue composition of the region of interest [238]. Still, the only reliable way of quantifying the soft-tissue error is through cadaver studies, which often suffer from large statistical error due to a small number of subjects. Such studies have shown that the patient-to-patient accuracy is 5-7% [90, 235]. However, Bolotin *et al.* [236, 239] reported errors in accuracy exceeding 20% in a study where various phantoms and cadaveric lumber vertebra were analysed. These observations caused the authors to question the reliability of DEXA as a means for patient-specific inferences concerning osteoporotic/ostepenic categorisation and predictions of fracture risks, and to call for prudence and circumspection in assessments of treatment effects of particular drugs, diets or exercise therapies.

Finally, it is important to note that scanners from different manufacturers (Norland, Lunar, Hologic) have different reference values, leading to significantly

different BMD results. BMD values obtained on Hologic scanners are 10% lower on average than values obtained from Norland and Lunar scanners. Hence, a reliable monitoring of a patient's BMD requires that the same instrument be used for all examinations. When an old instrument is replaced with a new, a thorough cross-calibration between the two instruments is required in order to make past and future results comparable [234].

4.3.4 Correction for bone Sr content

BMD measurements of patients and animals treated with Sr presents another accuracy problem. In the calculations of the bone mass, the instrument assumes that the bone mineral consists of regular hydroxyapatite. Presence of any element with a mass higher than that of Ca in the bone mineral will interfere with the mass determination, because it significantly alters the attenuation coefficient of the bone. Because of its higher mass, Sr attenuates X-rays more than does Ca, and presence of Sr in more than trace concentrations will therefore lead to an overestimation of BMD and BMC. Testing several DEXA scanners from different manufactures, Nielsen *et al.* [240] found an average of 10% overestimation of BMD for 1 mol/mol% Sr. In a recent study, Liao *et al.* [241] found that the overestimation was different for scanners from different manufacturers. Consequently, interpretation of DEXA measurements in patients treated with strontium ranelate should therefore be exercised with great care [242, 243]. The Danish Institute for Rational Pharmacotherapy recommends that the increase in BMD (in %) after initiation of strontium ranelate treatment be divided by two as a rule of thumb [95].

4.4 Mechanical testing

Biomechanical testing of bones provides information about the mechanical integrity of the bone structure [244]. The biomechanical testing of the bone samples was conducted using a material testing machine (Figure 4.10). Bending tests were used for dog femur, and compression tests were used for vertebra biopsies. The load was applied by a twin-mounted crosshead, travelling between two columns. The applied force was measured by an exchangeable load cell and the displacement was measured as the distance travelled by the crosshead.

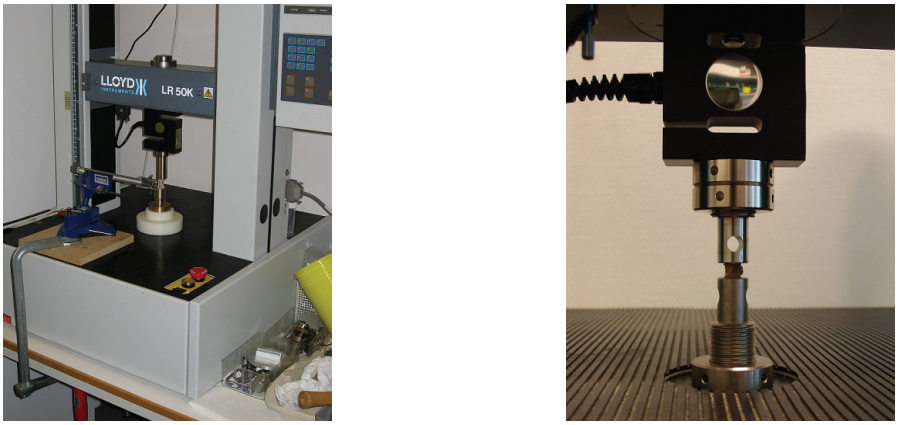

Figure 4.10 Photographs of the material testing machine used for mechanical strength measurements of bone. The picture on the right hand side shows compression testing of a dog vertebra biopsy. The load is measured by the black, square load-cell.

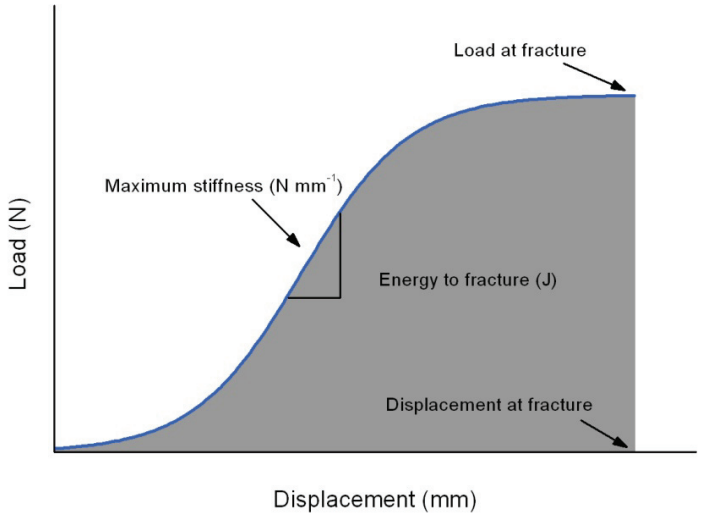

Figure 4.11 Load-displacement bending curve. The biomechanical properties of the bone were described by the load at failure (N), deformation at failure (mm), energy to failure (J) and stiffness (N mm^{-1}). Figure redrawn from [245].

Data was collected on-line at a sampling rate of 50 Hz, resulting in a load-displacement curve (Figure 4.11). From this curve the following biomechanical values could be calculated [244, 245]:

- the maximum load (load at fracture; breaking force)
- the deformation at osteoid collapse (displacement at fracture), representing reciprocal brittleness
- the energy absorption at fracture (area under the curve in N mm or J)

- the maximum stiffness (slope of the linear part of the load-displacement curve in N mm^{-1}), representing the elastic deformation.

Experimental details and a recorded load-displacement curve from a three-point bending test of a dog femur are presented in Chapter 8.

CHAPTER FIVE

Method development for determination of Sr, Mg, P and Ca in serum

5.1 Introduction

This chapter focuses on optimisation and validation of a procedure for determination of Sr and other key bone elements (Mg, P and Ca) in serum using ICP-MS. Serum samples were obtained from two animal studies, investigating strontium's influence on bone properties. The aim of the first study was to investigate the effect of strontium on healed bone fractures in normal rats after 3 and 8 weeks of healing, while the second study examined the effect of strontium and parathyroid hormone (PTH) on immobilised-induced bone loss. At the end of both studies, blood samples were obtained in order to monitor the effect of the treatment on the concentration of Sr in serum. The administration of strontium and the mechanical and morphological investigations were carried out by Dr. Annemarie Brüel and co-workers at Aarhus University [8].

5.2 Experimental

5.2.1 Animals and treatment

The experiments were performed in compliance with the guiding principles in the "Care and Use of Laboratory Animals", and they were approved by the Danish Animal Experiments Inspectorate. The measurements were blinded so that no information about dose and group distributions was given to our laboratory until the results of the analysis were reported back to the study coordinator.

5.2.1.1 Strontium's effect on fracture healing

The experiment is described in detail in reference [8]. Briefly, 84 female Wistar rats (Taconic, Lille Skensved, Denmark), 12 weeks old, were divided into four groups in such a manner that group means and standard deviations of body weight were matched as closely as possible. The animals were anaesthetised, and a closed fracture was produced at the right tibia by three-point bending. Groups 1 and 2 were allowed three weeks of healing, while groups 3 and 4 were allowed eight weeks of healing. Strontium ranelate (SrR) was administered to groups 2 and 4 in doses of 900 mg/kg/day (288 mg/kg/day Sr^{2+}) by mixing SrR with the rat feed. At the end of the study blood samples were obtained, serum was isolated and stored at -80°C and later at -18°C for subsequent analysis.

5.2.1.2 Effect of strontium and PTH on bone loss

72 female Wistar rats, 12 weeks old, were divided into six groups (no treatment, vehicle only, Botox, Botox + PTH, Botox + Sr + PTH, Botox + Sr) and treated for four weeks. As above, the Sr dose was 900 mg/kg/day and blood samples were extracted at the end of the study, except for the animals in the untreated group, which were killed at the start of the study.

5.2.2 Equipment and reagents for ICP-MS analysis

All glassware was cleaned overnight in 5% alkaline detergent (Extran MA 01, Merck), rinsed with ultra-pure water (18.2 MΩ·cm, Millipore), soaked in 10% (v/v) nitric acid (puriss p.a., Sigma-Aldrich) for 24 hours and again rinsed thoroughly with ultra-pure water. The measurements were performed using a Perkin-Elmer ELAN 6000 ICP-MS equipped with an ESI Apex Q (Elemental Scientific) sample inlet system. Instrument handling and data collection were performed using the software supplied with the instrument (ELAN v. 3.3 Patch 6), while the data processing for calibration and analysis was carried out by exporting the raw data to external software (Microsoft Excel®, Origin® and Minitab®). The applied settings of the ICP-MS and the Apex system are given in Table 5.1. At the beginning of each working day, before conducting measurements, the ICP-MS and the Apex were allowed to stabilise for 30 min, and the analytical performance was checked using a standard solution containing 10 μg L^{-1} Be, Mg, Ca, Rh, In, Ba, Ce and Pb.

Table 5.1 Settings on the ELAN 6000 ICP-MS and apex sample inlet system after full optimisation.

RF power	1000 W
Nebuliser argon flow	1.13 L min^{-1}
Secondary argon flow	0-50 mL min^{-1}
Sample flow	260 µL min^{-1}
Working pressure	$1.8 \cdot 10^{-3}$ Pa
Background pressure	$2.4 \cdot 10^{-4}$ Pa
Torch box temperature	40-43°C
Lens voltage	10.2 V
Detector mode	Dual
Pulse detector voltage	1500 V
Analogue detector voltage	-2587.5 V
Sweeps pr. reading	15
Scan mode	Peak hopping
Readings pr. replicate	1
No. of replicates	5
Dwell time pr. mass	100 ms
Measured isotopes	^{24}Mg, ^{25}Mg, ^{26}Mg ^{31}P ^{42}Ca, ^{43}Ca ^{84}Sr, ^{86}Sr, ^{87}Sr, ^{88}Sr ^{103}Rh (internal standard)

5.2.2.1 Apex sample inlet system

Due to the low natural concentration of strontium in serum, the analyses required a lower limit of detection than could be obtained using a standard cross-flow nebuliser. Furthermore, only a limited amount of serum (down to 150 µL for some animals) was available, resulting in a final sample volume after dilution of less than 2 mL, which would be insufficient for a reliable analysis using a cross-flow nebuliser. The combined problem of a low analyte concentration and a small sample volume was accommodated by applying the more advanced ESI Apex Q sample inlet system. By means of a concentric perfluoroalkoxy nebuliser (ES-2040 PFA-ST), the sample is self-aspirated, converted into an aerosol and transported to a quartz cyclonic spray-chamber heated to 140°C. For sample flow rates of 20-700 µL min^{-1}, the flow is controlled by the inner diameter of the sample tube; higher flow rates can be obtained with the aid of a peristaltic pump. From the spray-chamber, the aerosol is led through a first condenser loop cooled by air at room temperature to a second Peltier-cooled condenser kept at 2°C (Figure 5.1). At the second condenser, N_2 can be added to the sample aerosol, and additional Ar can be added at the end of the condenser before the aerosol is led to the plasma.

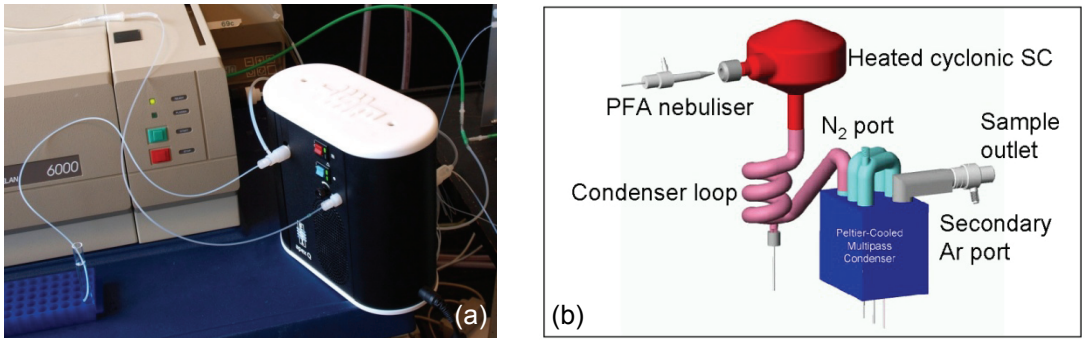

Figure 5.1 Photograph of the apex sample inlet system connected to the ELAN 6000 ICP-MS (a) and a schematic of the spray-chamber (SC) and condensers (b).

5.2.2.2 Standards

Standards were prepared in 0.1 M NHO_3 (Merck, Suprapur) by dilution of a multi-element stock standard solution (PlasmaCAL, SCP Science). A total of 17 standards were used, with concentrations ranging from 0.5 µg L^{-1} to 10 mg L^{-1}. An internal standard of 5 µg L^{-1} Rh (Fluka) was added to all standards and samples.

5.2.2.3 Sample pre-treatment

Nitrile gloves were worn at all times when handling undigested samples containing biological tissue. By the end of each day, work bench and tools were cleaned thoroughly with ethanol and water. After thawing at room temperature, 100-200 µL serum from each animal was transferred to a quartz tube, IS was added and the samples were diluted 1+11.5 with 0.1 M HNO_3 (Suprapur, Merck).

5.2.2.4 Quality control

The accuracy of the analytical procedure was assessed by repeatedly analysing a serum reference material (Seronorm Trace Elements Serum, Level 2, SERO AS). The lyophilised serum was reconstituted with 3.00 mL ultra-pure water according to the manufacturer's instructions. 30 min after the reconstitution, sample aliquots of 200 µL were transferred to a quartz tube and prepared as described above.

5.3 Results and discussion

5.3.1 Instrument optimisation

Before measuring the serum samples, a number of instrumental parameters were optimised with the aid of built-in procedures in the instrument software [214]. The optimisation included: RF power, nebuliser gas flow, lens voltage, the quadrupole mass filter and the detector voltage. Previous studies have used different criteria for

ICP-MS optimisation: best relative precision [246], highest sensitivity [224, 247, 248] and minimum matrix-induced interference [249-251]. The plasma conditions in particular can be adjusted with one of two objectives in mind: maximum sensitivity or good robustness. The term "robust conditions" in ICP context was introduced by Mermet and co-workers [252-254] for ICP-atomic emission spectroscopy and refers to the capability of the plasma to handle changes in matrix composition (acid concentration, interferents, etc.) without producing a change in the analytical signal. Earlier, Fernandez *et al.* [255] had demonstrated that low nebuliser gas flow and high RF power in ICP-MS produce a plasma that can accept changes to matrix acid concentration without changing plasma characteristics such as temperature and spatial conditions. In general, the two objectives lead to very different settings. Robust conditions are characterised by a reduced nebuliser gas flow and a low sample flow rate [256], conditions which are quite opposite to those required for maximum sensitivity. Hence, the purpose of the optimisation must be defined clearly from the onset. The plasma conditions used in this study were chosen mainly for optimum analyte sensitivity.

Strictly speaking, the procedure described below cannot be called a true optimisation, since this would involve the use of a statistically founded experimental setup such as Simplex optimisation [257, 258] or factorial designs [259]. However, these approaches require a single response function, i.e. they focus on optimisation of a single parameter, while, in the present study, several parameters had to be taken into account. Hence, the outcome of a single-response optimisation would likely have to be modified, in order to accommodate the remaining parameters. Considering the nature of the samples and the purpose of the analysis, the sensitivity and precision of the Sr response were given highest priority in the optimisation, but the other analyte responses, background noise and sample consumption were also included in the evaluation. It was therefore considered most practical to find the optimum setting for one parameter at a time and then iterate through the parameters until a set of satisfactory compromise values was reached (Table 5.1). Because of day-to-day variability, minor daily or weekly adjustments of the settings were necessary, in order to keep the instrument running consistently at peak performance.

5.3.1.1 Plasma parameters

As described in section 4.2.2, the sampling depth, nebuliser gas flow and RF power interact profoundly, making this stage of the method development susceptible to the inherent problems of the one-variable-at-a-time approach [260]. However, with the instrument used in this work, the tolerance of the sampling depth was quite low, requiring the torch to be positioned exactly right before the plasma could be

ignited. Once this position was established, it was left unchanged throughout the analysis, in effect fixing one of the optimisation factors. The remaining adjustments of nebuliser gas flow and RF power were a matter of reaching the best compromise between a high sensitivity and low degree of formation of oxides and doubly charged ions. Both parameters had a considerable impact on the ion intensity. Figure 5.2 shows the effect of RF power on the intensity of the isotopes determined in serum. Increasing the RF power from 700 to 1000 W gave a substantial increase in the response from Mg, P, Sr and Rh. At power settings above 1000 W, only slight signal increases were observed, and above 1150 W Sr and Rh intensities started decreasing. Only the response from Ca showed a steady increase up to 1500 W. Using conventional nebulisers, determination of Sr in the literature has been conducted with RF power settings ranging from 1000 to 1400 W. In comparison, the major part of the increase in ion intensity seen in Figure 5.2 occurs already in the range of 700-950 W. This may be a result of the dry aerosol produced by the desolvation process in the Apex inlet system (see section 5.3.5). With less solvent in the spray injected into the plasma, less energy is needed for evaporation and ionisation of the sample. Similar observations were reported by Pozebon *et al.* [248], who, also using an Apex-Q inlet system, found no significant increase in ion intensities of 10 different elements at RF power above 850 W. On the other hand, D'Ilio *et al.* [261] applied an RF power of 1500 W for determinations of 17 trace elements, using an Apex-IR inlet system and a dynamic reaction cell.

Increasing the RF power causes the levels of doubly charged ions to increase, because of the elevated temperature in the plasma. Sr has a much lower second ionisation potential (11.03 eV) than Rh (16.76 eV), and it would therefore be expected that the intensity of Sr would start decreasing at lower power settings than the intensity of Rh, but the two elements responded very similarly to the change in RF power. The formation of M^{2+} ions is commonly monitored using the ratio of Ba^{2+}/Ba^{+}, because of the very low second ionisation energy of the element (10.00 eV). Based on previous studies [256], a maximum level of 3% Ba^{2+}/Ba^{+} was accepted in this work. At the optimum nebuliser gas flow, an RF power of 1000 W resulted in a Ba^{2+}/Ba^{+} ratio of 2.5% (Table 5.5, p 77). Since higher power settings had no obvious benefits, the serum measurements were conducted at an RF power of 1000 W. It is interesting to note that, even though the aim here was maximum sensitivity, this power setting is identical to one recommended by Tromp *et al.* [256] for obtaining a robust plasma. The authors reported that while a higher RF power in some cases marginally reduced the matrix interferences, it was not enough to recommend operating at an RF power above 1000 W.

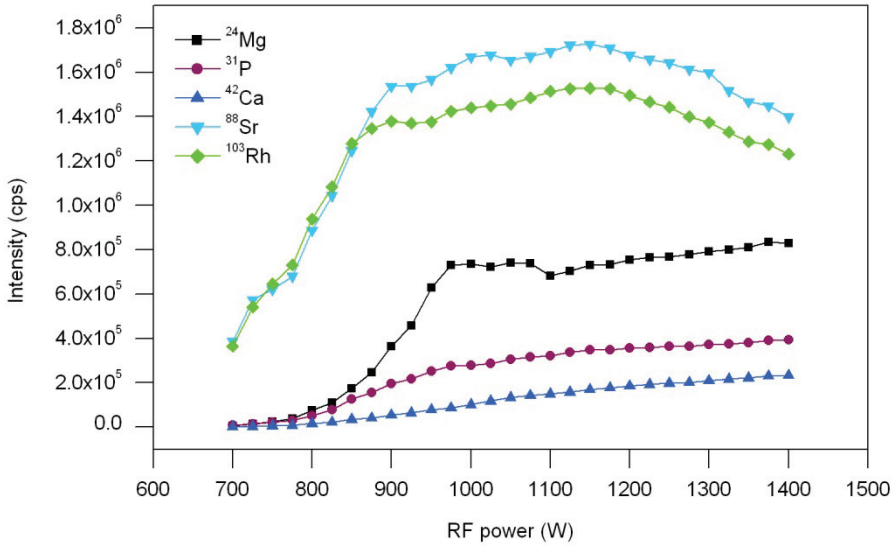

Figure 5.2 Influence of RF power on the response from the elements determined in serum (^{24}Mg, ^{88}Sr, ^{103}Rh: 10 µg L^{-1}; ^{31}P, ^{42}Ca: 100 µg L^{-1}). Nebuliser gas flow rate: 1.13 L min^{-1}.

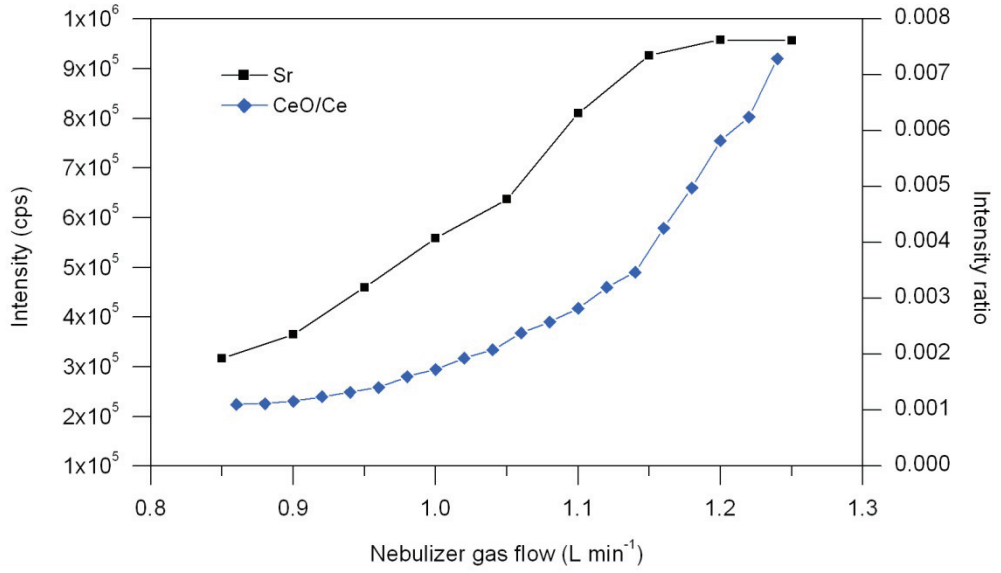

Figure 5.3 Effect of nebuliser gas flow on the signal intensity (10 µg L^{-1} ^{88}Sr) and formation of oxides (CeO/Ce). The best compromise was found at 1.13 L min^{-1}. RF power was 1000 W.

As a result of using the Apex nebuliser with free aspiration, the sample uptake rate increases with the nebuliser gas flow. It is therefore expected that the ion intensity increases correspondingly. Figure 5.3 shows that the signal is indeed enhanced by a factor of 3 when the gas flow is increased from 0.7 to 1.15 L min^{-1}. At gas flows above 1.15 L min^{-1} a plateau is reached. This observation is somewhat in contrast to previous reports [262, 263], where the Apex-Q system was used for determination of ^{226}Ra and ^{236}U/^{238}U with nebuliser flow rates no higher than 0.99 L

min^{-1}. Pozebon *et al.* [248] reported that the maximum response across a broad mass range was seen already at a nebuliser gas flow of 0.9 L min^{-1}. Conversely, Epov *et al.* [264] determined Pu using a gas flow of 1.15 min L^{-1}.

Clearly, the varying operational conditions found in the literature are partly due to the differences in mass and ionisation potential of the determined elements, but, nevertheless, the discrepancy is quite substantial. The most likely explanation seems to be the complex interactions between the plasma parameters. The sampling depth and the nebuliser gas flow both have an impact on the position of the plasma's ionisation zone, which deliver the analyte ions to the sampler cone. Instruments of different makes and models may have different sampling depths and plasma/auxiliary gas flow rates, which would result in different optimum nebuliser flow rates and power settings. However, the instrument used by Pozebon *et al.* was a Perkin-Elmer ELAN 6100, which is in many respects similar to the ELAN 6000 used in this work. The control of the sample flow rate is another factor adding to the complexity of the optimisation. When the nebuliser is used in self-aspiration mode, the sample flow is mainly controlled by the inner diameter of the sample tubing, but also by the nebuliser gas flow. Changing the nebuliser gas flow therefore not only affects the ion intensity via the plasma conditions but also through the amount of injected sample.

The oxide formation was investigated by analysing a sample containing 10 µg L^{-1} Ce, an element often used for this purpose because of its characteristic tendency to form CeO^+ [221]. The CeO^+/Ce^+ ratio was monitored as a function of the nebuliser gas flow as shown in Figure 5.3. As a result of the solvent removal performed by the Apex, the oxide formation was kept at a very low level (<1%). Still, the figure reveals a steep increase in formation of CeO^+ at gas flows above 1.13 L min^{-1}, and therefore this value was chosen as the best compromise setting. The effect of the secondary argon flow on the ion intensities was less systematic than the nebuliser gas flow. The setting giving the highest Sr signals varied between 0 and 50 mL min^{-1} from day to day.

5.3.1.2 Lens voltage

The voltage of the ion lens determines the transmission of ions from the interface to the quadrupole. The optimum lens voltage depends on the mass of the isotope of interest and on the condition of the lens. The ion lenses on the ELAN 6000 can be operated in two different modes:

1) Static ion lens voltage optimised for a particular isotope. When measuring several elements across a mass range, a suitable compromise setting based on a medium mass is used.

2) Variable lens voltage, in which case the lens voltage is changed automatically in concert with the quadrupole mass filter for each measured isotope during the analysis. This mode provides an optimum lens voltage for the entire mass range.

Appling a variable lens voltage requires an optimisation procedure, during which the lens voltage is changed while isotopes covering the mass range of interest are measured. Be, Co and In are often recommended because they are monoisotopic, they typically have well-defined lens voltage maxima and they span sufficiently well the entire mass range (masses of 9, 59 and 115 amu, respectively) [214]. The optimisation showed that the optimum lens voltage increased with increasing analyte mass, going from 9.1 V for Be to 11.8 V for In. At a first glance, this feature seemed to be a very compelling option for a sensitive determination of Mg at mass 23 through to Sr at mass 88. Compared to a static lens voltage optimised for determination of Sr, sensitivities for Mg, P and Ca improved by 19%, 8% and 13%, respectively. Unfortunately, this was accompanied by a poorer precision (up to 50% higher RSD) for all measured isotopes. The reason for this loss of signal stability is unclear, but it may indicate that either the settling time of the lens was longer than that of the quadrupole, or that lens and quadrupole were not completely coordinated when scanning through the mass range.

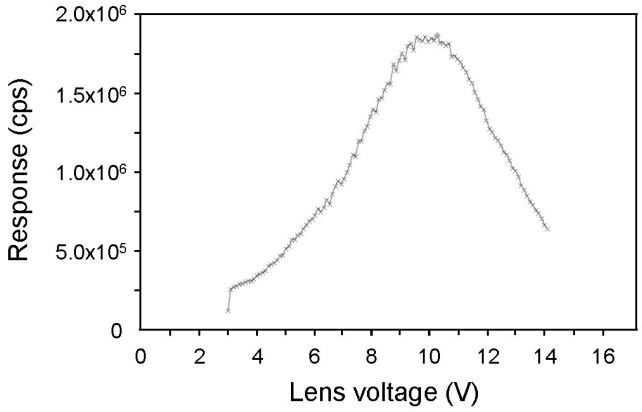

Figure 5.4 Effect of lens voltage on the signal intensity (10 µg L^{-1} ^{88}Sr). The optimum setting was found to be 10.2 V.

Given that maximum sensitivity for Ca, Mg and P would not be required due to their high natural concentrations, the minor increase in sensitivity could not justify the loss

of precision. It was therefore decided to optimise the lens voltage for determination of Sr (Figure 5.4), which had the highest sensitivity at 10.2 V.

5.3.1.3 Quadrupole mass filter tuning

When the mass filter is set in the peak-hop mode, only a single mass/charge ratio is measured for each isotope (cf. Figure 4.8, p 48). Consequently, for the best sensitivity to be achieved, the mass filter electronics must be properly calibrated or *tuned*, so that the quadrupole settles exactly on the maximum of the analytes' mass peaks. The instrument was tuned across the mass range by using spectral peaks of ^{3}He (present as an impurity in the Ar gas), ^{9}Be, ^{24}Mg, ^{103}Rh and ^{208}Pb. The tuning was repeated until all mass peaks were positioned within 0.05 amu of their true value. Spectral peaks for Mg, Rh and Pb are shown in Figure 5.5.

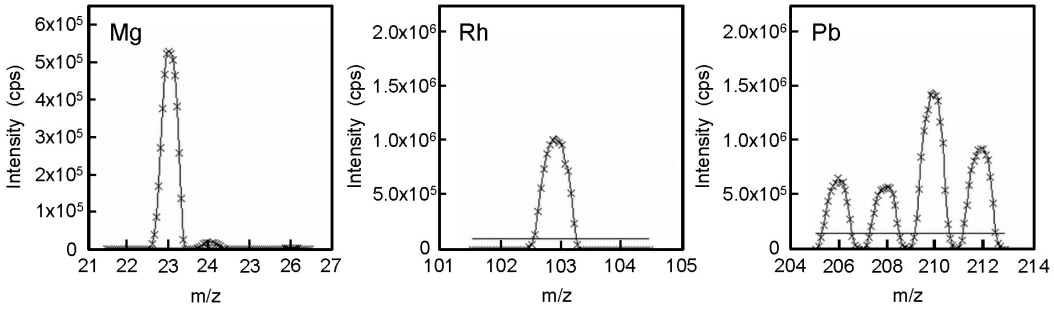

Figure 5.5 Spectral peaks of Mg, Rh and Pb obtained after tuning of the quadrupole mass filter. The horizontal lines mark the intensity at 10% of the peak maximum, which is where the resolution (peak width) is measured.

5.3.1.4 Detector voltage and dual-detector calibration

The optimum detector voltage depends primarily on the age of the detector. As the detector ages, its saturation point shifts towards higher values. Operating the detector at low voltages decrease the sensitivity, while voltages at or above the saturation point increase the noise level and reduce the lifetime of the detector [214]. The pulse detector stage was considered to be close to the saturation point when a further voltage increase of 50 V yielded less than 5% increase in the response. This approach arrived at 1500 V as an appropriate pulse voltage (Figure 5.6). In practise, the pulse stage was optimised both before and after the analogue stage adjustment, as the settings of the two detector stages may influence each other.

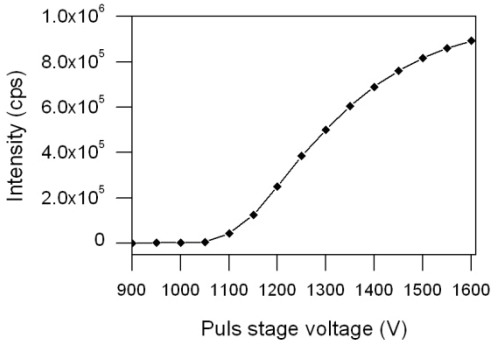

Figure 5.6 Response curve from the final pulse detector stage optimisation (10 µg L^{-1}Rh). The detector pulse voltage was subsequently set to 1500 V.

The voltage of the analogue detector stage was adjusted by defining a maximum signal that could be measured by the detector. Converting from the analogue signal current to ion counts, the threshold was set to $1 \cdot 10^9$ cps and the detector gain was adjusted accordingly by measuring a test solution of 200 µg L^{-1} Mg. The resulting gain and voltage were $1.2 \cdot 10^4$ and -2587.5 V, respectively.

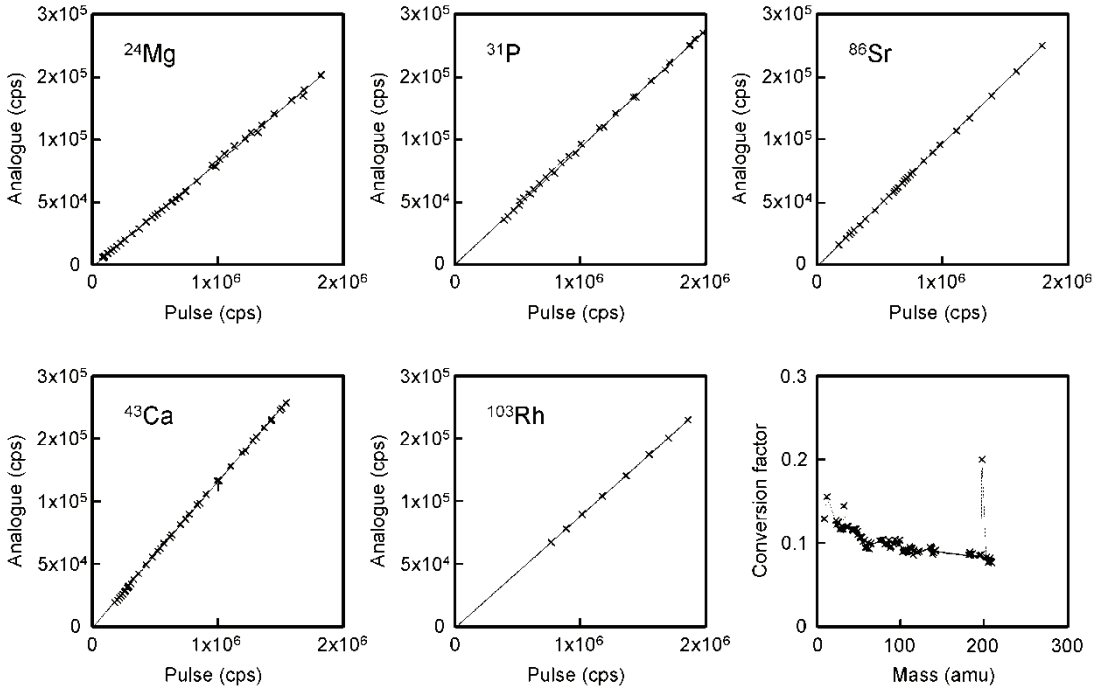

Figure 5.7 Examples of cross calibrations between the detector's analogue and pulse modes, providing an expanded dynamic range for each isotope. The lower right-hand graph shows how the conversion factors (the slopes of the individual calibrations) depend on the isotope masses.

After the final pulse stage adjustment, a cross calibration was performed between the two detector stages (Figure 5.7). As pointed out by Mestek and Koplik [226], it is important that such a calibration be carried out for each analyte, rather than merely

using a few isotopes to represent the entire mass range. Since the detector gain varies with isotope mass, the relationship between the analogue and pulse stages is also mass dependent and must be determined individually for each isotope, in order to obtain the best precision. With the aid of the ELAN software, the calibration was conducted by applying a single multielement solution of relatively high concentration (approx. 200 µg L^{-1} of 39 elements). The calibration points shown in Figure 5.7 were obtained by making 20 scans of each mass at different lens potentials. By varying the voltage of the lens, the ion transmission is reduced, in effect creating a dilution of the ion beam. The slopes of the all the cross-calibrations represent the conversion factor between the two detector stages for each mass. The lower right-hand graph in Figure 5.7 shows the mass dependence of the conversion factor. The pulse mode is approximately 10 times more sensitive than the analogue mode for most isotopes.

5.3.1.5 Daily performance check

In order to continuously asses the performance of the apparatus, a test solution was measured before the first standard, recording sensitivity, background intensity, precision and levels of oxides and doubly charged ions (Figure 5.8).

Daily Performance Report

Sample ID: Sample
Sample Date/Time: Friday, February 19, 2010 15:23:35
Sample Description:
Method File: C:\Elandata\Method\Daily.mth
Dataset File: C:\Elandata\Dataset\daily performance\Sample.376
Tuning File: C:\Elandata\Tuning\default.tun
Optimization File: c:\elandata\optimize\default_apex.dac
Dual Detector Mode: Pulse
Acq. Dead Time(ns): 50
Current Dead Time (ns): 50

Summary

	Analyte	Mass	Meas. Intens. Mean	Net Intens. Mean	Net Intens. SD	Net Intens. RSD
	Mg	24.0	354560.0	354559.993	3153.949	0.9
	Rh	102.9	1600493.3	1600493.341	12165.225	0.8
	In	114.9	1642537.7	1642537.696	16333.140	1.0
	Pb	208.0	909957.0	909956.988	16145.965	1.8
⎡>	Ba	137.9	1210792.8	1210792.804	31734.522	2.6
⎣	Ba++	69.0	30380.5	0.025	0.000	2.0
⎡>	Ce	139.9	1352018.2	1352018.247	29128.885	2.2
⎣	CeO	155.9	3543.1	0.003	0.000	2.7
	Bkgd	220.0	3.3	3.333	1.021	30.6

Figure 5.8 Excerpt from a daily performance report. Reports were obtained every day before the analysis was commenced. Sensitivity, background, precision, oxides and doubly charged ions were monitored as indictors of the instruments' performance.

Since undigested samples were analysed, it was particularly important to ensure that the instrument had been cleaned properly between two sample sets. Poor sensitivity was an indicator of reduced sample flow or clogged cones, while reduced precision

often was a result of nebulisation problems or unstable plasma, caused by a dirty torch.

5.3.2 Spectral interferences and selection of target isotopes

The elemental composition of serum is well-documented (Table 5.2). Ca, P and Mg are major elements, found in the mg L^{-1} concentration range, while Sr is a trace element normally found in the low µg L^{-1} range. The natural molar ratios are about 1.9:1, 2.7:1 and 7500:1 for Ca/P, Ca/Mg and Ca/Sr, respectively. For animals treated with strontium, concentrations of more than 15 mg L^{-1} have been reported [39].

Table 5.2 Concentration ranges of Mg, P, Ca and Sr in human serum [170, 265-268].

(mg L^{-1})			(µg L^{-1})
Mg	P	Ca	Sr
17-23	23-51	80-106	4-47

Table 5.3 p. 71 shows ionisation energies, naturally occurring isotopes and potentially interfering ions of all measured elements. Mg, Ca and Sr have several isotopes, with both high (^{24}Mg, ^{40}Ca, ^{88}Sr), medium (^{25}Mg, ^{26}Mg, ^{86}Sr, ^{87}Sr) and low (^{42}Ca, ^{43}Ca, ^{44}Ca, ^{46}Ca, ^{48}Ca, ^{84}Sr) abundance. Considering the natural concentration ratios between these elements, it was expected that an analytical protocol determining the low-abundant isotopes of Mg and Ca together with the high- and medium-abundant Sr isotopes would lead to ion intensities that fell within the dynamic range of the instrument. For the potentially very high Sr concentrations in the treated animal groups, the least abundant ^{84}Sr could be exploited. The high concentration of phosphorous would have to be determined through ^{31}P, the only exiting P isotope. However, as the first ionisation energy of P is much higher than that of the other measured elements, P is ionised to a much lesser degree in the ICP, resulting in a lower sensitivity.

De Muynck and Vanheacke [166] compiled a very comprehensive list of potential interfering ions for ICP-MS determination of Ca, P and Sr (Table 5.3). Some interfering ions can be corrected for mathematically by entering so-called elemental equations in the instrument software. The principle of this method is to monitor the interfering isotope at the analyte mass by measuring a different, ideally interference-free, isotope of the same element at an alternative mass, and then use the ratio of the natural abundances to correct the analytical result. For instance, the interference of ^{84}Kr on ^{84}Sr is corrected by simultaneously monitoring the combined ion intensity of ^{84}Kr + ^{84}Sr and the intensity of ^{83}Kr. The ELAN software supplied with the instrument suggests relevant equations for each measured isotope.

All the isotopes of interest suffer from spectral interferences. Most notably, the most abundant Ca isotope, ^{40}Ca, is unavailable for analysis by standard Ar-ICP due to severe spectral interference from the vast concentration of $^{40}Ar^+$ in the ion beam. The overlap cannot be resolved even by a high resolution instrument [166], but the Ar interference can be removed by applying a dynamic reaction cell with NH_3 as the reactant gas [269]. Of the five remaining Ca isotopes, ^{44}Ca, ^{46}Ca and ^{48}Ca were not considered suitable for analysis. ^{46}Ca has a very low abundance, while the P-based interferences on $^{48}Ca^+$ and the interference of $^{12}C^{16}O_2^+$ on ^{44}Ca are both potentially very significant. The interference from $^{26}Mg^{16}O^+$ on ^{42}Ca was expected to be less pronounced, since ^{26}Mg is only medium abundant. The two measured Ca isotopes, ^{42}Ca and ^{43}Ca, are both susceptible to interferences from doubly charged Sr^{2+} ions. In serum taken from untreated animals, this interference would be negligible due to the large Ca/Sr concentration ratio and the low amount of M^{2+} formed in the ICP ($M^{2+}/M^+ < 3\%$, see p. 62). However, the serum Ca/Sr ratio in animals treated with Sr is potentially raised to the order of 20:1, thus increasing the possibility for Sr interference. The effect was expected to be very low for ^{42}Ca, due to the low abundance of ^{84}Sr.

High concentrations of C, Ca and Na have been reported to interfere with determination of Mg in low concentrations due to spectral interferences from $^{48}Ca^{2+}$, $^{23}Na^+$(tailing), $^{23}Na^1H^+$ and $^{12}C^{14}N$ [270], but in view of the high concentration of serum Mg, no significant interference was expected. This was confirmed by the method validation, where a good agreement between the three Mg isotopes was observed.

Several investigators have used ICP-MS for determination of P and P-compounds [271-274], even though the single phosphorous isotope, ^{31}P, suffers from serious interference from carbon- and nitrogen based polyatomic species. In general, the presence of C has been reported to enhance the signal of elements with ionisation potentials of 9-11 eV [275], an observation that was later confirmed specifically for P [276]. NO^+ and NOH^+ are of course especially problematic if nitric acid is used for dilutions of samples and standards. The interferences can be overcome by using a high resolution instrument [277, 278] or a reaction cell [279-281]. Alternatively, the molecular ion PO^+ has been used for quantification of P at m/z 47 [276, 282], but since other interferences exist at this mass ($^{15}N^{16}O_2^+$, $^{14}N^{16}O^{17}O^+$, $^{14}N^{16}O_2^1H^+$), this approach was not pursued in the present study.

Table 5.3 First and second ionisation energies, natural isotope abundances [16] and some potentially interfering ions [166, 270, 276, 283-285] for Mg, Ca, P, Sr and Rh.

Element	Ionisation energy (eV)	Isotope	Abundance (%)	Potentially interfering ions
Magnesium	I: 7.646 II: 15.035	^{24}Mg	78.99	$^{12}C_2^+$, $^{23}Na^1H^+$, $^{23}Na^+$(tailing), $^{6}Li^{18}O^+$, $^{7}Li^{17}O^+$, $^{48}Ca^{2+}$, $^{48}Ti^{2+}$
		^{25}Mg	10.00	$^{12}C^{13}C^+$, $^{12}C_2^1H^+$, $^{9}Be^{16}O^+$, $^{24}Mg^1H^+$, $^{7}Li^{18}O^+$, $^{50}Ti^{2+}$
		^{26}Mg	11.01	$^{12}C^{14}N^+$, $^{13}C_2^+$, $^{12}C^{13}C^1H^+$, $^{25}Mg^1H^+$,
Phosphorous	I: 10.487 II: 19.769	^{31}P	100	$^{14}N^{16}O^1H^+$, $^{15}N^{16}O^+$, $^{14}N^{17}O^+$, $^{12}C^{18}O^1H^+$, $^{12}C^{16}O^1H_3^+$, $^{30}Si^1H^+$
Calcium	I: 6.113 II: 11.872	^{40}Ca	96.94	$^{40}Ar^+$, $^{40}K^+$, $^{24}Mg^{16}O^+$, $^{38}Ar^1H_2^+$, $^{39}K^1H^+$,
		^{42}Ca	0.647	$^{26}Mg^{16}O^+$, $^{14}N_3^+$, $^{16}O^{12}C^{14}N^+$, $^{40}Ar^1H_2^+$, $^{40}Ca^1H_2^+$, $^{84}Sr^{2+}$
		^{43}Ca	0.135	$^{27}Al^{16}O^+$, $^{26}Mg^{17}O^+$, $^{14}N_3^1H^+$, $^{12}C^{16}O^{15}N^+$, $^{13}C^{16}O^{14}N^+$, $^{12}C^{17}O^{14}N^+$, $^{40}Ar^1H_2^+$, $^{42}Ca^1H^+$, $^{86}Sr^{2+}$
		^{44}Ca	2.086	$^{26}Si^{16}O^+$, $^{12}C^{16}O_2^+$, $^{14}N_2^{16}O^+$, $^{28}Si^{16}O^+$, $^{44}Ca^1H^+$, $^{13}C^{16}O^{15}N^+$, $^{13}C^{17}O^{14}N^+$, $^{12}C^{17}O^{15}N^+$
		^{46}Ca	0.004	$^{46}Ti^+$, $^{28}Si^{18}O^+$, $^{14}N^{16}O_2^+$, $^{15}N_2^{16}O^+$, $^{12}C^{17}O_2^+$, $^{13}C^{18}O^{15}N^+$, $^{92}Zr^{2+}$
		^{48}Ca	0.187	$^{48}Ti^+$, $^{31}P^{16}O^1H^+$, $^{31}P^{17}O^+$, $^{15}N_2^{18}O^+$, $^{12}C^{18}O_2^+$, $^{96}Zr^{2+}$, $^{36}Ar^{12}C^+$, $^{32}S^{16}O^+$
Strontium	I: 5.695 II: 11.030	^{84}Sr	0.56	$^{84}Kr^+$, $^{36}Ar^{48}Ca^+$, $^{38}Ar^{46}Ca^+$, $^{40}Ar^{44}Ca^+$, $^{36}Ar^{48}Ti^+$, $^{38}Ar^{46}Ti^+$, $^{40}Ca^{44}Ca^+$, $^{42}Ca_2^+$, $^{66}Zn^{18}O^+$, $^{67}Zn^{17}O^+$, $^{68}Zn^{16}O^+$, $^{168}Er^+$, $^{168}Yb^{2+}$
		^{86}Sr	9.86	$^{86}Kr^+$, $^{38}Ar^{48}Ca^+$, $^{40}Ar^{46}Ca^+$, $^{36}Ar^{50}Ti^+$, $^{38}Ar^{48}Ti^+$, $^{40}Ar^{46}Ti^+$, $^{36}Ar^{50}Cr^+$, $^{40}Ca^{46}Ca^+$, $^{42}Ca^{44}Ca^+$, $^{43}Ca_2^+$, $^{68}Zn^{18}O^+$, $^{70}Zn^{16}O^+$, $^{69}Ga^{17}O^+$, $^{70}Ge^{16}O^+$, $^{172}Yb^{2+}$, $^{172}Lu^{2+}$
		^{87}Sr	7.00	$^{87}Rb^+$, $^{38}Ar^{49}Ti^+$, $^{40}Ar^{47}Ti^+$, $^{36}Ar^{51}V^+$, $^{43}Ca^{44}Ca^+$, $^{70}Zn^{17}O^+$, $^{69}Ga^{18}O^+$, $^{71}Ga^{16}O^+$, $^{70}Ge^{17}O^+$, $^{174}Yb^{2+}$, $^{174}Hf^{2+}$, $^{174}Lu^{2+}$
		^{88}Sr	82.58	$^{40}Ar^{48}Ca^+$, $^{38}Ar^{50}Ti^+$, $^{40}Ar^{48}Ti^+$, $^{38}Ar^{50}V^+$, $^{38}Ar^{50}Cr^+$, $^{40}Ca^{48}Ca^+$, $^{70}Zn^{18}O^+$, $^{71}Ga^{17}O^+$, $^{70}Ge^{18}O^+$, $^{72}Ge^{16}O^+$, $^{176}Yb^{2+}$, $^{176}Hf^{2+}$, $^{176}Lu^{2+}$,
Rhodium	I: 7.459 II: 18.08	^{103}Rh	100	$^{40}Ar^{63}Cu^+$, $^{38}Ar^{65}Cu^+$, $^{36}Ar^{67}Zn^+$, $^{40}Ar_2{}^{23}Na^+$, $^{87}Sr^{16}O^+$, $^{87}Rb^{16}O^+$, $^{85}Rb^{18}O^+$, $^{206}Pb^{2+}$

As the main element in this investigation, all four Sr isotopes were applied in the analysis. The least abundant isotope, ^{84}Sr, was included in anticipation of the elevated serum Sr concentrations present in the treated animal groups, where the high Sr sensitivity might result in ion counts above the range of the detector. The Sr isotopes are all potentially affected by spectral overlap from $ArCa^+$ molecular ions and/or Ca dimers, especially since Ca and Ar are both present in high concentrations in the ICP. Nevertheless, determination of Sr in Ca-rich matrices has not been reported to suffer from such interferences. In fact, it has been argued that elements with masses above 82 are essentially free of serious spectral interference from polyatomic species [286]. Of the interfering ions listed in Table 5.3, corrections were only made for spectral interference from singly charged monoatomic ions (Kr and Rb). All serum analyses showed excellent agreement between the three most abundant Sr isotopes. In the samples with low Sr contents, ion intensities for ^{84}Sr were often too low for a reliable quantification, whereas, in the Sr-treated groups, all four isotopes were in agreement within the measurement uncertainty. This confirmed that no serious spectral interferences for Sr were present.

The monoisotopic internal standard ^{103}Rh is subject to interference from $^{87}Sr^{16}0^+$ as well as several Ar-based species. Using an ELAN 6000 with a cross-flow nebuliser for analysis of environmental materials, Djingova *et al.* [285] found that a correction of 0.003% · [Sr] was necessary to achieve a good accuracy for determination of Rh. In the present study, however, the sample desolvation reduced the extent of oxide formation tenfold compared with a cross-flow nebuliser (Table 5.5, p 77). Therefore, the SrO^+ interference was assumed to be negligible and no correction was performed.

Based on the considerations above, it was decided to measure the isotopes ^{24}Mg, ^{25}Mg, ^{26}Mg, ^{31}P, ^{42}Ca, ^{43}Ca, ^{84}Sr, ^{86}Sr, ^{87}Sr and ^{88}Sr. Taking advantage of the expanded dynamic range of the dual detector mode, it was expected that this protocol would enable simultaneous determinations of all the analytes within their potential concentration ranges.

5.3.3 Non-spectral interference and internal standardisation

The serum matrix induced a severe suppression (>50%) of the analytical responses for all measured isotopes (Figure 5.9). The presence of biological constituents such as salts, proteins and lipids in the serum may suppress the signal through different mechanisms. Firstly, it may be a simple sample transport effect brought on by the sample components' impact on the flow dynamics and surface properties of the sample. A change in these properties would alter the formation of

aerosol droplets in the nebuliser and the droplet selection in the spray-chamber. The sample uptake rate may also be affected if the diluted serum has a different viscosity than the pure standards. Secondly, the signal suppression may be induced by a shift in the ionisation equilibrium [287] in the ICP. The ions in the plasma exist in equilibrium with their corresponding atoms:

$$M \leftrightharpoons M^{+} + e^{-} \qquad (5\text{-}1)$$

The serum matrix contains high amounts of easily ionisable matrix elements (e.g. Li, Na, and K) that may give rise to a high density of free electrons. The mass-action effect of these electrons might shift equation (5-1) towards the left, thus suppressing the formation of analyte ions. Finally, some of the plasma energy is used to vaporise and atomise the heavy biological components in the samples, which in effect cool down the plasma, leaving less energy for the ionisation of the analyte atoms.

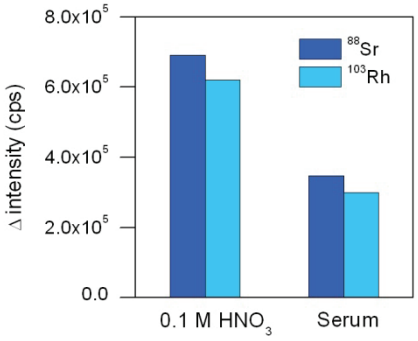

Figure 5.9 Signal increase after addition of 5 µg L^{-1} Sr and Rh to 0.1 M HNO_3 and diluted serum (1+11.5). The Sr and Rh responses were suppressed by 50 and 52 %, respectively.

The matrix interference made it absolutely essential to apply a suitable internal standard (IS) to correct the measured ion intensities of the analytes. Studies by Vanhaecke *et al.* [288] indicated that an IS with a mass close to that of the analyte is to be preferred for all elements, and both ^{89}Y, ^{103}Rh and ^{115}In have previously been used with success for determination of Sr (cf. section 3.5). In our laboratory, Rh is measured on a regular basis as a part of the instrument optimisation and daily performance checks. Consequently, extensive documentation concerning precision, sensitivity, long-term drift and day-to-day variability of Rh measurements was available, making it a good candidate for monitoring the analyses of standards and samples throughout the study. Rh was tested as IS during the initial method development and was found to provide a satisfactory correction of the Sr response.

The analyte signals were normalised by dividing the ion intensity of each analyte with that of the internal standard according to the general expression [169]

$$\frac{I_A}{I_{IS}} C_{IS} = a + bC_A \qquad (5\text{-}2)$$

where a is the intercept and b the slope of the calibration function, I_A is the analyte intensity in cps, I_{IS} the intensity in cps for the internal standard, C_{IS} the internal standard concentration in µg L^{-1}, C_A is the concentration of the analyte in µg L^{-1}. Since the IS concentration was identical for all standards and samples, C_{IS} could be omitted in the calculations.

^{103}Rh has also been used as IS for determinations of Mg and Ca [173, 289], though, admittedly, Rh is unlikely to be the best choice for these analytes due to the relatively large differences in mass and ionisation potential. Other investigators have used ^{59}Co as IS for determination of Mg, ^{35}Cl and ^{51}V for P, while ^{45}Sc and ^{51}V have been used for Ca [166, 290-292], but, as the main focus of this investigation was on Sr, no other IS than Rh was tested. This may have contributed to the large measurement uncertainty for these elements, as well as the poor accuracy of the P determination (cf. section 5.3.9).

5.3.4 Digestion vs. dilution

As described in Chapter 3, the primary motivation for digesting biological liquids is to avoid matrix-induced signal suppression, as well as clogging of the nebuliser, injector tubes and cones. This is especially true for a nebuliser with a concentric design, which is more prone to clogging because of the very fine liquid capillary. The perhaps most widespread method for preparation of serum samples is microwave assisted acid-digestion [168, 188]. However, considering the large number of samples (>150) to be analysed in this project, digestion would be very time consuming. Moreover, as the minimum solvent volume required for the laboratory's microwave digestion system is 7 mL, the small amount of serum available from each animal would risk being diluted below the limit of quantification. With this in mind, the more straightforward "dilute and shoot" approach was tested. A serum sample with a Sr concentration close to that of the animal control groups was divided into 8 subsamples, one half of which was diluted and the other one digested (500 µL serum was digested with HNO_3, HCl and H_2O_2 by a similar procedure to the one used for digestion of bone marrow in Appendix II).The analytical results obtained by the two methods (Table 5.4) were not significantly different, and consequently it was decided to avoid the labour-intensive digestion procedure.

Table 5.4 Results (mean ± SD) of analysis of several sub-samples taken from the same serum sample after microwave assisted acid digestion and dilution.

	Result (µg L^{-1} Sr)	*p* (student t-test)
Diluted serum (n = 4)	42.4 ± 3.7	
Digested serum (n = 4)	38.8 ± 5.2	0.31

The major drawback of this approach was a severe clogging of the line going from the Apex to the ICP-MS as shown in Figure 5.10a. After analysis of even a moderate number of samples, salts and organic sample material built up on the inner tube wall and eventually blocked the tube completely, at which point the plasma had to be stopped and the sample line disconnected and cleaned. Furthermore, sample material deposited on the inner wall of the plasma torch (Figure 5.10a). As a result, plasma ignition was hampered and ultimately the torch had to be replaced.

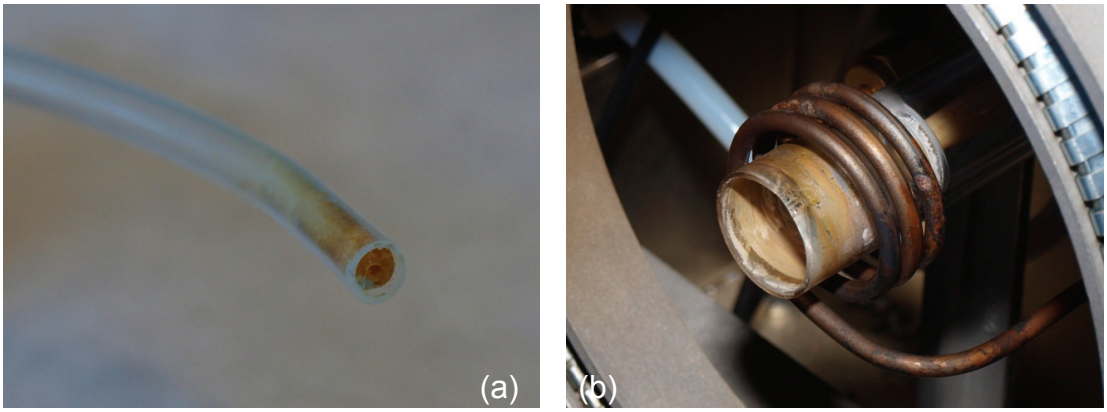

Figure 5.10 Photographs of the Apex aerosol tube (a) and the ICP-MS quartz nebuliser (a) after analysis of undigested serum samples illustrate the disadvantage of merely diluting the samples as opposed to performing a full digestion. Organic sample material is deposited on the inner tube wall, hindering and eventually blocking the sample flow.

The clogging of the aerosol line could to some extent be prevented by aspirating a solution of HNO_3 in high concentration (>5 M) between each sample, but even so, no more than 15-20 samples could be analysed before the sensitivity started to deteriorate. Similar, albeit less pronounced, effects was reported by Krahcler *et al.* [191], who used ICP-MS for determination of trace elements in serum, urine and even whole blood, which is a matrix much richer in organic material than serum. A dilution of 1+19 was necessary to achieve a good long-term stability (>24 h) for all three types of liquids, but a 1+9 dilution was reported very effective for serum and urine alone. Using ICP sector field mass spectrometry, Rodushkin *et al.* [293] reported that a 1+9 dilution of serum and urine allowed the instruments to remain stable for 6 h, corresponding to 30-35 clinical samples. de Boer e*t al.* [194] used a special Hewlett-Packard V-groove nebuliser and a 2.4 mm torch injector tube to

avoid blockage. These instrumental features allowed for 600-1000 blood samples to be measured without blocking the nebuliser. The somewhat lower tolerance to clogging seen in the present study must be attributed to the Apex inlet system. Contrary to preceding expectations, the clogging did not occur in the narrow capillary of the nebuliser, but rather at the aerosol outlet of the Apex. This suggests that a conventional cyclonic spray-chamber without a desolvation unit might have been more robust to clogging. Clearly, further dilution of the serum would allow more samples to be analysed without clogging, but the low Sr concentrations in serum from untreated animals set a limit to the extent of dilution.

5.3.5 Apex inlet system

Apex-Q sample inlet systems have previously been used for ICP-MS analysis of trace elements in acid-digested blood [261] diluted serum [188] and biological tissues [248]. The two main functions of the system are

1) to limit the amount of liquid entering the plasma, which reduces solvent-induced spectral interferences such as oxides, hydrides and argon/solvent-based polyatomic species. This is achieved by first heating the aerosol in the spray-chamber, which promotes solvent evaporation and analyte transport, and subsequently by cooling and condensing the evaporated solvent, thus creating a dry aerosol,

2) to increase sensitivity by adding N_2 to the sample aerosol.

Besides minimising solvent-based interferences, the low amount of solvent reaching the plasma reduces the energy needed to vaporize the solvent, which allows more energy to be available for ionisation of the analyte ions. Finally, controlling the temperature of the spray chamber can help minimising signal drift caused by changes in the ambient temperature [204, 219]. Addition of N_2 to argon-ICP has been studied extensively and has been shown to reduce formation of oxides [294] and other polyatomic species [295-297], while both enhancement [294, 298] and suppression [299] of the analyte sensitivity have been reported. Addition of N_2 fundamentally changes the physical and electrical properties of the plasma, but the mechanism by which N_2 affects the analyte sensitivity is uncertain. At a temperature of 7000 K, the thermal conductivity of N_2 is 32 times that of Ar, which may facilitate a greater heat transfer to the central channel of the plasma, causing a higher degree of ionization [300]. This view is supported by the measurements of the Ba^{2+}/Ba^{+} ratios shown in Table 5.5. The desolvation system operating without N_2 yields a Ba^{2+}/Ba^{+} level similar to a cross-flow nebuliser. Adding N_2 to the sample aerosol more than doubles the ratio, indicating that the gas facilitates ionisation. Contradicting this view, Lam

and Horlick [294] found no clear correlation between ionisation potential and signal enhancement after addition of N_2, which would have been expected if the mixed gas effect were related to the energy of the ionisation zone. This may be investigated further by looking at the degree of ionisation in the plasma. Using the Saha [301] equation, Houk [302] calculated the degree of ionisation in an ICP expressed as $M^+/(M^+ + M)$ for 79 elements and found a ratio of > 90% for both Mg, Sr, Rh and In. Table 5.5 shows that adding N_2 to the Apex aerosol increased the sensitivity 44-111% for these elements. With more than 90% of the elements already ionised, it would clearly be impossible to achieve the observed sensitivity enhancement solely by further ionisation of the elements, which also speaks against an energetic explanation of the N_2 effect.

Table 5.5 Comparison of sensitivities and formation of oxides and doubly-charged ions using a cross-flow nebuliser and the Apex inlet system. The sensitivities have been corrected for the difference in sample flow (cross-flow: 480 µL min^{-1}, Apex: 260 µL min^{-1}). Instrument settings were optimised for determination of Sr.

	Sensitivity (counts fg^{-1})			3σ-limit of detection (µg L^{-1})	
Nebuliser	Cross-flow	Apex, no N_2	Apex with N_2	Cross-flow	Apex with N_2
^{24}Mg	0.54	3.5	5.1	0.11	0.025
^{31}P	0.043	0.12	0.24	1.8	1.14
^{42}Ca	0.063	0.42	0.44	7.1	3.33
^{88}Sr	4.2	27	42	0.009	0.005
^{103}Rh	3.5	18	37	0.002	0.0007
^{115}In	4.1	19	38	0.002	0.001
^{138}Ba	3.7	16	28	0.004	0.002
^{140}Ce	4.0	16	31	0.003	0.002
^{208}Pb	4.0	10	21	0.008	0.005
CeO/Ce	2.8%	0.33%	0.26%	-	-
Ba^{2+}/Ba^+	1.2%	1.1%	2.5%	-	-

Compared with the most common injector combination of a cross-flow nebuliser and a double-pass spray chamber, the Apex provides a considerable increase in sensitivity for all analysed elements except Ca (Table 5.5). Being the target element of the optimisation, Sr sensitivity increased by a factor of 14, but large enhancements were also seen for both lighter (Mg, 8 x increase) and heavier (Rh 10 and Pb 5 x increase) elements. The improvement is due to the high efficiency of the concentric nebuliser and cyclonic spray chamber combined with the solvent removal and addition of N_2 in the Apex. Concomitantly, the CeO/Ce ratio was reduced with one order of magnitude, showing that the desolvation provided a marked decrease in the oxide levels. Finally, the microflow nebuliser allowed for much lower sample consumption (260 µL min^{-1}) than the cross-flow nebuliser (480 µL min^{-1}).

As discussed above, a possible disadvantage of the Apex is a more pronounced tendency to clogging, leading to a lower tolerance to heavy matrices. In addition, the efficient removal of the sample solvent enables more sample material to reach that plasma, which may amplify the signal suppression caused by the matrix.

5.3.6 Sample containers

Controlling and minimising blank contributions in trace and ultra-trace analysis of clinical samples is at least as important as maximising instrument sensitivity [303]. Different containers made from plastic, borosilicate glass (Duran) and quartz were tested as vessels for dilution and storage of the serum samples. The blank levels for both plastic and borosilicate containers showed a very large vessel-to-vessel variance with up to 60 times higher blank responses for Sr than found using quartz vessels. The highest observed contaminations were in the order of 0.5 $\mu g\ L^{-1}$, a level which would have had a serious impact on the means and standard deviations of the final results, particularly in the untreated groups. To keep the blank values consistently at a minimum, 70 quartz vessels were custom made for the analysis. The calibration standards were produced using volumetric flasks made from Duran. Only flasks showing consistent, low background levels were applied.

5.3.7 Dynamic range

The purpose of operating in dual detector mode is to increase the linear range of the ICP-MS, thus reducing the need for sample dilution. In principle, the cross-calibration of the two detector stages should enable a single linear calibration function to cover concentrations in both the pulse and the analogue regions. However, Campbell and Burns [227] reported nonlinearity of the detector response when applying the dual-detector mode on an ELAN 6000. Despite a satisfactory linear correlation in the cross-calibration (similar to the ones shown in Figure 5.7, p 67), the slopes of the calibration curves for the two stages were found to be different. Confirmed by other investigators [228], this nonlinearity leads to bias if a single calibration function is fitted to both response ranges. To investigate if a similar behaviour could be identified with the instrument used in the present work, calibration functions were calculated for Mg, P, and Sr for both the combined and separate detector stages (Table 5.6). The results showed that the slopes for the two regions did in fact differ significantly with the analogue stage giving systematically higher slopes than the pulse stage. This trend is in agreement with previous findings [227, 228]. As a consequence, separate calibration functions were calculated for the two regions. Isotopes with signal intensities below $2 \cdot 10^6$ cps were quantified using

the pulse mode calibration, while higher signal intensities were processed using the analogue mode calibration.

Table 5.6 Sensitivities for pulse, analogue and dual stages for the ELAN 6000.

	Slope ± standard deviation (L · µg^{-1})			P/A-ratio
	Dual mode	Pulse mode	Analogue mode	
^{24}Mg	(46.8±0.1) ·10^{-3}	(45.1±0.3)·10^{-3}	(46.9±0.3) ·10^{-3}	0.96
^{31}P	(21.9±0.1)·10^{-4}	(20.7±0.3)·10^{-4}	(21.8±0.1) ·10^{-4}	0.95
^{42}Ca	(47.1±0.1) ·10^{-4}	(39.2±0.1) ·10^{-4}	(48.6±0.8)·10^{-4}	0.81
^{86}Sr	(28.2±0.1) ·10^{-3}	(23.9±0.2) ·10^{-3}	(28.3±0.2) ·10^{-3}	0.84
^{88}Sr	(26.2±0.2) ·10^{-2}	(21.48±0.07) ·10^{-2}	(26.3±0.3) ·10^{-2}	0.82

Without the application of an internal standard, the response showed a pronounced curvature at high analyte concentrations, starting above 500 µg L^{-1} (Figure 5.11). This was observed for all isotopes, irrespective of the ion intensity or the detector mode. The curve shape bears resemblance to a signal approaching detector saturation, but, since the curving is independent of the ion count, it cannot be attributed to the detector. Rather, it must be taken as an indication of a lower efficiency in the generation and transmission of ions by the ICP and the ion lens at high analyte concentrations.

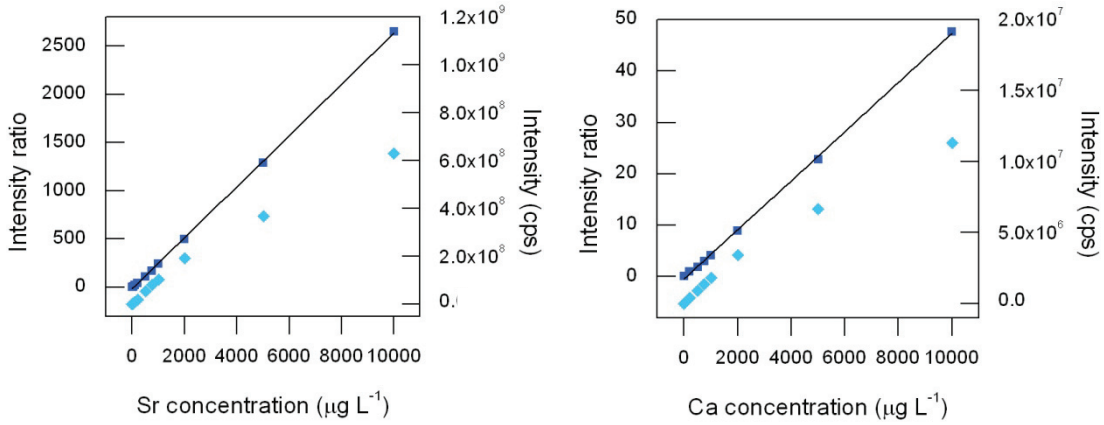

Figure 5.11 Calibration with respect to ^{88}Sr and ^{44}Ca up to 10,000 µg L^{-1} using the analogue detector mode. The ion intensity (◆) shows a pronounced curvature starting above 500 µg L^{-1}. Correcting the ^{88}Sr response using 5 µg L^{-1} Rh as IS (■) results in a good linearity in the whole concentration range. The curvature was seen for all isotopes irrespective of the ion intensity.

The explanation may be linked to the nature of the calibration standards. In addition to the analytes, the multi-element solution used for preparation of the standards contained similar concentrations of heavier elements such as Pb and Cd. Early investigations [304] showed that the magnitude of signal suppression increased with

the masses of elements concomitantly present in the sample. It was later suggested that the primary cause of this interference is the so-called *space charge effect* [305], which causes the heavier matrix elements to dominate the ion beam and deflect the lighter elements, in effect defocusing the beam and reducing ion transmission [306, 307]. It was observed that the suppression depended on the absolute concentrations of the analyte and matrix ions as well as their concentration ratios [304]. It has also been suggested that the distribution of analyte ions in the presence of concomitant matrix ions is affected by ambipolar diffusion in the ICP [304, 308]. Shifts in ionisation equilibria may also play a role, as discussed in section 5.3.3. As a final note, some investigators [309, 310] found that signal suppression cannot be explained by a single mechanism, but must be due to a combination of several causes.

In the present work, the curvature could be corrected by normalising the intensities with the internal Rh standard, and a good linearity could be obtained throughout the whole concentration range. This shows that whatever the cause of the suppression may be, it affects equally the analytes in the mg L^{-1} range and the internal standard at 5 μg L^{-1}.

5.3.8 Ruggedness

From the discussion in section 5.3.1 it is clear that all the optimisation parameters need to be carefully controlled during operation, as they greatly affect the analytical signal. Other factors influencing the performance of the instrument include the background pressure ($1.7\text{-}2.4 \cdot 10^{-4}$ Pa) and working pressure ($1.5\text{-}2.1 \cdot 10^{-3}$ Pa) of the mass spectrometer as well as the torch box temperature (39-43°C). Such factors are determined by the instrumental design and the laboratory's facilities (ambient temperature, cooling water, ventilation etc.) and cannot be readily adjusted by the operator. The values were noted daily in the instruments logbook together with the results of the performance check described in section 5.3.1.5.

The main factor affecting the analytical performance was deposition of sample material on the tubing. During analysis, the extent of clogging was monitored by recording the response of the internal standard. The first serum sample to be analysed typically gave a Rh response of approximately $3 \cdot 10^5$ cps. As more samples were measured, the response decreased due to the reduced aerosol flow. The measurements were stopped when the signal fell below approx. $1 \cdot 10^5$ cps. Sample depositions on cones and torch caused a need for these components to be removed and cleaned regularly.

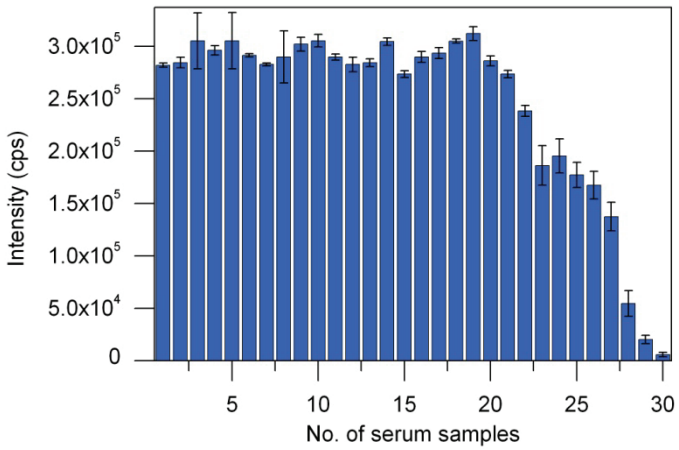

Figure 5.12 The Rh signal from the internal standard (mean ± SD) was monitored during the measurements. The intensity decreases as the aerosol flow is reduced due to clogging of the tubing.

5.3.9 Quality control

The precision was <2.5% for all isotopes when measured in the standards and <5% in the diluted serum. Sr and Rh measurements tended to exhibit better precision than those of the lighter isotopes, but the trend was not consistent in all samples.

The accuracy of the analytical procedure was evaluated by analysing a Seronorm serum reference material acquired from Sero, Norway. Despite its shortcomings, this material was the best of its kind commercially available. As discussed in Chapter 3, the manufacturer states up to three different reference intervals for each analyte concentration, and none of the analytical values are certified. In this context, it is worth mentioning that several investigators have reported analytical results for Mo and Se that differed significantly from the reported values in the serum material [191, 311, 312]. However, to this author's knowledge, no discrepancies regarding P, Mg, Ca and Sr have been reported.

The Seronorm reference material was analysed at regular intervals and it was always included at least once when a series of serum samples was measured. Table 5.7 presents a summary of the measured concentrations. Excellent agreement between measured and reported values was found for Sr.

Table 5.7 Measured (mean ± SD) and reported (95% confidence interval) values for the serum reference material Seronorm Trace Elements Serum, Level 2.

	Sr (μg L^{-1})	Sr (mg L^{-1})	Mg (mg L^{-1})	P (mg L^{-1})	Ca (mg L^{-1})
Found	134 ± 11	1.08 ± 0.078	31.5 ± 8.6	108 ± 31	120 ± 22
Reported	130 ± 5*	1.01†	27.3-32.2	39-44	108-126

*Mean ± SD, †Prepared by adding Sr to the Seronorm material

It should be noted that the strontium concentration in the certified reference sample was about 4 times higher than the lowest concentration found in a sample. Therefore, the accuracy of these analyses may not be properly evaluated by using the reference material. The measured concentrations were, however, at least three orders of magnitude above the LOD and 5 times higher than the lower limit of analysis (cf. Chapter 6) for which reason the validation was expected to be adequate.

The mean values of Mg and Ca were also within the reported reference interval, whereas the concentration of P was considerably overestimated as compared with the reported value. The reason for poor accuracy in the P determination was not investigated further, but it is most likely a result of N- and C-based spectral interferences (cf. Table 5.3, p 71), arising from the organic material in the serum samples. Likewise, the relatively large standard deviation observed for Mg is probably also a result of spectral interferences disturbing mass peak resolution at the low masses. A control chart showing all individual Sr results is presented in Chapter 6, p 92.

5.3.10 Analysis of rat serum

5.3.10.1 Strontium

The results of the analysis are presented in the tables below. The Sr concentrations found in the control groups were generally in good agreement with previously reported natural Sr levels in serum [112, 313, 314]. As expected [118], treatment with SrR caused a dramatic increase in serum Sr concentrations. In both studies, serum Sr levels in the Sr treated groups increased with approximately two orders of magnitude compared with the control groups.

Table 5.8 Animals, treatment and serum Sr (mean ±SD) in the fracture study [8].

	Group 1	Group 2	Group 3	Group 4
No. of animals	21	18	19	18
Fracture healing	3 weeks	3 weeks	8 weeks	8 weeks
SrR treatment	No	Yes	No	Yes
Serum Sr (μg L^{-1})	92 ± 101	(10.37 ± 0.89)·10^3	45 ± 16	(8.99 ± 0.77)·10^3
Serum Mg (mg L^{-1})	31.1 ± 6.3	28.9 ± 5.6	29.2 ± 7.2	30.1 ± 4.9
Serum P (mg L^{-1})	184 ± 43	160 ± 60	176 ± 55	134 ± 33
Serum Ca (mg L^{-1})	99.6 ± 10.2	98.9 ± 8.9	101.3 ±11.2	98.7 ± 16.3

Perhaps a bit surprisingly, the group mean of Group 2 in the fracture study was significantly higher than that of Group 4, even though Group 4 was treated for a longer period of time. This indicates that the transport of Sr from the intestine to the blood has reached saturation already after 3 weeks. Tentatively, it may also suggest

that the longer treatment time induced a more efficient transport of Sr from the blood to the intestinal lumen, supporting the idea put forth by Nielsen [13] that active transport of Sr to the lumen may act as a mechanism for homeostatic control of Sr at high Sr blood levels.

The large relative standard deviations observed in Group 1 in the fracture study and Groups 2 and 4 in the Botox study are results of one or more sample values that were significantly different to the other samples in the respective groups. In the fracture study, three samples in Group 1 contained significantly higher Sr concentrations (317-388 μg L^{-1} Sr) than the remaining samples (44-77 μg L^{-1} Sr). In the Botox study, Group 2 contained one value that was abnormal (424 μg L^{-1} Sr) compared to the rest of the group (42-76 μg L^{-1} Sr), while three samples (0.35-3.2 mg L^{-1} Sr) in Group 4 contained significantly different concentrations (remaining range 49-103 μg L^{-1} Sr). Since none of these groups were treated with Sr, it was much unexpected to find such high serum concentrations. The reason remains unclear, but it may be a result of cross-contamination during the sampling or preparation steps. However, as no errors or irregularities could be identified by consulting the study journals, the abnormal results could not be marked as outliers and they are therefore included in the group means and SDs.

Table 5.9 Animals, treatment and serum Sr (mean ±SD) in the Botox study.

	Group 1	Group 2	Group 3	Group 4	Group 5	Group 6
No. of animals	12	12	12	12	12	12
Treatment	None	Vehicle	Botox	Botox PTH	Botox Strontium PTH	Botox Strontium
Treatment time	0 days	4 weeks	4 weeks	4 weeks	4 weeks	4 weeks
Killed	Study start	Study end	Study end	Study end	Study end	Study end
Serum Sr (μg L^{-1})	43.5±5.2	84±109	48.5±6.7	$(0.57\pm1.1)\cdot10^3$	$(9.4\pm1.0)\cdot10^3$	$(7.85\pm0.49)\cdot10^3$

5.3.10.2 Magnesium, Calcium and Phosphorous

Mg, Ca and P were determined in the fracture study only (Table 5.8). In agreement with previous studies on strontium treatment in rats, no significant differences in serum concentrations of the three elements were observed between the groups. The observed Ca concentrations were in excellent agreement with values previously reported in rats, while the Mg concentrations were approx. 25% lower

[112, 313, 314]. However, the observed Mg levels were in very good agreement with rat serum Mg measured by another technique in the study presented in Chapter 7.

The measured P concentrations were much higher than what has been reported earlier, owing to the poor accuracy of the P determination. No statistical difference in serum P was found between the groups. Omdahl *et al.* [48] reported consistently lower serum phosphate in rats kept on a Sr-rich diet compared with rats kept on a low-Sr diet, while Schrooten *et al.* observed no significant differences in serum phosphorous between rats treated with Sr and a control group [314]. In the present study, the poor accuracy and large group SDs make it difficult to make any reliable biological inference about the treatment effect on serum P.

5.4 Conclusion

A procedure for determination of Mg, P, Ca and Sr in serum using ICP-MS has been established and optimised. Rh was found to be a suitable internal standard for all analytes. By running the instrument in dual detector mode, a linear response range of more than four orders of magnitude was obtained. To enable determination of the natural trace-levels of Sr, a sample introduction system with a concentric nebuliser and a desolvation unit was applied. The inlet system reduced the generation of oxides in the ICP and increased the sensitivity for Sr by a factor of 14 compared with a conventional cross-flow nebuliser. The sample preparation was based on direct dilution with diluted nitric acid, omitting sample digestion. This approach considerably reduced the time required for sample preparation, but the high content of organic material in the samples gave rise to a severe clogging of the sample inlet tube. Good accuracy was obtained for Mg, Ca and Sr, whereas serum P was grossly overestimated, probably due to spectral interferences from organic serum components. It must be concluded that the analytical procedure was very well suited for determination of Ca and Sr, adequate for determination of Mg, but unsuited for determination of P. The analysed serum samples from two studies in rats showed that treatment with strontium ranelate for 3, 4 and 8 weeks increased the concentration of Sr in serum about two orders of magnitude, while concentrations of Mg, P and Ca were maintained.

CHAPTER SIX

Uncertainty calculations and sampling

6.1 Introduction

This chapter presents a discussion of measurement uncertainty calculations associated with the ICP-MS analysis of Sr. Before the samples from the first animal study (4-week dog) were analysed, a complete uncertainty budget was constructed for the analytical procedure. The assessment of the uncertainties associated with the ICP-MS measurements was used for evaluating whether the methods were fit for the analytical purpose. In order to reach reliable clinical conclusions regarding the treatment effects of strontium on the tested animals, it was essential that the measurement uncertainty was considerably lower than the expected biological variations related to the treatment. In addition, the sampling procedure that was used for taking samples from bones from test animals is also discussed.

6.2 Uncertainty budget

The uncertainty budget was produced in accordance with the guidelines presented in the *Guide to the expression of uncertainty in measurement* (GUM) [195] and the Eurachem/CITAC guide *Quantifying Uncertainty in Analytical measurement* (QUAM) [196]. The sample preparation procedure and the magnitude of the uncertainty contributions from weighing, dilutions, measurement and traceability are presented in Appendix II. It was concluded that the uncertainty originating from the ICP-MS analysis was by far the most dominating contribution to the total uncertainty, while the repeatability and tolerance of the equipment used for preparing the sample solutions were negligible in comparison. Similar conclusions were

reached for the two long-term animal studies (26-week rat and 52-week dog), even though the samples from these studies were analysed using a more recent apparatus (ELAN 6000 ICP-MS) than the one used for the 4-week dog study (ELAN 5000). Hence, the uncertainty of the sample preparation will not be discussed further in this chapter.

6.3 Measurement uncertainty of the ICP-MS analysis

6.3.1 Regression equations

Being the dominating uncertainty contribution, it was particularly important that the uncertainty of the ICP-MS measurements was properly evaluated. This section presents the most important equations used for the calculations. The remaining regression equations are summarised in Appendix III.

In order to avoid complex, non-linear regression calculations, it was firstly ensured that the relation between the normalised response and the analyte concentration was well described by a linear function. Contrary to common practise, evaluation of linearity was not based on the magnitude of the correlation coefficient (r^2), but rather performed by testing for a random sign distribution of the regression residuals (Wald-Wolfowitz runs test [315]). Once linearity was established, the calibration data was fitted to the function

$$\frac{I_{Sr}}{I_{Rh}} = \alpha C_{Sr} + \beta \qquad (6\text{-}1)$$

where C_{Sr} is the concentration of Sr, and I_{Sr} and I_{Rh} are the intensities of Sr and Rh, respectively. α (slope) and β (intercept) denotes the regression coefficients. Figure 6.1 shows a calibration curve and the corresponding regression residuals obtained from five replicate measurements at each standard concentration. Inspection of the residuals revealed clear heteroscedasticity, which in theory require application of weighted least-squares regression (WLSR). In ordinary least-squares regression (OLSR) all calibration points are given equal weight in the calculations, which is technically incorrect if they do not have equal variance [230].

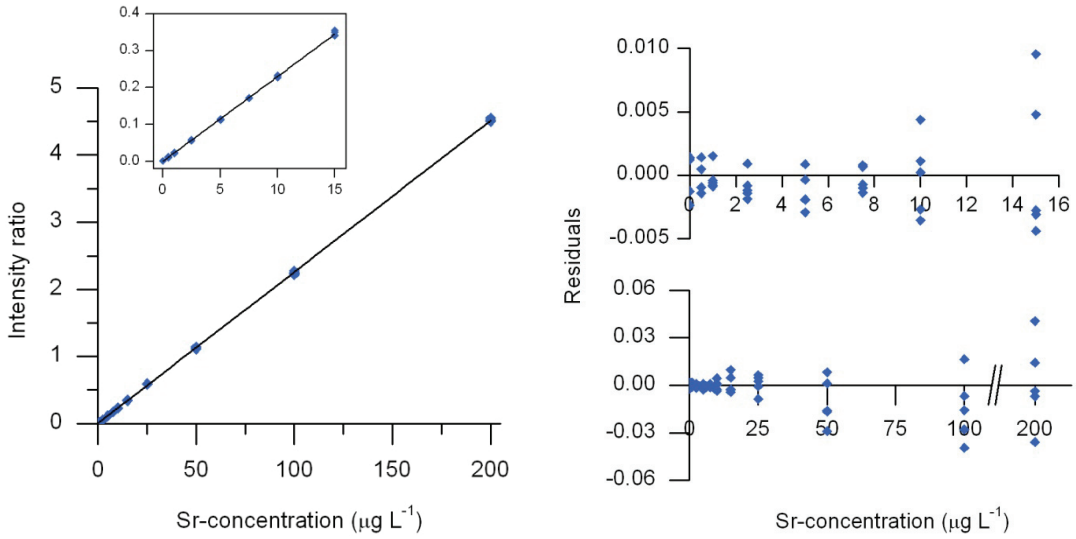

Figure 6.1 Calibration line (WLSR) and residuals for ^{86}Sr for the concentration range 0.5-200 µg L^{-1} (pulse mode). Five replicates were measured at each concentration.

The idea behind weighing is to attach most importance to data that is known with the highest statistical precision. However, it is rarely straightforward to assign proper weights to the individual calibration points. For any least-squares fit, the most statistically precise parameter estimates are obtained only if the data are weighed inversely as the true response variance ($w_i = \sigma_i^{-2}$). Unfortunately, σ^2 is never truly known for real data. It is well established that merely using the variance of repeated measurements to assign weights is not adequate, and the estimation of the variance function is therefore very important [316, 317]. Many different weights have been applied for different analytical applications. For a calibration function, $y = ax + b$, weights such as $x^{-0.5}$, x^{-1}, x^{-2}, $y^{-0.5}$, y^{-1} and y^{-2} have been suggested [318]. In this project, the variance was assumed to follow the empirical equation suggested in the CITAC/Eurachem guide [196]:

$$u^2\left(\frac{I_{Sr}}{I_{Rh}}\right) = s_0^2 + \left(\frac{I_{Sr}}{I_{Rh}} \cdot s_1\right)^2 \qquad (6\text{-}2)$$

This equation satisfies the residual pattern seen in Figure 6.1, where the variance is practically constant at the low response limit and proportional to $u(I_{Sr}/I_{Rh})$ at the high response limit. The response variance was measured for each standard concentration, and the data was fitted to equation (6-2) using the Solver function in Microsoft Excel®. The weights were then calculated by

$$w_i = \frac{1}{u_i^2} \cdot \sum_i \frac{1}{m \cdot u_i^2} \qquad (6\text{-}3)$$

where $u = u(I_{Sr}/I_{Rh})$ from equation (6-2) and m is the number of calibration standards. In equation (6-3) the weights are scaled such that the sum of the weights equal the number of calibration standards: $\sum_i w_i = m$.

Clearly, the calculations involved in WLSR are far more complex than those required for OLSR. Even so, it has been our experience there is no or very little practical difference between the calibrations functions obtained by OLSR and WLSR when working with ICP-MS (cf. Table 2, Appendix II). This is supported by the regression equations calculated from the data in Figure 6.1. Table 6.1 shows that the regression parameters were similar within their respective uncertainties. Based on these observations, it can be debated whether it was worthwhile going through the time-consuming WLSR routine. However, it was thought to be necessary for obtaining a complete and theoretically sound treatment of the calibration data.

Table 6.1 Parameter estimates for calibration functions determined by ordinary least squares regression (OLSR) and weighted least squares regression (WLSR) for ^{86}Sr.

Regression method	Calibration function
OLSR	$\frac{I_{Sr}}{I_{Rh}} = 0.02255(\pm 0.000047) \cdot C_{Sr} + 0.0035(\pm 0.0031)$
WLSR	$\frac{I_{Sr}}{I_{Rh}} = 0.02275(\pm 0.00015) \cdot C_{Sr} + 0.00081(\pm 0.00058)$

After calculation of a (weighted or unweighted) calibration function, the concentration of Sr in a sample can be found by rearranging equation (6-1):

$$C_{Sr} = \frac{\frac{I_{Sr}}{I_{Rh}} - \beta}{\alpha} \qquad (6\text{-}4)$$

The uncertainty estimate of the predicted concentration can be calculated by propagating the uncertainties associated with the quantities in equation (6-4), resulting in [195, 319]

$$u(C_{Sr}) = \frac{1}{\alpha}\sqrt{u(I_{Sr}/I_{Rh})^2 + u(\beta)^2 + (u(\alpha) \cdot C_{Sr})^2 + 2C_{sr}u(\alpha)u(\beta)r(\alpha,\beta)} \qquad (6\text{-}5)$$

where $u(I_{Sr}/I_{Rh})$ is the uncertainty of the normalised sample response, $u(\alpha)$ and $u(\beta)$ are the uncertainties of the regression coefficients and $r(\alpha,\beta)$ is the coefficient of correlation between α and β given by [320]

$$r(\alpha,\beta) = -\frac{1}{\sqrt{m}} \cdot \frac{\sum_i C_{Sr,i}}{\sqrt{\sum_i C_{Sr,i}^2}} \quad (6\text{-}6)$$

The above equations were applied for evaluation of the measurement uncertainty as described in the following sections.

6.3.2 Single-day calibrations

Throughout this project, a suitable reference material (RM) was always included in the ICP-MS analysis of samples from test animals. Prior to analysis, the performance of the instrument was optimised and validated as described in Chapter 5. As described above, the calibration of the instrument, and the calculations of sample concentrations and associated uncertainties, were performed in accordance with conventional recommendations [196, 230, 315, 321]. However, it was soon observed that the uncertainty estimates calculated from the linear regressions (either weighted or unweighted) did not correspond well with our observations. This can be illustrated by looking at results from analysis of the Seronorm Serum RM at four different days (Table 6.2). The first result was perfectly in agreement with the reported value of the RM, while the next two were respectively below and above the reported range. The second measurement was close to the upper limit of the reported range, but because of the low uncertainty (1.9%), the result was not within the reported concentration range, and thus significantly different from the reference value. The fourth result was, within the uncertainty, again in agreement with the reference value. Furthermore, the table reveals a large difference in the uncertainty estimates of the four measurements, ranging from 1.9 – 8.3% relative uncertainty. This is unfortunate, as identical samples with identical levels of analyte would be expected to give very similar uncertainty estimates. The calibration of the ICP-MS and the application of an internal standard were expected to correct appropriately for day-to-day variations in the instrumental response, but, as judged from Table 6.2 this seems not be the case.

Table 6.2 Results from analysis of Seronorm Trace Elements Serum RM. WLSR was applied for the calibration.

Repetition (separate days)	Result ± expanded uncertainty (coverage factor, k = 2)
1	131 ± 11
2	145 ± 3
3	106 ± 4
4	143 ± 7
Reference value (± 2SD)	130 ± 10

After seeing these results, the ICP-MS and the sample introduction system were thoroughly checked for clogging, unstable sample flow and other factors that might have disturbed the measurements. In addition, performance checks for precision, sensitivity, oxides, etc. were conducted regularly, and the response of the internal standard was monitored continually during the measurements. We could identify no errors or signs of reduced instrumental performance. Hence, it was found that the measurements had not been compromised, and consequently we could not justify rejection of any results as outliers. We therefore concluded that the measurement uncertainty was underestimated.

6.3.3 Pooled calibrations

In view of the above observations, we abandoned the uncertainty estimates based on single-day calibrations and applied instead an alternative method of pooled calibrations, which has previously proven useful for a variety of analytical techniques at our laboratory: ICP-MS [10], ETAAS [322], UV/Vis spectroscopy [323], gas chromatography-MS [324, 325] and ion chromatography [326]. In an attempt to explain and predict the spread of the sample results by exploiting the long-term variation in the calibration data, all of the calibrations and RM data were collected and pooled into one single dataset. The determination of ^{86}Sr in the Seronorm serum RM is used again as an example. ^{86}Sr was chosen because the abundance of this isotope allows for measurement in a reasonably wide concentration range (up to 200 μg L^{-1}) without producing intensities that saturate the pulse stage of the detector. The high abundance of the most abundant isotope, ^{88}Sr, resulted in pulse stage saturation already at 15 μg L^{-1}.

The serum RM was analysed through a period of approximately four weeks. During this time a total of 13 sets of calibration data were recorded. The graph shown in Figure 6.2 was produced by collecting all this calibration data and calculating a single calibration function using ordinary least-squares regression. An estimate of the predicted uncertainty of the Sr determination was then calculated from this calibration line, using equation (6-5). In this case, $u(I_{Sr}/I_{Rh})$ for the sample was estimated from the pooled calibrations using equation (1-4). This led to a standard uncertainty estimate of ±10.5 μg L^{-1} Sr for the serum RM analysis. It should be noted that the pooled calibration can only be used for uncertainty calculations and not for determining the concentration of the RM.

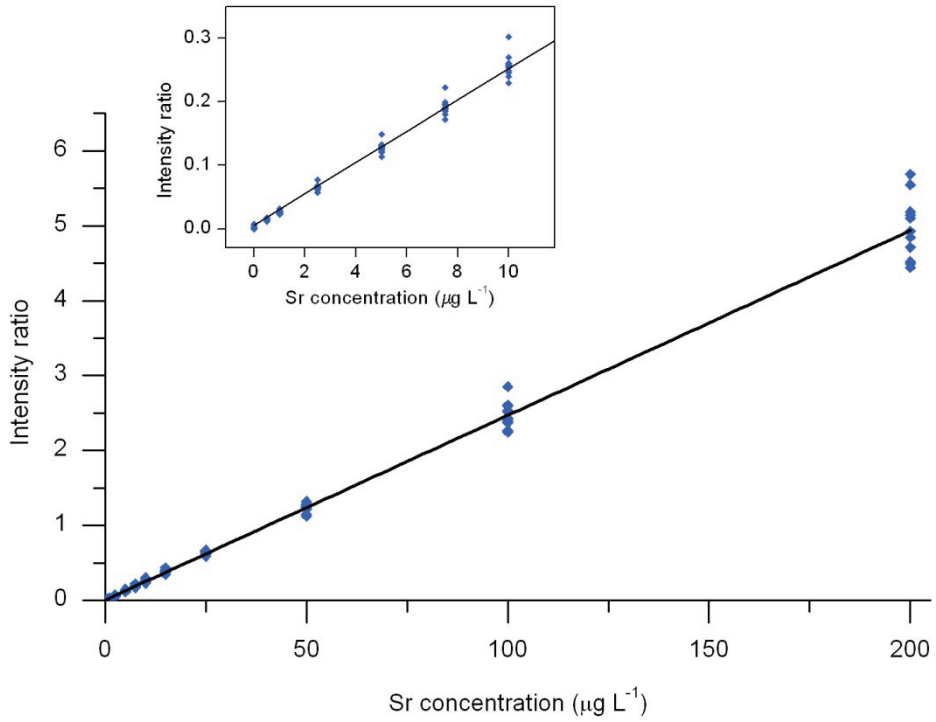

Figure 6.2 Pooled calibration data recorded during a period of four weeks. A single calibration function was calculated from all the data. The Sr intensities were normalised using an internal standard of 5 µg L^{-1} Rh.

The uncertainty estimate was evaluated by comparing it with the SD of the results from the individual serum measurements:

$$SD(C_{Sr}) = \sqrt{\sum_{i=1}^{n} \frac{([C_{Sr}]_i - \overline{C_{Sr}})^2}{n-1}} \qquad (6\text{-}7)$$

where C_{Sr} is the Sr concentration found by each individual analysis. The SD of the individual determinations was determined as ±11.2 µg L^{-1} Sr.

The results of the RM analyses are summarised in Table 6.3, showing excellent correspondence between the uncertainty estimate calculated from the pooled calibrations and the observed SD of the 20 individual determinations. Conversely, the uncertainties calculated from the single-day calibrations were often underestimated compared with the observed variation. Figure 6.3 presents a control chart showing the individual results and uncertainties together with the reported concentration range of the RM. The mean of the 20 measurements was 134 µg L^{-1}, which is within 1 SD of the reference value. The chart shows that three of the results are in disagreement with the reported concentration, when the individual

uncertainties were applied. However, as no experimental or instrumental errors had been identified, it was considered incorrect to reject these results. Instead, pooled data were applied to obtain a better estimate of the measurement uncertainty.

Table 6.3 Results, standard uncertainties (SU), standard deviations (SD) and relative uncertainty/deviation (RSU/RSD) for determination of Sr in Seronorm Serum RM.

	Result (μg L^{-1})		*RSU/RSD (%)*
Range of individual determinations (result ± SU)	106.1 – 152.4	(±3.2) – (±10.1)	2.0 – 7.1
Combined individual determinations (mean ± SD)	133.7	±11.2	8.4
Pooled calibrations (SU)	-	± 10.5	7.8
Reported concentration	130	5	3.8

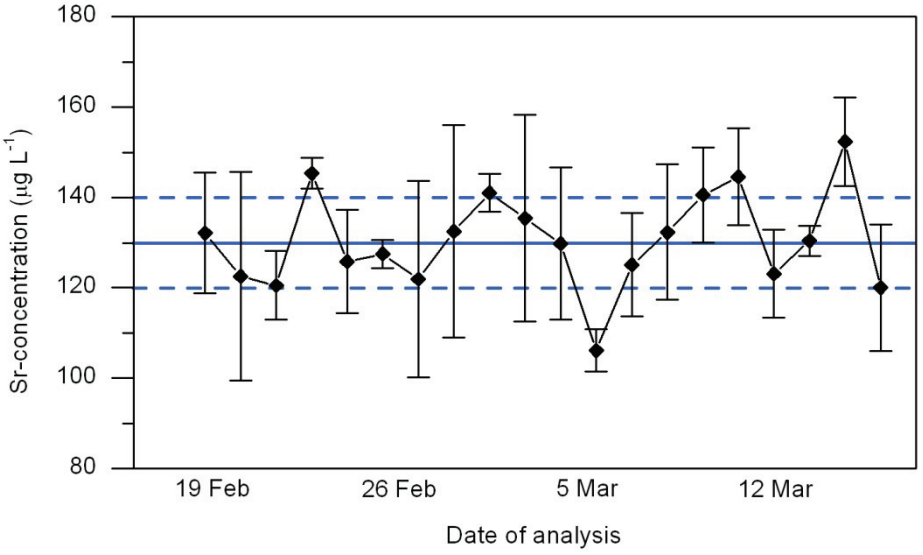

Figure 6.3 Control chart of 20 determinations of Sr in a serum CRM. Error bars show expanded uncertainty (k =2). Blue lines indicate the reported concentration (solid) and 2 standard deviations. The mean and SD of all the repetitions were determined as 133.7 ± 11.2

The mean value of the 20 Sr measurements was in very good agreement with the reported value, demonstrating that the accuracy of the analysis was satisfactory. The determinations of Ca and Mg also showed good accuracy and a good correspondence between the predicted and observed variation (Table 6.4). As described in Chapter 5, the determination of serum P suffered from very poor accuracy due to an unidentified interference.

For the analysis of calcified tissues described in the following chapters, a bone meal reference material was used for quality control. As with the serum RM, the observed SD of the analytical results was seen to be larger than the uncertainties that were predicted by applying single-day calibrations in the uncertainty budget. The method of pooled calibrations was therefore also applied for measurements of this RM; the results are summarised in Table 6.4. Generally, the SDs of the individual bone meal measurements were slightly lower than predicted by the pooled calibration data, but the correspondence was found to be very good for the purpose of the analysis. For both serum and bone, the determinations of Mg, P and Ca showed considerably higher SDs than the Sr determinations. This is due to the higher occurrence of interferences at the low masses (cf. Table 5.3, p 71).

Table 6.4 Analytical results, standard uncertainties (SU), standard deviations (SD) and certified/reported values for the reference materials Seronorm Serum and NIST bone meal.

Seronorm Trace Elements Serum	Sr (μg L^{-1})	Mg (mg L^{-1})	P (mg L^{-1})	Ca (mg L^{-1})
Individual determinations (mean ± SD)	134 ± 11	31.5 ± 8.6	108 ± 31	120 ± 22
Pooled calibrations (± SU)	± 11	± 9.0	± 13	± 20
Reported value / range (mean ± SD / 95% conf. int.)	130 ± 5	27.3 – 32.2	39 – 44	108 – 126
NIST 1486 Bone meal	Sr (μg g^{-1})	Mg (mg g^{-1})	P (mg g^{-1})	Ca (mg g^{-1})
Individual determinations (mean ± SD)	269 ± 14	4.58 ± 0.30	122.8 ± 9.3	265 ± 27
Pooled calibrations (± SU)	± 19	± 0.61	± 13	± 40
Certified value (mean ± expanded uncertainty)	264 ± 7	4.66 ± 0.17	123.0 ± 1.9	265.8 ± 2.4

Figure 6.4 shows a control chart of 63 determinations of Sr in the bone SRM. The average of the analyses was within the expanded uncertainty of the certified value, and it was concluded that the measured concentration was in agreement with the certified value. Similar conclusions were reached for Mg, P and Ca the in the bone SRM (Table 6.4).

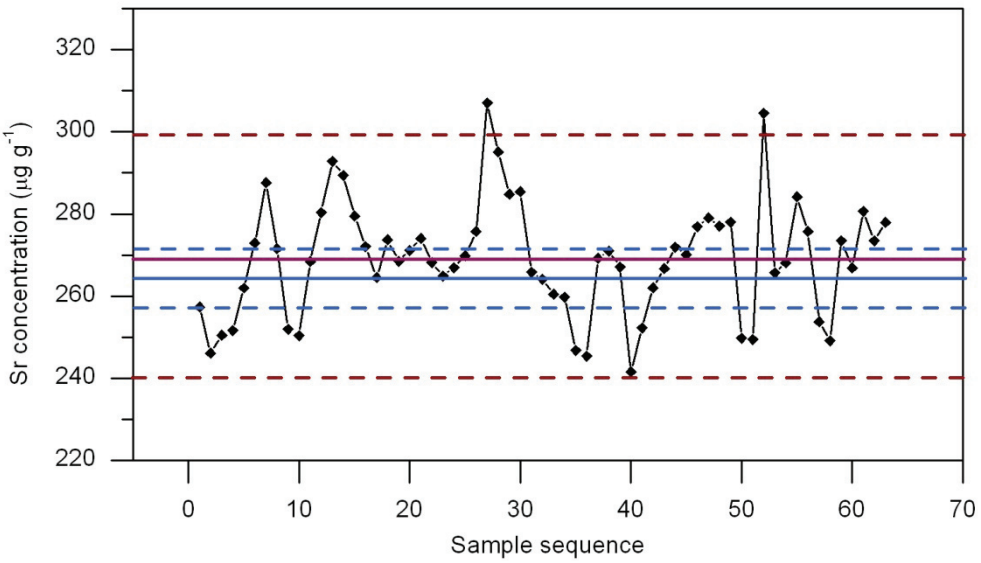

Figure 6.4 Control chart of 63 determinations of Sr in NIST Bone meal. Blue lines indicate the reported concentration (solid) and the expanded uncertainty (dashed) of the SRM. The red lines indicate the mean (solid) and 2SD (dashed) of all the determinations.

Based on these findings it was concluded that the pooled calibration data provided a reliable and realistic uncertainty estimate of the analysis. Consequently, this method was used for determining the measurement uncertainty for ICP-MS analysis of serum, bone and tooth samples.

6.3.4 LLA

Pooling all calibration data allows for calculation of the lower limit of analysis (LLA) [322, 323]. The LLA value is defined as the lowest concentration that can be determined from the pooled calibrations with an uncertainty of less than 50%. The LLA is given by

$$\mathrm{LLA} = \frac{1}{\alpha}\sqrt{\frac{s_{blank} + s_{\beta}}{2}} \qquad (6\text{-}8)$$

where s_{blank} is the SD of a series of blank measurements, s_β the SD of the intercept of the pooled calibration function and α is the slope. The LLAs for the most abundant analyte isotopes are shown in Table 6.5. For comparison, the limit of quantification (LOQ) was also calculated using the common $10 \cdot s_{blank}$ formula. The LLA exceeds considerably the LOQ for all analytes, in particular for Sr and Mg, where a difference of respectively three and one orders of magnitude is seen. This shows that using the instrumental LOQ as a basis for deciding the lowest quantifiable

concentration may lead to very large measurement uncertainties at concentrations below the LLA. According to the pooled calibrations, analysis is not feasible at Sr concentrations below 0.69 µg L^{-1}, strongly contradicting the manufacturer's specifications (ELAN 6000 without Apex: LOD < 1 ng L^{-1} Sr).

Table 6.5 LLA and LOQ (10σ) for the Apex-ICP-MS analysis.

	Concentration (µg L^{-1})			
	^{88}Sr	^{24}Mg	^{31}P	^{44}Ca
LLA	0.69	0.88	18	26
LOQ	0.02	0.08	4	11

As the variance of the instrumental response depends on the analyte concentration (cf. Figure 6.1), it is worthwhile investigating how the relative measurement uncertainty changes with the concentration. Figure 6.5 shows that the uncertainty generally decreases with increasing concentration, attaining values of <10% at concentrations above 5 µg L^{-1}. As a consequence, it may be suggested that samples should not be diluted to a Sr concentration below 5 µg L^{-1}, if the uncertainty associated with the ICP-MS analysis is desired to be less than 10%.

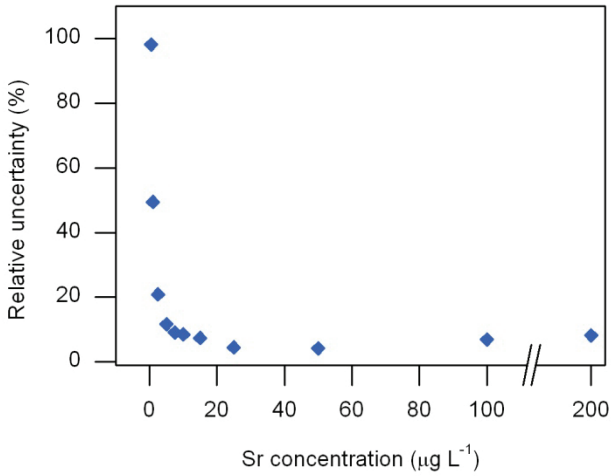

Figure 6.5 Relative uncertainty estimate calculated by equation (6-5) vs. the Sr concentration.

6.4 Sampling

6.4.1 Theory of sampling

Generally, the purpose of taking samples is to collect a smaller, manageable portion of the material of interest, which can then be used to describe the original material. Hence, the sample should be *representative* of the material. Procedures and

theoretical background for obtaining representative samples are included in the Theory of Sampling (TOS), which was introduced and developed by Gy [327]. Detailed explanations about the fundamental aspects of TOS are beyond the scope of this text but can be found in the literature [327-330]. It will merely be mentioned that, in TOS terms, a *correct sampling procedure* means that all constituent elements of the original material have an even, non-zero, probability of being selected. This is called the *Fundamental Sampling Principle* (FSP), which can never be compromised if a representative sample is to be obtained. The need for developing a correct sampling procedure for this project arose as the results from the first animal study showed that Sr was very heterogeneously distributed in the bones (cf. Appendix II). The variance associated with sampling (TOS: *sampling error*) is caused by the existence of heterogeneity, and representativity is therefore closely linked to heterogeneity.

6.4.2 Sampling for bone and teeth analysis

After the 4-week dog study, mid-sections of the femurs were sent to our laboratory for analysis (Figure 6.6). These bones were too large to be digested whole, and sampling was therefore required. A cleaned bone was submerged in liquid nitrogen for an hour, placed in a plastic bag and fractured with a hammer. The bone pieces were then dried at 110°C for five hours. The dried fragments were spread out on a piece of weigh-paper and a suitable amount of bone was collected by taking out pieces at random with a pair of tweezers. These bone pieces were then weighed and digested.

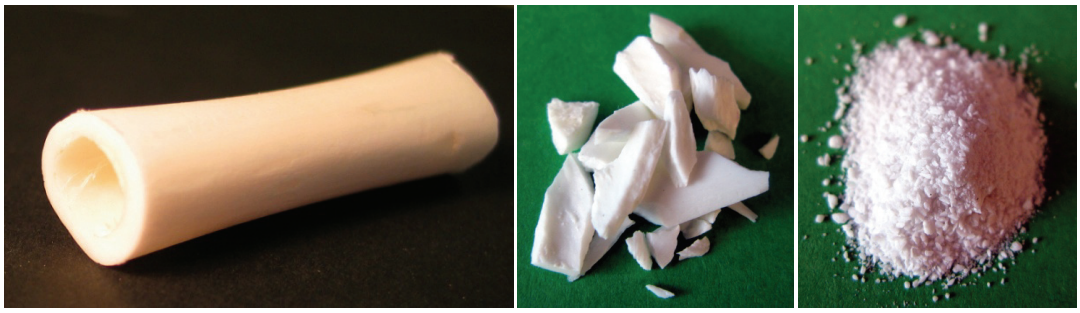

Figure 6.6 Photos of the cleaned mid-shaft of a femur (left), the large bone pieces from fractionating the femur with a hammer (middle) and the small bone pieces after 2 min of grinding (right). Notice the large size difference of the bone pieces in the middle picture.

Because of the large size difference between the bone pieces (Figure 6.6), all bone material did not have equal probability of being selected, the probability being close to zero for the smallest bone pieces. This was a violation of the FSP. By taking several subsamples from the same femur, it was confirmed that the variance of the Sr

concentration in these samples was much too large to be explained exclusively by the analytical uncertainty (Figure 6.7).

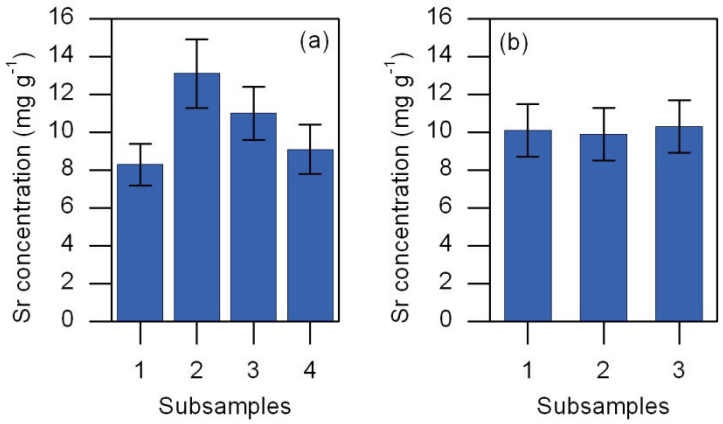

Figure 6.7 Analytical results from repeated sampling of a femur from an animal treated with 3000 mg kg^{-1} day^{-1} SrM for 4-weeks. The charts illustrate the sample heterogeneity after fractionation using a hammer (a) and an analytical mill (b). Error bars show the expanded uncertainty according to the uncertainty budget.

Consequently, it was concluded that the applied sampling procedure was not representative and had to be improved. With the principles of TOS in mind, it was necessary to 1) reduce the heterogeneity of the primary sample (the whole femur) before taking subsamples and 2) to observe the FSP. This was achieved by applying an analytical mill to reduce the grain size of the bone pieces. The sampling procedure was therefore changed to include 2 min of grinding of the bone pieces. After the grinding, the mill was left to stand for a few minutes, in order to allow the finer particles to settle. The bone powder was then carefully poured out in a thin line on a weigh-paper, in effect making all the bone material accessible for sampling. Increment samples were taken by passing a folded piece of thin paper through the line, while making sure that each increment covered the whole cross-section of the material. In TOS, such a design is known as 1-dimensional sampling. The increments were collected, weighed and transferred to the digestion vessel, thus creating a representative composite sample.

6.5 Conclusion

This chapter has demonstrated that the measurement uncertainty associated with determination of Sr using ICP-MS was often underestimated when applying WLSR to calibration data obtained on a single day. To account for the observed variation in the analytical results, calibration data from many different days were pooled into one data set. The uncertainties predicted by these combined calibrations were in very

good agreement with the observed variation in the RM results. This new principle of processing calibration data successfully provided a satisfactory estimate of the measurement uncertainty related to the ICP-MS analysis, ensuring reliable determinations of the analytes of interest. The analytical procedure showed excellent accuracy for all analytes in the bone CRM and for Sr, Mg and Ca in the serum RM.

Substantial differences between the LOQ and LLA were observed, and it was suggested that the LLA is a useful parameter for estimating the lowest concentration at which a sample can be reliably measured. Thus, analysis between the LOQ and the LLA cannot be expected to provide reliable results.

Exploiting the concepts of TOS, a new sampling procedure reduced the sampling error related to the collection of subsamples from bone and teeth. This was accomplished by decreasing the heterogeneity of the sample through a substantial reduction in the average particle size, and through a thorough mixing of the sample material. Additionally, the FSP was observed by ensuring that all sample material was equally accessible for sampling.

CHAPTER SEVEN

Influence of strontium on mineral composition in rats after 26 weeks of treatment with strontium malonate

7.1 Introduction

This chapter presents a 26-week study on the effects of strontium malonate (SrM) treatment on teeth, bone and serum in rats. Concentrations of Sr, Mg, Ca and P in incisors and femur were determined using ICP-MS, and bone mineral density (BMD) of femur and vertebrae was measured using DEXA. The ICP-MS analyses were performed in collaboration with Søren R. Sørensen [10], MSc. The BMD measurements were performed by Dr. Jens-Erik Beck Jensen, MD, at Hvidovre Hospital.

As described in Chapter 2, the incorporation of Sr happens faster in newly formed mineralised tissue than in old. In humans, there is an almost complete absence of remodelling of the dentine matrix, and the propensity for incorporation Sr is therefore very small in adult humans. The situation is different in rodents, as rodent incisors are open-rooted and continue to erupt and grow throughout life [331, 332]. It was therefore expected that rat incisors would be suitable indicators for SrM's ability to make Sr available for incorporation in calcified tissues. Femur bone was chosen for comparison because the mid-shaft of the femur is purely cortical and therefore has a relatively low turnover rate.

7.2 Experimental

7.2.1 Animals

7.2.1.1 Study design

The experiment was performed in 80 male and 80 female SPF Wistar rats of the strain HanTac:WH (GALAS) from Taconic M&B A/S, Ejby, Denmark. The in-life part of the study was conducted at LAB Scantox, Ejby, Denmark under GLP conditions. At the start of the acclimatisation period, the rats were approximately 5 - 6 weeks old. An additional 20 animals (10 of each sex) were available until completion of the acclimatisation period for replacement purposes. An acclimatisation period of 22 days was allowed in order to reject animals in poor condition or at the extremes of the weight range and to allow animals to adjust to the housing conditions and recover from any adverse effects induced by the transport. On the day of arrival, the animals were allocated randomly to 4 treatment groups and a group of extra animals, using a randomisation scheme. Prior to commencement of treatment, 11 animals were re-allocated in order to reduce possible differences in average body weight between the groups [333].

Table 7.1 Design of 26-week study of strontium malonate treatment in rats.

Group	SrM dose (mg kg^{-1} day^{-1})	SrM dose formulation (mg mL^{-1})	No of animals	
			Males	Females
1	0	0	20	20
2	100	20	20	20
3	300	60	20	20
4	1000	200	20	20

7.2.1.2 Treatment

The vehicle for preparation of the dose formulation was 0.5% carboxymethyl cellulose (0.5% CMC). The vehicle was prepared with de-ionized water for all treatment groups. The dose formulations were prepared by suspending SrM in the vehicle. The animals in Group 1 (control) were treated with vehicle (0.5% CMC). The animals in Groups 2, 3 and 4 were treated respectively with 100, 300 and 1000 mg strontium malonate per kg body weight per day, corresponding to 46, 138 and 460 mg $kg^{-1}day^{-1}$ Sr^{2+}. All animals were weighed upon arrival, on the day of re-allocation, on the first day of treatment (Day 1) and weekly thereafter. The daily dose was given by oral gavage according to the most recent body weight data, and the dose volume was 5 ml per kg body weight [333].

7.2.1.3 Diet and drinking water

A complete pelleted rodent diet "Altromin 1314" (for growing animals) was available *ad libitum* until Day 49 of the dosing period. On Day 50 and throughout the remaining part of the study, the animals were offered *ad libitum* "Altromin 1324" (for adult animals). Altromin was supplied by Chr. Petersen, Ringsted, Denmark. The animals had free access to bottles with domestic quality drinking water acidified with hydrochloric acid to pH 2.5 in order to prevent microbial growth. Analyses for relevant possible contaminants were performed regularly on the drinking water prior to acidification [333].

7.2.1.4 Collection of blood samples

In week 26 blood samples were taken from all animals (approx. 750 µl) for clinical pathology assessment. Blood samples were drawn from the orbital venous plexus during CO_2/O_2 anaesthesia. The samples were analysed for Mg, Ca, P and bone specific alkaline phosphatase (BSAP) on a Hitachi 902 automated clinical chemistry analyser by a commercial accredited laboratory. Two additional sets of blood samples for determination of strontium in serum were collected halfway through the study (week 13) and at the end of the study (week 26). 2 and 24 hours after Sr administration, 0.5-0.6 ml blood from orbital venous plexus was taken from 96 animals during CO_2/O_2 anaesthesia. After 30-60 minutes the collected blood was centrifuged (10 minutes, 1270 G, 20°C) and the serum stored at -18°C. The serum samples were analysed by a commercial accredited laboratory [333].

7.2.1.5 Collection of bone and teeth samples

A piece of the lumbar vertebral column (L_2-L_4), the left femur, and a tooth (front incisor) was removed from each animal. The tissue samples were stored in suitable plastic containers at -18°C until analysis. Incisors from all animals as well as 24 femurs (3 males and 3 females from each group) were analysed for concentrations of Mg, P, Ca and Sr.

7.2.2 Densitometry

Bone densitometry measurements were performed on cleaned and dried femur and vertebra samples, using a Lunar PIXImus DEXA scanner designed especially for small samples. The femur samples were scanned once each for quantitative measurements of bone mineral content and density.

7.2.3 ICP-MS analysis of bone and teeth

7.2.3.1 Equipment and reagents

The chemicals used were of at least p.a. grade. The samples were digested with 65% nitric acid (Merck Suprapur), 30% hydrochloric acid (Merck Suprapur) and 35% hydrogen peroxide (Riedel de Haën p.a.) in an Anton-Paar Multiwave 3000 microwave oven. Ultra-pure water (18.2 MΩ·cm, Milli-Q Plus, Millipore) was used throughout. All applied glassware was cleaned in 4 M HNO3 at 80°C for 40 min in an automatic acid washer (Miele). Measurements were performed using a Perkin-Elmer ELAN 6000 ICP-MS equipped with a cross-flow nebuliser. The parameter settings are presented in Table 7.2. Instrument control and data collection were performed using the software supplied with the instrument (ELAN v. 3.3 Patch 6), while the data processing for calibration and analysis was carried out by exporting the raw data to external software (Microsoft Excel®, Origin® and Minitab®). The ICP-MS was allowed to stabilise for 30 min before analysis was commenced. The analytical performance (sensitivity, precision, oxides and doubly-charged ions) was checked using a standard solution containing 10 µg L-1 Be, Mg, Ca, Rh, In, Ba, Ce and Pb.

Table 7.2 Settings on the ELAN 6000 ICP-MS.

RF power	1000 W
Nebuliser argon flow	0.95-1.0 L min^{-1}
Sample flow	0.480 mL min^{-1}
Working pressure	$1.8 \cdot 10^{-3}$ Pa
Background pressure	$2.4 \cdot 10^{-4}$ Pa
Torch box temperature	40-43 °C
Lens voltage	7.5-8.75 V
Pulse detector voltage	1500
Detector mode	Pulse
Sweeps pr. reading	10
Scan mode	Peak hopping
Readings pr. replicate	1
No. of replicates	3
Dwell time pr. mass	100 ms
Measured isotopes	^{24}Mg, ^{25}Mg, ^{26}Mg ^{31}P ^{42}Ca, ^{43}Ca ^{84}Sr, ^{86}Sr, ^{87}Sr, ^{88}Sr ^{103}Rh (internal standard)

7.2.3.2 Standards

Standards were prepared in 0.1 M NHO_3 (Merck, Suprapur) by dilution of two multi-element stock standard solutions (1000 mg L^{-1} Sr PlasmaCAL, SCP Science; P/N 4000 ICP-MS ICS solution A, CPI International). A total of 20 standards

containing concentrations of 1 µg L^{-1} to 5 mg L^{-1} of all analytes were used. 10 µg L^{-1} Rh (Fluka) was added to all standards and samples for internal standardisation.

7.2.3.3 Cleaning procedure

Nitrile gloves were worn at all times when handling undigested biological samples. Tools and lab bench were cleaned with ethanol and water at the end of each working day. The tooth and bone samples were stored at -18°C until analysis. The first step in the preparation was to heat the samples for 4-5 min in a standard domestic microwave oven at a low power (270W). This eased the following removal of soft tissue, which was carried out using a stainless steal scalpel. The samples were then submerged in 35% H_2O_2 (Riedel de Haën, p.a.) for 10 min, and washed with ethanol and copious amounts of ultra-pure water. Any remaining lean tissue, periosteum, cartilage or marrow was removed with a scalpel and water, and the incisors were separated from the jaw (Figure 7.1). The samples were dried at 110 °C for 2 hours and cooled to room temperature in a dessicator before being weighed (Mettler AE 260 DeltaRange) and transferred to a quartz vessel (Figure 7.2a) for digestion.

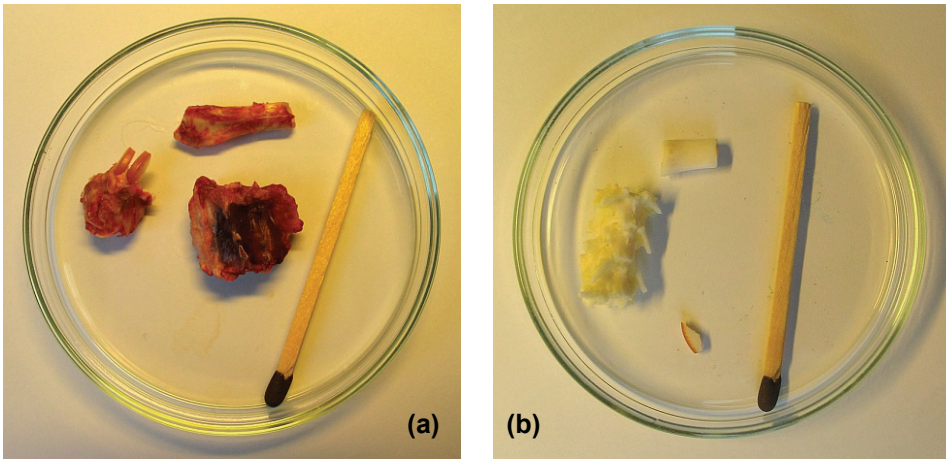

Figure 7.1 Photographs of femur, lumbar vertebral column (L_2-L_4) and tooth from 26-week rat before (a) and after (b) the cleaning procedure.

7.2.3.4 Digestion

The samples were dissolved by microwave assisted high-pressure acid digestion. A rotor with eight quartz vessels (Figure 7.2b) was used, each vessel containing a sample weighing 22-130 mg (incisors) or 120-300 mg (femurs). The digestion procedure is presented in Table 7.3.

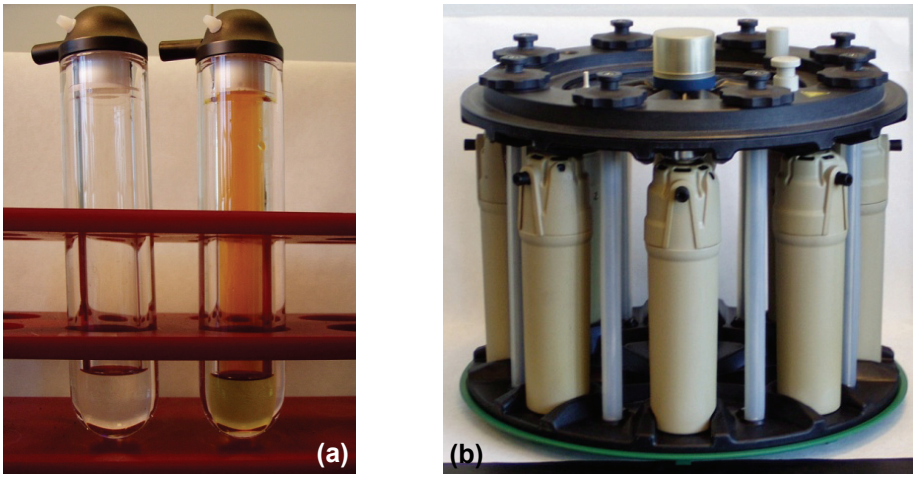

Figure 7.2 Anton-Paar quartz vessels with Teflon cap and digested bone samples (a) and rotor for 8 vessels (b).

Table 7.3 Procedure and chemicals used for digestion of incisor and femur from 26-week rat.

Step	Duration (min)	Power (W)	Chemicals	Volume per vessel (mL)
1 (ramp)	10	$0 \rightarrow 1200$	65 % HNO_3	5
2 (digestion)	10	1200	35% H_2O_2	3
3 (cooling)	20	0	30% HCl	0.5

7.2.3.5 Quality control

The accuracy of the analytical procedure was validated by using the standard reference material NIST SRM 1486 Bone Meal. The material was dried and digested using the procedure described above. The material provides certified values for all elements of interest to this study.

7.2.4 Statistics

Data was processed to give mean values and standard deviations for groups and gender. Each continuous variable was tested for homogeneity of variance using Bartlett's test. If the variance was accepted as homogeneous, analysis of variance (ANOVA) was carried out for the variable. If the ANOVA detected any significant differences, possible inter-group differences were assessed with Dunnett's test (comparing treated groups with a control group). Sr data for both serum and mineralised tissues was invariably heteroscedastic, and the data was therefore log-transformed before analysis. Comparison of regression slopes (OLSR) was performed using analysis of covariance (ANCOVA). If the variance was heterogeneous, each variable was tested for normality by the Shapiro-Wilk test. In

case of normal distribution, possible inter-group differences were identified with Student's t-test. Otherwise the possible inter-group differences were assessed by Kruskal-Wallis's test. If any significant inter-group differences were detected, the subsequent identification of the groups was carried out with Wilcoxon Rank-Sum test. For all tests, the level of significance was defined as $p < 0.05$. Calculations were performed using Minitab®, Microsoft Excel® and Origin®.

7.3 Results and discussion

7.3.1 Cleaning procedure

The initial sampling from the terminated animals was fairly crude, leaving adhering skin, muscles, fat, marrow, etc. on the bones. The purpose of cleaning the samples before analysis was to ensure that the analytical results only reflected the analytes present in the mineralised tissue and not in the surrounding soft tissues. In addition, each incisor had to be separated from the jaw in order to avoid contamination from the jawbone. Because of the high number of samples, the cleaning step was by far the most time-consuming step in the analytical procedure, but it was essential for the purpose of the analysis. Once the samples were cleaned and dried, they could be digested directly without sub-sampling; due to their limited size, whole samples could easily be contained in the digestion vessels.

The validation of the analytical method was performed on bone powder, which had already been cleaned and homogenised by the manufacturer. Consequently, the effect of the initial heating, as well as the cleaning with H_2O_2 and ethanol, was not covered by the validation. There is, however, no reason to presume that these steps introduced significant contamination or loss of analytes. Using a similar procedure, Roberts *et al.* [164] found that the loss of sample in the washing solutions from cleaning of bones with H_2O_2 and ethanol were only of minor importance.

7.3.2 Digestion

The applied digestion procedure has previously been applied for digestion of teeth and femurs from dogs (cf. Appendix II). It was developed using the trial-and-error method and validated using a certified bone material. During the method development, it was observed that inclusion of HCl and H_2O_2 tended to give slightly better recoveries than HNO_3 alone. Digestions without HCl sometimes resulted in cloudy digestion solutions. Similar observations were reported by Oitridge *et al.* [165], who found that use of a mixture (3:1) of HNO_3 and HCl provided a more complete dissolution of bone tissue than a pure HNO_3 solution. H_2O_2 was added in

order to improve oxidation of organic matter. Moreover, inclusion of H_2O_2 resulted in solutions virtually free from nitrous fumes, which eased the subsequent handling.

In the microwave oven, the temperature and pressure in the digestion vessels was monitored continually during the digestion (Figure 7.3). The maximum pressure of 80 bar was reached after about 20 minutes of digestion. At this point, the power was reduced as to maintain the maximum pressure for the remainder of the digestion program. During this time, the temperature continued to rise and reached its maximum level after about 25 minutes. Since NIST suggests that bone powder be digested using HF [186], such a procedure was also tested. This did not result in better recoveries than those obtained with $HNO_3/HCl/H_2O_2$, and, in view of the safety issues of working with HF, the application of HF for digestion of bones was therefore abandoned.

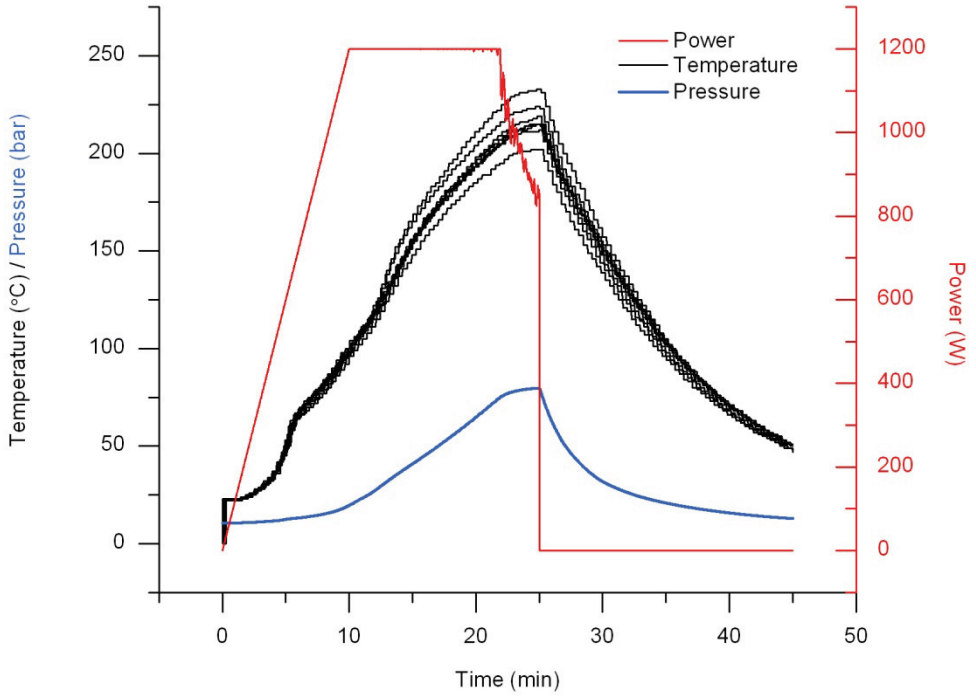

Figure 7.3 Graphs showing temperature, pressure and power during digestion of 8 bone samples. The temperature was measured in each individual vessel by an IR sensor, while the pressure was measured as the combined pressure in all vessels.

7.3.3 ICP-MS analysis

The procedures used to establish optimum values for RF power, gas flow, lens voltage, quadrupole tuning and detector voltage were similar to those described in

Chapter 5. From an analytical point of view, the major differences between the two studies can be summarised in the following points:

1) The digested bone samples contained higher concentrations of Sr than the diluted serum samples and were also available in ample volumes. This allowed for a conventional cross-flow nebuliser to be used for sample introduction instead of the Apex desolvation system.

2) Contrary to the serum samples, all bone and teeth samples were of necessity digested, and therefore all organic macromolecules were completely dissolved. Hence, the problems of tube clogging experienced with the serum samples were non-existent in this study.

3) Another consequence of the sample digestion was an absence of any noticeable non-spectral interferences in this study. Therefore, it was not strictly necessary to include an internal standard for correction of the analyte signals. During the method development, it was observed that application of Rh as IS increased the measurement uncertainty for determinations of Ca, Mg and P, without providing a notable improvement of the accuracy of the CRM analysis. Hence, Rh was used as internal standard for determination of Sr only.

4) The ICP-MS was operated exclusively in pulse mode in this study, whereas the serum samples were measured in dual mode.

7.3.3.1 Quality control

The NIST reference material was analysed at regular intervals and was always included when a series of samples was measured (cf. Chapter 6). Table 7.4 presents a summary of the measured and certified concentrations. There was very good agreement for all analytes.

Table 7.4 Measured (mean ± SD) and reported (expanded uncertainty) values for the serum reference material NIST SRM 1486 Bone Meal.

	Sr (µg L^{-1})	Mg (mg L^{-1})	P (mg L^{-1})	Ca (mg L^{-1})
Found (mean)	269 ± 14	4.58 ± 0.30	122.8 ± 9.3	265 ± 27
Certified value	264 ± 7	4.66 ± 0.17	123.0 ± 1.9	265.8 ± 2.4
Recovery	102%	98.2%	99.8%	99.7

7.3.4 Serum

Serum was sampled in study weeks 13 and 26. Samples were taken at 2 and 24 hours after oral administration, as these times were expected to represent respectively the highest and lowest concentrations of circulating strontium. The mean values of each group are shown in Figure 7.4. Serum Sr increased substantially in each of the treated groups, demonstrating that strontium administered orally as strontium malonate was highly available for absorption into the blood.

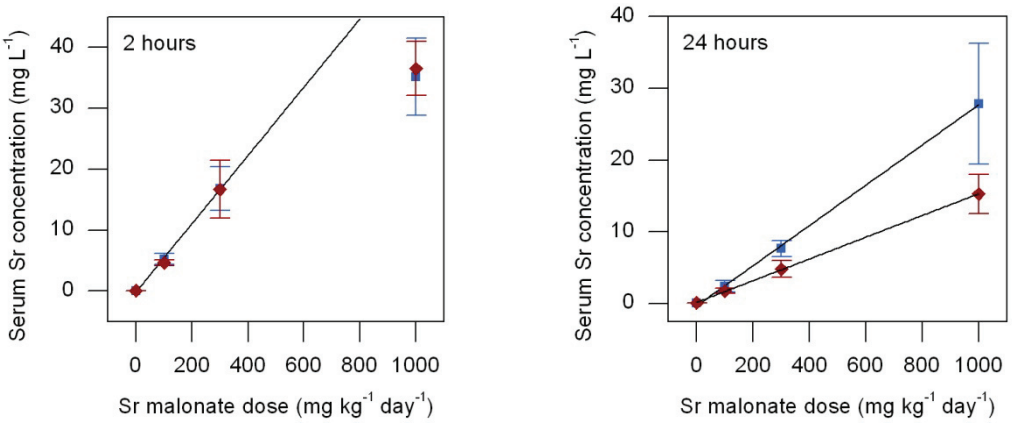

Figure 7.4 Mean serum Sr concentrations (error bars show SD) 2 and 24 hours after administration of Sr malonate for males (■) and females (■). The trend lines indicate linear response to the SrM dose for Groups 1-3 after 2 h and all groups after 24 h). Pooled data for samples taken after 13 and 26 weeks.

The strontium concentration was analysed in a linear model with dose groups, gender, week and time of day as effects. In order to obtain a homogeneous variance, the serum data was log-transformed before analysis. The data analysis showed that dose group, gender, time and study week were all significant ($p \leq 0.001$ for all effects), with interactions between time and dose group, as well as between time and gender. The analysis was therefore performed separately by time and gender. In the control group, overall means and SDs of 71 ± 10 for males and 72 ± 18 for females showed no significant differences between the genders. In order to evaluate whether the absorption of strontium in the blood was linearly related to the administered dose of strontium malonate, the following linear model was formulated:

$$C_{Sr} = \alpha \cdot dose^{\beta} \qquad (7\text{-}1)$$

C_{Sr} is the concentration of Sr in the serum, *dose* is the administered dose of SrM, and α and β are model parameters. If $\beta = 1$, i.e. β is not significantly different from 1, the

relationship between dose and serum Sr is linear. By taking the natural logarithm of both sides of the equation, we obtain

$$\ln(C_{Sr}) = \ln(\alpha) + \beta \cdot \ln(dose) \quad (7\text{-}2)$$

Hence, a test for dose linearity can be performed as a test of the hypothesis H_0: $\beta = 1$ against the alternative hypothesis H_1: $\beta \neq 1$. Linearity was concluded if H_0 was accepted. The analysis showed that 24 hours after administration, dose linearity was accepted ($\beta = 1.02$, p = 0.64) for all treated groups. It was therefore concluded that circulating serum Sr concentrations were proportional to the administered dose at the time of expected minimum Sr concentrations (just before the next dose administration). In contrast, 2 hours after administration, linearity had to be rejected ($\beta = 0.86$, p = 0.001). Figure 7.4 shows that the lack of linearity is caused by the highest dose group, whose serum Sr did not increase proportionally to the dose. This may be an indication that the absorption of strontium at dose levels above 300 mg kg^{-1} day^{-1} was limited by saturation of the gastrointestinal tract.

The bioavailability was found to be higher for males than for females, in accordance with previous reports [39]. In the treated groups, the males showed a significantly higher serum Sr response than females after 24 hours (OLSR slopes: males 28.0 ± 2.2, females 15.1 ± 0.7, $p < 0.001$, ANCOVA). This observation is in contrast to observations in 4-week dog, where Sr administered as SrM had higher bioavailability in females (cf. Appendix II), showing that the test organism can have a profound influence on the clinical conclusions.

Finally, it was observed that the average of all treated groups were 10% lower at week 26 than at week 13, demonstrating that steady-state conditions had been obtained for serum Sr. It is unclear why the serum Sr levels were lower by the end of the study than at week 13, but since the serum was taken from different animals at the two time-points, it may be a result of biological variation between individual animals. It is worth noting that a similar trend was observed in the fracture study described in Chapter 5, where the average serum Sr of the group treated for 3 weeks were higher than for the group treated for 8 weeks (Table 5.8, p 82). However, because of the different time-scale of the two studies, a direct comparison may not be feasible.

The serum was also analysed for Mg, P, Ca and bone specific alkaline phosphatise (BSAP) at the end of the study (Figure 7.5). The concentrations of phosphorous showed opposite trends for the two genders. Serum P was significantly increased for males in Group 3 and 4, while a minor (non-significant) decrease with

dose was observed in the females. Decrease in serum P in mice following short-term Sr treatment has previously been reported [334]. The Mg concentrations were unaffected by the treatment, while Ca concentrations were significantly decreased in the highest dose group for both genders. These observations are in agreement with those of Skoryna and Fuskova [60], who found that after 12 weeks of Sr supplementation (up to 0.34% $SrCl_2$ in the drinking water), no changes in serum Ca and Mg were observed in rats.

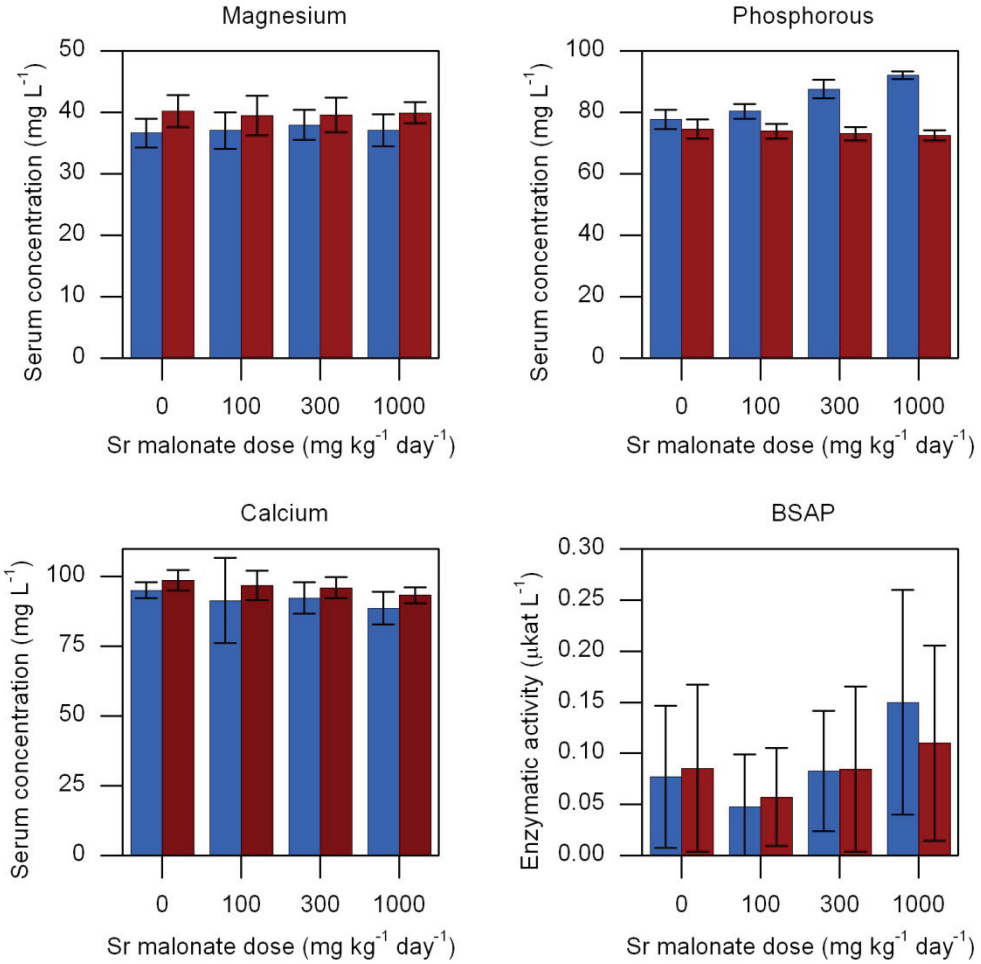

Figure 7.5 Serum levels (mean ±SD) of P, Mg, Ca and bone specific alkaline phosphatase (BSAP) for males (■) and females (■) The unit µkat L^{-1} denotes catalytic activity and is a measure for the amount of enzyme present [335, 336].

BSAP is regarded as a marker for osteoblastic activity [337]. Despite very large intra-group variations, BSAP levels were significantly increased in the highest dose group (Figure 7.5). This indicates a Sr-induced increase in osteoblastic (bone-forming) activity in this group, in agreement with previous reports [115, 120].

7.3.5 Calcified tissues

The results of the ICP-MS analysis are summarised in Tables 7.5 and 7.6. The analysis demonstrated that administration of strontium malonate resulted in a significant, dose-dependent increase in the strontium contents of both incisor and femur. All dose groups showed considerably higher Sr concentrations than the placebo group for both types of tissues. In the incisors, the Sr increased approximately 400 – 500 folds in the highest dose group, while femur Sr increased 280 – 400 folds in this group. The Sr/(Sr+Ca)mol% for the four groups were respectively 0.015, 1.2, 5.8 and 7.7 for incisors, and 0.015, 0.6, 1.9 and 5.0 for femurs. In agreement with previous investigations [39, 73], these observations clearly demonstrate the bone-seeking properties of strontium (cf. Chapter 2). Both incisors and femurs showed significant differences between males and females, with males having the highest degree of Sr incorporation in the treated groups. This difference is apparently linked to differences in the gastrointestinal absorption of Sr, as serum Sr was also higher in males than in females. No gender differences were observed in the untreated control groups.

Table 7.5 Summarised results (mean ± SD) for ICP-MS analysis of incisors from rats treated with strontium malonate for 26 weeks.

	Concentration (mg g^{-1})			
Dose (mg kg^{-1} day^{-1})	Sr	Mg	P	Ca
0 (placebo)	0.103 ± 0.011	20.2 ± 2.8	165 ±16	298 ±57
Males (n=20)	0.104 ± 0.010	21.7 ±2.9	170 ±18	289 ± 60
Females (n=20)	0.102 ± 0.011	18.7 ± 1.6	160 ± 12	306 ± 54
100	6.7 ±1.5	19.0 ± 2.1	156.5 ±8.3	260 ±25
Males (n=20)	7.8 ± 1.3	20.2 ± 1.9	158 ± 10	258 ± 29
Females (n=20)	5.6 ± 0.6	17.9 ± 1.6	154.8 ± 5.5	262 ± 22
300	34 ± 18	18.6 ± 2.9	152.5 ± 6.8	255.3 ±64
Males (n=20)	22.9 ± 3.0	19.4 ± 1.5	159.3 ± 3.8	256.3 ± 9.6
Females (n=20)	17.8 ± 2.0	18.2 ± 1.2	155.3 ± 7.3	263 ± 15
1000	45 ± 11	18.8 ± 2.9	150.8 ± 4.8	243 ± 65
Males (n=20)	51 ± 10	19.0 ± 3.9	149.6 ± 4.9	248 ± 90
Females (n=20)	38.4 ± 8.1	18.6 ± 1.4	152.0 ± 4.4	238 ± 17

For the key apatite elements, Mg, P and Ca, the incisors revealed significant differences between treated groups and placebo, as well as significant gender differences. For Mg and P, the interactions between dose and gender were significant, and the analyses were therefore performed separately by gender. The males showed a dose-dependent reduction in incisor Mg, with significant differences in both the medium and high dose groups compared with placebo. Conversely, the females showed no significant differences between the groups. The males had significantly higher Mg contents than females in all groups. There was a significant loss of P in the highest dose groups for both sexes, but, while a significant loss was

found in all the treated groups in males, the females showed no significant changes in the low and medium dose groups. The opposing trends for Mg and P make it difficult to draw clear conclusions regarding the treatment effect of Sr on these elements. In contrast to P and Mg, Ca showed a clear trend, as Ca concentrations were significantly reduced for both genders in all treated groups as compared with placebo. This observation is in agreement with previous reports of decreasing mineralisation with increasing Sr dose in rats [107, 111].

Table 7.6 Analytical results for ICP-MS analysis of whole femur (n =24) taken from rats treated with strontium malonate for 26 weeks.

	Concentration (mg g^{-1})			
Dose (mg kg^{-1} day^{-1})	Sr	Mg	P	Ca
0 (placebo)	0.0912 ± 0.0050	4.60 ± 0.25	144.1 ± 4.0	280 ± 11
Males (n=3)	0.092 ± 0.010	4.59 ± 0.18	143.6 ± 4.5	277.6 ± 8.5
Females (n=3)	0.0906 ± 0.0049	4.62 ±0.35	144.6 ± 4.3	283 ± 14
100	4.3 ± 1.5	5.4 ±1.3	168 ± 40	341 ± 80
Males (n=3)	5.3 ± 1.4	5.8 ±1.9	181 ± 58	368 ± 116
Females (n=3)	3.2 ± 0.2	5.05 ±0.21	153.7 ± 2.7	313.0 ± 5.9
300	11.3 ± 3.8	4.91 ±0.17	145.1 ± 5.6	274 ± 17
Males (n=3)	14.3 ± 2.7	4.79 ±0.13	141.3 ± 3.2	260.4 ± 6.5
Females (n=3)	8.3 ± 1.0	5.03 ±0.10	148.8 ± 5.1	287.4 ±9.9
1000	31.2 ± 9.6	5.43 ±0.18	148.8 ± 4.5	276.4 ± 6.6
Males (n=3)	37 ± 10	5.53 ±0.62	152.4 ± 1.4	281.5 ± 2.7
Females (n=3)	25.4 ± 4.6	5.33 ±0.22	145.2 ± 3.1	271.2 ± 4.4

Table 7.7 Summarised results for DEXA analysis of femur and vertebrae from rats treated with strontium malonate for 26 weeks. P-values indicate level of significance for the difference between each group and the placebo group (Dunnett's test). The values have not been corrected for Sr content.

Dose level	BMD (g cm^{-2})			
(mg kg^{-1} day^{-1})	Femur		Vertebrae	
0 (placebo)	0.184 ± 0.026		0.134 ± 0.026	-
Males (n=20)	0.187 ± 0.028		0.142 ± 0.025	
Females (n=20)	0.181 ± 0.023		0.125 ± 0.025	
100	0.202 ± 0.027	p = 0.02	0.141 ± 0.023	p = 0.49
Males (n=20)	0.220 ± 0.025		0.149 ± 0.021	
Females (n=20)	0.184 ± 0.015		0.132 ± 0.022	
300	0.207 ± 0.037	p = 0.002	0.164 ± 0.036	p < 0.001
Males (n=20)	0.228 ± 0.033		0.186 ± 0.029	
Females (n=20)	0.185 ± 0.028		0.142 ± 0.028	
1000	0.234 ± 0.042	p < 0.001	0.172 ± 0.041	p < 0.001
Males (n=20)	0.249 ± 0.046		0.190 ± 0.044	
Females (n=20)	0.218 ± 0.031		0.156 ± 0.030	

In femur (Table 7.6), no significant differences in Mg, P and Ca concentrations were observed. The large variation observed in Group 2 (100 mg kg^{-1} day^{-1}) is caused by a single sample from a male, the analysis of which showed much higher concentrations of Mg, P and Ca than the other samples. Suspecting the sample result

to be an outlier, the statistical analysis was performed both with and without the sample, which did not change the primary conclusions. As no gross errors could be identified in the analysis, the sample was included in the reported group means.

The results of the DEXA analysis of femur and vertebrae are summarised in Table 7.7. Except the vertebrae in the low dose group, all groups showed significant increases in BMD compared with placebo.

7.3.6 Clinical observations

The study director reported [333] that the animals in the highest dose group started to show changes in teeth condition after approximately 2 months of treatment, seen as white teeth and rough enamel. All males and 80% of the females in this group had poor teeth condition during the study, and one animal from the high dose group was euthanized due to poor teeth. These observations are in accordance with previous reports of abnormal mineralisation in rat incisor after injection with $SrCl_2$ [332, 338]. The deleterious effects in calcified tissues following administration of high doses of Sr have been tentatively explained as a combination of inhibited calcium metabolism and distortion of the apatite crystal lattice due to displacement of Ca by Sr (cf. section 2.13). The present observations seem to confirm an effect on body levels of Ca, as the highest dose group show a reduced concentration of Ca in serum. This effect may be a combination of inhibited intestinal absorption and increased renal excretion of Ca. The high teeth Sr found in the highest dose group may also indicate that strontium has indeed substituted calcium in the enamel apatite crystal to such a degree that it affects the normal appearance and structure of the teeth. This is further supported by the observation that the animal that must be killed prematurely due to poor teeth condition had the second highest strontium concentration (70 mg g^{-1} tooth) in calcified tissue that has been observed throughout this entire project.

7.3.7 Sampling sites

In accordance with previous reports [39], the amount of Sr incorporated into the mineralised tissues depended strongly on the concentration of Sr in serum. Figure 7.6 shows a clear correlation between serum Sr measured 24 hours after administration and incisor Sr. The OLSR residuals reveal a slight curvature, suggesting a beginning saturation of the incorporation mechanism at the highest serum Sr concentrations.

As described in Chapter 2, Sr is incorporated more efficiently into newly formed HAp than into old. Rodent incisors grow continuously throughout the animal's life, and, considering the long duration of the treatment, the incisors were therefore

expected to incorporate relatively large amounts of Sr into the mineralised matrix. Femur bone was chosen for comparison because of the relatively low turnover rate of the mid-diaphyseal cortical tissue. The relationship between strontium contents in the incisors and femurs is shown in Figure 7.6.

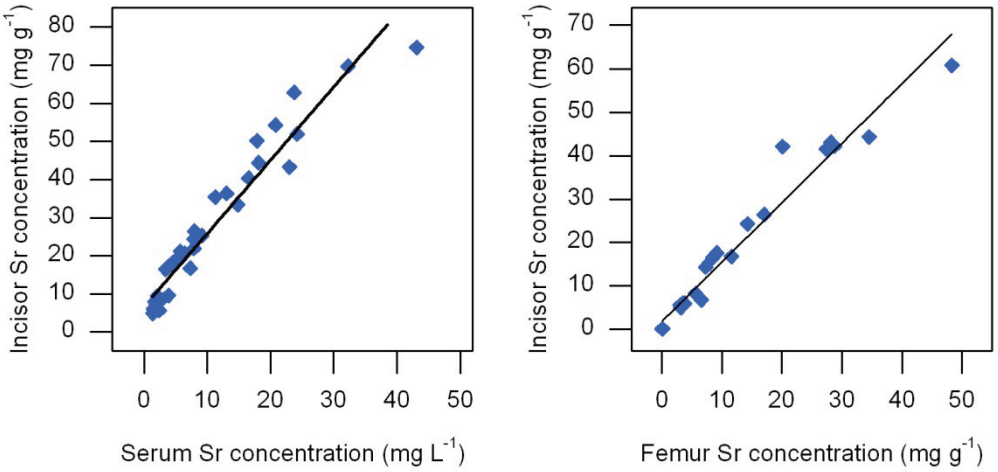

Figure 7.6 Relations between strontium concentrations in incisors and femur (left), and incisors and serum (right) in rats from the three active dose groups. OLSR: IncisorSr = (1.31±0.08)·FemurSr + (1.8 ± 1.1), $r^2 = 0.94$, $p < 0.001$, IncisorSr = (1.92±0.09)·SerumSr + (6.6 ±1.2), $r^2 = 0.93$, $p < 0.001$.

Independent of dose, there was a significant correlation ($p < 0.001$) between the Sr concentrations in the two types of tissue. The slope of the regression line (OLSR) is 1.31 ± 0.08, indicating that Sr is indeed incorporated more efficiently into the constantly growing incisors than into the cortical bone of the femur.

7.3.8 Correction of femur BMD measurements

The observed increase in BMD in the active dose groups was expected to be strongly influenced by the large amounts of strontium deposited in the bones (cf. section 4.3.4). In the 52-week dog study described in Chapter 8, a correction factor was elucidated for the influence of Sr on BMD measurements using a Norland XR-26 DEXA scanner. This correction factor was used as a tentative correction for the PIXImus measurements of the 24 rat femurs in which the concentration of Sr was determined (Figure 7.7). After correction for Sr contents, there was a small but non-significant decrease in BMD in the active dose-groups, confirming that the increase in measured BMD with increasing SrM dose was predominately caused by the associated increase in bone Sr, rather than an actual increase in bone mineralisation. It is reasonable to assume that a similar effect is present in vertebrae, and the BMD increase seen in Table 7.7 must therefore be interpreted with care.

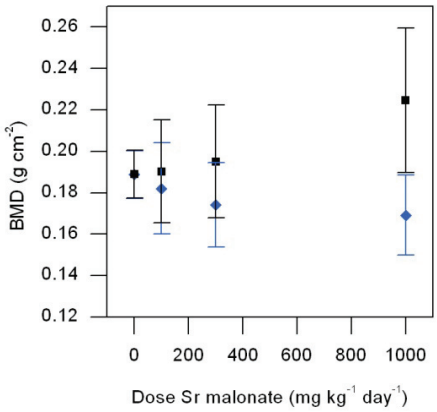

Figure 7.7 Means and SDs (error bars) of measured (■) and corrected (◆) BMD results for rat femur. The correction is approximate, as it was calculated using a different DEXA scanner than the PIXImus used in this study.

7.3.9 A model for incorporation of Sr into hydroxyapatite

The results presented above (Table 7.5, p. 111) seem to indicate that administration of high doses of SrM was associated with decreased concentrations of Ca, Mg and P. However, in the evaluation of the analytical results, it is important to keep in mind that the concentrations are expressed on a weight-to-weight basis. Consequently, the observed reduction in the concentrations of cations may have come about in two ways:

1) An *actual* reduction in the amount of Ca in the apatite crystal lattice, due to replacement by Sr and/or disturbed Ca metabolism.

2) A *perceived* reduction in the Ca/apatite mass ratio, resulting from an increased incorporation or adsorption of strontium in the mineralised matrix. Strontium's high molar mass (88 g/mol) compared with that of calcium (40 g/mol), increases the weight of the hydroxyapatite, which, all other things being equal, will be seen as a reduction in the concentrations of Ca, P and Mg in the dentine.

The latter may lead to an overestimation of the resorption of Ca, P and Mg if large amounts of strontium are incorporated into the mineralised matrix. This point was made already in 1951 by McDonald *et al.* [97], who recognised that a drop in the measured mass ratio of Ca in bone ash might not be due to a decrease in the amount of Ca deposition, but rather to the addition of Sr to the total weight of inorganic matter. Under the assumption that all Ca, Mg, P and Sr found in bone is imbedded in the inorganic apatite matrix, we can formulate a simple substitution model to further investigate this effect (Figure 7.8).

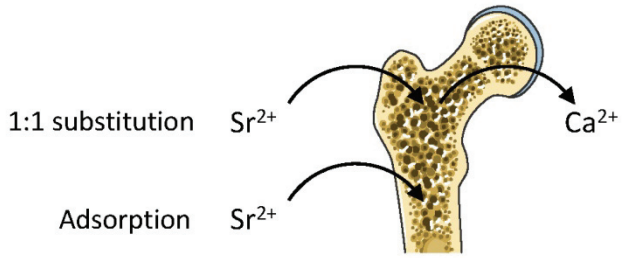

Figure 7.8 Simplified illustration of stoichiometry behind the substitution model, which assumes that apatite Ca is substituted 1:1 by Sr. Alternatively, Sr may be adsorbed without replacing Ca. The figure was produced using Servier Medical Art [78].

Pure hydroxyapatite has the composition

$$\mathrm{Ca_{10}(PO_4)_6(OH)_2} \tag{7-3}$$

As described in Chapter 2, Ca^{2+} in the HAp lattice can be replaced by both Mg^{2+} and Sr^{2+}. The equation for formation of magnesium-strontium-hydroxyapatite (MgSr-HAp) can be written as [339]

$$(10-x-y)\mathrm{Ca^{2+}} + x\mathrm{Mg^{2+}} + y\mathrm{Sr^{2+}} + 6\mathrm{PO_4^{3+}} + 2\mathrm{OH^-} \rightarrow \mathrm{Ca_{10-x-y}Mg_xSr_y(PO_4)_6(OH)_2} \tag{7-4}$$

where x and y represent the degree of substitution by Mg and Sr, respectively. It is assumed that Ca is substituted 1:1 by Sr or Mg. The molecular weight (MW) of the substituted apatite is thus given by

$$MW_{MgSr-HAp} = (10-x-y)MW_{Ca^{2+}} + xMW_{Mg^{2+}} + yMW_{Sr^{2+}} + 6MW_{PO_4^{3+}} + 2MW_{OH^-} \tag{7-5}$$

The coefficients x and y can be expressed in terms of molar ratios (MR) between the substituting ions and the substituted apatite:

$$x = MR_{Mg} = \frac{n_{Mg^{2+}}}{n_{MgSr-HAp}} \tag{7-6}$$

$$y = MR_{Sr} = \frac{n_{Sr^{2+}}}{n_{MgSr-HAp}} \tag{7-7}$$

Similarly, the molar ratio between Ca^{2+} and substituted apatite can be written as

$$10-x-y = \frac{n_{Ca^{2+}}}{n_{MgSr-HAp}} \tag{7-8}$$

The ICP-MS analysis determines the mass ratio between the individual analytes and the dry calcified tissue, e.g. for Sr

$$C_{Sr} = \frac{m_{Sr}}{m_{calcified\ tissue}} \tag{7-9}$$

In order to obtain an estimate, *w*, for the mass ratio between each analyte and MgSr-HAp, the ICP-MS results must be corrected for the contents of organic material in the samples:

$$w_{Sr^{2+}} \equiv \frac{m_{Sr^{2+}}}{m_{MgSr-HAp}} = \frac{1}{HAp-ratio} \cdot \frac{m_{Sr^{2+}}}{m_{calcified\ tissue}} \tag{7-10}$$

Based on the literature [67-69] it was expected that the apatite would constitute 60 – 80% of the total sample weight, depending on the type of tissue. The incisors were expected to contain a higher ratio of HAp than the femurs, because tooth enamel contains very little organic material. In the present calculations, the HAp-ratio was adjusted to give the best fit between the model and the analytical data. Using equations (7-4) and (7-5), the theoretical mass ratio between Sr and HAp can be expressed as

$$w_{Sr^{2+}} = \frac{m_{Sr^{2+}}}{m_{MgSr-HAp}} = \frac{y \cdot MW_{Sr^{2+}}}{MW_{MgSr-HAp}} \tag{7-11}$$

Similarly, the theoretical mass ratios for magnesium, phosphorous and calcium are given by

$$w_{Mg^{2+}} = \frac{m_{Mg^{2+}}}{m_{MgSr-HAp}} = \frac{x \cdot MW_{Mg^{2+}}}{MW_{MgSr-HAp}} \tag{7-12}$$

$$w_{Ca^{2+}} = \frac{m_{Ca^{2+}}}{m_{MgSr-HAp}} = \frac{(10-x-y) \cdot MW_{Ca^{2+}}}{MW_{MgSr-HAp}} \tag{7-13}$$

$$w_{P} = \frac{m_{P}}{m_{MgSr-HAp}} = \frac{6MW_{P}}{MW_{MgSr-HAp}} \tag{7-14}$$

With the mass ratios, *w*, determined experimentally, the molar ratios, *x* and *y*, can be found for each individual sample by combining the above equations, inserting the relevant molecular weights and solving for x and y. Figure 7.9 shows the measured mass ratios of Ca, P and Mg in the incisor hydroxyapatite matrix plotted against the molar ratio of Sr. The lines in the figure represent the theoretical mass ratios as a function of *y* according to equations (7-5) and (7-12) – (7-14). The molar ratio of

Mg, *x*, did not change significantly with the Sr concentrations (*x* was in the range 0.83 – 1.15), and the value used in Figure 7.9 was therefore calculated as an average of all the teeth samples, resulting in $x = 1.03$. The model slopes represent the reduction in mass ratios of Mg, P and Ca solely due to the increase in apatite weight, while the intercepts correspond to the mass ratios in Sr-free apatite. The estimate of apatite content in the samples (equation (7-10)) affected only the intercepts, while it had no effect on the slopes. The figure demonstrates a very good agreement between the proposed model for Sr incorporation and the analytical results, indicating that at least a part of the perceived loss of Ca at high Sr concentrations must be attributed to the added weight of Sr to the apatite matrix.

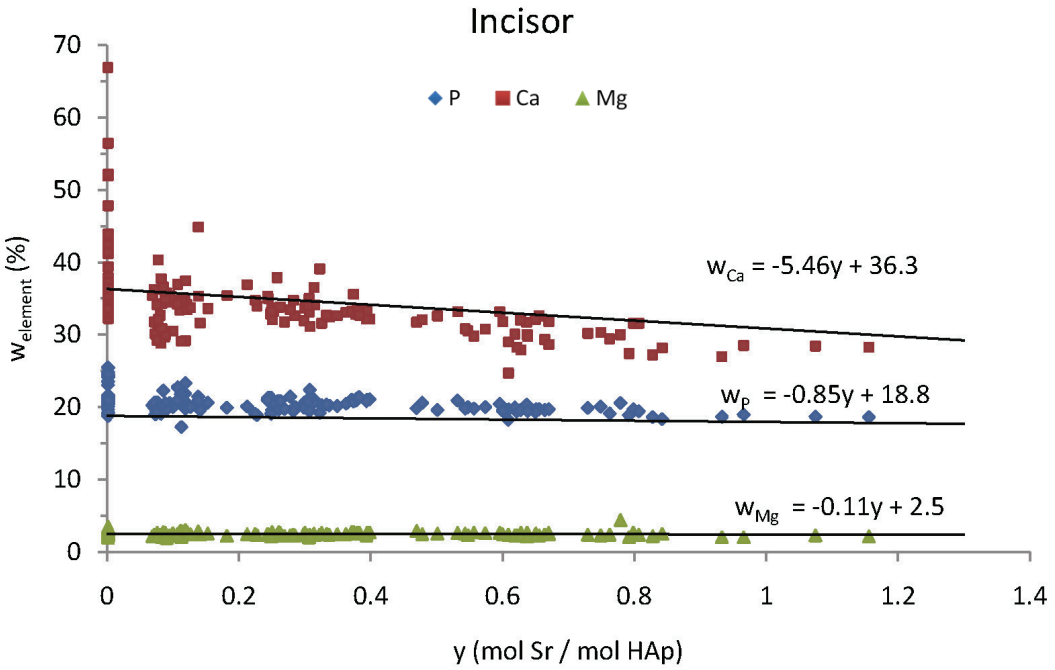

Figure 7.9 Analytical results (data points) and modelled lines (substitution model) for mass ratios of Ca, P and Mg in the hydroxyapatite matrix as a function of the molar fraction of Sr in rat incisor. The best correspondence between model and data was found with a teeth apatite content of 78%. The equations show the slopes and intercepts of the model. The molar ratio of Mg was fixed at x = 1.03 in the model.

In view of the proposed incorporation mechanisms presented in Chapter 2, an alternative model was formulated, in which Sr was assumed to be adsorbed on the mineralised tissue without replacing other divalent ions (cf. Figure 7.8). The calculated slopes and intercepts (using ordinary least-squares regression) from the analytical data and the two models are listed in Table 7.8.

Table 7.8 Theoretical and observed (OLSR) slopes and intercepts for the relationship between the molar ratio of Sr (y) and the mass ratios of Mg, P and Ca in rat dentine apatite. The exchange model assumes that Sr replaces Ca 1:1 in the apatite crystal. The adsorption model assumes that Sr is adsorbed in dentine without replacing other ions. The best correspondence was found with a teeth apatite content of 78%.

	Measured mass ratios	p (slope = 0)	Exchange model	Adsorption model
Mg	(-0.19±0.09) · y + (2.55±0.35)	0.03	-0.11 · y + 2.5	-0.20 · y + 2.5
P	(-2.10±0.37) · y + (21.00±0.14)	< 0.001	-0.85 · y + 18.8	-1.49 · y + 18.8
Ca	(-9.9±1.3) · y + (36.7±0.49)	< 0.001	-5.46 · y + 36.3	-2.88 · y + 36.3

By comparing the slopes given in the table, it is evident that, in theory, apatite adsorption of Sr can account for nearly all the apparent loss of Mg and P in the teeth. A considerable part of the perceived loss of Ca may also be explained by the increased weight of HAp, but even the model based on pure Sr adsorption cannot account for the entire reduction of the Ca content. This suggests that Ca mineralisation has in fact been reduced by the Sr treatment. The reason that Sr affects Ca more than it does Mg and P may be linked to the fact that Ca and Sr share the same transport pathways in the organism, causing competitive inhibition in intestinal absorption and perhaps also in incorporation into apatite.

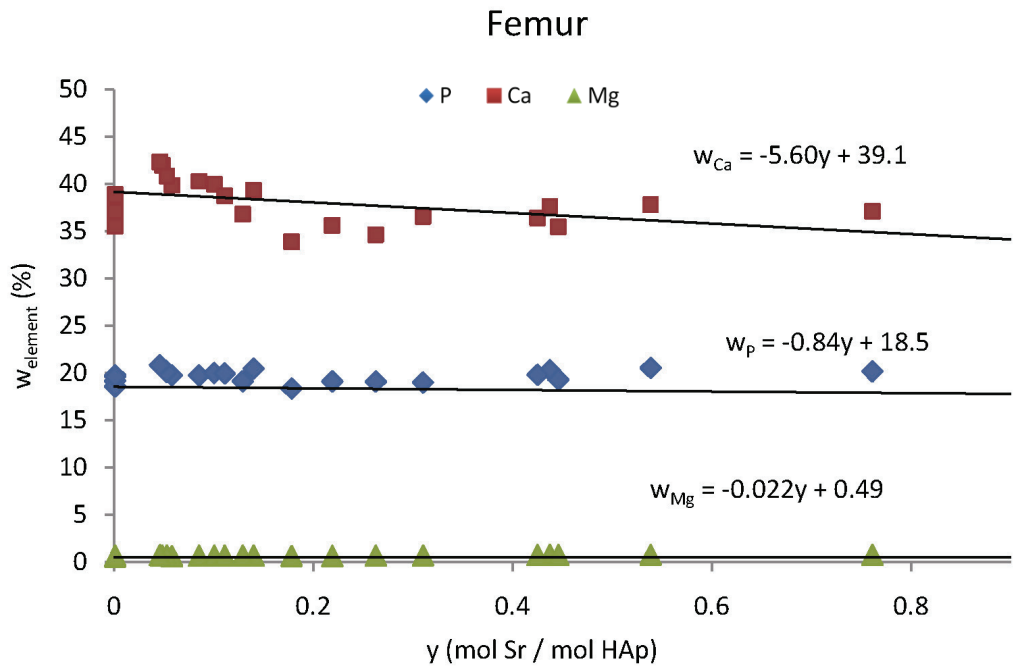

Figure 7.10 Analytical results (data points) and modelled lines (substitution model) for mass ratios of Ca, P and Mg in the hydroxyapatite matrix as a function of the molar fraction of Sr. The best correspondence between model and data was found with a femur apatite content of 72%. The equations show the slopes and intercepts of the model. The molar ratio of Mg was fixed at x = 0.2 in the model.

The substitution model was also applied to the 24 femur samples (Figure 7.10), showing a very good model agreement with an estimated femur HAp content of 72%. However, as described above (Table 7.6, p 112), the administration of strontium induced no significant changes in the concentrations of Mg, P and Ca in femur, and, as a consequence, the slopes calculated from the data points in Figure 7.10 are not significantly different from zero. This may be due to the relatively low number of femur samples.

7.4 Conclusion

This 26-week rat study has shown that strontium administered orally as strontium malonate is highly bioavailable for transport to the blood and for incorporation into calcified tissues. 2 hours after administration, serum Sr increased linearly with the administered dose up to 138 mg kg^{-1} day^{-1} Sr^{2+}. A treatment dose of 460 mg kg^{-1} day^{-1} Sr^{2+} resulted in increases in Sr concentrations of up to 500 and 400 folds in incisor and femur, respectively. Significant gender differences were observed, as Sr had a higher bioavailability in male rats than in females. The incorporation of Sr in the mineralised tissues was strongly correlated with the concentration of Sr in serum.

High doses of Sr reduced Ca concentrations in both serum and incisors, indicating that Sr influenced Ca metabolism and the mineralisation of the dentine tissue. Opposing trends in Mg and P concentrations in both serum and teeth make it difficult to make any conclusive statements on the treatment effect on these elements. Treatment with SrM induced a significant increased in BMD in femur and lumbar vertebrae, but the measurements were much affected by the high Sr concentrations in the bones. After correction for Sr-content, no treatment-related change in BMD was observed in 24 femur samples.

A simple stoichiometric model was proposed for incorporation and adsorption of Sr in hydroxyapatite. The model showed excellent agreement with the analytical data and it was found that the incisors and femurs contained an average of 78% and 72% hydroxyapatite, respectively. Finally, it was demonstrated that at least a part of the perceived loss of Ca in teeth was caused by the adsorption or incorporation of Sr in the teeth apatite.

CHAPTER EIGHT

Mineral composition, bone mineral density and bone strength in dogs after 52 weeks of treatment with strontium malonate

8.1 Introduction

This chapter presents a 52-week study on the effects of strontium malonate on mineral composition, bone mineral density and biomechanical properties of various calcified tissues in dogs. In order to obtain correct BMD results in the Sr-rich bones, the influence of Sr on the DEXA measurements was determined by analysing Sr-doped hydroxyapatite. The effect of strontium malonate treatment on cortical and trabecular bone strength was studied by testing the biomechanical properties of femurs and vertebra biopsies. In addition, structural analysis of the bone samples was performed using extended X-ray absorption fine structure (EXAFS) in order to gain information on the local environment of the Sr-ions in the samples.

8.2 Experimental

8.2.1 Animals

8.2.1.1 Study design

The study was performed in 40 beagle dogs (20 males and 20 females) from Harlan Winkelmann GmbH, Germany. The in-life part of the study was conducted at LAB Scantox, Ejby, Denmark. The first day of treatment was designated Day 1. At the start of the acclimatisation period (Day -5), the animals were approximately 5 to 6 months old with body weights within a range of 8.9 – 14.2 kg for males and 8.1 – 12.0 kg for females. Two extra animals (one of each sex) were available until

completion of the pre-treatment period for replacement purposes. The animals were allocated to 4 groups each consisting of 4 males and 4 females per main study group, and 2 males and 2 females in the recovery groups (Groups 1 and 4). The animals were allocated so as to distribute litter-mates evenly between groups and to reduce inter-group mean body weight differences [340].

8.2.1.2 Treatment

The vehicle for preparation of the dose formulation was 0.5% carboxymethyl cellulose (0.5% CMC). The vehicle was prepared with de-ionized water for all treatment groups. The dose formulations were prepared by suspending SrM in the vehicle. The animals in Group 1 (control) were treated with vehicle (0.5% CMC). The animals in Groups 2, 3 and 4 were treated with 100, 300 and 1000 mg strontium malonate per kg body weight per day, respectively. Treatment of the recovery animals was performed daily for 52 weeks after which a treatment free period of 4 weeks was inserted. The daily dose was given by oral gavage with a dose volume of 5 ml per kg body weight. All animals were weighed upon arrival, one week before start of dosing (Day -7), on the day of group allocation (Day -1) and weekly thereafter. The dose for the following 7 days was calculated on the basis of the most recent weight. At the end of the in-life phase, the animals were killed and subjected to necropsy [340].

Table 8.1 Design of 52-week study of strontium malonate treatment in dogs.

Group	SrM dose (mg kg^{-1} day^{-1})	SrM dose formulation (mg mL^{-1})	No of animals (n) (main study)		No of animals (recovery)	
			Males	Females	Males	Females
1	0	0	4	4	2	2
2	100	20	4	4		
3	300	60	4	4		
4	1000	200	4	4	2	2

8.2.1.3 Diet and drinking water

A commercially available diet (Teklad 2021, Harlan, Blackthorn, England) was offered twice daily (150 g per animal twice daily). From Day 42 the amount of diet was increased to 175 g twice daily. In order to allow the animals a reasonable growth, the amount of diet was further increased on Day 71 to 200 g and on Day 241 to 225 g twice daily. The animals had ad libitum access to domestic quality drinking water. Analyses for relevant possible contaminants were performed regularly [340].

8.2.1.4 Blood sampling

Before start of treatment and during Weeks 13, 26, 39 and 52, blood samples were taken from all animals. Blood samples were drawn from the jugular vein, frozen to -18°C and then analysed at a commercial accredited laboratory [340].

8.2.1.5 Sampling for bone and teeth analysis

The entire right femur, the entire right tibia, the calvaria (skullcap) and a tooth (first molar) as well as lumbar vertebrae L_2-L_4 were dissected from each animal. The bones were dissected free of as much muscular tissue as possible, wrapped in cotton bandage, soaked in isotonic 0.9% NaCl and placed in plastic bags. The samples were stored at -18ºC until analysis.

8.2.2 ICP-MS analysis

The procedure for the ICP-MS analysis was similar to one used for the 26-week study in rats described in Chapter 7. The reader is referred to Chapters 5 - 7 for details on instrument optimisation and validation.

8.2.2.1 Sampling and sample pre-treatment

Sampling of femur and skull samples was performed according to the regions of interest (ROI) selected for the bone densitometry measurements (cf. section 8.2.3). The mid-diaphyseal (mid-shaft) section of femur was sampled at the fracture site of the three-point bending test using a stainless steel saw. Four skull biopsies were sampled from the top part of the skull (Figure 8.1) using a Rochester Bone Biopsy Kit (7 mm i.d.). A skull sample was composed of 3 randomly selected biopsies, each weighing approximately 180 mg. The teeth were removed from the jaw bone using a clamp and a scalpel, the root was separated from the dentine/enamel with a saw, and the pulp was removed.

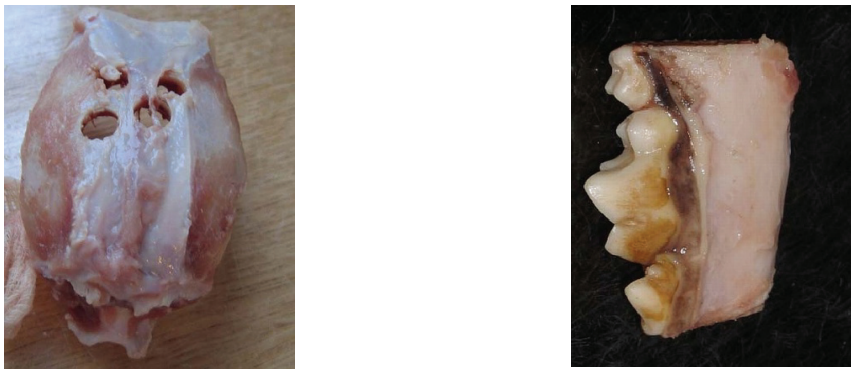

Figure 8.1 Photos of a dog skullcap after sampling of biopsies (left) and a jaw bone before removal of the teeth (right). The first molar is seen as the middle tooth.

Prior to analysis, remaining adhering soft tissue was removed by submerging the samples in 35% H_2O_2 for approximate 30 min, and subsequently placing the sample in an ultrasonic bath for 10 minutes. The samples were then rinsed with ethanol and ultra-pure water. The tooth and femur samples were ground with an IKA A11 analytical mill (cf. Chapter 6) before digestion. All samples were digested in microwave oven as described in Chapter 7.

Vertebra body specimens were produced by first removing the cranial and caudal ends of the L_3 lumbar vertebral body with a low-speed saw. A biopsy of trabecular tissue (5 mm i.d.) was then taken from the vertebral body using a hollow drill, and a specimen for mechanical testing (7 mm high) was produced by cutting the biopsy with a twin circular saw (Figure 8.2)

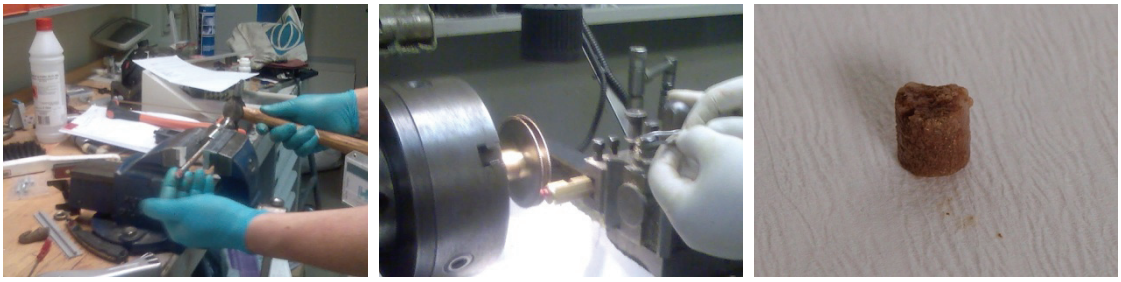

Figure 8.2 Photos of the sampling procedure for producing vertebral body specimens for compression tests. The extracted vertebra biopsy was carefully removed from the hollow drill (left) and cut to uniform height with a twin circular saw (middle), producing a specimen used for mechanical testing (right).

8.2.3 Bone densitometry

8.2.3.1 Calibration

The densitometry measurements were performed using a Norland XR-26 Mark II, X-ray bone densitometer with a pencil beam X-ray source. The instrument is used for routine scanning of patients at Hvidovre Hospital. The scanner performed self-calibration on start-up, and the calibration was verified by scanning a hydroxyapatite phantom. The results of the phantom scans were recorded in order to monitor the long-term stability of the apparatus.

8.2.3.2 Scanning

The samples were scanned using the *Small subjects* mode, with a scan resolution of 1.0 x 1.0 mm and a scan speed of 40 mm s^{-1}. The samples were positioned on a 2-3 cm layer of rice placed on a 5 cm polymethylmethacrylate (PMMA, acrylic glass) block in order to imitate measuring conditions in the presence of soft tissue (Figure 8.3).

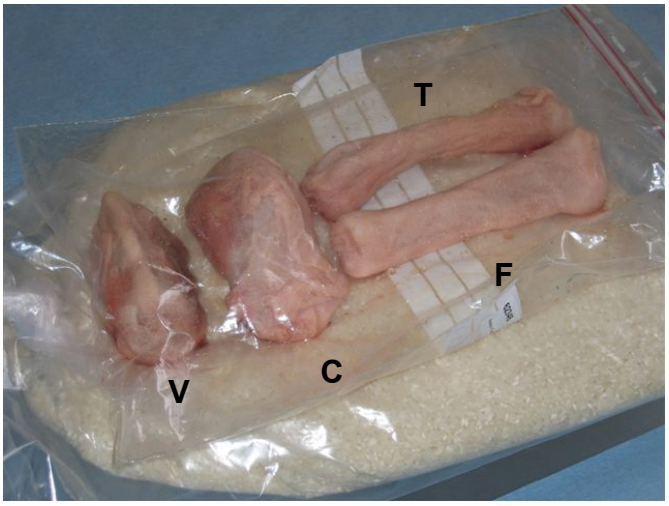

Figure 8.3 Photos of vertebra (V), calvaria (C), tibia (T) and femur (F) positioned for DEXA analysis. The samples were wrapped in sodium chloride soaked cloths to prevent them from drying out. The PPMA plate and the bag of rice were used to simulate soft tissue and provided a useful foundation for positioning the samples.

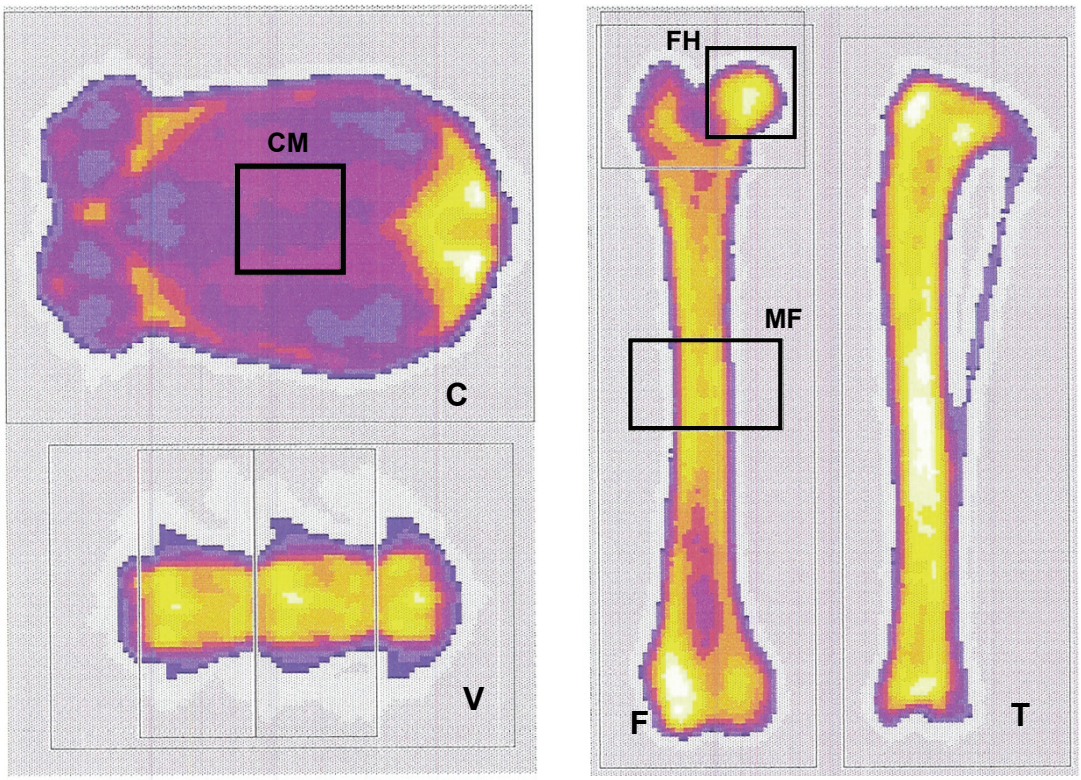

Figure 8.4 DEXA scanning image of vertebra (V), calvaria (C), tibia (T) and femur (F) from dogs. High density areas are shown in light colours and the lower density areas in dark colours. The squares mark selected regions of interest (ROI). The black squares represent ROIs for which BMD is given in Table 8.5: calvaria mid-section (CM), 2 x 3.5 cm; femur head (FH), 2 x 2 cm; mid-diaphyseal femur (MF), 2 x 2 cm. Scan resolution: 1.0 x 1.0 mm.

All samples were scanned in polyethylene bags while frozen, with cloths soaked in 0.9 g L^{-1} NaCl solution wrapped around each bone. In order to obtain adequate resolution when selecting ROIs, each sample set was scanned in two sections, with femur and tibia in one scan and vertebra and skull in another. A background correction was done for each measurement. The selected ROIs are shown in Figure 8.4.

8.2.4 Biomechanical analysis

The biomechanical properties of femurs and vertebra biopsies were evaluated using a material testing machine (Lloyd LR 50K). 24 hours before the measurements, the bones were removed from the freezer, submersed in an isotonic sodium chloride solution (9 g L^{-1} NaCl in sterile water) and allowed to reach room temperature. All specimens were tested in hydrated condition. Femur bone strength was evaluated by a three-point bending test and a bending test of the femur neck. For three-point bending, the femurs were placed on the posterior surface on two bars spaced 75 mm apart, and the load was applied half-way between the bars to the anterior side of the mid-diaphyseal femur. For the bending test of the femur neck, the femurs were sawed in half across the mid-shaft using a stainless steel saw. The proximal half of the bone was fixed by six Allan screws and load was applied laterally to the femur head (Figure 8.5). The compression strength of biopsies taken from the core of lumbar vertebra L_3 was performed by applying a compression load to the biopsy in the longitudinal direction as shown in Figure 4.10, p 54.

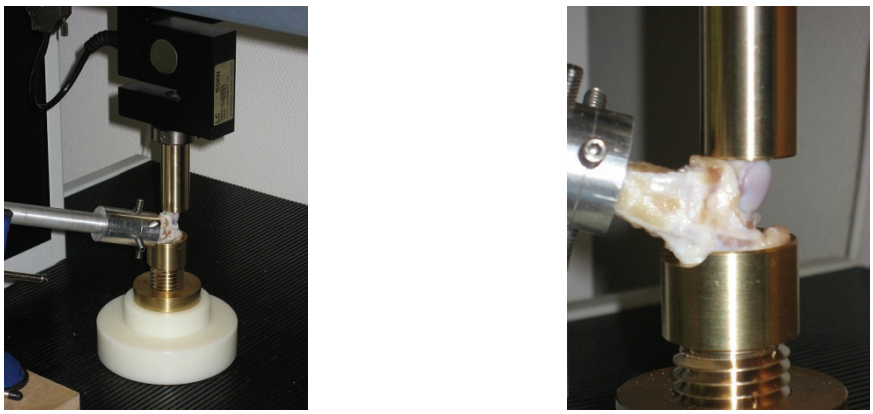

Figure 8.5 Experimental setup for mechanical testing of dog femur neck strength. After sampling from the mid-section

A loading speed of 2 mm min^{-1} and a zero-point load of 50 N were used for all samples. The displacement was measured as the distance travelled by the crosshead. Load-displacement curves were recorded and the maximum load (N), displacement

at failure (mm), stiffness (N/mm) and the energy absorption at failure (J) were calculated as shown in Chapter 4.

8.2.5 Correction of BMD measurements

The influence of Sr on the BMD measurements were assessed by producing six different mixtures of hydroxyapatite in which 0-5% of the Ca atoms were replaced by Sr.

8.2.5.1 Synthesis of Sr-doped hydroxyapatite

White solid crystals of calcium hydroxyapatite (HAp) and hydroxyapatite with approximately 5% (w/w) calcium substituted by strontium (Sr-HAp) were prepared by the method of Kumta *et al.* [341] with minor modifications. The synthesis of Sr-HAp was performed according to the equation

$$9.41Ca^{2+} + 0.59Sr^{2+} + 6PO_4^{3-} + 2OH^- \rightarrow Ca_{9.41}Sr_{0.59}(PO_4)(OH)\ (s) \qquad (8\text{-}1)$$

190 g of trisodiumphosphate, Na_3PO_4, (Sigma-Aldrich) was partly dissolved in 1 L of ultra-pure water. After addition of 15.5 g of sodium hydroxide, NaOH, (Sigma-Aldrich), the suspension was gently heated to approximately 50°C until all material was dissolved. 268 g of calcium chloride dihydrate, $CaCl_2 \cdot 2H_2O$, (Fluka) and 30.4 g of strontium chloride hexahydrate, $SrCl_2 \cdot 6H_2O$, (Fluka) was dissolved in 1 L of ultra-pure water. The solution containing Na_3PO_4 and NaOH was transferred to a large beaker and the Sr/Ca solution was added under vigorous stirring over a time period of six hours. A finely-grained white precipitate was formed and the solution was centrifuged for 5 min at 2000 rpm and flushed 5 times in Millipore water. The powder was heated to 1000°C for 10 hours and allowed to cool to room temperature over 12 hours. The powder was ground in a mortar and the structure was confirmed by X-ray powder diffraction (XRPD).

Figure 8.6 Photo of the PMMA block used for assessing the influence of strontium on the BMD results in Sr-rich bones. The DEXA measurements were performed with the rubber stoppers removed.

The six HAp mixtures were produced by accurately weighing appropriate quantities of pure Ca-hydroxyapatite and the Sr-doped apatite and transferring the powders to holes drilled in PMMA block. The size and of the holes and the amount of Sr-HAp transferred were selected so as to obtain an areal density close to that of the dog bone samples (0.7-1 g cm^{-2}). BMD and BMC was measured in each hole by the same DEXA scanner that was used for the bone analysis. Subsequently, the exact Sr content in each hole was determined using ICP-MS.

8.2.6 EXAFS

EXAFS was performed on skull samples from all active dose groups. Femur samples from the 4-week study in dogs were also analysed by EXAFS. Experimental work and data analysis was performed by Christian G. Frankær and described elsewhere [342].

8.2.7 Statistics

The statistical treatment followed the procedures outlined in Chapter 7.

8.3 Results

8.3.1 Ca in serum

Throughout the study, the concentration of calcium (not shown) was significantly lower for both sexes in the highest dose group (Group 4) as compared with the control group. In addition, the level of calcium was lower for the males in the medium dose group (Group 3) after 39 weeks of treatment and onwards. Although not statistically significant in all cases, the results indicated a dose dependent reduction in the calcium level for both sexes in Group 3 from Week 26 and for Groups 2 and 3 from Week 39 and onwards.

8.3.2 BSAP in serum

The levels of bone specific alkaline phosphatase (not shown) were significantly increased throughout the entire study (Weeks 13, 26, 39 and 52 of treatment) in Group 4 for both males and females. On a few occasions, BSAP had also increased in the lower dosed groups.

8.3.3 Elemental analysis of calcified tissues

The results of the ICP-MS analysis of femur, calvaria and molar are summarised in Tables 8.2 – 8.4 below.

Table 8.2 Results for ICP-MS analysis of mid-diaphyseal femur from dogs treated with strontium malonate for 52 weeks.

	Concentration (mg g^{-1})			
Dose (mg kg^{-1} day^{-1})	Sr	Mg	P	Ca
0 (placebo)	0.078 ± 0.013	3.32 ± 0.37	148 ± 16	328 ± 41
Males (n=4)	0.081 ± 0.016	3.22 ± 0.43	139 ± 17	305 ± 46
Females (n=4)	0.074 ± 0.010	3.43 ± 0.32	156.0 ± 9.9	352 ± 21
100	15.4 ± 5.4	3.47 ± 0.20	132.0 ± 9.8	271 ± 15
Males (n=2)	17.2 ± 6.0	3.45 ± 0.22	131.4 ± 9.9	269 ± 14
Females (n=4)	11.6 ± 0.14	3.52 ± 0.23	133 ± 13	277 ± 19
300	22.7 ± 6.6	3.28 ± 0.46	128.7 ± 7.9	263 ± 25
Males (n=4)	24.0 ± 4.8	3.64 ± 0.33	135.0 ± 5.1	276 ± 11
Females (n=4)	21.5 ± 8.7	2.93 ± 0.21	122.5 ± 3.6	250 ± 29
1000	28 ± 12	3.38 ± 0.52	131.8 ± 9.6	275 ± 26
Males (n=4)	29 ± 14	3.40 ± 0.34	129.7 ± 1.6	265 ± 13
Females (n=4)	27 ± 12	3.35 ± 0.71	134 ± 14	285 ± 34

The treatment with Sr resulted in a marked, dose-dependent increase in Sr concentrations in all the sampled skeletal sites. The highest level of Sr incorporation for all the active dose groups was seen in the skull biopsies, with an approximate 350-fold increase in Sr content in Group 4 compared with the control group. Of the three sample types, the molar showed the lowest Sr contents in all treated groups. The Sr/(Sr+Ca)mol% for the four groups were respectively 0.011, 2.5, 3.8 and 4.4 for femurs; 0.019, 3.3, 4.7 and 6.5 for calvaria and 0.013, 0.75, 1.1 and 1.6 for teeth. In the placebo group, the Sr contents in the different samples were quite similar, with the highest natural levels found in skull. There were no significant differences in Sr content between males and females in any of the analysed tissues.

The concentrations of calcium and phosphorous were significantly reduced in both femur and skull in all treated groups. There was not, however, any differences in Ca and P concentrations between any of the active dose groups. Hence, increasing the SrM dose from 100 to 1000 mg kg^{-1} day^{-1} was not accompanied by a decrease in the Ca and P concentrations.

Table 8.3 Analytical results for ICP-MS analysis of calvaria (skullcap) biopsies from dogs treated with strontium malonate for 52 weeks.

	Concentration (mg g^{-1})			
Dose (mg kg^{-1} day^{-1})	Sr	Mg	P	Ca
0 (placebo)	0.116 ± 0.017	3.29 ± 0.13	141.0 ± 9.8	279 ± 19
Males (n=4)	0.118 ± 0.014	3.34 ± 0.16	148.6 ± 5.5	294 ± 10
Females (n=4)	0.114 ± 0.021	3.23± 0.057	133.5 ± 6.7	263 ± 13
100	19.3 ± 5.2	3.48 ± 0.11	128.0 ± 3.3	253 ± 16
Males (n=3)	22.9 ± 6.7	3.41 ± 0.046	125.6 ± 1.3	243 ± 22
Females (n=4)	16.6 ± 0.76	3.54 ± 0.12	129.8 ± 3.2	260.9 ± 7.6
300	27.4 ± 5.2	3.76 ± 0.16	125.9 ± 3.6	254.3 ± 8.2
Males (n=4)	28.7 ± 4.1	3.81 ± 0.22	124.5 ± 4.9	258.0 ± 6.5
Females (n=4)	26.2 ± 6.6	3.72 ± 0.044	127.2 ± 1.2	250.5 ± 8.8
1000	37.0 ± 8.1	3.48 ± 0.29	125.0 ± 4.8	244 ± 12
Males (n=4)	38 ± 11	3.56 ± 0.31	123.6 ± 5.2	242 ± 17
Females (n=4)	35.7 ± 4.1	3.41 ± 0.29	126.4 ± 4.7	246.4 ± 5.6

In teeth, Ca and P levels were similar in all groups. The concentration of Mg showed conflicting treatment responses. In the highest dose group, the Mg content was increased in skull, decreased in teeth while remaining unchanged in femur. The males had significantly higher concentrations of Mg in teeth than females.

Table 8.4 Analytical results for ICP-MS analysis of molar (dentine and enamel) taken from dogs treated with strontium malonate for 52 weeks.

	Concentration (mg g^{-1})			
Dose (mg kg^{-1} day^{-1})	Sr	Mg	P	Ca
0 (placebo)	0.093 ± 0.027	8.54 ± 0.97	171.1 ± 3.9	340 ± 12
Males (n=4)	0.081 ± 0.06	9.25 ± 0.85	168.4 ± 4.1	332.5 ± 6
Females (n=4)	0.106 ± 0.036	7.82 ± 0.32	173.7 ± 1.0	348 ± 11
100	5.5 ± 1.8	8.6 ± 1.9	178 ± 16	331 ± 49
Males (n=2)	6.2 ± 1.8	9.1 ± 2.2	178 ± 21	336 ± 62
Females (n=4)	4.02 ± 0.010	7.52 ± 0.20	175.9 ± 3.0	320 ± 22
300	7.3 ± 2.0	7.78 ± 0.96	169.9 ± 2.2	309.2 ± 9.2
Males (n=4)	8.4 ± 2.0	8.2 ± 1.3	169.2 ± 2.8	307 ± 11
Females (n=4)	6.3 ± 1.6	7.40 ± 0.26	170.5 ± 1.6	311 ± 8.3
1000	11.6 ± 5.6	6.72 ± 0.71	166.5 ± 6.5	319 ± 10.6
Males (n=4)	11.2 ± 6.0	6.72 ± 0.76	168.4 ± 7.7	326 ± 4.7
Females (n=4)	12.1 ± 6.1	6.71 ± 0.77	164.6 ± 5.5	313 ± 11

8.3.4 Bone densitometry

The results for the densitometric measurements are shown in Table 8.5. The bone mineral density increased significantly with the SrM dose in femur mid-shaft, femur head and lumbar vertebra. In skull, only Groups 2 and 3 showed significant increases in BMD. No gender differences were observed. A large proportion of the BMD increase seen in the active dose groups was expected to be caused by the presence of Sr. The measurements of femur and calvaria were therefore corrected for Sr interference by using the results from the ICP-MS analysis (cf. section 8.4.8).

Table 8.5 Densitometry results for femur mid-shaft, femur head, calvaria (mid-section) and vertebra biopsies taken from dogs treated with strontium malonate for 52 weeks.

Dose (mg kg^{-1} day^{-1})	Bone mineral density (g cm^{-2})			
	Femur mid-shaft	Femur head	Calvaria mid-section	Lumbar vertebra L_3 biopsy
0 (placebo)	0.558 ± 0.018	0.556 ± 0.026	0.38 ± 0.10	0.151 ± 0.014
Males (n=4)	0.562 ± 0.021	0.552 ± 0.033	0.40 ± 0.10	0.145 ± 0.017
Females (n=4)	0.554 ± 0.016	0.560 ± 0.021	0.37 ± 0.10	0.157 ± 0.010
100	0.705 ± 0.082	0.734 ± 0.066	0.528 ± 0.087	0.186 ± 0.022
Males (n=2)	0.766 ± 0.094	0.777 ± 0.037	0.548 ± 0.098	0.168 ± 0.011
Females (n=4)	0.674 ± 0.067	0.713 ± 0.070	0.513 ± 0.090	0.194 ± 0.023
300	0.792 ± 0.095	0.845 ± 0.057	0.59 ± 0.12	0.219 ± 0.037
Males (n=4)	0.769 ± 0.040	0.867 ± 0.034	0.529 ± 0.14	0.223 ± 0.030
Females (n=4)	0.82 ± 0.13	0.823 ± 0.072	0.640 ± 0.091	0.215 ± 0.047
1000	0.712 ± 0.076	0.789 ± 0.083	0.504 ± 0.054	0.215 ± 0.032
Males (n=4)	0.700 ± 0.021	0.752 ± 0.040	0.53 ± 0.036	0.201 ± 0.049
Females (n=4)	0.72 ± 0.11	0.83 ± 0.11	0.473 ± 0.066	0.225 ± 0.010

8.3.5 Biomechanical measurements

The results for the biomechanical measurements are presented in Tables 8.6 – 8.8. The three-point bending test revealed a significant decrease in maximum load in the highest dose group. There was a slight but non-significant increase in the maximum load in Groups 2 and 3. Maximum displacement and work was not recorded for this test. The bending test of the femur neck showed significantly lower maximum force and absorbed energy in the highest dose group, similarly to the three-point bending test. The vertebra biopsies showed no significant differences between the groups for any parameters. No gender differences were observed.

Table 8.6 Biomechanical results for three-point-bending test of dog femur. M: males, F: females

	Dose (mg kg-1 day-1)			
	0 (placebo)	100	300	1000
Max force (kN)	2.81 ± 0.38	3.06 ± 0.35	3.08 ± 0.40	2.28 ± 0.44
Males	3.01 ± 0.30	3.30 ± 0.47	3.14 ± 0.44	2.17 ± 0.36
Females	2.62 ± 0.38	2.94 ± 0.27	3.01 ± 0.41	2.39 ± 0.54
No. of animals	M: 4, F: 4	M: 4, F: 4	M: 4, F: 4	M: 4, F: 4

Table 8.7 Biomechanical results for femur neck bending test.

Dose (mg kg-1 day-1)	Max force (kN)	Max displacement (mm)	Work (J)
0 (placebo)	1.70 ± 0.24	3.6 ± 0.6	4.8 ± 1.2
Males (n=4)	1.76 ± 0.32	3.5 ± 0.5	4.9 ± 1.8
Females (n=4)	1.63 ± 0.15	3.7 ± 0.6	4.67 ± 0.63
100	1.65 ± 0.19	3.9 ± 1.0	5.0 ± 1.1
Males (n=2)	1.56 ± 0.19	5.1 ± 0.1	6.29 ± 0.15
Females (n=4)	1.69 ± 0.19	3.3 ± 0.6	4.34 ± 0.46
300	1.74 ± 0.28	4.3 ± 0.6	4.9 ± 1.3
Males (n=4)	1.77 ± 0.35	4.2 ± 0.6	5.1 ± 1.6
Females (n=4)	1.71 ± 0.24	4.3 ± 0.6	4.6 ± 1.0
1000	1.29 ± 0.35	3.7 ± 0.6	3.2 ± 1.3
Males (n=4)	1.06 ± 0.36	3.6 ± 0.5	2.48 ± 0.58
Females (n=4)	1.52 ± 0.16	3.9 ± 0.8	4.0 ± 1.5

Table 8.8 Biomechanical results for compression test of vertebra biopsies.

Dose (mg kg-1 day-1)	Max force (kN)	Max displacement (mm)	Work (J)
0 (placebo)	0.93 ± 0.29	0.39 ± 0.06	0.60 ± 0.20
Males (n=4)	1.07 ± 0.24	0.45 ± 0.04	0.68 ± 0.17
Females (n=4)	0.89 ± 0.14	0.37 ± 0.05	0.60 ± 0.13
100	0.69 ± 0.28	0.63 ± 0.29	0.56 ± 0.27
Males (n=2)	0.42 ± 0.24	0.64 ± 0.47	0.29 ± 0.11
Females (n=4)	0.82 ± 0.20	0.63 ± 0.26	0.69 ± 0.20
300	0.82 ± 0.37	0.43 ± 0.12	0.65 ± 0.36
Males (n=4)	0.75 ± 0.34	0.41 ± 0.11	0.59 ± 0.28
Females (n=4)	0.89 ± 0.43	0.45 ± 0.14	0.71 ± 0.47
1000	0.72 ± 0.30	0.43 ± 0.13	0.57 ± 0.28
Males (n=4)	0.57 ± 0.34	0.42 ± 0.15	0.51 ± 0.32
Females (n=4)	0.87 ± 0.18	0.44 ± 0.11	0.65 ± 0.24

8.4 Discussion

8.4.1 Ca and BSAP in serum

The treatment effects on serum Ca and BSAP were similar to those observed in 26-week rat (Chapter 7). As previously described, the decrease in serum Ca in the active dose groups is most probably due to inhibited intestinal absorption of Ca. The increase in BSAP indicates that treatment with SrM stimulated osteoblastic activity. A similar trend was seen in 4-week dog, where a significant correlation between serum BSAP and bone Sr was observed (Fig. 2, Appendix II).

8.4.2 Effect of treatment time on Sr-incorporation

As described in Chapter 2, the duration of treatment is an important factor for determining the amount of Sr incorporated into bone. In the 4-week study in dogs, Sr-concentrations increased up to 95 fold in femur and 30 fold in molar after treatment with up to 3000 mg kg^{-1} day^{-1} SrM. Although the administered doses were lower in the present study, it was expected that the much longer treatment time would allow more Sr to be incorporated into the mineralised matrix. This is confirmed by comparing results for groups that received the same dose of SrM in the two studies (Table 8.9). When the treatment time was increased from 4 to 52 weeks, the Sr concentration in cortical bone increased approximately 3 fold. The relatively high levels of bone Sr seen after only 4 weeks of treatment seems to confirm that Sr is incorporated firstly by an initial rapid mechanism, which is eventually saturated, followed by a second, slower mechanism (cf. section 2.12).

Table 8.9 Comparison of Sr-concentrations in dog femur after 4 and 52 weeks of SrM treatment [11].

Treatment time	Administered dose (mg kg^{-1} day^{-1})	
	300	1000
4 weeks	7.2 ± 1.7 mg g^{-1}	9.5 ± 2.7 mg g^{-1}
52 weeks	22.7 ± 6.6 mg g^{-1}	28 ± 12 mg g^{-1}

8.4.3 The effect of skeletal site on Sr-incorporation

As previously mentioned, the amount of Sr incorporated into mineralised tissue is largely determined by the rate of bone turnover. In dogs, the highest levels of Sr incorporation were seen in calvaria, as all active dose groups had significantly higher average Sr concentrations in the skullcap than in femur and teeth. These findings are

most likely related to the structure of the cranial bone. In contrast to the purely cortical femur shaft, the calvarial bone consists of three layers: the *outer table* and the *inner table* are both made up by cortical bone, while the middle layer (*the diploë*) is made up by trabecular bone [343]. The higher Sr concentration in the skullcap biopsies may then be explained by the higher remodelling rate of trabecular bone compared with that of cortical bone [39], resulting in a more efficient incorporation of Sr .

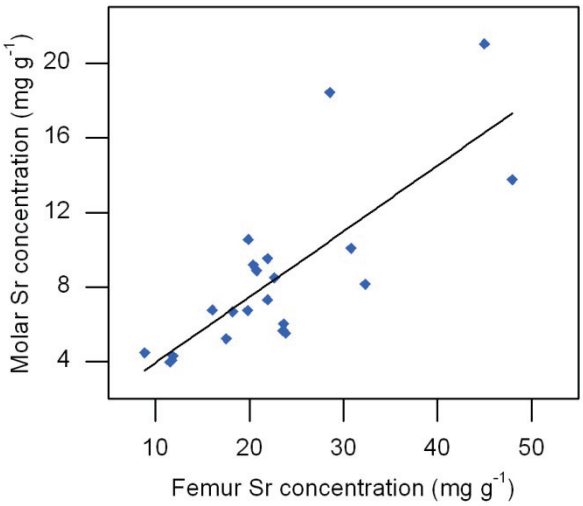

Figure 8.7 The plot shows a significant correlation between Sr concentrations in femur and molar. The slope of the line (OLSR) is 0.35 ± 0.06. $r^2 = 0.059$, $p < 0.001$.

In both the short-term and the long-tern study in dogs, the incorporation of Sr was much lower in teeth than in bone. In the 52-week study, the content of Sr in teeth was on average one third of the femur Sr content (Figure 8.7). This is in accordance with the lower remodelling rate of teeth in dogs compared with that of bone. The trend was opposite in rats (Figure 7.6, p 114), where the level of incorporation was significantly higher in teeth than in femur, reflecting the continuous modelling (growth) of rodent incisors [331].

8.4.4 Substitution model

The substitution/adsorption model that was developed for Sr incorporation in bone and teeth in Chapter 7 was also applied to the data in this study. Figure 8.8 shows the analytical data together with the modelled relationships between the molar ratio of Sr and the mass ratios of Mg, Ca and P. For both tissues, the substitution model showed a good agreement with the analytical values. The parameters for substitution and adsorption are presented in Table 8.10, demonstrating that a considerable proportion of the observed reduction in the concentrations of Ca and P

in these tissues (cf. section 8.3.3) is caused by the increased weight of the apatite matrix following incorporation of heavier Sr ions. As was the case in the rats, however, the model does not seem to account for all of the reduction in Ca and P, which suggests that the mineralisation of Ca and P was affected by the Sr treatment. The best fit was found by letting 70% of the bone weight be made up by apatite in the model. The data for teeth were fitted best using an apatite ratio of 85%, corresponding well to the high apatite content of enamel. While dentine and bone contains similar amounts of HAp, fully mature enamel contain up to 99% HAp, reflecting the increased demand for hardness in teeth [344].

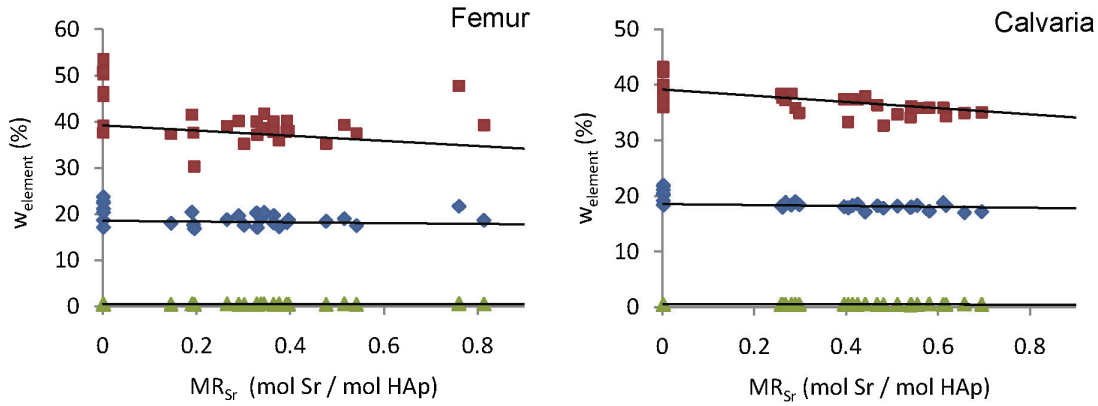

Figure 8.8 Analytical results (points) and modelled lines for mass ratios of Ca, P and Mg in the hydroxyapatite matrix as a function of the molar fraction of Sr in dog femur and calvaria. The best correspondence between model and data was found with a bone apatite content of 70%. The equations show the theoretical slopes and intercepts of the model. The molar ratio of Mg was fixed at ML_{Mg} = 0.21 in the model.

Table 8.10 Theoretical and observed (OLSR) slopes and intercepts for the relation between the molar ratio of Sr (y) and the mass ratios of Mg, P and Ca in dog bone apatite. The substitution model assumes that Sr replaces Ca 1:1 in the apatite crystal. The adsorption model assumes that Sr is adsorbed in the tissue without replacing other ions. The best correspondence was found with a bone apatite content of 70%. The molar ratio of Mg was set at MR_{Mg} = 0.21 for calvaria and MR_{Mg} = 0.20 for femur.

	Measured mass ratios	p (slope = 0)	Substitution model	Adsorption model
Femur				
Mg	(0.065±0.047) · y + (0.460±0.017)	0.18	-0.11 · y + 2.5	-0.038 · y + 0.48
P	(-2.9±1.5) · y + (20.11±0.53)	0.066	-0.85 · y + 18.8	-1.46 · y + 18.5
Ca	(-9.7±4.3) · y + (43.4±1.5)	0.032	-5.46 · y + 36.3	-3.08 · y + 39.1
Calvaria				
Mg	(0.051±0.35) · y + (0.48±0.010)	0.12	-0.023 · y + 0.51	-0.041 · y + 0.51
P	(-3.75±0.61) · y + (19.89±0.26)	< 0.001	-0.84 · y + 18.6	-1.46 · y + 18.5
Ca	(-8.1±1.3) · y + (39.67±0.57)	< 0.001	-5.60 · y + 39.1	-3.08 · y + 39.1

8.4.5 EXAFS

X-ray absorption spectroscopy was used for analysis of femur samples from 4-week dog, skull samples from 52-week dog and Sr-doped HAp. The EXAFS spectra, *X(k)*, are shown in Figure 8.9 together with the modulus of the Fourier transform of *X(k)*. The latter gives information on the radial distribution of electronic density around an average Sr atom, which can be used to identify different coordination spheres around Sr. By comparing the radial electron distribution functions from bone and Sr-doped HAp, it is observed that the coordination shells occur at similar distances, *R*, from the absorbing Sr atom, indicating that Sr has similar local environments in bone and Sr-doped HAp. This demonstrates that some Sr was incorporated into the bone hydroxyapatite lattice by substitution of Ca.

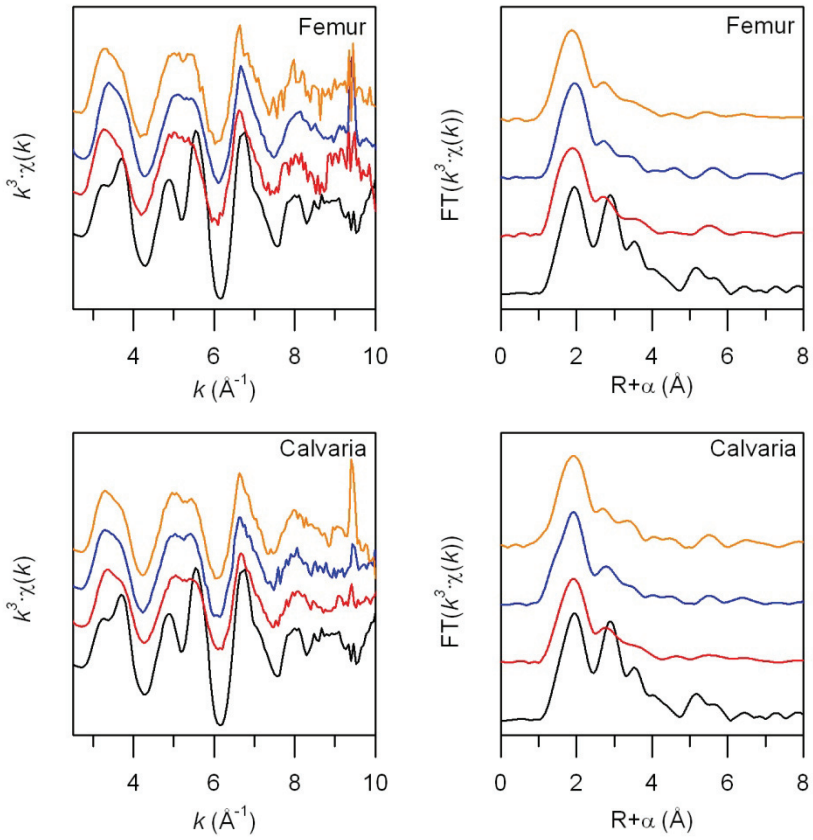

Figure 8.9 Background subtracted and k^3-weighed EXAFS functions, *X(k)*, (left) and radial electron density distributions given as the modulus of the Fourier transform of *X(k)* (right) for 4-week dog femur and 52-week dog calvaria. The figures show data for samples taken from the high dose groups (orange), medium dose groups (blue), low dose groups (red) and 5% doped Sr-HAp (black).

Within the apatite lattice, the Sr atoms are highly coordinated and expected to be very tightly bound compared with Sr atoms bound to e.g. collagen outside the apatite structure. Such loosely bound Sr will result in a dampening of the EXAFS signal. Seeing that the spectra for bone samples have lower amplitudes than the spectrum for Sr-doped HAp, this suggests that some Sr is coordinated to other materials than HAp. This is supported by the radial electron distribution functions for the bone samples, which have a higher relative height for the first peak than the Sr-doped HAp, indicating a coordination of Sr to other material at distances around 2.5 Å. This distance is close to an average Sr-O distance, suggesting that Sr may be coordinated to oxygen atoms in collagen or water in addition to the apatite coordination.

The spectra for the bone samples all look very similar, showing that the local environments for Sr are similar in all cases. Thus, the local chemical coordination of the Sr ions in the bones was largely independent of dose, type of bone and treatment time. The peak heights (amplitude) of the EXAFS spectra increased with increasing dose, demonstrating that more Sr was incorporated into the bone apatite with increasing Sr dose [342].

8.4.6 Biomechanical measurements

Previous studies have shown that strontium treatment improved bone strength in femur and vertebra in healthy rats [119] and in healed, previously fractured, tibiae in osteoporotic rats [121]. In this study, strontium's effect on the biomechanical properties of cortical and trabecular bone was assessed by testing the strength of femurs and vertebrae. The mainly cortical femoral mid-shaft was subjected to a three-point bending test, while the trabecular bone in the core of the vertebral body was tested by compression. The femoral neck was tested by a bending test. This site contains both cortical and trabecular tissue and is a frequent site of fracture in osteoporotic patients [345]. The data for the biomechanical measurements was analysed by plotting load-displacement curves and recording the maximum load, maximum displacement and absorbed energy (cf. section 4.4). Figure 8.10 shows an example of a load-displacement curve for a three-point bend test.

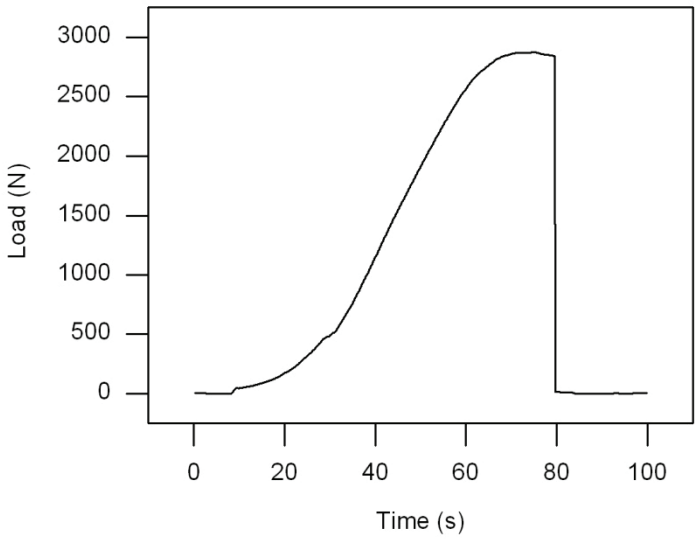

Figure 8.10 Example of a recorded load-displacement curve for three-point bending test of dog femur. The highest point on the curve was taken as the load-to-failure value.

The measurements all showed very large intra-group variances, which, in combination with the relatively low number of samples, made it difficult to identify treatment effects. It was attempted to normalise the results with respect to the size (weight) of the individual animals, but that did not reduce the intra-group variance. Bone size is a major determinant for bone strength [100, 119], and the large variability may therefore be due to intra-group differences in bone volume. The results from the two tests of femur were correlated (Figure 8.11a), the maximum tolerated load of the mid-shaft being 1.2 kN higher than that of the neck, irrespective of strength (slope = 1).

Groups 2 and 3 showed a slight but non-significant increase in cortical strength (maximum load, three-point bending), while group 4 showed a significant decrease in strength (Figure 8.11b). A similar decrease in strength was seen in the femur neck in Group 4. This demonstrates that the dose of 1000 mg kg^{-1} day^{-1} induced deleterious effects in the bone apatite structure, comparable to the observations of poor teeth condition in the high dose group in 26-week rat (section 7.3.6). As previously discussed, the effect may be linked to the reduced bone calcium in the high dose groups, or to a distortion of the apatite crystal lattice due to strontium's larger ion radius [12].

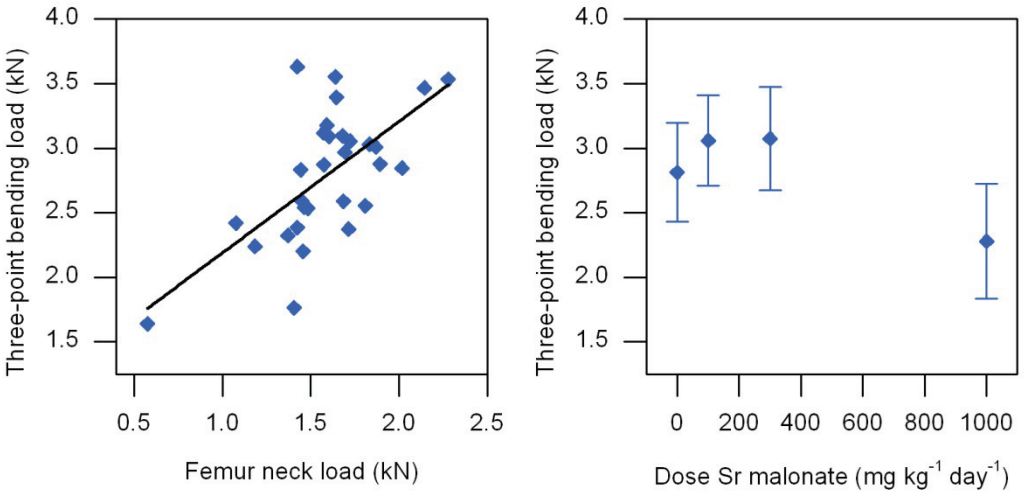

Figure 8.11 (a) maximum loads measured for femur (mid-shaft and femur neck) were correlated. Mid-shaft = (1.02±0.22)·neck + (1.2±0.4), $r^2 = 0.40$, $p < 0.001$. (b) maximum load of femoral mid-shaft for the four animal groups. The strength was significantly reduced in Group 4.

Somewhat surprisingly, no significant effects were seen in the vertebrae. Since trabecular tissue incorporates more Sr than cortical tissue, it was expected that any biomechanical effects of the Sr treatment would be evident in these samples. However, the intra-group variance was too large to identify any differences between the groups (Table 8.8). The variability may have been caused by presence of various amounts of cortical tissue in the biopsies. The diameter of the applied drill only just allowed for a trabecular biopsy to be taken from the inner part of the vertebral body, and some biopsies may have included some of the cortical bone making up the cortex of the vertebrae, which would affect the biomechanical properties of the biopsy. Although great care was taken to avoid it, the microstructure of biopsies may also have been damaged by the sampling process.

8.4.7 Validation of bone densitometry measurements

The accuracy of the DEXA analysis was evaluated using the hydroxyapatite mixture containing 0% Sr in the PMMA block. The nominal value for BMC was the amount of HAp transferred to the hole, while the area was calculated from the diameter (2.1 cm) of the hole. The nominal BMD was calculated as the ratio between nominal BMD and area. The accuracies of the BMD, BMC and area determinations were then calculated as the ratios between the measured and nominal values (Table 8.11). The accuracy for all parameters was found to be satisfying and within previously reported ranges for similar instruments [240].

Table 8.11 Accuracy and precision (n = 15) for DEXA analysis of pure hydroxyapatite**.**

	Nominal value	Measured (mean ± SD)	Accuracy (%)
BMC (g)	2.66	2.82 ± 0.02	106
Area (cm^2)	3.63	3.95± 0.03	109
BMD	0.732	0.715 ± 0.003	97.7

The total repeatability of the analysis depends on the precision of the detector, the repeatability of the positioning of the samples and the operators' ability to select the same ROI after each scan. The repeatability was evaluated by repeating measurements of the same set of bone samplings over several days, resulting in a precision of 0.9-1.0% for BMD, BMC and area of mid-diaphyseal femur.

8.4.8 Influence of Sr on BMD measurements

Strontium's effect on DEXA measurements was described in Chapter 4. In order to obtain a reliable evaluation of the effect of SrM treatment on bone BMD, strontium's influence on DEXA measurements was assessed, using mixtures of hydroxyapatite with various concentrations of Sr. The calculations follow the procedure presented by Nielsen *et al.* [240], who published correction factors for a range of different DEXA scanners. The overestimation or the relative error (RE) of the BMD measurement for each apatite mixture was calculated by the difference in measured BMD between pure Ca-HAp and the individual mixture of Sr-doped HAp:

$$RE_{BMD} = \frac{BMD_{Sr-HAp} - BMD_{Pure\ HAp}}{BMD_{Pure\ HAp}} \quad (8\text{-}2)$$

The RE was calculated for the area and BMC in a similar fashion. After determination of the exact Sr-concentration in each of the six mixtures, the molar ratios between Sr and Sr-doped HAp were calculated, providing a measure for the amount of Ca atoms that had been substituted by Sr in the apatite. RE was then plotted against the molar ratio of Sr, showing the relationship between the amount of Sr present and the scanner's overestimation of BMD (Figure 8.12).

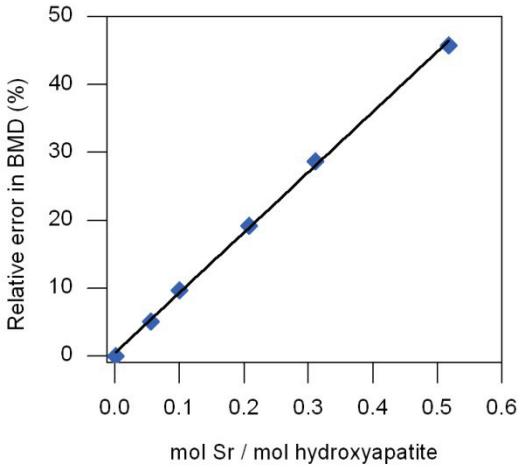

Figure 8.12 The relative error of BMD measurements of hydroxyapatite at different molar ratios of Sr. A linear relation with a slope of k_{BMD} = 91.0 ± 1.1 was found.

Linearity was accepted for the data in Figure 8.12 and the overestimation was therefore expected to be well-described by a linear model. As expected, the intercept was not significantly different from zero (corresponding to no correction for pure HAp), and the level of overestimation was therefore calculated using OLSR for the model

$$RE_{BMD} = k \cdot MR_{Sr} \tag{8-3}$$

where k is the correction factor [mol HAp / mol Sr] and MR_{Sr} the concentration of Sr given as a molar ratio with respect to HAp. A correction factor of k = 0.910 ± 0.014 was found. For the purpose of comparison with literature values, the correction factor was recalculated by using the molar fraction of Sr/(Ca+Sr) as a measure for Sr substitution. The resulting correction factors are presented in Table 8.12, together with data reported by Nielsen *et al.* [240]. The authors found that the correction factor depended on whether the HAp was placed directly on the scanner table or positioned between a total of 5.5 cm acrylic glass and 9.5 cm of water. In this work, the positioning of HAp on 2 mm of acrylic glass and 3 cm of rice resulted in correction factors close to those obtained without water and acrylic glass. One important difference is that Nielsen *et al.* [240] found that the estimates of the mineral-containing areas were not correlated to the Sr-contents in the apatites, whereas, in the present study, the area estimate increased systematically with increasing Sr-concentration. Since all the holes had the same diameter, it was concluded that the scanner's edge detection was affected by the amount of Sr in the HAp. The reason for this effect has not been identified.

Table 8.12 Comparison of values for correction of strontium's influence on DEXA measurements of BMC, BMD and area. The means, standard deviations and confidence intervals (CI) quoted from [240] are based on measurements from a range of different DEXA-scanners, with the HAp samples placed directly on the scanner table.

	Present work	Nielsen *et al.* [240]		
	Mean ± SD	Norland XR-26	Mean ± SD	95% CI
BMC	0.0910 ± 0.0011	0.0926	0.0883 ± 0.0107	0.0794-0.0973
Area	0.0116 ± 0.0010	0.0001	0.0025 ± 0.0074	-0.0015-0.0064
BMD	0.0752 ± 0.0011	0.0966	0.0869 ± 0.0089	0.0794-0.0944
BMD incl. areal correction	0.0910 ± 0.011	-	-	-

The area effect of the Sr-content was assumed to be related to the design of the acrylic block rather than being a general property of the DEXA-scanner. The effect was expected to be absent, or at least less pronounced, for the animal samples, and it was therefore decided to adjust the BMD correction factor for the overestimation of the area. This resulted in a 21% increase in the correction factor compared with that obtained directly from the BMD measurements.

Using the molar ratios of Sr, MR_{Sr}, that were calculated for the evaluation of the substitution model (cf. sections 7.3.9 and 8.4.4), the corrected BMD in each bone sample can be calculated using the following formula:

$$BMD_{corrected} = \frac{BMD_{measured}}{1 + RE_{BMD}} = \frac{BMD_{measured}}{1 + k \cdot MR_{Sr}} \qquad (8\text{-}4)$$

Figure 8.13 shows the effect of the BMD correction in femur. The uncorrected BMD results were significantly correlated with the Sr concentration in the bones, whereas the corrected values showed no such correlation. Thus, the interference from Sr on the X-ray attenuation was eliminated, allowing for a more reliable evaluation of the mineral density in the bones.

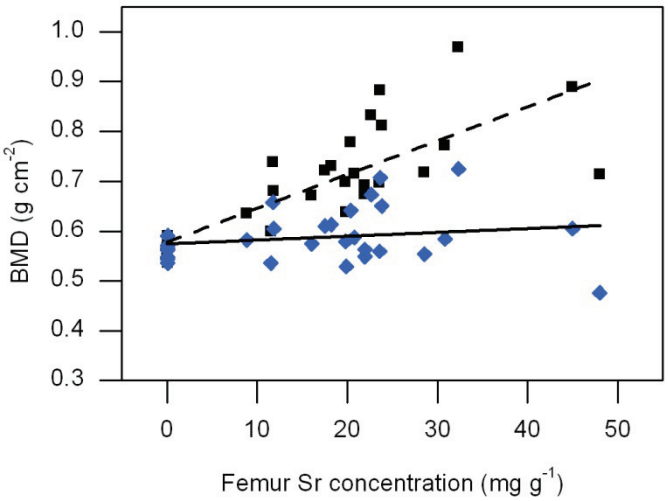

Figure 8.13 Relationships between measured (■) and corrected (◆) BMD results and the directly determined strontium concentrations in dog femur. There is a significant correlation between measured BMD and femur Sr ($p < 0.001$), whereas the corrected BMD is not correlated to the Sr concentration ($p = 0.33$).

Nielsen *et al.* [240] clearly demonstrated that the magnitude of the correction factor depends on whether the X-rays are also attenuated by other materials than apatite. Consequently, the application of a correction factor calculated from pure HAp was challenged by fact that the mineral phase in the real animal samples was surrounded by various organic materials. Made up by mineralised collagen, marrow, bone cells, etc. the microstructure of the bones is much more complex than the pure inorganic powders. Additionally, the bones were surrounded by adhering soft tissues and wrapped in cotton soaked in isotonic water in order to keep them hydrated for the subsequent mechanical measurements. Together, these tissues and materials may affect the interference from Sr. However, as there was no way to predict a possible deviation, the value determined from the HAp powders represented the best attainable estimate of the correction. It should be noted that other techniques for determination of bone mass and density, such as bone ash weight [119] and density fractionation [107, 112], would also be expected to be influenced by the purely physical effect of strontium's high weight.

8.4.9 Effect of SrM treatment on BMD

The group averages of measured and corrected BMD for femur and calvaria are shown in Figure 8.14. As expected, the correction for Sr reduced considerably the average BMD in all the active dose groups, while the placebo group BMD remained essentially unchanged.

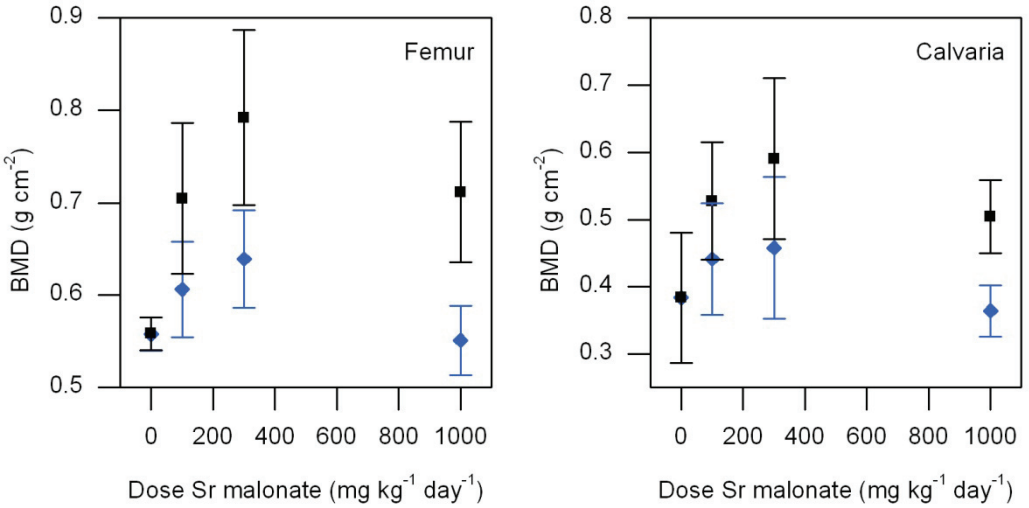

Figure 8.14 Means and SDs (error bars) of measured (■) and corrected (◆) BMD results for dog femur and calvaria. Femurs from the animals in Group 3 (300 mg kg^{-1} day^{-1} SrM) had significantly increased BMD in femur compared with placebo.

Both femur and calvaria show similar trends: compared with placebo, BMD increases with dose in Groups 2 and 3, while the BMD in Group 4 is marginally lower than in the placebo group. An analysis of variance with corrected BMD as response and dose group as effect showed a significant inter-group difference only in femur BMD. Further investigation (Dunnett's test) revealed that Group 3 had significantly higher corrected BMD in femur than the placebo group ($p = 0.0017$). This indicates that a dose of 300 mg kg^{-1} day^{-1} SrM increased the mineral density of mid-diaphyseal femur.

The increase in BMD is somewhat in contrast to the results of the elemental analysis, which showed that Ca concentrations were decreased in the active dose groups. In order to asses whether this disparity may be explained by the increased amounts of Sr in the treated groups, the molar concentrations of Sr + Ca were calculated, and the substitution model was used to express the concentrations with respect to hydroxyapatite (Table 8.13). The results showed that the molar concentrations of Sr + Ca were similar in calvaria in all four groups ($p = 0.29$), while Sr + Ca in femur was (barely) significantly lower ($p = 0.021$) in the treated groups. There were no differences between any of the active dose groups, demonstrating that loss of Ca did not increase with increased SrM dose. Still, these observations do not support the increase in corrected BMD seen in Groups 2 and 3. One explanation for this difference might be that the correction of the Sr interference on the DEXA scans was inadequate, due to the potential problems with soft-tissue attenuation as discussed above. It is also possible that the areal density measured by DEXA and the weight-to-weight concentrations measured by ICP-MS were affected differently by

the SrM treatment and the addition of Sr to the bone matrix. If SrM stimulated formation of new bone within the bone structure, e.g. on the inner surface of the medullary cavity of the femurs, it might be seen as an increase in areal mineral density. It would not, however, necessarily be perceived as an increase in the concentrations of Sr + Ca as measured by ICP-MS, because of the accompanying increase in the total weight of the bone. As a final point, the EXAFS measurements showed that some of the Sr ions imbedded in the bone tissue was bound to atoms outside the apatite structure. Rather than substituting Ca in the apatite, these Sr ions may be therefore have been adsorbed as an amorphous phase of inorganic salts such as $Sr_3(PO_4)_2$ and $SrCO_3$. Having higher densities than hydroxyapatite [16, 346], presence of such compounds would influence both the DEXA measurements and ICP-MS analyses.

Table 8.13 Concentrations of Ca and Sr in dog femur and calvaria. The ICP-MS results were converted to molar concentrations in order to asses the sum of

Dose (mg kg^{-1} day^{-1})	Concentration			
	Sr	Ca	Sr + Ca	Sr + Ca
	(mg g^{-1} bone)		(mmol g^{-1} bone)	(mol mol^{-1} HAp)
Femur				
0 (n=8)	0.078 ± 0.013	328 ± 41	8.2 ± 1.0	10.5 ± 1.4
100 (n=6)	15.4 ± 5.4	271 ± 15	6.94 ± 0.36	9.30 ± 0.70
300 (n=8)	22.7 ± 6.6	263 ± 25	6.82 ± 0.66	8.96 ± 0.85
1000 (n=8)	28 ± 12	275 ± 26	7.18 ± 0.74	8.97 ± 0.50
Calvaria				
0 (n=8)	0.116 ± 0.017	279 ± 19	6.95 ± 0.48	9.95 ± 0.69
100 (n=7)	19.3 ± 5.2	253 ± 16	6.54 ± 0.36	9.50 ± 0.48
300 (n=8)	27.4 ± 5.2	254.3 ± 8.2	6.66 ± 0.21	9.73 ± 0.31
1000 (n=8)	37.0 ± 8.1	244 ± 12	6.51 ± 0.22	9.59 ± 0.28

The validity of the BMD measurements was evaluated by comparing the corrected BMD results with the biomechanical measurements. The inter-group pattern of the corrected BMD results resembles that which was seen for the three-point bending tests of the femurs (Figure 8.11). A small (non-significant) increase in maximum load was observed in Groups 2 and 3 compared with placebo, while a significant decrease was seen in Group 4. The degree of mineralisation is a very important factor in determining the mechanical strength of bone [77, 100], and the corrected BMD was therefore expected to be related to the maximum load. Amman *et al.* [119] reported a clear correlation between BMD as measured by DEXA and bone strength in rat femoral mid-shaft after 2 years of treatment with SrR. However, the authors did not adjust the BMD results for the large concentrations of Sr (up to

5.4 mol% Sr/(Sr + Ca)) present in the femurs. The measured BMD must therefore be assumed to have been strongly affected by the presence of Sr, and the results may therefore not represent the true mineral density of the bones. In the present work, the corrected BMD in mid-diaphyseal femur was compared with the maximum load of the three-point bending test (Figure 8.15).

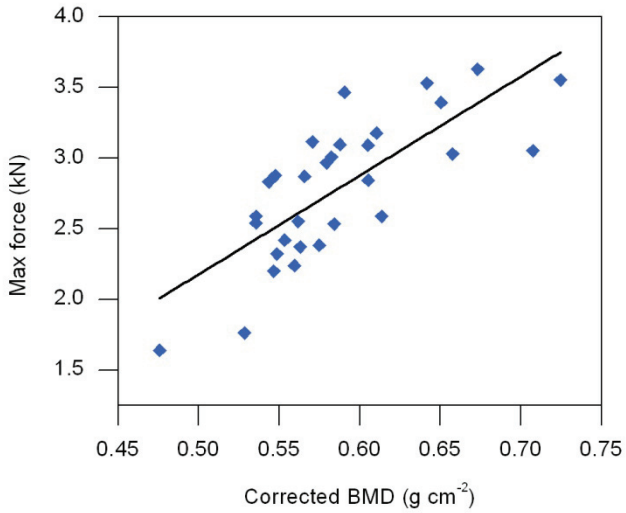

Figure 8.15 Relationship between bone strength (three-point bending) and corrected BMD for dog femur. Slope = 6.99±1.1, $r^2 = 0.56$, $p < 0.001$.

There was a very strong correlation between the two observations, demonstrating that the corrected BMD can be used as a predictor for the maximum load. The correlation also suggests that the increase in corrected BMD following SrM treatment was associated with concomitant increase of bone strength.

8.5 Conclusion

This study showed that Sr was readily incorporated into molar tooth, calvaria and mid-diaphyseal femur in dogs after 52 weeks of treatment with strontium malonate. The highest concentrations of Sr were found in calvaria, where administration of up to 460 mg kg^{-1} day^{-1} Sr^{2+} resulted in an approximate 350-fold increase in bone Sr compared with placebo. The lowest degree of Sr incorporation was seen in molar, which is attributed to the low remodelling rate of dog teeth. The concentrations of Sr in femur and molar were correlated. By comparing the femur Sr concentrations with those found in a 4-week study in dogs, it was observed that approximately one third of the Sr found after 52 weeks was incorporated already after 4 weeks, suggesting that initial incorporation of Sr happens by a rapid mechanism which is eventually saturated and replaced by a slower mechanism. All the active dose groups had reduced concentrations of Ca and P in both calvaria and femur.

EXAFS measurements indicated that Sr had substituted Ca in the bone apatite structure but that Sr also coordinated to other atoms, most likely oxygen in collagen and water. The coordination of Sr was similar in the calvaria and femur, and the incorporation of Sr into the HAp increased with increasing dose. A higher resolution in the EXAFS data would be needed in order to obtain more detailed information on the coordination of Sr.

The mechanical strength of the femurs was significantly reduced in the highest dose group, indicating a weakening of the apatite structure. A small but non-significant increase in strength was seen in the low and medium dose groups.

Measurement of BMD using DEXA was found to be heavily influenced by presence of Sr in the mineralised matrix. A direct linear relation between overestimation of BMD and Sr concentration was identified, and a correction of 9% for a 1:10 molar ratio of Sr:HAp was determined. The correction was applied to BMD measurements of femur and calvaria, resulting in a significant increase in corrected BMD in femur mid-shaft in the group treated with 300 mg kg^{-1} day^{-1} SrM. The corrected BMD was found to be correlated with bone strength, irrespective of SrM dose.

CHAPTER NINE

Concluding remarks and outlook

9.1 Strontium's effect on bone tissue

This work has shown that strontium administered orally as strontium malonate (SrM) is highly bioavailable for transport to the blood and for incorporation into calcified tissues in rats and dogs. Long-term treatment with 100, 300 and 1000 mg kg^{-1} day^{-1} SrM (corresponding to 46, 138 and 460 mg kg^{-1} day^{-1} Sr^{2+}, respectively) resulted in dose-dependent increases in Sr concentrations of up to 500 folds in rat incisor and 350 folds in dog femur. Significant gender differences were observed in both rats and dogs. In rats, Sr had a higher bioavailability in males than in females, while the opposite trend was seen in dogs after four weeks of treatment. Sr concentrations in different skeletal sites were correlated, and the degree of incorporation depended on the rate of turnover in the mineralised matrix. It was observed that approximately one third of the Sr found after 52 weeks was incorporated already after 4 weeks. This suggests that initial incorporation of Sr proceeds by a rapid mechanism which is eventually saturated and replaced by a slower mechanism. High doses of Sr reduced Ca concentrations in both serum and calcified tissues, indicating that Sr influenced Ca metabolism and the mineralisation of the bones and teeth.

A stoichiometric model was proposed for incorporation of Sr in hydroxyapatite. The model showed excellent agreement with the analytical data and it was found that respectively 70 – 72% of femur, 78% of rat incisor and 85% of dog molar was made up by hydroxyapatite (HAp). The model demonstrated that a part of the perceived loss of Ca in the calcified tissues was caused by the adsorption or incorporation of Sr in the HAp. EXAFS measurements indicated that some apatite Ca was substituted by Sr in the SrM-treated animals and that the incorporation increased with increasing Sr

dose. However, Sr also coordinated to other atoms, most likely oxygen in collagen and water.

The mechanical strength of dog femur was slightly but non-significantly increased in the low and medium dose groups, while the highest Sr dose group showed significantly reduced bone strength, indicating a weakening of the apatite structure at the highest dose.

Measurement of BMD using DEXA was heavily influenced by presence of Sr in the mineralised matrix, and a direct linear relation of 9% for a 1:10 molar ratio of Sr:HAp was identified. By applying the correction, a significant increase was observed in corrected BMD in femur mid-shaft in the group treated with 300 mg kg^{-1} day^{-1} SrM. The corrected BMD was found to be clearly correlated with bone strength, irrespective of SrM dose. This strongly indicated that the increase in corrected BMD following SrM treatment was associated with concomitant increase of bone strength.

9.2 Methodology

Direct measurements of the treatment effects of SrM on bone were complicated by the fact than Sr affects bone both on the cellular and molecular level. Incorporation of Sr ions into the apatite matrix affected evaluations of bone mineralisation by both DEXA and ICP-MS. Adjustments for Sr contents were therefore essential in order to correctly interpret the results.

ICP-MS proved to be a very suitable analytical technique for determining key bone elements in serum and mineralised tissues due to its high accuracy, multi-element capability, low quantification limits and broad linear range. The low natural concentrations of Sr in serum required application of a high-sensitivity desolvation unit for sample introduction, which constituted a major improvement in performance with respect to sample consumption, sensitivity, precision and oxide levels compared with a conventional cross-flow nebuliser.

The measurement uncertainty associated with the ICP-MS analysis was frequently underestimated when applying conventional calibration procedures. To obtain reliable uncertainty estimates, calibration data from many different days were pooled into one data set. This new principle of processing calibration data successfully provided a satisfactory estimate of the measurement uncertainty related to the ICP-MS analysis, ensuring reliable determinations of the analytes of interest. Substantial differences between the LOQ and lower limit of analysis (LLA) were

observed, and it was suggested that the LLA is a useful parameter for estimating the lowest concentration at which a sample can be reliably analysed at an RSD of less than 50%.

9.3 Outlook

It would be of great interest to examine further the impact of SrM on bone mineral density and strength. In order to obtain more conclusive results about the beneficial effects of Sr, it might be suggested to set up an animal study with lower treatment doses, longer treatment time and, ideally, with more animals in each dose group. With respect to the current results, it would be of interest to normalise the biomechanical measurements with respect to the physical dimensions (e.g. thickness or cross-section) of the bones. Bone size is a major determinant of bone strength, and adjusting the biomechanical results for bone volume might therefore reduce the variability within the dose groups, thus allowing for a stronger identification of potential treatment effects.

Further method development is necessary in order to achieve a satisfactory accuracy for determination of P in serum using ICP-MS. The main objective would be to identify and overcome the disturbing interferences. Application of another internal standard than Rh might also be of use.

A better resolution of the EXAFS data would be very useful for drawing more detailed conclusions about the position and coordination of Sr in bone tissue. This would require collection of a new set of EXAFS data over a higher energy range. For the purpose of comparison, EXAFS spectra of collagen coordinated to Sr may also be useful.

As a final point, the role of the malonate anion has not been specifically investigated in this project. In order to obtain a complete picture of the biological effects of SrM treatment, it might be worthwhile to include analysis of malonate in any future animal studies of SrM.

10 References

1. F. Lehnerdt. On the topic of the substitution of calcium with strontium in the bone system. II. Announcement. Strontium feeding of lactating animals, the influence of strontium on the bone system of nursing young. *Beitrage zur pathologischen Anatomie und zur allgemeinen Pathologie* (1910) **47**, 215-247.

2. E. Shorr & A. Carter. The usefulness of strontium as an adjuvant to calcium in the remineralization of the skeleton in man. *Bulletin of the Hospital for Joint Diseases* (1952) **13**, 59-66.

3. S. Christgau, K. Stahl & J. E. T. Andersen. Synthesis and characterisation of strontium carboxylates formed at room temperature and under hydrothermal conditions. *Journal of Coordination Chemistry* (2006) **59**, 2023-2030.

4. K. Ståhl, J. E. T. Andersen & S. Christgau. Strontium diibuprofenate dihydrate, strontium malonate sesquihydrate, strontium diascorbate dihydrate and strontium 2-oxidobenzoate hydrate at 120 K. *Acta Crystallographica Section C-Crystal Structure Communications* (2006) **62**, M144-M149.

5. K. Krogsgaard, M. Weis & S. Christgau. A new strontium salt available in tablet form with improved bioavailablity of strontium compared to strontium ranelate. *Osteoporosis International* (2006) **17**, S221-S221.

6. S. Christgau, M. Weis & K. Krogsgard. Improved strontium bioavailability in a new tablet formulated strontium salt. *Journal of Bone and Mineral Research* (2007) **22**, T411.

7. L. A. Sorbera, J. Castaner, P. A. Leeson & M. Bayes. Strontium ranelate. Treatment and prevention of osteoporosis, bone resorption inhibitor, bone formation stimulant. *Drugs of the Future* (2003) **28**, 328-335.

8. A. Brüel, J. Olsen, H. Birkedal, M. Risager, T. T. Andreassen, A. C. Raffalt, J. E. T. Andersen & J. T. Thomsen. Strontium is Incorporated into the Fracture Callus, but Does not Influence the Mechanical Strength of Healing Rat Fractures. *Calcified Tissue International* (2011).

9. A. C. Raffalt. Bestemmelse med ICP-MS af strontium og andre Gruppe II metaller i knogler, knoglemarv og tænder og kvalitetssikring af resultaterne. Eksamensprojekt. DTU Kemi, (2006).

10. S. R. Sørensen. Determination of key elements in rat teeth and bone and quality assurance of the results. Master thesis. (2007).

11. A. C. Raffalt, J. E. T. Andersen & S. Christgau. Application of inductively coupled plasma-mass spectrometry (ICP-MS) and quality assurance to study the incorporation of strontium into bone, bone marrow, and teeth of dogs after one month of treatment with strontium malonate. *Analytical and Bioanalytical Chemistry* (2008) **391**, 2199-2207.

12. S. Inoue, Chemistry of strontium, in *Handbook of stable strontium,* (ed. S. C. Skoryna)ch. 2, 11-18, Plenum Press, New York, 1981.

13. S. P. Nielsen. The biological role of strontium. *Bone* (2004) **35**, 583-588.

14. S. G. Hibbins, Strontium and strontium compounds, in *Kirk-Othmer Encyclopedia of chemical technology,* (ed. M. Howe-Grant), 947-955, John Wiley & Sons, New York, NY, 1997.

15. S. Christgau, J. Odderhede, K. Ståhl & J. E. T. Andersen. Strontium D-glutamate hexahydrate and strontium di(hydrogen L-glutamate) pentahydrate. *Acta Crystallographica Section C-Crystal Structure Communications* (2005) **61**, M259-M262.

16. D. R. Lide (ed.), in *CRC handbook of chemistry and physics*, 82nd edn., CRC Press, Boca Raton, 2005.

17. J. Reeve, R. Wootton & R. Hesp. New Method for Calculating Accretion Rate of Bone Calcium and some Observations on Suitability of Strontium-85 as a Tracer for Bone Calcium. *Calcified tissue research* (1976) **20**, 121-135.

18. J. S. Wand, T. Smith, J. R. Green, R. Hesp, J. N. Bradbeer & J. Reeve. Whole-Body and Site-Specific Bone Remodeling in Patients with Previous Femoral Fractures - Relationships between Reduced Physical-Activity, Reduced Bone Mass and Increased Bone-Resorption. *Clinical science* (1992) **83**, 665-675.

19. O. G. Finlay, M. D. Mason & M. Shelley. Radioisotopes for the palliation of metastatic bone cancer: a systematic review. *Lancet Oncology* (2005) **6**, 392-400.

20. Toxicological profile for strontium. U.S. Department of Health and Human Services, Public Health Service. Agency for Toxic Substances and Disease Registry, Atlanta, GA (2004) http://www.atsdr.cdc.gov/toxprofiles/tp159.html, retrieved 8 January 2010.

21. H. J. M. Bowen & J. A. Dymond. Strontium and Barium in Plants and Soils. *Proceedings of the Royal Society of London Series B-Biological Sciences* (1955) **144**, 355-368.

22. R. C. Capo, B. W. Stewart & O. A. Chadwick. Strontium isotopes as tracers of ecosystem processes: theory and methods. *Geoderma* (1998) **82**, 197-225.

23. H. A. Schroeder, I. H. Tipton & A. P. Nason. Trace Metals in Man - Strontium and Barium. *Journal of chronic diseases* (1972) **25**, 491-&.

24. R. Loren. Strontium i grundvand og drikkevand. Roskilde Amt, Roskilde (2005).

25. Wikipedia article:Celestine (mineral). (2010) http://en.wikipedia.org/wiki/Celestine_(mineral), retrieved 12 June 2010.

26. Amethyst Galleries: (2010) http://www.galleries.com/minerals/carbonat/strontia/strontia.htm, retrieved 12 June 2010.

27. A. P. Vonderheide, M. V. Zoriy, A. V. Izmer, C. Pickhardt, J. A. Caruso, P. Ostapczuk, R. Hille & J. S. Becker. Determination of Sr-90 at ultratrace levels in urine by ICP-MS. *Journal of Analytical Atomic Spectrometry* (2004) **19**, 675-680.

28. S. M. Vakulovsky, A. I. Nikitin, V. B. Chumichev, I. Y. Katrich, O. A. Voitsekhovich, V. I. Medinets, V. V. Pisarev, L. A. Bovkum & E. S. Khersonsky. Cesium-137 and Sr-90 Contamination of Water Bodies in the Areas Affected by Releases from the Chernobyl-Nuclear-Power-Plant Accident - an Overview. *Journal of environmental radioactivity* (1994) **23**, 103-122.

29. P. Froidevaux, F. Bochud & M. Haldimann. Retention half times in the skeleton of plutonium and Sr-90 from above-ground nuclear tests: A retrospective study of the Swiss population. *Chemosphere* (2010) **80**, 519-524.

30. C. Minoia, E. Sabbioni, A. Ronchi, A. Gatti, R. Pietra, A. Nicolotti, S. Fortaner, C. Balducci, A. Fonte & C. Roggi. Trace-Element Reference Values in Tissues from Inhabitants of the European-Community .4. Influence of Dietary Factors. *Science of the Total Environment* (1994) **141**, 181-195.

31. A. Howe, L. Fung, G. Lalor, R. Rattray & M. Vutchkov. Elemental composition of Jamaican foods 1: A survey of five food crop categories. *Environmental Geochemistry and Health* (2005) **27**, 19-30.

32. K. Isermann, Uptake of stable strontium by plants and effects on plant growth, in *Handbook of stable strontium,* (ed. S. C. Skoryna), 65-86, Plenum Press, New York, 1981.

33. J. L. Groff & S. S. Gropper, in *Advanced nutrition and human metabolism,* Wadsworth/Thomson Learning, Belmont, CA, 2000.

34. Council directive 98/83/EF of 3 November 1998 on the quality of water intended for human consumpation. European Union, (2003) http://europa.eu/legislation_summaries/environment/water_protection_management/l28079_en.htm.

35. Guidelines for drinking-water quality. World Health Organization, Geneva (2008) http://www.who.int/water_sanitation_health/dwq/fulltext.pdf, retrieved 19 August 2010.

36. Liste over kvalitetskriterier i relation til forurenet jord og kvalitetskriterier for drikkevand. Miljøministeriet, (2010) http://www.mst.dk/NR/rdonlyres/95F9ABE9-485B-4D83-A3FF-62E420A5BE8D/0/Kvalitetskriterierjord_og_drikkevandfinaljuni2010.pdf, retrieved 19 August 2010.

37. P. J. Marie, P. Ammann, G. Boivin & C. Rey. Mechanisms of action and therapeutic potential of strontium in bone. *Calcified tissue international* (2001) **69**, 121-129.

38. W. E. Cabrera, I. Schrooten, M. E. De Broe & P. C. D'Haese. Strontium and bone. *Journal of Bone and Mineral Research* (1999) **14**, 661-668.

39. S. G. Dahl, P. Allain, P. J. Marie, Y. Mauras, G. Boivin, P. Ammann, Y. Tsouderos, P. D. Delmas & C. Christiansen. Incorporation and distribution of strontium in bone. *Bone* (2001) **28**, 446-453.

40. R. D. Shannon. Revised Effective Ionic-Radii and Systematic Studies of Interatomic Distances in Halides and Chalcogenides. *Acta Crystallographica Section a* (1976) **32**, 751-767.

41. K. Kostial, Simonovi.i & M. Pisonic. Effect of Calcium and Phosphates on Gastrointestinal Absorption of Strontium and Calcium in Newborn Rats. *Nature* (1967) **215**, 1181.

42. K. Kostial, S. Vojvodic & C. L. Comar. Effects of Dietary Levels of Phosphorus and Calcium on Comparative Behaviour of Strontium and Calcium. *Nature* (1965) **208**, 1110.

43. G. Patrick. Inhibition of Strontium and Calcium Uptake by Rat Duodenal Slices - Comparison of Polyuronides and Related Substances. *Nature* (1967) **216**, 815.

44. J. Z. Hendrix, R. M. Archibald & N. W. Alcock. Competition between Calcium, Strontium, and Magnesium for Absorption in Isolated Rat Intestine. *Clinical chemistry* (1963) **9**, 734.

45. D. G. Papworth & G. Patrick. Kinetics of Influx of Calcium and Strontium into Rat Intestine In-Vitro. *Journal of Physiology-London* (1970) **210**, 999.

46. P. A. Dumont, P. F. Curran & A. K. Solomon. Calcium and Strontium in Rat Small Intestine their Fluxes and their Effect on Na Flux. *Journal of General Physiology* (1960) **43**, 1119-1136.

47. U. Karbach & W. Rummel. Strontium Transport in the Rat Colon. *Naunyn-Schmiedebergs Archives of Pharmacology* (1987) **335**, 91-96.

48. J. L. Omdahl, L. A. Hunsaker & V. A. Aschenbrenner. Control of Kidney 25-Hydroxyvitamin-D3 Metabolism - Strontium and Involvement of Parathyroid-Hormone .2. *Archives of Biochemistry and Biophysics* (1977) **184**, 172-178.

49. C. S. Marcus & F. W. Lengemann. Absorption of Ca45 and Sr85 from Solid and Liquid Food at various Levels of Alimentary Tract of Rat. *Journal of Nutrition* (1962) **77**, 155-&.

50. S. Milsom, K. Ibbertson, S. Hannan, D. Shaw & J. Pybus. Simple Test of Intestinal Calcium-Absorption Measured by Stable Strontium. *British medical journal* (1987) **295**, 231-234.

51. J. M. Warren & H. Spencer. Metabolic Balances of Strontium in Man. *Clinical orthopaedics and related research* (1976), 307-320.

52. M. E. J. Curzon, P. C. Spector & H. P. Iker. Association between Strontium in Drinking-Water Supplies and Low Caries Prevalence in Man. *Archives of Oral Biology* (1978) **23**, 317-321.

53. M. E. J. Curzon. The Relation between Caries Prevalence and Strontium Concentrations in Drinking-Water, Plaque, and Surface Enamel. *Journal of dental research* (1985) **64**, 1386-1388.

54. M. E. J. Curzon, M. H. Ashrafi & P. C. Spector. Effects of Strontium Administration on Rat Molar Morphology. *Archives of Oral Biology* (1982) **27**, 667-671.

55. M. Riyat & D. C. Sharma. Analysis of 35 Inorganic Elements in Teeth in Relation to Caries Formation. *Biological trace element research* (2009) **129**, 126-129.

56. M. Burguera, J. L. Burguera, M. L. Di Bernardo, O. M. Alarcon, E. Nieto, J. R. Salinas & E. Burguera. Age and sex-related calcium and strontium concentrations in different types of human bones. *Trace Elements and Electrolytes* (2002) **19**, 143-151.

57. P. C. D'Haese, I. Schrooten, W. G. Goodman, W. E. Cabrera, L. V. Lamberts, M. M. Elseviers, M. M. Couttenye & M. E. De Broe. Increased bone strontium levels in hemodialysis patients with osteomalacia. *Kidney international* (2000) **57**, 1107-1114.

58. M. Cohen-Solal. Strontium overload and toxicity: impact on renal osteodystrophy. *Nephrology Dialysis Transplantation* (2002) **17**, 30-34.

59. I. Schrooten, M. M. Elseviers, L. V. Lamberts, M. E. De Broe & P. C. D'Haese. Increased serum strontium levels in dialysis patients: An epidemiological survey. *Kidney international* (1999) **56**, 1886-1892.

60. S. C. Skoryna & M. Fuskova, Effects of stable strontium supplementation, in *Handbook of stable strontium,* (ed. S. C. Skoryna), 593-617, Plenum Press, New York, 1981.

61. F. E. McCaslin & J. M. Janes. The Effect of Strontium Lactate in the Treatment of Osteoporosis. *Proceedings of the Staff Meetings of the Mayo Clinic* (1959) **34**, 329-334.

62. F. E. McCaslin & J. M. Janes, Effects of stable strontium in treatment of Osteoporosis, in *Handbook of stable strontium,* (ed. S. C. Skoryna)ch. 33, 563-567, Plenum Press, New York, 1981.

63. S. C. Skoryna. Effects of Oral Supplementation with Stable Strontium. *Canadian Medical Association journal* (1981) **125**, 703-712.

64. S. C. Skoryna, P. J. Marie, E. Yeghiayan & J. F. Stara. Effects of Neoadjuvant Stable Strontium Therapy on Metastatic Bone Cancer. *Cancer drug delivery* (1986) **3**, 78-78.

65. P. J. Marie *et al.*, Histomorphometry of bone changes in stable strontium therapy, in *Trace substances in environmental health XIX,* (ed. D. D. Hemphill), 193-208, University of Missouri, Columbia, Missouri, 1985.

66. J. P. Bilezikian, R. Marcus & M. A. Levine (eds.), in *The Parathyroids: Basic and Clinical Concepts,* 2nd edn., Academic Press, San Diego, CA, United States, 2001.

67. M. E. Launey, M. J. Buehler & R. O. Ritchie. On the Mechanistic Origins of Toughness in Bone. *Annual Review of Materials Research, Vol 40* (2010) **40**, 25-53.

68. E. Seeman & P. D. Delmas. Mechanisms of disease - Bone quality - The material and structural basis of bone strength and fragility. *New England Journal of Medicine* (2006) **354**, 2250-2261.

69. S. Weiner & H. D. Wagner. The material bone: Structure mechanical function relations. *Annual Review of Materials Science* (1998) **28**, 271-298.

70. E. S. Orwoll & M. Bliziotes (eds.), in *Contemporary Endocrinology: Osteoporosis: Pathophysiology and Clinical Management,* 1st edn., Humana Press, Inc., Totowa, NJ, United States, 2002.

71. Bone health and osteoporosis. A report of the Surgeon General. Department of Health and Human Services, Rockville, MD, United States (2004) http://www.surgeongeneral.gov/library/bonehealth/, retrieved 9-11-2010.

72. B. Wopenka & J. D. Pasteris. A mineralogical perspective on the apatite in bone. *Materials Science & Engineering C-Biomimetic and Supramolecular Systems* (2005) **25**, 131-143.

73. G. Boivin, P. Deloffre, B. Perrat, G. Panczer, M. Boudeulle, Y. Mauras, P. Allain, Y. Tsouderos & P. J. Meunier. Strontium distribution and interactions with bone mineral in monkey iliac bone after strontium salt (S 12911) administration. *Journal of Bone and Mineral Research* (1996) **11**, 1302-1311.

74. K. Sudarsanan & R. A. Young. Structure of Partially Substituted Chlorapatite (Ca,Sr)5(PO4)3Cl. *Acta Crystallographica Section B-Structural Science* (1980) **36**, 1525-1530.

75. S. Cazalbou, C. Combes, D. Eichert & C. Rey. Adaptative physico-chemistry of bio-related calcium phosphates. *Journal of Materials Chemistry* (2004) **14**, 2148-2153.

76. J. D. Currey. The design of mineralised hard tissues for their mechanical functions. *Journal of Experimental Biology* (1999) **202**, 3285-3294.

77. J. D. Currey. Physical Characteristics Affecting the Tensile Failure Properties of Compact-Bone. *Journal of Biomechanics* (1990) **23**, 837-844.

78. Servier Medical Art. www.servier.com.

79. J. Warberg, in *Human fysiologi - en grundbog. 4. udg*, Polyteknisk Forlag, Lyngby, 2001.

80. Who are candidates for prevention and treatment for osteoporosis? *Osteoporosis international* (1997) **7**, 1-6.

81. D. W. Dempster, E. Shane, W. Horbert & R. Lindsay. A Simple Method for Correlative Light and Scanning Electron-Microscopy of Human Iliac Crest Bone Biopsies - Qualitative Observations in Normal and Osteoporotic Subjects. *Journal of Bone and Mineral Research* (1986) **1**, 15-21.

82. About osteoporosis. 2010, International Osteoporosis Foundation, (2009) http://www.iofbonehealth.org/health-professionals/about-osteoporosis.html, retrieved 20/9/2010.

83. B. L. Riggs, S. Khosla & L. J. Melton. Sex steroids and the construction and conservation of the adult skeleton. *Endocrine reviews* (2002) **23**, 279-302.

84. L. J. Melton 3rd, E. J. Atkinson, M. K. O'Connor, W. M. O'Fallon & B. L. Riggs. Bone density and fracture risk in men. *Journal of bone and mineral research : the official journal of the American Society for Bone and Mineral Research* (1998) **13**, 1915-1923.

85. L. J. Melton 3rd, E. A. Chrischilles, C. Cooper, A. W. Lane & B. L. Riggs. Perspective. How many women have osteoporosis? *Journal of bone and mineral research* (1992) **7**, 1005-1010.

86. J. A. Kanis, O. Johnell, A. Oden, I. Sernbo, I. Redlund-Johnell, A. Dawson, C. De Laet & B. Jonsson. Long-term risk of osteoporotic fracture in Malmo. *Osteoporosis International* (2000) **11**, 669-674.

87. P. Vestergaard, L. Rejnmark & L. Mosekilde. Osteoporosis is markedly underdiagnosed: a nationwide study from Denmark. *Osteoporosis International* (2005) **16**, 134-141.

88. J. A. Kanis. Diagnosis of osteoporosis and assessment of fracture risk. *Lancet* (2002) **359**, 1929-1936.

89. Dansk knoglemedicinsk selskab. Guide til udredning og behandling af osteoporose. (2009) www.dkms.dk, retrieved 21-09-2010.

90. G. M. Blake & I. Fogelman. An Update on Dual-Energy X-Ray Absorptiometry. *Seminars in nuclear medicine* (2010) **40**, 62-73.

91. The WHO study group on osteoporosis. Assessment of fractrue risk and its application to screening for postmenopausal osteoporosis. World Health Organization, Geneva (1994).

92. O. Johnell, J. A. Kanis, A. Oden, H. Johansson, C. De Laet *et al*. Predictive value of BMD for hip and other fractures. *Journal of Bone and Mineral Research* (2005) **20**, 1185-1194.

93. W. D. Leslie, J. F. Tsang, P. A. Caetano, L. M. Lix & Monitoba Bone Density Program. Effectiveness of bone density measurement for predicting osteoporotic fractures in clinical practice. *Journal of Clinical Endocrinology & Metabolism* (2007) **92**, 77-81.

94. J. A. Kanis & C. C. Gluer. An update on the diagnosis and assessment of osteoporosis with densitometry. *Osteoporosis International* (2000) **11**, 192-202.

95. Protelos (strontium ranelat). 2010, Institut for rationel farmakoterapi, (2006) http://irf.dk/dk/praeparatnyt/arkiv/protelos_strontium_ranelat.htm.

96. N. H. Bjarnason & B. Krølner. Osteoporose - farmakologisk behandling. 2010, Institut for rationel farmakoterapi, (2006).

97. N. S. Macdonald, R. E. Nusbaum, R. Stearns, F. Ezmirlian, C. Mcarthur & P. Spain. The Skeletal Deposition of Non-Radioactive Strontium. *Journal of Biological Chemistry* (1951) **188**, 137-143.

98. N. S. Macdonald, F. Ezmirlian, P. Spain & C. Mcarthur. The Ultimate Site of Skeletal Deposition of Strontium and Lead. *Journal of Biological Chemistry* (1951) **189**, 387-399.

99. J. Reeve, J. R. Green, C. J. Maletskos & R. M. Neer. Skeletal Retention of Ca-45 and Sr-85 Compared - Further-Studies on Intravenously Injected Sr-85 as a Tracer for Skeletal Calcium. *Calcified tissue international* (1983) **35**, 9-15.

100. G. Boivin & P. J. Meunier. The mineralization of bone tissue: a forgotten dimension in osteoporosis research. *Osteoporosis International* (2003) **14**, S19-S24.

101. O. J. Kirkeby & T. Berglarsen. Regional Blood-Flow and Sr-85 Incorporation Rate in the Rat Hindlimb Skeleton. *Journal of Orthopaedic Research* (1991) **9**, 862-868.

102. J. Reeve, M. Arlot, R. Wootton, C. Edouard, M. Tellez, R. Hesp, J. R. Green & P. J. Meunier. Skeletal Blood-Flow, Iliac Histomorphometry, and Strontium Kinetics in Osteoporosis - a Relationship between Blood-Flow and Corrected Apposition Rate. *Journal of Clinical Endocrinology & Metabolism* (1988) **66**, 1124-1131.

103. T. Morohashi, T. Sano & S. Yamada. Effects of Strontium on Calcium-Metabolism in Rats .1. A Distinction Between the Pharmacological and Toxic Doses. *Japanese journal of pharmacology* (1994) **64**, 155-162.

104. A. E. Sobel, J. Cohen & B. Kramer. The nature of the injury to the calcifying mechanism in rickets due to strontium. *The Biochemical journal* (1935) **29**, 2640-2645.

105. R. A. Corradino, J. G. Ebel, P. H. Craig, A. N. Taylor & R. H. Wasserman. Calcium Absorption and Vitamin D3-Dependent Calcium-Binding Protein Inhibition by Dietary Strontium. *Calcified tissue research* (1971) **7**, 81-&.

106. H. J. Armbrecht, R. H. Wasserman & M. E. H. Bruns. Effect of 1,25-Dihydroxyvitamin D3 on Intestinal Calcium-Absorption in Strontium-Fed Rats. *Archives of Biochemistry and Biophysics* (1979) **192**, 466-473.

107. M. D. Grynpas & P. J. Marie. Effects of Low-Doses of Strontium on Bone Quality and Quantity in Rats. *Bone* (1990) **11**, 313-319.

108. R. Boland, A. R. Deboland, E. Ritz & W. Hasselbach. Effect of 1,25-Dihydroxycholecalciferol on Sarcoplasmic-Reticulum Calcium-Transport in Strontium-Fed Chicks. *Calcified tissue international* (1983) **35**, 190-194.

109. J. C. Bartley & E. F. Reber. Toxic Effects of Stable Strontium in Young Pigs. *Journal of Nutrition* (1961) **75**, 21-&.

110. S. Ozgur, H. Sumer & G. Kocoglu. Rickets and soil strontium. *Archives of Disease in Childhood* (1996) **75**, 524-526.

111. P. J. Marie, M. T. Garba, M. Hott & L. Miravet. Effect of Low-Doses of Stable Strontium on Bone Metabolism in Rats. *Mineral and electrolyte metabolism* (1985) **11**, 5-13.

112. M. D. Grynpas, E. Hamilton, R. Cheung, Y. Tsouderos, P. Deloffre, M. Hott & P. J. Marie. Strontium increases vertebral bone volume in rats at a low dose that does not induce detectable mineralization defect. *Bone* (1996) **18**, 253-259.

113. E. Canalis, M. Hott, P. Deloffre, Y. Tsouderos & P. J. Marie. The divalent strontium salt S12911 enhances bone cell replication and bone formation in vitro. *Bone* (1996) **18**, 517-523.

114. E. Bonnelye, A. Chabadel, F. Saltel & P. Jurdic. Dual effect of strontium ranelate: Stimulation of osteoblast differentiation and inhibition of osteoclast formation and resorption in vitro. *Bone* (2008) **42**, 129-138.

115. P. J. Marie, M. Hott, D. Modrowski, C. Depollak, J. Guillemain, P. Deloffre & Y. Tsouderos. An Uncoupling Agent Containing Strontium Prevents Bone Loss by Depressing Bone-Resorption and Maintaining Bone-Formation in Estrogen-Deficient Rats. *Journal of Bone and Mineral Research* (1993) **8**, 607-615.

116. R. K. Fuchs, M. R. Allen, K. W. Condon, S. Reinwald, L. M. Miller, D. McClenathan, B. Keck, R. J. Phipps & D. B. Burr. Strontium ranelate does not stimulate bone formation in ovariectomized rats. *Osteoporosis International* (2008) **19**, 1331-1341.

117. M. Hott, P. Deloffre, Y. Tsouderos & P. J. Marie. S12911-2 reduces bone loss induced by short-term immobilization in rats. *Bone* (2003) **33**, 115-123.

118. P. Delannoy, D. Bazot & P. J. Marie. Long-term treatment with strontium ranelate increases vertebral bone mass without deleterious effect in mice. *Metabolism-Clinical and Experimental* (2002) **51**, 906-911.

119. P. Ammann, V. Shen, B. Robin, Y. Mauras, J. P. Bonjour & R. Rizzoli. Strontium ranelate improves bone resistance by increasing bone mass and improving architecture in intact female rats. *Journal of Bone and Mineral Research* (2004) **19**, 2012-2020.

120. S. D. Bain, C. Jerome, V. Shen, I. Dupin-Roger & P. Ammann. Strontium ranelate improves bone strength in ovariectomized rat by positively influencing bone resistance determinants. *Osteoporosis International* (2009) **20**, 1417-1428.

121. K. E. Ozturan, B. Demir, I. Yucel, H. Cakıcı, F. Yilmaz & A. Haberal. Effect of strontium ranelate on fracture healing in the osteoporotic rats. *Journal of Orthopaedic Research* (2011) **29**, 138-142.

122. M. Shahnazari, D. H. Lang, G. J. Fosmire, N. A. Sharkey, A. D. Mitchell & R. M. Leach. Strontium administration in young chickens improves bone volume and architecture but does not enhance bone structural and material strength. *Calcified tissue international* (2007) **80**, 160-166.

123. E. M. Brown. Is the calcium receptor a molecular target for the actions of strontium on bone? *Osteoporosis International* (2003) **14**, S25-S34.

124. P. J. Marie. The calcium-sensing receptor in bone cells: A potential therapeutic target in osteoporosis. *Bone* (2010) **46**, 571-576.

125. J. Coulombe, H. Faure, B. Robin, Y. Tsouderos & M. Ruat. Activation of the rat and mouse cation-sensing receptor by strontium ranelate and its modulation by extracellular calcium. *Osteoporosis International* (2002) **13**, S25-S25.

126. J. Coulombe, H. Faure, B. Robin & M. Ruat. In vitro effects of strontium ranelate on the extracellular calcium-sensing receptor. *Biochemical and biophysical research communications* (2004) **323**, 1184-1190.

127. T. C. Brennan, M. S. Rybchyn, W. Green, S. Atwa, A. D. Conigrave & R. S. Mason. Osteoblasts play key roles in the mechanisms of action of strontium ranelate. *British journal of pharmacology* (2009) **157**, 1291-1300.

128. A. S. Hurtel-Lemaire, R. Mentaverri, A. Caudrillier, F. Cournarie, A. Wattel, S. Kamel, E. F. Terwilliger, E. M. Brown & M. Brazier. The Calcium-sensing Receptor Is Involved in Strontium Ranelate-induced Osteoclast Apoptosis NEW INSIGHTS INTO THE ASSOCIATED SIGNALING PATHWAYS. *Journal of Biological Chemistry* (2009) **284**, 575-584.

129. J. Y. Reginster, R. Deroisy, M. Dougados, I. Jupsin, J. Colette & C. Roux. Prevention of early postmenopausal bone loss by strontium ranelate: The randomized, two-year, double-masked, dose-ranging, placebo-controlled PREVOS trial. *Osteoporosis International* (2002) **13**, 925-931.

130. P. J. Meunier, D. O. Slosman, P. D. Delmas, J. L. Sebert, M. L. Brandi *et al*. Strontium ranelate: Dose-dependent effects in established postmenopausal vertebral osteoporosis - A 2-year randomized placebo controlled trial. *Journal of Clinical Endocrinology and Metabolism* (2002) **87**, 2060-2066.

131. P. J. Meunier & J. Y. Reginster. Design and methodology of the phase 3 trials for the clinical development of strontium ranelate in the treatment of women with postmenopausal osteoporosis. *Osteoporosis International* (2003) **14**, S66-S76.

132. P. J. Meunier, C. Roux, E. Seeman, S. Ortolani, J. E. Badurski *et al*. The effects of strontium ranelate on the risk of vertebral fracture in women with postmenopausal osteoporosis. *New England Journal of Medicine* (2004) **350**, 459-468.

133. P. J. Meunier, C. Roux, S. Ortolani, M. Diaz-Curiel, J. Compston *et al*. Effects of long-term strontium ranelate treatment on vertebral fracture risk in postmenopausal women with osteoporosis. *Osteoporosis International* (2009) **20**, 1663-1673.

134. J. Y. Reginster, E. Seeman, M. C. de Vernejoul, S. Adami, J. Compston *et al*. Strontium ranelate reduces the risk of nonvertebral fractures in postmenopausal women with osteoporosis: Treatment of Peripheral Osteoporosis (TROPOS) study. *Journal of Clinical Endocrinology and Metabolism* (2005) **90**, 2816-2822.

135. J. Reginster, D. Felsenberg, S. Boonen, A. Diez-Perez, R. Rizzoli *et al*. Effects of long-term strontium ranelate treatment on the risk of nonvertebral and vertebral fractures in postmenopausal osteoporosis - Results of a five-year, randomized, placebo-controlled trial. *Arthritis and Rheumatism* (2008) **58**, 1687-1695.

136. J. Y. Reginster, O. Bruyere, A. Sawicki, A. Roces-Varela, P. Fardellone, A. Roberts & J. P. Devogelaer. Long-term treatment of postmenopausal osteoporosis with strontium ranelate: Results at 8 years. *Bone* (2009) **45**, 1059-1064.

137. R. Barto, A. J. A. M. Sips, W. J. F. Vandervijgh & J. C. Netelenbos. Sensitive Method for Analysis of Strontium in Human and Animal Plasma by Graphite-Furnace Atomic-Absorption Spectrophotometry. *Clinical chemistry* (1995) **41**, 1159-1163.

138. T. Prohaska, C. Latkoczy, G. Schultheis, M. Teschler-Nicola & G. Stingeder. Investigation of Sr isotope ratios in prehistoric human bones and teeth using laser ablation ICP-MS and ICP-MS after Rb/Sr separation. *Journal of Analytical Atomic Spectrometry* (2002) **17**, 887-891.

139. J. P. Goulle, L. Mahieu, J. Castermant, N. Neveu, L. Bonneau, G. Laine, D. Bouige & C. Lacroix. Metal and metalloid multi-elementary ICP-MS validation in whole blood, plasma, urine and hair - Reference values. *Forensic science international* (2005) **153**, 39-44.

140. M. Piette, B. Desmet & R. Dams. Determination of Strontium in Human Whole-Blood by ICP-AES. *Science of the Total Environment* (1994) **141**, 269-273.

141. P. J. Parsons & F. Barbosa Jr. Atomic spectrometry and trends in clinical laboratory medicine. *Spectrochimica Acta Part B-Atomic Spectroscopy* (2007) **62**, 992-1003.

142. W. H. Evans & J. I. Read. Determination of Lithium, Rubidium and Strontium in Foodstuffs. *Analyst* (1985) **110**, 619-623.

143. C. A. Helsby. Determination of Strontium in Human Tooth Enamel by Atomic-Absorption Spectrometry. *Analytica Chimica Acta* (1974) **69**, 259-265.

144. M. Burguera, J. L. Burguera, M. L. Di Bernardo, C. Rondon, P. Carrero, E. Nieto, R. Salinas & E. Burguera. Strontium determination in human bone digests by flame atomic absorption spectrometry. *Quimica Analitica* (1999) **18**, 305-312.

145. M. Burguera, J. L. Burguera, C. Rondon, M. L. Di Bernardo, M. Gallignani, E. Nieto & J. Salinas. Appraisal of different electrothermal atomic absorption spectrometric methods for the determination of strontium in biological samples. *Spectrochimica Acta Part B-Atomic Spectroscopy* (1999) **54**, 805-818.

146. J. Scancar, R. Milacic, M. Benedik & P. Bukovec. Determination of trace elements and calcium in bone of the human iliac crest by atomic absorption spectrometry. *Clinica Chimica Acta* (2000) **293**, 187-197.

147. D. L. Tsalev, in *Atomic absorption spectrometry in occupational and and environmental health practice. Vol II,* CRC Press, Boca Raton, Florida, 1984.

148. D. L. Tsalev, in *Atomic absorption spectrometry in occupational and and environmental health practice. Vol III,* CRC Press, Boca Raton, Florida, 1995.

149. *Analytical methods for atomic absorption spectrometry,* The Perkin-Elmer Corporation, 1994.

150. A. Sanz-Medel, R. R. Roza & C. Perezconde. A Critical Comparative-Study of Atomic-Spectrometric Methods (Atomic-Absorption, Atomic Emission and Inductively Coupled Plasma Emission) for Determining Strontium in Biological-Materials. *Analyst* (1983) **108**, 204-212.

151. P. C. D'haese, G. F. VanLandeghem, L. V. Lamberts, V. A. Bekaert, I. Schrooten & M. E. Debroe. Measurement of strontium in serum, urine, bone, and soft tissues by Zeeman atomic absorption spectrometry. *Clinical chemistry* (1997) **43**, 121-128.

152. C. A. Helsby. Determination of Strontium in Human Tooth Enamel by Flameless Atomic-Absorption Spectrometry. *Talanta* (1977) **24**, 46-48.

153. O. R. Leeuwenkamp, W. J. F. Vandervijgh, B. C. P. Husken, P. Lips & J. C. Netelenbos. Quantification of Strontium in Plasma and Urine with Flameless Atomic-Absorption Spectrometry. *Clinical chemistry* (1989) **35**, 1911-1914.

154. I. Peltz-Csaszma, E. Andrasi, A. Lasztity & S. Kosel. Determination of strontium and its relation to other alkaline earth elements in human brain samples. *Microchemical Journal* (2005) **79**, 375-381.

155. G. P. Sighinolfi, C. Gorgoni, O. Bonori, E. Cantoni, M. Martelli & L. Simonetti. Comprehensive Determination of Trace-Elements in Human-Saliva by ETA-AAS. *Mikrochimica acta* (1989) **1**, 171-179.

156. L. A. Powell & R. L. Tease. Determination of Calcium, Magnesium, Strontium, and Silicon in Brines by Graphite-Furnace Atomic-Absorption Spectrometry. *Analytical Chemistry* (1982) **54**, 2154-2158.

157. K. Matsusaki. Mechanism and Removal of Halide Interferences in the Determination of Metals by Atomic-Absorption Spectrometry with Electrothermal Atomization. *Analytica Chimica Acta* (1982) **141**, 233-240.

158. H. S. Mahanti & R. M. Barnes. Determination of Major, Minor and Trace-Elements in Bone by Inductively-Coupled Plasma Emission-Spectrometry. *Analytica Chimica Acta* (1983) **151**, 409-417.

159. K. Shiraishi, H. Kawamura & G. Tanaka. Determination of Alkaline-Earth Metals in Fetus Bones by Inductively-Coupled Plasma Atomic-Emission Spectrometry. *Talanta* (1987) **34**, 823-827.

160. I. Martinsen & Y. Thomassen. Multielemental Characterization of Human-Lung Tissues by Icp-Aes. *Acta Pharmacologica et Toxicologica* (1986) **59**, 620-623.

161. K. Shiraishi, G. I. Tanaka & H. Kawamura. Simultaneous Multielement Analysis of various Human-Tissues by Inductively-Coupled Plasma Atomic-Emission Spectrometry. *Talanta* (1986) **33**, 861-865.

162. Y. Mauras, K. S. Ang, P. Simon, B. Tessier, F. Cartier & P. Allain. Increase in Blood-Plasma Levels of Boron and Strontium in Hemodialyzed Patients. *Clinica Chimica Acta* (1986) **156**, 315-320.

163. S. S. Q. Hee & J. R. Boyle. Simultaneous Multielemental Analysis of Some Environmental and Biological Samples by Inductively Coupled Plasma Atomic Emission-Spectrometry. *Analytical Chemistry* (1988) **60**, 1033-1042.

164. N. B. Roberts, H. P. J. Walsh, L. Klenerman, S. A. Kelly & T. R. Helliwell. Determination of elements in human femoral bone using inductively coupled plasma atomic emission spectrometry and inductively coupled plasma mass spectrometry. *Journal of Analytical Atomic Spectrometry* (1996) **11**, 133-138.

165. P. M. Outridge, R. J. Hughes & R. D. Evans. Determination of trace metals in teeth and bones by solution nebulization ICP-MS. *Atomic Spectroscopy* (1996) **17**, 1-8.

166. D. De Muynck & F. Vanhaecke. Development of a method based on inductively coupled plasma-dynamic reaction cell-mass spectrometry for the simultaneous determination of phosphorus, calcium

and strontium in bone and dental tissue. *Spectrochimica Acta Part B-Atomic Spectroscopy* (2009) **64**, 408-415.

167. T. Hasegawa, H. Matsuura, K. Inagaki & H. Haraguchi. Major-to-ultratrace elements in bone-marrow fluid as determined by ICP-AES and ICP-MS. *Analytical Sciences* (2003) **19**, 147-150.

168. J. Dombovari, Z. Varga, J. S. Becker, J. Matyus, G. Kakuk & L. Papp. ICP-MS determination of trace elements in serum samples of healthy subjects using different sample preparation methods. *Atomic Spectroscopy* (2001) **22**, 331-335.

169. C. S. Muniz, J. M. Larchante-Gayon, J. I. G. Alonso & A. Sanz-Medel. Multi-elemental trace analysis of human serum by double-focusing ICP-MS. *Journal of Analytical Atomic Spectrometry* (1999) **14**, 193-198.

170. C. S. Muniz, J. L. Fernandez-Martin, J. M. Marchante-Gayon, J. I. G. Alonso, J. B. Cannata-Andia & A. Sanz-Medel. Reference values for trace and ultratrace elements in human serum determined by double-focusing ICP-MS. *Biological trace element research* (2001) **82**, 259-272.

171. C. Latkoczy, T. Prohaska, G. Stingeder & M. Teschler-Nicola. Strontium isotope ratio measurements in prehistoric human bone samples by means of high-resolution inductively coupled plasma mass spectrometry (HR-ICP-MS). *Journal of Analytical Atomic Spectrometry* (1998) **13**, 561-566.

172. R. Djingova, B. Zlateva & I. Kuleff. On the possibilities of inductively coupled plasma mass spectrometry for analysis of archaeological bones for reconstruction of paleodiet. *Talanta* (2004) **63**, 785-789.

173. M. Gerotto, E. Dellandrea, A. Bortoli, M. Marchiori, M. Palonta & A. Troncon. Interference Effects and Their Control in Icp-Ms Analysis of Serum and Saline Solutions. *Microchemical Journal* (1995) **51**, 73-87.

174. N. K. Aras, G. Yilmaz, F. Korkusuz, I. Olmez, B. Sepici, F. Eksioglu & P. Bode. Multielement analysis of iliac crest bone by neutron activation. *Journal of Radioanalytical and Nuclear Chemistry* (2000) **244**, 185-188.

175. M. K. Takata & M. Saiki. INAA of cortical and trabecular bone samples from animals. *Journal of Radioanalytical and Nuclear Chemistry* (2004) **259**, 375-379.

176. V. Zaichick. INAA application in the age dynamics assessment of Ca, Cl, K, Mg, Mn, Na, P and Sr in the cortical bone of human femoral neck. *Journal of Radioanalytical and Nuclear Chemistry* (2004) **259**, 351-354.

177. J. Versieck, L. Vanballenberghe, A. Wittoek & H. Vanhoe. The Determination of Strontium in Human Blood-Serum and Packed Blood-Cells by Radiochemical Neutron-Activation Analysis. *Journal of Radioanalytical and Nuclear Chemistry-Articles* (1993) **168**, 243-248.

178. H. Vanhoe, C. Vandecasteele, J. Versieck & R. Dams. Determination of Trace-Elements in a Human Serum Reference Material by Inductively Coupled Plasma Mass-Spectrometry. *Mikrochimica acta* (1989) **3**, 373-379.

179. A. P. Packer, D. Lariviere, C. Li, M. Chen, A. Fawcett, K. Nielsen, K. Mattson, A. Chatt, C. Scriver & L. S. Erhardt. Validation of an inductively coupled plasma mass spectrometry (ICP-MS)

method for the determination of cerium, strontium, and titanium in ceramic materials used in radiological dispersal devices (RDDs). *Analytica Chimica Acta* (2007) **588**, 166-172.

180. M. L. Carvalho, J. Brito & M. A. Barreiros. Study of trace element concentrations in human tissues by EDXRF spectrometry. *X-Ray Spectrometry* (1998) **27**, 198-204.

181. M. L. Carvalho, C. Casaca, T. Pinheiro, J. P. Marques, P. Chevallier & A. S. Cunha. Analysis of human teeth and bones from the chalcolithic period by X-ray spectrometry. *Nuclear Instruments & Methods in Physics Research Section B-Beam Interactions with Materials and Atoms* (2000) **168**, 559-565.

182. T. Akyuz, A. Bassari & S. Akyuz. Determination of elements in bone of tuberculous-arthritis patients by radioisotope X-ray fluorescence analysis. *Journal of Radioanalytical and Nuclear Chemistry* (1998) **232**, 253-255.

183. A. Pejovic-Milic, I. M. Stronach, J. Gyorffy, C. E. Webber & D. R. Chettle. Quantification of bone strontium levels in humans by in vivo x-ray fluorescence. *Medical physics* (2004) **31**, 528-538.

184. Y. X. Zhang, Y. P. Zhang, Y. P. Tong, S. J. Qiu, X. T. Wu & K. R. Dai. Multi-element determination in cancellous bone of human femoral head by PIXE. *Journal of Radioanalytical and Nuclear Chemistry-Letters* (1996) **212**, 341-351.

185. S. P. Nielsen, O. Barenholdt, C. Barenholdt-Schioler, Y. Mauras & P. Allain. Noninvasive measurement of bone strontium. *Journal of Clinical Densitometry* (2004) **7**, 262-268.

186. Certificate of analysis. Standard Reference Material 1486 Bone Meal. National Institute for Standards,and Technology, (1992).

187. F. E. Smith & E. A. Arsenault. Microwave-assisted sample preparation in analytical chemistry. *Talanta* (1996) **43**, 1207-1268.

188. S. D'Ilio, N. Violante, S. Caimi, M. Di Gregorio, F. Petrucci & O. Senofonte. Determination of trace elements in serum by dynamic reaction cell inductively coupled plasma mass spectrometry - Developing of a method with a desolvating system nebulizer. *Analytica Chimica Acta* (2006) **573**, 432-438.

189. J. Begerow, M. Turfeld & L. Dunemann. Determination of physiological palladium, platinum, iridium and gold levels in human blood using double focusing magnetic sector field inductively coupled plasma mass spectrometry. *Journal of Analytical Atomic Spectrometry* (1997) **12**, 1095-1098.

190. J. Begerow, M. Turfeld & L. Dunemann. Determination of physiological platinum levels in human urine using magnetic sector field inductively coupled plasma mass spectrometry in combination with ultraviolet photolysis. *Journal of Analytical Atomic Spectrometry* (1996) **11**, 913-916.

191. M. Krachler, C. Heisel & P. Kretzer. Validation of ultratrace analysis of Co, Cr, Mo and Ni in whole blood, serum and urine using ICP-SMS. *Journal of Analytical Atomic Spectrometry* (2009) **24**, 605-610.

192. D. Beauchemin. Inductively coupled plasma mass spectrometry. *Analytical Chemistry* (2004) **76**, 3395-3415.

193. E. Barany, I. A. Bergdahl, A. Schutz, S. Skerfving & A. Oskarsson. Inductively coupled plasma mass spectrometry for direct multi-element analysis of diluted human blood and serum. *Journal of Analytical Atomic Spectrometry* (1997) **12**, 1005-1009.

194. J. L. M. de Boer, R. Ritsema, S. Piso, H. van Staden & d. B. van. Practical and quality-control aspects of multi-element analysis with quadrupole ICP-MS with special attention to urine and whole blood. *Analytical and Bioanalytical Chemistry* (2004) **379**, 872-880.

195. Guide to the expression of uncertainty in measurement. DS/ENV 13005, 1. edn. Dansk Standard, (1999).

196. S. Ellison, M. Rosslein & A. (.). Williams. EURACHEM/CITAC Guide: Quantifying Uncertainty in Analytical Measurement, 2. udg. (2000).

197. M. Bettinelli. ICP-MS determination of Pt in biological fluids of patients treated with antitumor agents: evaluation of analytical uncertainty. *Microchemical Journal* (2005) **79**, 357-365.

198. M. Breda, M. Maffini, A. Mangia, C. Mucchino & M. Musci. Development and validation of an inductively coupled plasma mass spectrometry method with optimized microwave-assisted sample digestion for the determination of platinum at ultratrace levels in plasma and ultrafiltrate plasma. *Journal of pharmaceutical and biomedical analysis* (2008) **48**, 435-439.

199. M. Patriarca, M. Castelli, F. Corsetti & A. Menditto. Estimate of uncertainty of measurement from a single-laboratory validation study: Application to the determination of lead in blood. *Clinical chemistry* (2004) **50**, 1396-1405.

200. D. Stockl, K. Van Uytfanghe, D. R. Cabaleiro & L. M. Thienpont. Calculation of measurement uncertainty in clinical chemistry. *Clinical chemistry* (2005) **51**, 276-277.

201. M. Patriarca, M. Castelli, F. Corsetti & A. Menditto. Calculation of measurement uncertainty in clinical chemistry - Reply. *Clinical chemistry* (2005) **51**, 277-277.

202. M. Patriarca, M. Castelli, F. Corsetti & A. Menditto. Estimate of uncertainty of measurement from a single-laboratory validation study: Application to the determination of lead in blood (vol 50, pg 1396, 2004). *Clinical chemistry* (2005) **51**, 281-281.

203. A. Taylor, S. Branch, M. P. Day, M. Patriarca & M. White. Atomic spectrometry update. Clinical and biological materials, foods and beverages. *Journal of Analytical Atomic Spectrometry* (2006) **21**, 439-491.

204. R. Thomas, in *Practical guide to ICP-MS - A tutorial for beginners,* 2nd edn., CRC Press, Boca Raton, 2008.

205. D. De Muynck, C. Cloquet & F. Vanhaecke. Development of a new method for Pb isotopic analysis of archaeological artefacts using single-collector ICP-dynamic reaction cell-MS. *Journal of Analytical Atomic Spectrometry* (2008) **23**, 62-71.

206. M. Y. Perez-Jordan, A. Salvador & l. G. de. Determination of Sr, K, Mg and Na in human teeth by atomic spectrometry using a microwave-assisted digestion in a closed flow system. *Analytical Letters* (1998) **31**, 867-877.

207. Elements in blood or tissue. Method 8005, issue 2, in *NIOSH manual of analytical methods.* ch. 4 U.S. Department of Health and Human Services. National Institute for Occupational Safety and Health, Cincinnati, OH, 1994.

208. R. S. Houk, V. A. Fassel, G. D. Flesch, H. J. Svec, A. L. Gray & C. E. Taylor. Inductively Coupled Argon Plasma as an Ion-Source for Mass-Spectrometric Determination of Trace-Elements. *Analytical Chemistry* (1980) **52**, 2283-2289.

209. D. Beauchemin. Inductively coupled plasma mass spectrometry. *Analytical Chemistry* (2002) **74**, 2873-2893.

210. D. Beauchemin. Inductively coupled plasma mass spectrometry. *Analytical Chemistry* (2006) **78**, 4111-4135.

211. D. Beauchemin. Inductively coupled plasma mass spectrometry. *Analytical Chemistry* (2008) **80**, 4455-4486.

212. D. Beauchemin. Inductively Coupled Plasma Mass Spectrometry. *Analytical Chemistry* (2010) **82**, 4786-4810.

213. D. Beauchemin. Environmental Analysis by Inductively Coupled Plasma Mass Spectrometry. *Mass spectrometry reviews* (2010) **29**, 560-592.

214. M. Reijnen, in *Basic STD and DRC Elan ICPMS training - course module,* Perkin-Elmer Corporation, Netherlands.

215. K. L. Linge & K. E. Jarvis. Quadrupole ICP-MS: Introduction to Instrumentation, Measurement Techniques and Analytical Capabilities. *Geostandards and Geoanalytical Research* (2009) **33**, 445-467.

216. A. A. Ammann. Inductively coupled plasma mass spectrometry (ICP MS): a versatile tool. *Journal of Mass Spectrometry* (2007) **42**, 419-427.

217. A. Montaser (ed.), in *Inductively coupled plasma mass spectrometry,* Wiley-VCH, New York, 1998.

218. S. M. Nelms (ed.), in *ICP mass spectrometry handbook,* 1st edn., CRC Press, Boca Raton, 2005.

219. J. Todoli & J. Mermet, in *Liquid sample introduction in ICP spectrometry - A practical guide,* 1st edn., Elsevier, Amsterdam, 2008.

220. D. J. Douglas & S. D. Tanner, Fundamental considerations in ICPMS, in *Inductively Coupled Plasma Mass Spectrometry,* (ed. A. Montaser), 615-679, Wiley-WCH, New York, 1998.

221. L. A. Simpson, M. Thomsen, B. J. Alloway & A. Parker. A dynamic reaction cell (DRC) solution to oxide-based interferences in inductively coupled plasma mass spectrometry (ICP-MS) analysis of the noble metals. *Journal of Analytical Atomic Spectrometry* (2001) **16**, 1375-1380.

222. G. Horlick, S. H. Tan, M. A. Vaughan & C. A. Rose. The Effect of Plasma Operating Parameters on Analyte Signals in Inductively Coupled Plasma-Mass Spectrometry. *Spectrochimica Acta Part B-Atomic Spectroscopy* (1985) **40**, 1555-1572.

223. M. A. Vaughan, G. Horlick & S. H. Tan. Effect of Operating Parameters on Analyte Signals in Inductively Coupled Plasma Mass-Spectrometry. *Journal of Analytical Atomic Spectrometry* (1987) **2**, 765-772.

224. W. G. Diegor & H. P. Longerich. Parameter interaction in signal optimization of an ICP mass spectrometer. *Atomic Spectroscopy* (2000) **21**, 111-117.

225. K. Sakata & K. Kawabata. Reduction of Fundamental Polyatomic Ions in Inductively-Coupled Plasma-Mass Spectrometry. *Spectrochimica Acta Part B-Atomic Spectroscopy* (1994) **49**, 1027-&.

226. O. Mestek & R. Koplik. Dual Detector Calibration of PE-Elan Inductively Coupled Plasma Mass Spectrometers. *Chemia Analityczna* (2009) **54**, 1245-1252.

227. M. J. Campbell & K. I. Burns. Non-linearity of detector response in ICP-MS. *Journal of Analytical Atomic Spectrometry* (2001) **16**, 970-974.

228. K. Simitchiev, V. Stefanova, V. Kmetov, G. Andreev, N. Kovachev & A. Canals. Microwave-assisted cloud point extraction of Rh, Pd and Pt with 2-mercaptobenzothiazole as preconcentration procedure prior to ICP-MS analysis of pharmaceutical products. *Journal of Analytical Atomic Spectrometry* (2008) **23**, 717-726.

229. J. A. Kanis, P. Delmas, P. Burckhardt, C. Cooper & D. Torgerson. Guidelines for diagnosis and management of osteoporosis. *Osteoporosis International* (1997) **7**, 390-406.

230. K. Danzer & L. A. Currie. Guidelines for calibration in analytical chemistry - Part 1. Fundamentals and single component calibration (IUPAC recommendations 1998). *Pure and Applied Chemistry* (1998) **70**, 993-1014.

231. H. K. Genant, C. Cooper, G. Poor, I. Reid, G. Ehrlich *et al*. Interim report and recommendations of the World Health Organization task-force for osteoporosis. *Osteoporosis International* (1999) **10**, 259-264.

232. W. W. Peppler & R. B. Mazess. Total-Body Bone-Mineral and Lean Body-Mass by Dual-Photon Absorptiometry .1. Theory and Measurement Procedure. *Calcified tissue international* (1981) **33**, 353-359.

233. G. M. Blake & I. Fogelman. Technical principles of dual energy x-ray absorptiometry. *Seminars in nuclear medicine* (1997) **27**, 210-228.

234. B. Abrahamsen, H. A. Sørensen, B. Rud, A. P. Hermann, J. B. Jensen, C. Mølgaard & O. H. Sørensen. Normalområder og kvalitetskontrol for dual energy X-ray absortiometry-scanning. *Ugeskrift for læger* (2005) **167**, 878-882.

235. G. M. Blake & I. Fogelman. The clinical role of dual energy X-ray absorptiometry. *European Journal of Radiology* (2009) **71**, 406-414.

236. H. H. Bolotin. Inaccuracies inherent in dual-energy X-ray absorptiometry in vivo bone mineral densitometry may flaw osteopenic/osteoporotic interpretations and mislead assessment of antiresorptive therapy effectiveness. *Bone* (2001) **28**, 548-555.

237. R. B. Mazess, H. S. Barden, J. P. Bisek & J. Hanson. Dual-Energy X-Ray Absorptiometry for Total-Body and Regional Bone-Mineral and Soft-Tissue Composition. *American Journal of Clinical Nutrition* (1990) **51**, 1106-1112.

238. O. R. Madsen, J. E. B. Jensen & O. H. Sorensen. Validation of a dual energy X-ray absorptiometer: Measurement of bone mass and soft tissue composition. *European journal of applied physiology and occupational physiology* (1997) **75**, 554-558.

239. H. H. Bolotin & H. Sievanen. Inaccuracies inherent in dual-energy X-ray absorptiometry in vivo bone mineral density can seriously mislead diagnostic/prognostic interpretations of patient-specific bone fragility. *Journal of Bone and Mineral Research* (2001) **16**, 799-805.

240. S. P. Nielsen, D. Slosman, O. H. Sorensen, B. Basse-Cathalinat, P. De Cassin, C. Roux & P. J. Meunier. Influence of strontium on bone mineral density and bone mineral content measurements by dual X-ray absorptiometry. *Journal of Clinical Densitometry* (1999) **2**, 371-379.

241. J. Liao, G. M. Blake, A. H. McGregor & R. Patel. The effect of bone strontium on BMD is different for different manufacturers' DXA Systems. *Bone* (2010) **47**, 882-887.

242. G. M. Blake, E. M. Lewieck, D. L. Kendler & I. Fogelman. A review of strontium ranelate and its effect on DXA scans. *Journal of Clinical Densitometry* (2007) **10**, 113-119.

243. S. J. Gallacher & T. Dixon. Impact of Treatments for Postmenopausal Osteoporosis (Bisphosphonates, Parathyroid Hormone, Strontium Ranelate, and Denosumab) on Bone Quality: A Systematic Review. *Calcified tissue international* (2010) **87**, 469-484.

244. C. H. Turner & D. B. Burr. Basic Biomechanical Measurements of Bone - a Tutorial. *Bone* (1993) **14**, 595-608.

245. C. Sonne, H. Wolkers, F. F. Riget, J. B. Jensen, J. Teilmann *et al*. Mineral density and biomechanical properties of bone tissue from male Arctic foxes (Vulpes lagopus) exposed to organochlorine contaminants and emaciation. *Comparative Biochemistry and Physiology C-Toxicology & Pharmacology* (2009) **149**, 97-103.

246. E. H. vanVeen, S. Bosch & M. T. C. deLoosVollebregt. Precision-based optimization of multicomponent analysis in inductively coupled plasma mass spectrometry. *Spectrochimica Acta Part B-Atomic Spectroscopy* (1996) **51**, 591-608.

247. C. Sartoros, D. M. Goltz & E. D. Salin. Program considerations for simplex optimization of ion lenses in ICP-MS. *Applied Spectroscopy* (1998) **52**, 643-648.

248. D. Pozebon, V. L. Dressler, J. S. Becker, A. Matusch, M. Zoriy & J. S. Becker. Biomonitoring of essential and toxic elements in small biological tissues by ICP-MS. *Journal of Analytical Atomic Spectrometry* (2008) **23**, 1281-1284.

249. I. I. Stewart & J. W. Olesik. Steady state acid effects in ICP-MS. *Journal of Analytical Atomic Spectrometry* (1998) **13**, 1313-1320.

250. I. I. Stewart & J. W. Olesik. The effect of nitric acid concentration and nebulizer gas flow rates on aerosol properties and transport rates in inductively coupled plasma sample introduction. *Journal of Analytical Atomic Spectrometry* (1998) **13**, 1249-1256.

251. E. H. Evans & J. A. Caruso. Optimization Strategies for the Reduction of Nonspectroscopic Interferences in Inductively Coupled Plasma Mass-Spectrometry. *Spectrochimica Acta Part B-Atomic Spectroscopy* (1992) **47**, 1001-1012.

252. I. Novotny, J. C. Farinas, J. L. Wan, E. Poussel & J. M. Mermet. Effect of power and carrier gas flow rate on the tolerance to water loading in inductively coupled plasma atomic emission spectrometry. *Spectrochimica Acta Part B-Atomic Spectroscopy* (1996) **51**, 1517-1526.

253. X. Romero, E. Poussel & J. M. Mermet. The effect of sodium on analyte ionic line intensities in inductively coupled plasma atomic emission spectrometry: Influence of the operating conditions. *Spectrochimica Acta Part B-Atomic Spectroscopy* (1997) **52**, 495-502.

254. X. Romero, E. Poussel & J. M. Mermet. Influence of the operating conditions on the efficiency of internal standardization in inductively coupled plasma atomic emission spectrometry. *Spectrochimica Acta Part B-Atomic Spectroscopy* (1997) **52**, 487-493.

255. A. Fernandez, M. Murillo, N. Carrion & J. M. Mermet. Influence of Operating-Conditions on the Effects of Acids in Inductively-Coupled Plasma-Atomic Emission-Spectrometry. *Journal of Analytical Atomic Spectrometry* (1994) **9**, 217-221.

256. J. W. Tromp, M. Pomares, M. Alvarez-Prieto, A. Cole, H. Ying & E. D. Salin. Exploration of robust operating conditions in inductively coupled plasma mass spectrometry. *Spectrochimica Acta Part B-Atomic Spectroscopy* (2003) **58**, 1927-1944.

257. S. N. Deming & L. R. Parker. Review of Simplex Optimization in Analytical-Chemistry. *Crc Critical Reviews in Analytical Chemistry* (1978) **7**, 187-202.

258. E. H. Evans & L. Ebdon. Comparison of Normal and Low-Flow Torches for Inductively Coupled Plasma Mass-Spectrometry using Optimized Operating-Conditions. *Journal of Analytical Atomic Spectrometry* (1991) **6**, 421-430.

259. D. C. Montgomery, in *Design and analysis of experiments,* 5th edn., John Wiley & Sons, Hoboken, 2001.

260. B. Karlberg & R. Torgrip. Increasing the scope and power of flow-injection analysis through chemometric approaches. *Analytica Chimica Acta* (2003) **500**, 299-306.

261. S. D'Ilio, N. Violante, M. Di Gregorio, O. Senofonte & F. Petrucci. Simultaneous quantification of 17 trace elements in blood by dynamic reaction cell inductively coupled plasma mass spectrometry (DRC-ICP-MS) equipped with a high-efficiency sample introduction system. *Analytica Chimica Acta* (2006) **579**, 202-208.

262. K. Benkhedda, D. Lariviere, S. Scott & D. Evans. Hyphenation of flow injection on-line preconcentration and ICP-MS for the rapid determination of Ra-226 in natural waters. *Journal of Analytical Atomic Spectrometry* (2005) **20**, 523-528.

263. S. F. Boulyga & K. G. Heumann. Determination of extremely low U-236/U-238 isotope ratios in environmental samples by sector-field inductively coupled plasma mass spectrometry using high-efficiency sample introduction. *Journal of environmental radioactivity* (2006) **88**, 1-10.

264. V. N. Epov, K. Benkhedda, R. J. Cornett & R. D. Evans. Rapid determination of plutonium in urine using flow injection on-line preconcentration and inductively coupled plasma mass spectrometry. *Journal of Analytical Atomic Spectrometry* (2005) **20**, 424-430.

265. P. Rustad, P. Felding, A. Lahti & P. H. Petersen. Descriptive analytical data and consequences for calculation of common reference intervals in the Nordic Reference Interval Project 2000. *Scandinavian Journal of Clinical & Laboratory Investigation* (2004) **64**, 343-369.

266. S. Caroli, A. Alimonti, E. Coni, F. Petrucci, O. Senofonte & N. Violante. The Assessment of Reference Values for Elements in Human Biological Tissues and Fluids - a Systematic Review. *Critical Reviews in Analytical Chemistry* (1994) **24**, 363-398.

267. R. Forrer, K. Gautschi & H. Lutz. Simultaneous measurement of the trace elements Al, As, B, Be, Cd, Co, Cu, Fe, Li, Mn, Mo, Ni, Rb, Se, Sr, and Zn in human serum and their reference ranges by ICP-MS. *Biological trace element research* (2001) **80**, 77-93.

268. R. Rahil-Khazen, B. J. Bolann & R. J. Ulvik. Trace element reference values in serum determined by inductively coupled plasma atomic emission spectrometry. *Clinical Chemistry and Laboratory Medicine* (2000) **38**, 765-772.

269. S. F. Boulyga, U. Kloetzli, G. Stingeder & T. Prohaska. Optimization and application of ICPMS with dynamic reaction cell for precise determination of Ca-44/Ca-40 isotope ratios. *Analytical Chemistry* (2007) **79**, 7753-7760.

270. G. De Wannemacker, A. Ronderos, L. Moens, F. Vanhaecke, M. J. C. Bijvelds & Z. I. Kolar. Use of double-focusing sector field ICP-mass spectrometry in tracer experiments, aiming at the quantification of Mg2+ transport across the intestine of tilapia fish. *Journal of Analytical Atomic Spectrometry* (2001) **16**, 581-586.

271. G. Esslemont, W. Maher, P. Ford & F. Krikowa. The determination of phosphorus and other elements in plant leaves by ICP-MS after low-volume microwave digestion with nitric acid. *Atomic Spectroscopy* (2000) **21**, 42-45.

272. W. Maher, S. Forster, F. Krikowa, P. Snitch, G. Chapple & P. Craig. Measurement of trace elements and phosphorus in marine animal and plant tissues by low-volume microwave digestion and ICP-MS. *Atomic Spectroscopy* (2001) **22**, 361-370.

273. R. G. Fernandez, J. I. G. Alonso & A. Sanz-Medel. Coupling of ICP-MS with ion chromatography after conductivity suppression for the determination of anions in natural and waste waters. *Journal of Analytical Atomic Spectrometry* (2001) **16**, 1035-1039.

274. M. Kovacevic, A. Gartner & M. Novic. Determination of bisphosphonate by ion chromatography-inductively coupled mass spectrometry. *Journal of Chromatography a* (2004) **1039**, 77-82.

275. P. Allain, L. Jaunault, Y. Mauras, J. M. Mermet & T. Delaporte. Signal Enhancement of Elements due to the Presence of Carbon-Containing Compounds in Inductively Coupled Plasma Mass-Spectrometry. *Analytical Chemistry* (1991) **63**, 1497-1498.

276. M. Kovacevic, W. Goessler, N. Mikac & M. Veber. Matrix effects during phosphorus determination with quadrupole inductively coupled plasma mass spectrometry. *Analytical and Bioanalytical Chemistry* (2005) **383**, 145-151.

277. M. Wind, A. Eisenmenger & W. D. Lehmann. Modified direct injection high efficiency nebulizer with minimized dead volume for the analysis of biological samples by micro- and nano-LC-ICP-MS. *Journal of Analytical Atomic Spectrometry* (2002) **17**, 21-26.

278. M. Wind, M. Edler, N. Jakubowski, M. Linscheid, H. Wesch & W. D. Lehmann. Analysis of protein phosphorylation by capillary liquid chromatography coupled to element mass spectrometry with P-31 detection and to electrospray mass spectrometry. *Analytical Chemistry* (2001) **73**, 29-35.

279. D. Profrock, P. Leonhard & A. Prange. Determination of phosphorus in phosphorylated deoxyribonucleotides using capillary electrophoresis and high performance liquid chromatography hyphenated to inductively coupled plasma mass spectrometry with an octopole reaction cell. *Journal of Analytical Atomic Spectrometry* (2003) **18**, 708-713.

280. M. Kovacevic, R. Leber, S. D. Kohlwein & W. Goessler. Application of inductively coupled plasma mass spectrometry to phospholipid analysis. *Journal of Analytical Atomic Spectrometry* (2004) **19**, 80-84.

281. D. R. Bandura, V. I. Baranov & S. D. Tanner. Detection of ultratrace phosphorus and sulfur by quadrupole ICPMS with dynamic reaction cell. *Analytical Chemistry* (2002) **74**, 1497-1502.

282. S. Kozono, S. Takahashi & H. Haraguchi. Determination of trace phosphorus in high purity tantalum materials by inductively coupled plasma mass spectrometry subsequent to matrix separation with on-line anion exchange/coprecipitation. *Analytical and Bioanalytical Chemistry* (2002) **372**, 542-548.

283. J. S. Becker, K. Fuellner, U. D. Seeling, G. Fornalczyk & A. J. Kuhn. Measuring magnesium, calcium and potassium isotope ratios using ICP-QMS with an octopole collision cell in tracer studies of nutrient uptake and translocation in plants. *Analytical and Bioanalytical Chemistry* (2008) **390**, 571-578.

284. A. P. Krushevska, Y. Zhou, V. Ravikumar, Y. Kim & J. Hinrichs. Chromium based polyatomic interferences on rhodium in ICP-MS. *Journal of Analytical Atomic Spectrometry* (2006) **21**, 847-855.

285. R. Djingova, H. Heidenreich, P. Kovacheva & B. Markert. On the determination of platinum group elements in environmental materials by inductively coupled plasma mass spectrometry and microwave digestion. *Analytica Chimica Acta* (2003) **489**, 245-251.

286. C. S. Hsiung, J. D. Andrade, R. Costa & K. O. Ash. Minimizing interferences in the quantitative multielement analysis of trace elements in biological fluids by inductively coupled plasma mass spectrometry. *Clinical chemistry* (1997) **43**, 2303-2311.

287. J. A. Olivares & R. S. Houk. Suppression of Analyte Signal by various Concomitant Salts in Inductively Coupled Plasma Mass-Spectrometry. *Analytical Chemistry* (1986) **58**, 20-25.

288. F. Vanhaecke, H. Vanhoe, R. Dams & C. Vandecasteele. The use of Internal Standards in Icp Ms. *Talanta* (1992) **39**, 737-742.

289. H. Falk, R. Geerling, B. Hattendorf, K. KrengelRothensee & K. P. Schmidt. Capabilities and limits of ICP-MS for direct determination of element traces in saline solutions. *Fresenius Journal of Analytical Chemistry* (1997) **359**, 352-356.

290. J. Riondato, F. Vanhaecke, L. Moens & R. Dams. Fast and reliable determination of (ultra-)trace and/or spectrally interfered elements in water by sector field ICP-MS. *Journal of Analytical Atomic Spectrometry* (2000) **15**, 341-345.

291. I. E. Vasilyeva, E. V. Shabanova, Y. V. Sokolnikova, O. A. Proydakova & V. I. Lozhkin. Selection of internal standard for determination of boron and phosphorus by ICP-MS in silicon photovoltaic materials. *Journal of Analytical Atomic Spectrometry* (1999) **14**, 1519-1521.

292. P. Masson, T. Dalix & S. Bussiere. Determination of Major and Trace Elements in Plant Samples by Inductively Coupled Plasma-Mass Spectrometry. *Communications in Soil Science and Plant Analysis* (2010) **41**, 231-243.

293. I. Rodushkin, E. Engstrom, A. Stenberg & D. C. Baxter. Determination of low-abundance elements at ultra-trace levels in urine and serum by inductively coupled plasma-sector field mass spectrometry. *Analytical and Bioanalytical Chemistry* (2004) **380**, 247-257.

294. J. W. H. Lam & G. Horlick. A Comparison of Argon and Mixed Gas Plasmas for Inductively Coupled Plasma Mass-Spectrometry. *Spectrochimica Acta Part B-Atomic Spectroscopy* (1990) **45**, 1313-1325.

295. J. M. Craig & D. Beauchemin. Reduction of the Effects of Concomitant Elements in Inductively Coupled Plasma Mass-Spectrometry by Adding Nitrogen to the Plasma Gas. *Journal of Analytical Atomic Spectrometry* (1992) **7**, 937-942.

296. D. Beauchemin & J. M. Craig. Investigations on Mixed-Gas Plasmas Produced by Adding Nitrogen to the Plasma Gas in Icp-Ms. *Spectrochimica Acta Part B-Atomic Spectroscopy* (1991) **46**, 603-614.

297. E. H. Evans & L. Ebdon. Effect of Organic-Solvents and Molecular Gases on Polyatomic Ion Interferences in Inductively Coupled Plasma Mass-Spectrometry. *Journal of Analytical Atomic Spectrometry* (1990) **5**, 425-429.

298. H. Louie & S. Y. P. Soo. Use of Nitrogen and Hydrogen in Inductively Coupled Plasma Mass-Spectrometry. *Journal of Analytical Atomic Spectrometry* (1992) **7**, 557-564.

299. Q. C. Zeng, E. Zhang & J. Tellinghuisen. Univariate calibration by reversed regression of heteroscedastic data: a case study. *Analyst* (2008) **133**, 1649-1655.

300. S. F. Durrant. Alternatives to All-Argon Plasmas in Inductively-Coupled Plasma-Mass Spectrometry (Icp-Ms) - an Overview. *Fresenius Journal of Analytical Chemistry* (1993) **347**, 389-392.

301. F. R. Meeks. Electron Number Density in a Slightly Ionized-Gas (Argon Inductively-Coupled Plasma). *Spectrochimica Acta Part B-Atomic Spectroscopy* (1993) **48**, 1537-1549.

302. R. S. Houk. Mass-Spectrometry of Inductively Coupled Plasmas. *Analytical Chemistry* (1986) **58**, A97-&.

303. R. M. Barnes. Advances in Inductively-Coupled Plasma-Mass Spectrometry - Human-Nutrition and Toxicology. *Analytica Chimica Acta* (1993) **283**, 115-130.

304. D. C. Gregoire. The Effect of Easily Ionizable Concomitant Elements on Nonspectroscopic Interferences in Inductively Coupled Plasma-Mass Spectrometry. *Spectrochimica Acta Part B-Atomic Spectroscopy* (1987) **42**, 895-907.

305. G. R. Gillson, D. J. Douglas, J. E. Fulford, K. W. Halligan & S. D. Tanner. Nonspectroscopic Interelement Interferences in Inductively Coupled Plasma Mass-Spectrometry. *Analytical Chemistry* (1988) **60**, 1472-1474.

306. H. Niu & R. S. Houk. Fundamental aspects of ion extraction in inductively coupled plasma mass spectrometry. *Spectrochimica Acta Part B-Atomic Spectroscopy* (1996) **51**, 779-815.

307. S. D. Tanner. Space-Charge in Icp-Ms - Calculation and Implications. *Spectrochimica Acta Part B-Atomic Spectroscopy* (1992) **47**, 809-823.

308. S. E. Hobbs & J. W. Olesik. Laser-Excited Fluorescence Studies of Matrix-Induced Errors in Inductively Coupled Plasma Spectrometry - Implications for Icp-Mass Spectrometry. *Applied Spectroscopy* (1991) **45**, 1395-1407.

309. Y. S. Kim, H. Kawaguchi, T. Tanaka & A. Mizuike. Non-Spectroscopic Matrix Interferences in Inductively Coupled Plasma-Mass Spectrometry. *Spectrochimica Acta Part B-Atomic Spectroscopy* (1990) **45**, 333-339.

310. D. Beauchemin, J. W. Mclaren & S. S. Berman. Study of the Effects of Concomitant Elements in Inductively Coupled Plasma Mass-Spectrometry. *Spectrochimica Acta Part B-Atomic Spectroscopy* (1987) **42**, 467-490.

311. A. Townsend, A. Featherstone, C. C. Chery, F. Vanhaecke, J. Kirby, F. Krikowa, B. Maher, G. Jacobson & G. Peterson. Increased selenium concentrations in seronorm trace elements serum. *Clinical chemistry* (2004) **50**, 1481-1482.

312. A. M. Featherstone, A. T. Townsend, G. A. Jacobson & G. M. Peterson. Comparison of methods for the determination of total selenium in plasma by magnetic sector inductively coupled plasma mass spectrometry. *Analytica Chimica Acta* (2004) **512**, 319-327.

313. I. Schrooten, W. Cabrera, W. G. Goodman, S. Dauwe, L. V. Lamberts, R. Marynissen, W. Dorrine, M. E. De Broe & P. C. D'Haese. Strontium causes osteomalacia in chronic renal failure rats. *Kidney international* (1998) **54**, 448-456.

314. I. Schrooten, G. J. S. Behets, W. E. Cabrera, S. R. Vercauteren, L. V. Lamberts *et al*. Dose-dependent effects of strontium on bone of chronic renal failure rats. *Kidney international* (2003) **63**, 927-935.

315. J. N. Miller & J. C. Miller, in *Statistics and chemometrics for analytical chemistry, 5. udg,* Paerson Education Limited, Edinburgh, 2005.

316. J. Tellinghuisen. Weighted least-squares in calibration: What difference does it make? *Analyst* (2007) **132**, 536-543.

317. L. Bruggemann, P. Morgenstern & R. Wennrich. Comparison of regression techniques for linear calibration. *Accreditation and Quality Assurance* (2005) **10**, 344-351.

318. A. G. Asuero & G. Gonzalez. Fitting straight lines with replicated observations by linear regression. III. Weighting data. *Critical Reviews in Analytical Chemistry* (2007) **37**, 143-172.

319. L. Cuadros-Rodriguez, L. Gamiz-Cracia, E. Almansa-Lopez & J. Laso-Sanchez. Calibration in chemical measurement processes: I. A metrological approach. *Trac-Trends in Analytical Chemistry* (2001) **20**, 195-206.

320. IUPAC Compendium of analytical nomenclature. Sections 2.3 - 2.4. International Union of Pure and Applied Chemistry, (2002) http://old.iupac.org/publications/analytical_compendium/, retrieved Feb 2007.

321. J. N. Miller. Basic Statistical-Methods for Analytical-Chemistry .2. Calibration and Regression Methods - A Review. *Analyst* (1991) **116**, 3-14.

322. J. E. T. Andersen. A step-wise approach to the determination of the lower limit of analysis of the calibration line. *Journal of Analytical Chemistry* (2008) **63**, 308-319.

323. J. E. T. Andersen. Exercise in Quality Assurance: A Laboratory Exercise. *Journal of chemical education* (2009) **86**, 733-737.

324. A. Klukowska. Identification of sulfur compunds responsible for flavor in liquid consumables. Master thesis. Technical University of Denmark, Kgs. Lyngby (2009).

325. H. Al-Faloje. Determination of volatile organic compounds in blue cheese using head space-mono trap with gas chromatograhpy mass spectrometry. Master thesis. Technical University of Denmark, Kgs. Lyngby (2009).

326. M. Mikolajczak. Determination of anions in pharmaceutical salts. Master thesis. Technical University of Denmark, Kgs. Lyngby (2010).

327. P. M. Gy, in *Sampling for analytical purposes,* 1st edn., John Wiley and Sons, Chichester, 1998.

328. L. Petersen, P. Minkkinen & K. H. Esbensen. Representative sampling for reliable data analysis: Theory of Sampling. *Chemometrics and Intelligent Laboratory Systems* (2005) **77**, 261-277.

329. J. B. Holm-Nielsen, C. K. Dahl & K. H. Esbensen. Representative sampling for process analytical characterization of heterogeneous bioslurry systems - a reference study of sampling issues in PAT. *Chemometrics and Intelligent Laboratory Systems* (2006) **83**, 114-126.

330. K. H. Esbensen, H. H. Friis-Petersen, L. Petersen, J. B. Holm-Nielsen & P. P. Mortensen. Representative process sampling - in practice: Variographic analysis and estimation of total sampling errors (TSE). *Chemometrics and Intelligent Laboratory Systems* (2007) **88**, 41-59.

331. C. Robinson, S. J. Brookes, J. Kirkham, R. C. Shore & W. A. Bonass. Uptake and Metabolism of Albumin by Rodent Incisor Enamel In-Vivo and Postmortem - Implications for Control of Mineralization by Albumin. *Calcified tissue international* (1994) **55**, 467-472.

332. S. Suga, H. Aoki, Y. Yamashita, M. Tsuno & M. Ogawa. A comparative study of disturbed mineralization of rat incisor enamel induced by strontium and fluoride administration. *Advances in Dental Research* (1987) **1**, 339-355.

333. A. Christensen. Strontium malonate. 26-week toxicity study in rats. Scantox study report 59146/NBS-T06-GE, Lab Scantox, Ejby, Denmark (2006).

334. P. J. Marie & M. Hott. Short-Term Effects of Fluoride and Strontium on Bone-Formation and Resorption in the Mouse. *Metabolism-Clinical and Experimental* (1986) **35**, 547-551.

335. R. Dybkaer. Unit "katal" for catalytic activity (IUPAC technical report). *Pure and Applied Chemistry* (2001) **73**, 927-931.

336. R. Dybkaer. The special name "katal" for the SI derived unit, mole per second, when expressing catalytic activity. *Metrologia* (2000) **37**, 671-676.

337. K. S. Leung, K. P. Fung, A. H. L. Sher, C. K. Li & K. M. Lee. Plasma Bone-Specific Alkaline-Phosphatase as an Indicator of Osteoblastic Activity. *Journal of Bone and Joint Surgery-British Volume* (1993) **75**, 288-292.

338. J. A. Yaeger. Recovery of rat incisor dentin from abnormal mineralization produced by strontium and fluoride. *The Anatomical Record* (1966) **154**, 661-673.

339. Raffalt, A. C., Sørensen, S. R., Jensen, J. B., Christgau, S. & Andersen, J. E. T. *Strontium treatment does not affect the mineralisation of calcified tissue in rats and dogs* (Euroanalysis XV, EuChems Division of analytical Chemistry, Innsbruck, Austria, 2009).

340. K. Kaaber. Strontium malonate. A 52-week toxicity study in dogs - oral (gavage) administration. Scantox study report 62346/NBS-T09-GE, Lab Scantox, Ejby, Denmark (2007).

341. P. N. Kumta, C. Sfeir, D. H. Lee, D. Olton & D. Choi. Nanostructured calcium phosphates for biomedical applications: novel synthesis and characterization. *Acta Biomaterialia* (2005) **1**, 65-83.

342. C. G. Frankær. Locating Sr-ions in bone tissue using EXAFS. X-ray and Protein Crystallography Group, DTU Chemistry, Lyngby (2010).

343. E. M. Barker, in *Neuroscience nursing: a spectrum of care*, 3rd edn., Elsevier Health Sciences, St. Louis, 2008.

344. S. Hillson, in *Teeth*, 2nd edn., Cambridge University Press, Cambridge, 2005.

345. S. L. Manske, T. Liu-Ambrose, D. M. L. Cooper, S. Kontulainen, P. Guy, B. B. Forster & H. A. McKay. Cortical and trabecular bone in the femoral neck both contribute to proximal femur failure load prediction. *Osteoporosis International* (2009) **20**, 445-453.

346. M. Potoczek. Hydroxyapatite foams produced by gelcasting using agarose. *Materials Letters* (2008) **62**, 1055-1057.

Appendix I

Investigation of hydrolysis of organic phosphorus compounds using stopped-flow analysis

1 Introduction

In view of the poor accuracy observed in the determination of phosphorous in serum using ICP-MS (cf. Chapter 5), the potential of flow injection analysis (FIA) and sequential injection analysis (SIA) for quantification of P in biological fluids was explored. These methods have been used extensively for quantification of P in environmental samples [1-4] and were thought to constitute suitable alternatives to ICP-MS. The most widely used method for determination of inorganic P is the molybdenum-blue spectrophotometric method, in which orthophosphate reacts with an acidified molybdenum reagent to form phosphomolybdate heteropolyacid, which is then reduced to form a blue compound and determined spectrophotometrically [1, 2]. Though most of the phosphate bound to organic compounds is unable to react directly with molybdenum, the highly acidic conditions may cause hydrolysis of some organic P compounds. This would make organic P available for reaction with molybdenum and lead to an overestimation of the inorganic P concentration. The aim of this work is to investigate three model P compounds, glucose-6-phosphate (G6P), phytic acid and penta-sodium triphosphate, to asses the extent of hydrolysis during P determination using the molybdenum-blue method.

2 Experimental

All glassware and bottles were cleaned overnight in nutrient free detergent (Neutracon®), rinsed three times with ultra-pure water (18.2 MΩ), soaked in 10% (v/v) HCl for 24 h and again rinsed three times with ultra-pure water. All solutions and reagents were prepared with ultra-pure water. A 100 mg/l PO_4-P stock solution was prepared by dissolving 0.4393 g of dried potassium dihydrogen orthophosphate in 1 l of ultra-pure water. Organic P stock solutions were prepared as shown in Table 1. Working standards were prepared by dilution of the stock solutions.

Table 1 Preparation of organic P stock standards. Fresh stock solutions were prepared every day.

Compound	Amount transferred (mg)	Final volume (ml)	Stock concentration (mg l^{-1} P)
Glucose-6-phosphate	96.3	100	100
Phytic acid	396.2	100	1000
Triphosphate	395.9	100	1000

2.1 Flow method

Two reagents were prepared: ammonium molybdate (5 g ammonium molybdate and 17.5 ml sulphuric acid in 500 ml ultra-pure water) and tin(II)chloride (0.1 g tin(II)chloride, 1 g hydrazinium sulphate and 14 ml sulphuric acid in 500 ml ultra-pure water). The measurements were performed using an in-house flow injection analyser (Figures 1 – 2) at the University of Plymouth and a FIAlab-3200 SIA instrument (Figure 3) at Monash University.

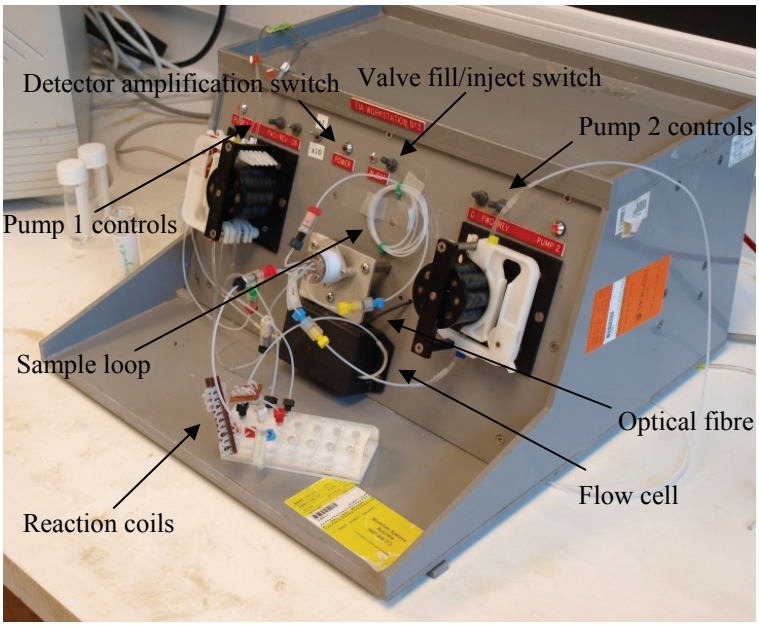

Figure 1 The flow injection analyser used for phosphate analysis at the University of Plymouth.

The FIA manifold consisted of two peristaltic pumps, PTFE tubing, a flow cell and an injection valve (Figure 1). All electronics, such as detectors, amplifiers and LED are contained in a gray housing. The analyser is connected to a PC via a USB connection. The valve is turned by applying pressurised N_2 gas. The pump tubing used for the FIA reagent streams are shown in Table 2. The system is designed for determination of phosphate using the molybdenum-blue method with tin(II)chloride as a reductant and detection at 690 nm. Pump 1 runs at 40 rpm and is used to propel

the carrier (ultra-pure water), molybdenum and tin(II)chloride streams. Pump 2 runs at 20 rpm and is used to fill the sample loop.

Table 2 Pump tubing (Elkay accu-rated) used with the flow analyser.

Stream	Colour code
Carrier	White/White
Acid molybdate	Orange/White
Tin(II)chloride	Orange/Yellow

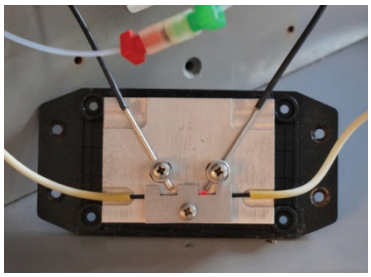

Figure 2 The multi-reflection flow cell. Red light from the LED is visible at the end of the fibre on the right hand side [5].

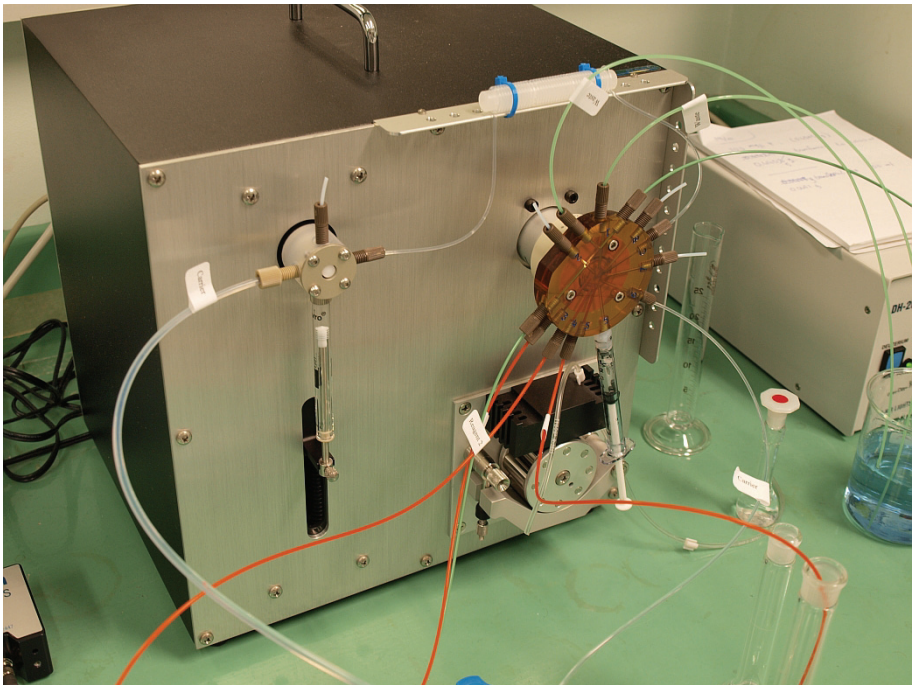

Figure 3 The FIAlab sequential injection system used for analysis of organic phosphate.

Details on the principles and operation of the SIA apparatus are given elsewhere [6, 7].

2.2 Batch method

Four reagents were prepared, sulphuric acid (70 ml concentrated sulphuric acid diluted with 500 ml ultra-pure water), ammonium molybdate (15 g ammonium molybdate in 500 ml of ultra-pure water), ascorbic acid (5.4 g ascorbic acid in 100 ml ultra-pure water) and potassium antimonyl tartrate (0.34 g potassium antimonyl tartrate in 500 ml ultra-pure water). A working reagent was prepared (fresh every time) by mixing

1. 75 ml sulphuric acid solution
2. 25 ml ammonium molybdate solution
3. 25 ml ascorbic acid solution
4. 12.5 ml potassium antimonyl tartrate solution

20 ml of sample or calibration standard was transferred to a 25 ml volumetric flask, 4 ml working reagent was added and the flask was filled to the mark with ultra-pure water and inverted several times. The reagent-sample solution was immediately transferred to a 1 cm quarts cell, and the absorbance (λ = 890 nm) was measured at selected reaction times (5-35 min) by leaving the cell in the spectrophotometer and taking 3-5 replicate readings when desired.

3 Results

3.1 Flow injection

The flow analyser has two different amplification settings. Typical calibrations are shown in Figure 4. The x10 setting increases the sensitivity with a factor of 10 compared with the 1x setting. The high amplification (LOD: 0.5 $\mu g\ l^{-1}$ P) is recommended for determination of phosphate concentrations below 10 $\mu g\ l^{-1}$ P.

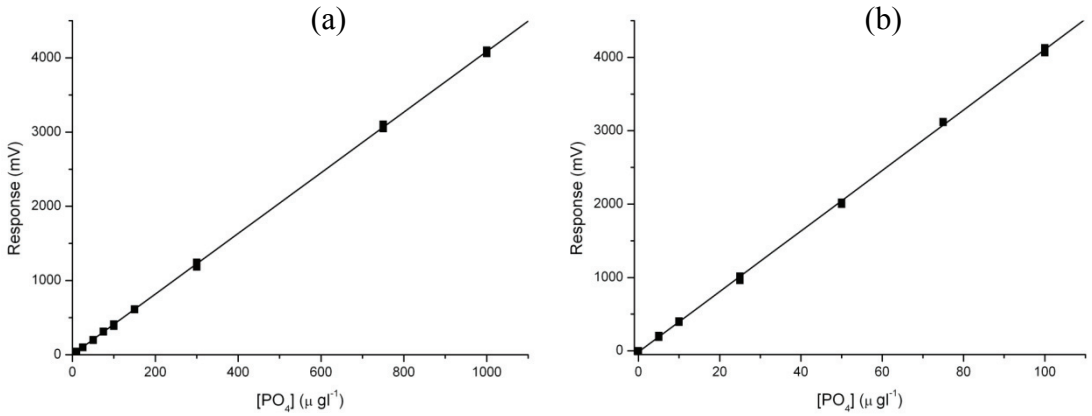

Figure 4 Calibrations with the detector amplification set on x1 (a) and x10 (b). The sensitivities were 4.08 and 41.2 mV l μg^{-1}, respectively.

3.2 Stopped flow

If the sample-reagent mixture is stopped within the flow cell, the rate of the colour reaction can be measured by monitoring the change in absorbance. Under normal circumstances, a program to automatically stop the flow precisely at the appropriate time could easily be created in the LabView software. However, due to noise problems, the onboard pumps could not be used, and hence external pumps had to be applied. The flow was therefore stopped manually and the correct timing was observed with the aid of a stop watch. Using the SIA system, the stopped-flow procedure and the data collection could be fully automated by the accompanying software.

3.2.1 Inorganic phosphate

In order to assess the timing and response of the flow analyser, a series of orthophosphate standards were analysed. The time between sample injection and the point where the flow was stopped was eventually set to 22 s. The (instantaneous) rate of reaction at a given time can be determined by the slope of the tangent drawn to the absorption curve (Figure 5).

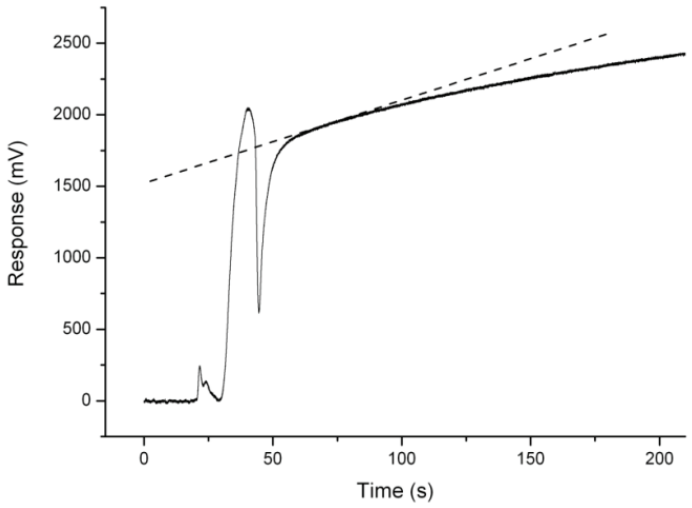

Figure 5 Stopped Flow analysis of 50 µg l^{-1} PO_4 using the FIA apparatus. The reaction rate is given by the slope of the tangent drawn to the curve (dashed line).

As can be seen from Figures 6-8, the rate of reaction increases with increasing phosphate concentration.

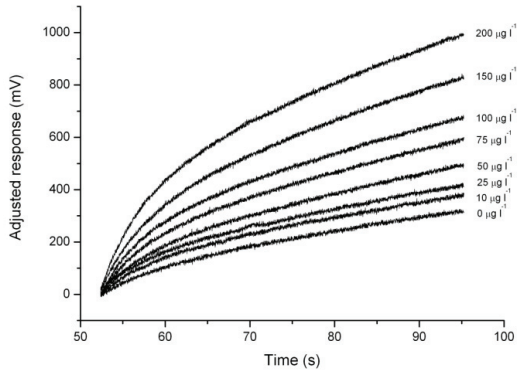

Figure 6 Sections of response curves for 0-200 µg l^{-1} PO_4.

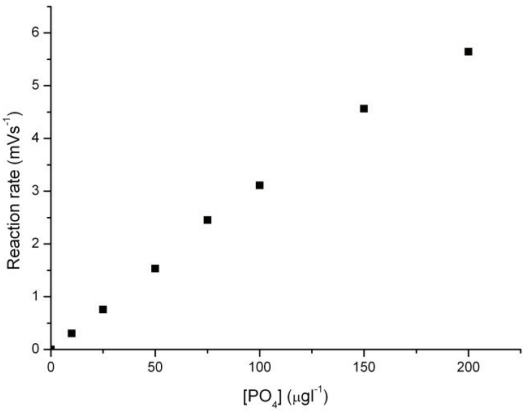

Figure 7 Reaction rate as a function of initial phosphate concentration.

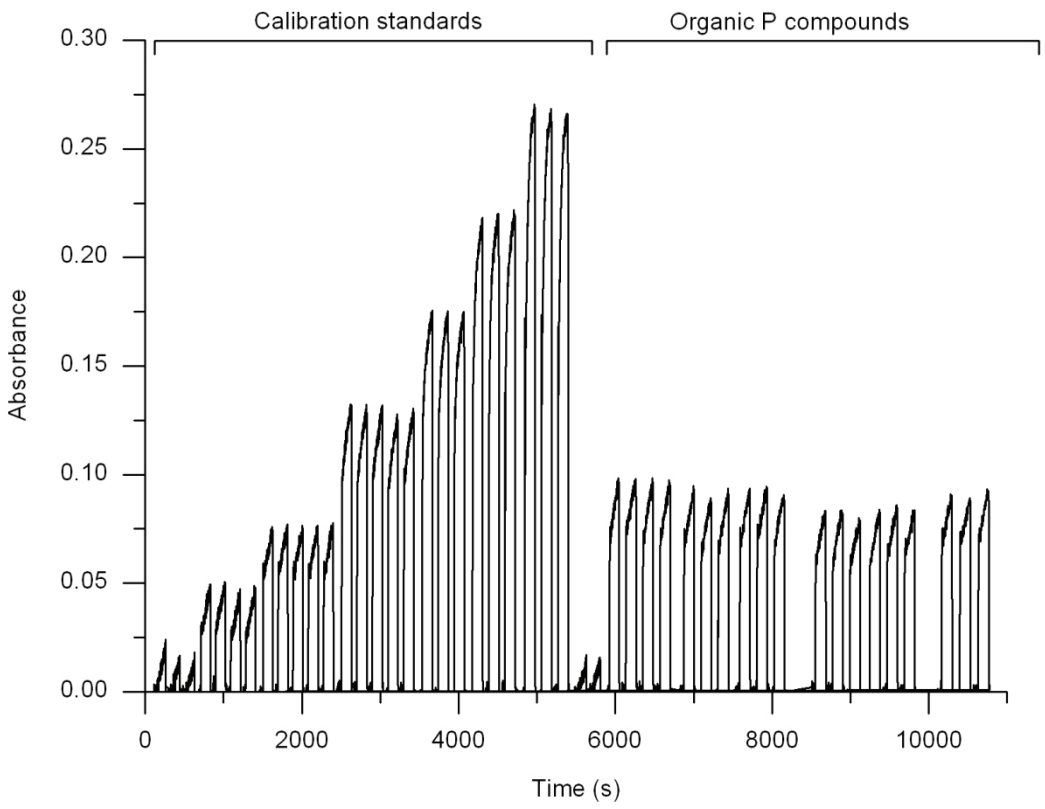

Figure 8 Recorded data from stopped flow analysis of organic phosphate compounds. Stopping the flow provide an incubation time for reaction rate measurements [7]. The stop-flow curves up to 4700 s originate from analysis of calibration standards containing 0-1 mg L^{-1} PO_4^-.

3.2.2 Reaction order

Let us assume that the general reaction

$$A + B \rightarrow C \tag{1}$$

has the rate law

$$r = -\frac{d[A]}{dt} = -\frac{d[B]}{dt} = \frac{d[C]}{dt} = k[A]^n[B]^m \tag{2}$$

where r is the rate, k the rate constant and $n + m$ the order of reaction. If the reactant B is present in large excess, we can write

$$r = k[A]^n[B]^m = k'[A]^n, \qquad k' = k[B]^m \tag{3-1}$$

which can be rearranged to

$$\ln r = \ln k' + n \ln[A] \quad (4)$$

With the reagents (ammonium molybdate and tin(II)chloride) in excess, a plot of ln(rate) against ln[PO_4] is expected to form a straight line with slope *n*. Figure 9 shows that the plot is indeed linear with a slope of 0.99, indicating a reaction order of 1 with respect to phosphate, in accordance with previous reports [8]. This shows that the flow analyser is capable of producing reliable kinetic measurements using the stopped-flow technique and that the instrument is very suitable for the current investigation.

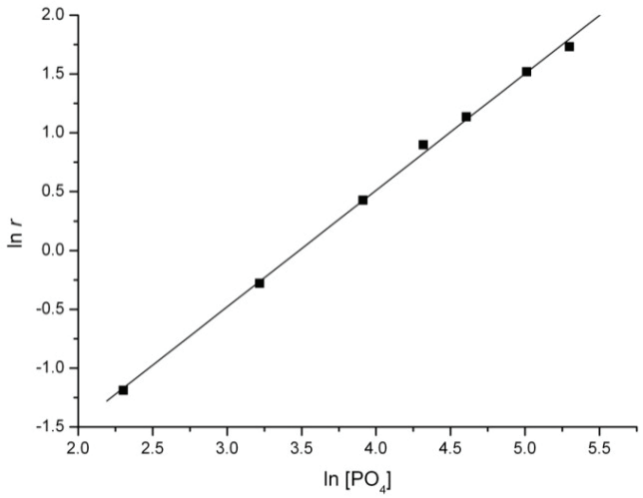

Figure 9 ln *r* vs. ln[PO_4]. The slope of the fitted line is 0.99, indicating a first order reaction (see text).

3.2.3 Organic phosphate compounds

As the most labile of the three investigated organic P compounds, G6P was expected to be the most susceptible to hydrolysis. However, the slopes of the response curves for 0-200 µg l^{-1} G6P (Figure 10) were constant within the noise level. Figure 11 shows the calculated reaction rate as a function of the G6P concentration. No significant relation was found (the slope of the fitted line is not significantly different from zero).

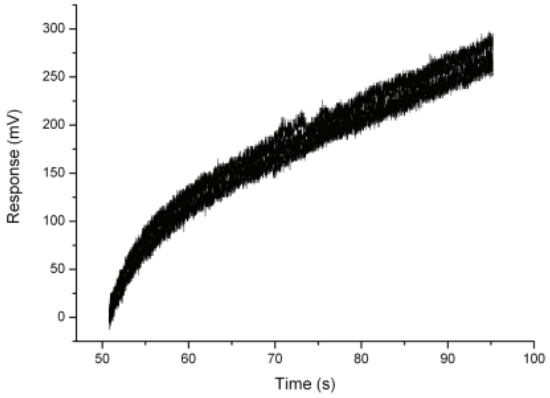

Figure 10 Overlaid sections of response curves for 0-200 µg l^{-1} P- glucose-6-phosphate.

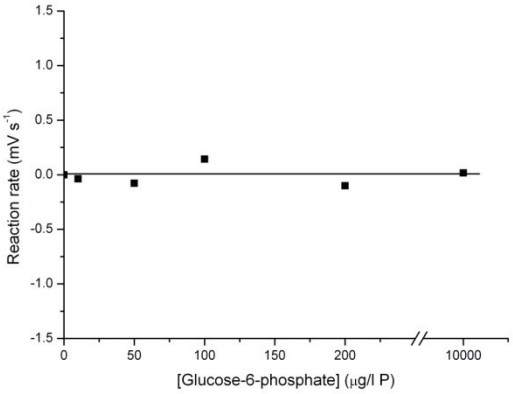

Figure 11 Reaction rate vs. glucose-6-phosphate concentration. No significant relation was found.

Seeing that no measurable hydrolysis had taken place with G6P, it was assumed that similar results would be obtained for triphosphate and particularly phytic acid. Hence, it was decided not to continue the investigation of these compounds using the flow injection analyser. Similar results were reached using the SIA instrument.

3.3 Batch measurements

With the flow injection analyser, data could be collected for no longer than 5 min per analysis. To allow for a longer reaction time, the batch method described in section 2.2 was applied.

3.3.1 Inorganic phosphate

Standards of 10-100 µg l^{-1} PO_4 were mixed with the working reagent and used to calibrate the spectrophotometer (Figure 12) at reaction times of 5, 12 and 20 min. The highest absorbance was seen after 12 min (Figure 13), confirming the recommendation stated in the SOP.

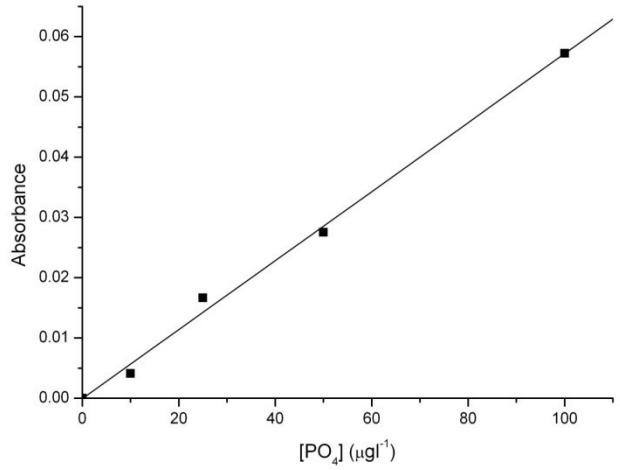

Figure 12 Batch method calibration. The reagent-sample mixture was left to react in the flow cell for 12 min as recommended in the SOP.

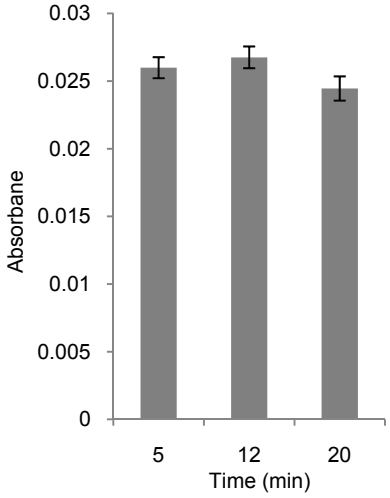

Figure 13 Absorbance of 50 µg l^{-1} phosphate at reaction times of 5, 12 and 20 minutes. The error bars show the standard deviation (precision).

3.3.2 Organic phosphate compounds

The sensitivity of the batch method (LOD: 3 µg l^{-1} P) was much lower than that of the flow injection analyser, and therefore much higher concentrations of the organic P compounds were required. The analysis of 2 mg l^{-1} G6P (Figure 14a) showed an absorbance maximum at a reaction time of 18-20 min, after which the response decreased. The PO_4 concentration after 20 min was 13 µg l^{-1}, corresponding to 0.7% hydrolysed G6P. However, this low concentration of PO_4 may well be explained by impurities in the stock G6P compound, as the certificate only guarantees > 95% purity. The decrease in absorbance after 20 min indicates that there was no ongoing formation of reactive PO_4 and therefore no (measureable) hydrolysis of G6P within 35 min. The 5 mg l^{-1} G6P solution showed maximum absorbance after 12 min (Figure 14b), corresponding to 16 µg l^{-1} PO_4 and 0.3% hydrolysed G6P. Again, the presence of reactive PO_4 may be a result of impurities.

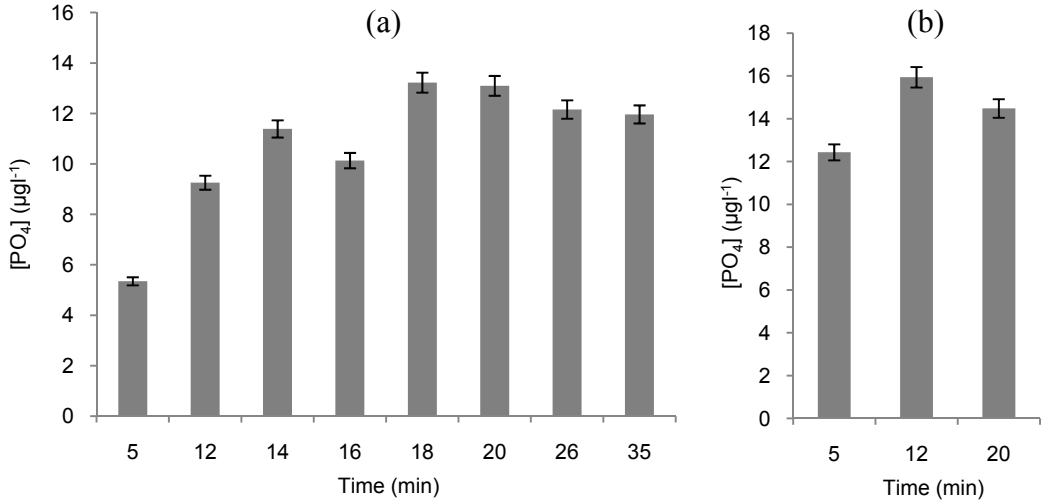

Figure 14 Glucose-6-phosphate, 2 mg l^{-1} (a) and 5 mg l^{-1} (b). The bar charts show the concentration of PO_4 after different reaction times. The error bars show the standard deviation (precision).

The absorbance of 1 mg l^{-1} phytic acid (Figure 15a) was below or very close to the limit of detection after 5 and 12 min. After 20 min the PO_4 concentration was 8 µg l^{-1}, corresponding to 0.8% hydrolysis. 10 mg L^{-1} phytic acid (Figure 15b) had an absorbance maximum after 12 min with a PO_4 concentration of 21 µg L^{-1}, corresponding to 0.2% hydrolysed phytic acid. As was the case with G6P, these low concentrations of reactive PO_4 may not be caused by hydrolysis of dissolved organic P, but instead by impurities in the stock compound.

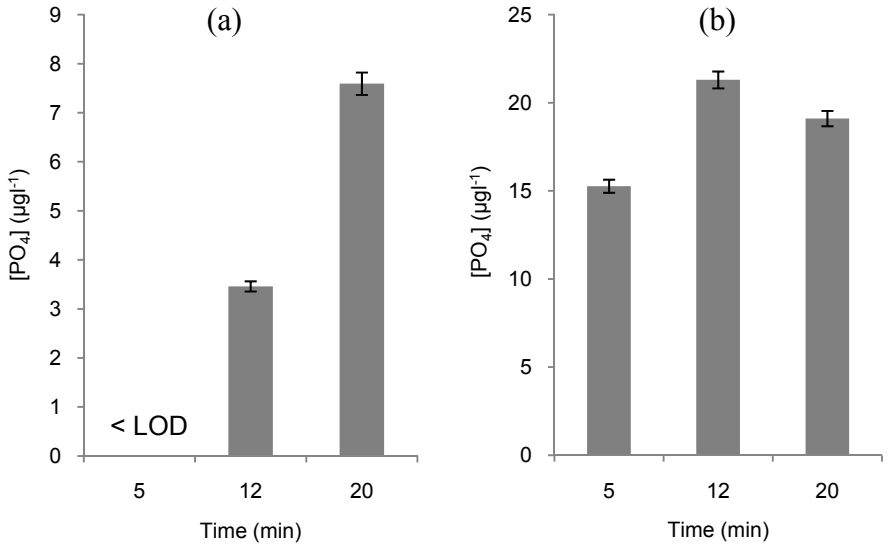

Figure 15 Phytic acid, 1 mg L^{-1} (a) and 10 mg L^{-1} (b). The bar charts show the concentration of PO_4 after different reaction times. The error bars show the standard deviation (precision).

The response pattern of 1 mg L^{-1} triphosphate (Figure 16a) was very similar to that of 5 mg L^{-1} G6P and 10 mg L^{-1} phytic acid. At the absorbance maximum at 12 min reaction time, the PO_4 concentration was 15 µg l^{-1}, corresponding to 1.5% hydrolysis. In contrast, the 10 mg L^{-1} triphosphate solution (Figure 16b) showed a steady increase in PO_4 concentration with time. After 5 min the PO_4 concentration was 35 µg L^{-1}, increasing to 65, 79 and 98 µg L^{-1} PO_4 after 12, 20 and 30 min, respectively. This suggests that triphosphate was hydrolysed continuously during the 30 min. The average reaction rate from 5 to 30 min was 2.4 µg L^{-1} min^{-1} PO_4, and the PO_4 concentration after 30 min corresponded to 1% hydrolysis.

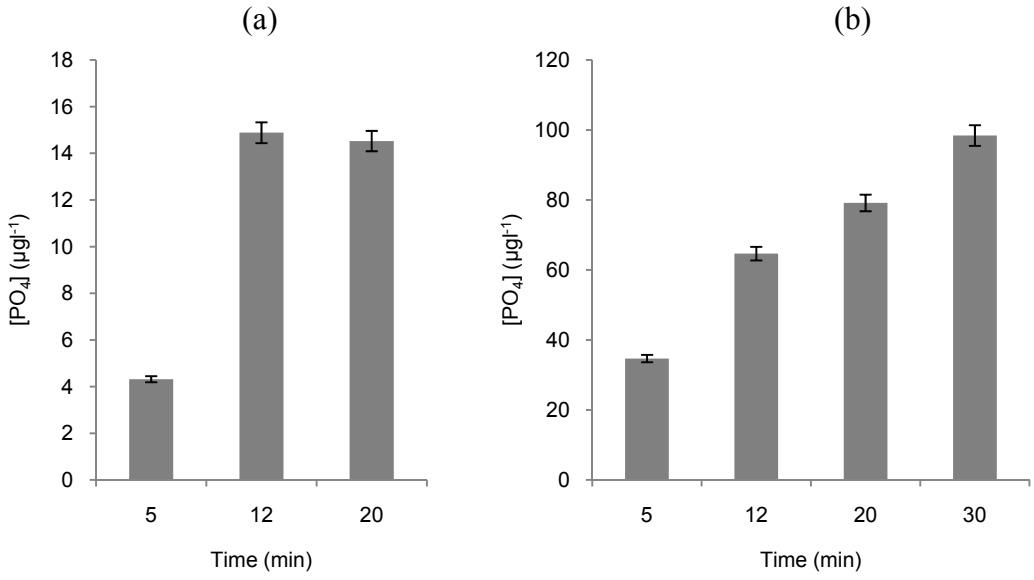

Figure 16 Triphosphate, 1 mg L^{-1} (a) and 10 mg L^{-1} (b). The bar charts show the concentration of PO_4 after different reaction times. The error bars show the standard deviation (precision).

4 Conclusion

The flow injection analyser and the SIA instrument used in the present work are capable of producing reliable kinetic measurements using the stopped-flow technique. The investigation showed that the acidic reagents used with the molybdenum-blue method caused no or very little hydrolysis of the three organic P compounds. In all cases, less than 2% of organic P was hydrolysed after 12-35 min exposure to the acidic environment. In fact, the concentrations of reactive PO_4 were so low that they may only be the results of impurities in the stock compounds. Thus, the molybdenum-blue method may be a feasible method for determination of P in biological fluids.

5 References

1. P. Monbett, I. D. Mckelvie, A. Saefumillah & P. J. Worsfold. A protocol to assess the enzymatic release of dissolved organic phosphorus species in waters under environmentally relevant conditions. *Environmental science & technology* (2007) **41**, 7479-7485.

2. L. J. Gimbert, P. M. Haygarth & P. J. Worsfold. Determination of nanomolar concentrations of phosphate in natural waters using flow injection with a long path length liquid waveguide capillary cell and solid-state spectrophotometric detection. *Talanta* (2007) **71**, 1624-1628.

3. P. J. Worsfold, L. J. Gimbert, U. Mankasingh, O. N. Omaka, G. Hanrahan, P. C. F. C. Gardolinski, P. M. Haygarth, B. L. Turner, M. J. Keith-Roach & I. D. McKelvie. Sampling, sample treatment and quality assurance issues for the determination of phosphorus species in natural waters and soils. *Talanta* (2005) **66**, 273-293.

4. P. J. Worsfold, P. Monbet, A. D. Tappin, M. F. Fitzsimons, D. A. Stiles & I. D. McKelvie. Characterisation and quantification of organic phosphorus and organic nitrogen components in aquatic systems: A review. *Analytica Chimica Acta* (2008) **624**, 37-58.

5. P. S. Ellis, A. J. Lyddy-Meaney, P. J. Worsfold & I. D. McKelvie. Multi-reflection photometric flow cell for use in flow injection analysis of estuarine waters. *Analytica Chimica Acta* (2003) **499**, 81-89.

6. Operations manual for the MicroSIA, FIAlab-3200, and FIAlab-3500 systems. FIAlab Instruments, Inc., (2005).

7. J. Ruzicka. Lab-on-valve: universal microflow analyzer based on sequential and bead injection. *Analyst* (2000) **125**, 1053-1060.

8. K. Grudpan, P. Ampan, Y. Udnan, S. Jayasvati, S. Lapanantnoppakhun, J. Jakmunee, G. D. Christian & J. Ruzicka. Stopped-flow injection simultaneous determination of phosphate and silicate using molybdenum blue. *Talanta* (2002) **58**, 1319-1326.

Appendix II

Application of inductively coupled plasma-mass spectrometry (ICP-MS) and quality assurance to study the incorporation of strontium into bone, bone marrow, and teeth of dogs after one month of treatment with strontium malonate

With kind permission from Springer Science + Business Media: *Analytical and Bioanalytical Chemistry,* 391(6), 2008, p 2199-2207, Anders C. Raffalt, Jens E.T. Andersen and Stephan Christgau.

Anal Bioanal Chem (2008) 391:2199–2207
DOI 10.1007/s00216-008-2171-0

ORIGINAL PAPER

Application of inductively coupled plasma–mass spectrometry (ICP–MS) and quality assurance to study the incorporation of strontium into bone, bone marrow, and teeth of dogs after one month of treatment with strontium malonate

Anders C. Raffalt · Jens E. T. Andersen · Stephan Christgau

Received: 21 January 2008 / Revised: 25 April 2008 / Accepted: 30 April 2008 / Published online: 23 May 2008

Abstract The strontium content of serum, bone, marrow, and teeth was determined by inductively-coupled plasma mass spectrometry (ICP–MS). Significant correlations were obtained after the data were subjected to quality assurance (QA) performed according to validated procedures. After four weeks of treatment with strontium malonate, strontium levels increased from 76±9 μg g^{-1} in placebo-treated dogs to levels of 7.2±1.7 mg g^{-1}, 9.5±2.7 mg g^{-1}, and 9.8±2.7 mg g^{-1} in groups treated with 300, 1000, and 3000 mg kg^{-1} day^{-1}, respectively. Strontium induced a highly significant increase in the bone formation marker, bone-specific alkaline phosphatase (BSAP), and an excellent correlation was found with the bone-strontium content. In females, the placebo-treated group showed a decrease in BSAP of 53%, whereas the three strontium malonate-treated groups showed an increase of 60, 276, and 278% for the groups treated with 300, 1000, and 3000 mg kg^{-1} day^{-1}, respectively. For males the corresponding values were −44%, +142%, +194%, and +247% increases in BSAP in the placebo, 300, 1000, and 3000 mg kg^{-1} day^{-1} groups respectively.

A. C. Raffalt · J. E. T. Andersen (✉)
Department of Chemistry, Technical University of Denmark,
Kemitorvet Building 207,
2800 Kgs. Lyngby, Denmark
e-mail: jeta@kemi.dtu.dk

S. Christgau
Osteologix A/S, Symbion Science Park,
Fruebjergvej 3,
2100 Copenhagen Ø, Denmark

Keywords Chemometrics/statistics · Quality assurance · Mass spectrometry/ICP–MS · Pharmaceuticals

Introduction

Early investigations [1, 2] revealed the beneficial effect of non-radioactive strontium on the structure of cartilage and bone. McCaslin and Janes [2] showed that patients suffering from bone pain, as a result of osteoporosis, experienced relief after oral intake of strontium lactate. The nature of the anion in strontium compounds has been investigated in detail with respect to transfer across cell membranes, and it has been suggested that strontium ions are able to coordinate rather strongly to small organic ligands. The introduction of strontium ranelate [3] (Protelos®) as a potent pharmaceutical for prevention and treatment of osteoporosis has initiated a search for other strontium salts with elevated skeletal efficacy and/or bioavailability of ionic strontium.

Bone turnover is mediated by mainly two types of cell, osteoclasts and osteoblasts, responsible for bone degradation and formation [4]. In-vitro studies have revealed that strontium ranelate can increase DNA synthesis and bone matrix protein production by osteoblasts, and, furthermore, on osteoclast cultures, a decreased maturation rate and resorbing activity has been observed [5, 6]. It is well established that strontium stimulates the formation of bone volume [7], and strontium is the only trace-metal of bone that can be positively correlated with the compression strength of bone [8]. The mineralized tissue of bone contains

approx. 40% organic material and 60% inorganic material, predominantly hydroxyapatite $Ca_{10}(PO_4)_6(OH)_2$, the calcium of which can to some extent may be substituted by strontium or other double-charged metallic ions. Strontium may be incorporated into the mineralized bone matrix by two main mechanisms. If strontium is present when apatite crystal formation is initiated in newly synthesized osteoid (i.e. organic bone matrix), it may be directly incorporated in the crystals, and affect the formation and properties of the inorganic matrix. A second mechanism involves hetero-ionic exchange of constituent ions of the apatite crystals with strontium ions present in the micro-environment. By this mechanism calcium in the inorganic bone matrix can be substituted with strontium [9].

In adults the bone is continuously remodelled, whereas remodelling of the dentine in teeth is very slow or even absent. This means that the propensity for incorporation of strontium in teeth is smaller in adult humans and also in other higher mammals. The mineral content, and the ratio between the different types of mineral in bone can be determined by ICP–MS, which allows detailed study of the interrelation of inorganic species that are constituents of bone. After four and eight weeks of treatment, the strontium content of the rat femur increased proportionally to strontium dose within the range 35–140 mg kg^{-1} day^{-1} administered as strontium ranelate [10]. Strontium uptake by rat bone saturated at doses close to 255 mg kg^{-1} day^{-1} after 10 days. However, several factors influence the incorporation of strontium by mineralized tissues—dose, strontium concentration of the plasma, gender, the duration of treatment and the bone type, or rather the turnover rate of the tissue. With respect to the last factor, the strontium content of trabecular bone of monkeys was higher than that of cortical bone after 13 weeks of treatment, in accordance with expectations, as trabecular bone has a substantially higher turnover rate than cortical bone [10].

In order to study the interrelationship between the more common metals of group II, a four-week study of beagle dogs was initiated in which the animals were treated with strontium malonate, $Sr(C_3H_2O_4)$ [11], by oral gavage [12]. Growth, clinical status, mineral content of bone and teeth, and serum levels of bone-specific alkaline phosphatase (BSAP), a marker for bone formation, were studied. The magnesium, calcium, and strontium content of the mineralized tissues was measured by ICP–MS in cortical bone and in teeth after the four-week treatment. Analysis of bone and teeth has previously been performed by atomic absorption spectrometry [13–18] but the technology is prone to interferences. No interferences have been identified in the determination of strontium in bone and teeth by ICP–MS [19–21]. All the results from this analysis were subjected to data processing that complied with the methods of the Eurachem/CITAC guide and the measurements were validated by analysis of a standard reference material (NIST SRM 1486 Bone Meal).

Experimental

Chemicals

The chemicals used were of at least p.a. grade and the bone samples were treated with nitric acid (Merck Suprapur), hydrochloric acid (Merck Suprapur), and hydrogen peroxide (Riedel–de Haën p.a.). Millipore water was used for dilutions throughout. The measurements were validated by using the standard reference material NIST SRM 1486 Bone Meal.

Sample pretreatment

Only the cortical part of the femur was used for analysis. Soft tissues, such as marrow, flesh, and pellicle, were removed from the bone samples by use of a scalpel prior to further processing. Each bone was cleansed by immersion in hydrogen peroxide (30%) in a beaker for one hour. The beaker was subsequently placed in an ultrasonic bath for ten minutes. The bone was then flushed with ethanol and water, dried, and immersed in liquid nitrogen for one hour. Roberts et al. [19] showed that the loss of analyte from the bone to the hydrogen peroxide solution and to ethanol was relatively minor. The bone was then placed in a plastic bag and crushed with a hammer to small pieces. In order to ensure homogeneity, about two grams of bone pieces were sampled from the bag by incremental sampling [22] and dried at 110°C for five hours. Two samples, denoted A and B, each containing approx. 0.5 g bone pieces, were weighed accurately for the analysis. The teeth were cleaned in a similar fashion, but no fractionation was necessary prior to digestion.

Digestion of samples

In order to ensure complete digestion of bone residues, the samples were digested under hydrothermal conditions in a microwave oven (Anton-Paar MW3000). A rotor of eight quartz vessels contained samples weighing 0.45–0.60 g in a solution of 5 mL conc. nitric acid, 0.5 mL conc. hydrochloric acid, and 3 mL of conc. hydrogen peroxide. The pressure controlled the progress of digestion and the power was ramped up to 1200 W at a rate of 100 W min^{-1}, and the maximum pressure was set at 80 bar that was reached after approx. 12 min. When this limit was reached, the power was reduced, to maintain the maximum pressure for three minutes. Within this period of time, the temperature continued to rise thus reaching its maximum after digestion for 25 min.

ICP–MS analysis

For analysis of strontium, the ICP–MS is virtually free from spectral interferences and isobaric overlap. Addition of 20 mg L^{-1} Al, Ba, Ca, Fe, K, Mg, Na, Zn, phosphate, or sulfate to a solution containing 200 μg L^{-1} strontium did not induce any interferences in the determination of strontium. The measurements were performed with an ICP–MS instrument (Perkin-Elmer Elan 5000) equipped with a cross-flow nebuliser. The operating conditions and all measured isotopes are listed in Table 1. All isotopes were analysed in the peak-hop mode.

Most frequently, only the more abundant isotope, ^{88}Sr, has been used for strontium analysis [19–24]. In this investigation the four naturally occurring non-radioactive isotopes of strontium, ^{84}Sr, ^{86}Sr, ^{87}Sr, and ^{88}Sr, were analysed. Elements of mass higher than 82 amu are usually free from spectral interferences from polyatomic species [24], which makes analysis of strontium practically free from interferences. Low LODs (3*s*) were obtained for determination of elements in bone, compared with values reported earlier [16–20]. Analysis of hair, however, could be performed at an LOD of 7 ng g^{-1} [25]. The LODs of this study were determined as LOD(^{24}Mg)=0.7 μg L^{-1}, LOD (^{44}Ca)=30 μg L^{-1}, LOD(^{64}Zn)=0.4 μg L^{-1}, LOD(^{88}Sr)= 0.04 μg L^{-1}, and LOD(^{138}Ba)=0.3 μg L^{-1}.

Animal study

Twenty-four beagle dogs (12 males and 12 females; approximately 6 months old at the start of the study) were allocated to four groups. The animals in one group (placebo/control) were treated with vehicle (0.5% carboxymethylcellulose) whereas the animals in the other three groups were treated with daily doses of 300, 1000, and 3000 mg strontium malonate kg^{-1}, respectively. The strontium malonate was administered in suspensions of 10 mg mL^{-1} by oral gavage in the morning before the dogs were given food. The dogs were given two daily meals and had free access to drinking water. The strontium content of the available drinking water was 2.6±0.6 mg L^{-1}, which is a high level that characterises the local hard water. Blood samples were taken at baseline and at the end of the study for analysis of BSAP. At study start and at administration of the last dose, more frequent sampling at 0, 1, 2, 4, 8, and 24 h was performed to assess strontium pharmacokinetic properties. At the end of the study period, the animals were killed and femur, vertebrae (L2–L4), and teeth (front incisors) were extracted and stored frozen until analysis.

Table 1 Elan 5000 ICP–MS operating conditions

RF Power	800 W
Plasma Ar flow	13 L min^{-1}
Nebulizer Ar flow	0.80 L min^{-1}
Sample injection flow	1.4 mL min^{-1}
Working pressure	1×10^{-8} bar
Background pressure	2×10^{-10} bar
Sweeps per reading	2
Readings per replicate	1
Points per spectral peak	3
Number of replicates	5
Time per reading	300 ms
Dwell time	150 ms
Isotopes measured	^{24}Mg, ^{42}Ca, ^{43}Ca, ^{44}Ca, ^{64}Zn, ^{67}Zn, ^{68}Zn, ^{84}Sr (^{84}Kr), ^{86}Sr (^{86}Kr), ^{87}Sr (^{87}Rb), ^{88}Sr, ^{136}Ba (^{136}Xe, ^{136}Ce), ^{137}Ba, ^{138}Ba (^{138}La, ^{138}Ce)

Correction for potentially interfering isotopes (in parentheses) is performed by the instrument software

BSAP method

Before the start of treatment and before termination of the treatment, blood samples were taken from all animals. The animals were fasted overnight before blood samples were taken, but water was available. Blood samples were drawn from the jugular vein. At least 3 mL blood was taken for clinical chemistry in plain glass tubes for serum. Measurements for BSAP were performed with an automated assay using a Hitachi 902 immuno-analyzer according to the manufacturer's instructions. Validated control serum samples were included in each analytical run.

Results and discussion

Uptake and elimination of strontium

Mean serum strontium concentrations at baseline before initiation of treatment were 62±15 and 56±7 μg L^{-1} for females and males, respectively. The areas under the curves (AUC) [26] were calculated for plasma concentration–time from 0 to 24 h after strontium malonate administration and for the maximum serum strontium concentration (C_{max}). After adjusting for baseline, the control group C_{max} ranged from 3–24 μg L^{-1}. For the three active-dose groups C_{max} fell within the ranges 22–109 mg L^{-1} for the 300 mg kg^{-1} dose, 39–126 mg L^{-1} for the 1000 mg kg^{-1} dose, and 24–180 mg L^{-1} for the 3000 mg kg^{-1} dose. The corresponding ranges for AUC were 31–367 h μg L^{-1}, 248–863 h μg L^{-1}, 415–1570 h μg L^{-1}, and 308–3465 h μg L^{-1}. Thus, substantial variation of both values was observed. When linearity between administered dose levels and AUC and C_{max} was assessed, the results demonstrated that for both quantities there was an increasing trend with dose. However, it was also demonstrated that these trends were not linear. Further, comparisons of the individual dose

levels showed that the AUC increased more from the 300 mg kg^{-1} dose to the 1000 mg kg^{-1} dose than from the 1000 mg kg^{-1} dose to the 3000 mg kg^{-1} dose. This indicated saturation in absorption, which was more pronounced for the highest-dose groups than for the medium-dose groups. The individual dose groups were also compared. When the dose was raised 3.33-fold from 300 mg kg^{-1} to 1000 mg kg^{-1}, a ratio of 1.53 was found for the AUC. For the 3000 mg kg^{-1} and 1000 mg kg^{-1} doses the ratio estimate was 1.11. For C_{max}, the corresponding ratio estimates were 1.21 in both comparisons. Both for AUC and for C_{max} the bioavailability was lower for males than for females with ratios of 0.80 and 0.67, respectively. The gender-by-dose-group interaction was significant for C_{max} (P=0.0013) and marginally significant for AUC. Due to the presence of an interaction effect, no conclusion can be drawn on the gender comparison [27, 28].

Strontium in bone

The natural strontium levels in bone and teeth were equal, while the strontium content of marrow was approx. half the bone value. The bar plot of Fig. 1 shows that the level of strontium increased by a factor of 85–100 for the low-dose group and by a factor of 110–145 for the two high-dose groups, compared with the placebo group. Beside the expected significant difference in strontium content of the control group and the treated groups, analysis of variance (ANOVA, not shown) for the results for bone showed that whereas significantly more strontium was incorporated into the bones of the females in the two highest-dose groups compared with the low-dose group, no such difference was observed in the males. This result demonstrates that, at least for the females, the incorporation of strontium increased when the dose increased from 300 mg kg^{-1} day^{-1} to 1000 mg kg^{-1} day^{-1} while an increment in dose to 3000 mg kg^{-1} day^{-1} did not increase amounts of strontium in the mineralized tissues substantially in this four-week intervention study. A similar saturation tendency has previously been reported in rats [10]. Additionally, this observation may be regarded as being in accordance with the pharmacokinetic analysis, which indicates saturation at the highest dose levels.

Effect of strontium on markers and bone turnover

The anabolic effects of strontium treatment on bone turnover were assessed by quantification of bone specific alkaline phosphatase (BSAP) as a specific marker of bone formation. Strontium resulted in a dose-dependent increase in BSAP for both males and females in the groups treated with 300 and 1000 mg kg^{-1} day^{-1}, while no further increase was observed in the 3000 mg kg^{-1} day^{-1} group. During the course of the study the placebo-treated females showed a decrease in BSAP of 53%, whereas the three strontium malonate-treated female groups showed increases of 60%, 276%, and 279% for the groups treated with 300, 1000, and 3000 mg kg^{-1} day^{-1}. For males the corresponding values were −44%, +142%, +192%, and +247% increase in BSAP in the placebo, 300, 1000, and 3000 mg kg^{-1} day^{-1} groups, respectively. The BSAP increase depends linearly on bone strontium content (Fig. 2), showing a highly significant ($P < 0.001$) positive correlation (r^2=0.83, ordinary least-squares regression). These observations indicate that strontium induced a dose-dependent increase in bone formation up to a dose level of 3000 mg kg^{-1} day^{-1}. This is in accordance with previous investigations in which strontium in the form of strontium ranelate increased bone formation and, in addition, reduced bone resorption [29], though, to the best of our knowledge, a direct correlation with bone strontium levels has not previously been reported. It is noted that both BSAP and strontium measurements have

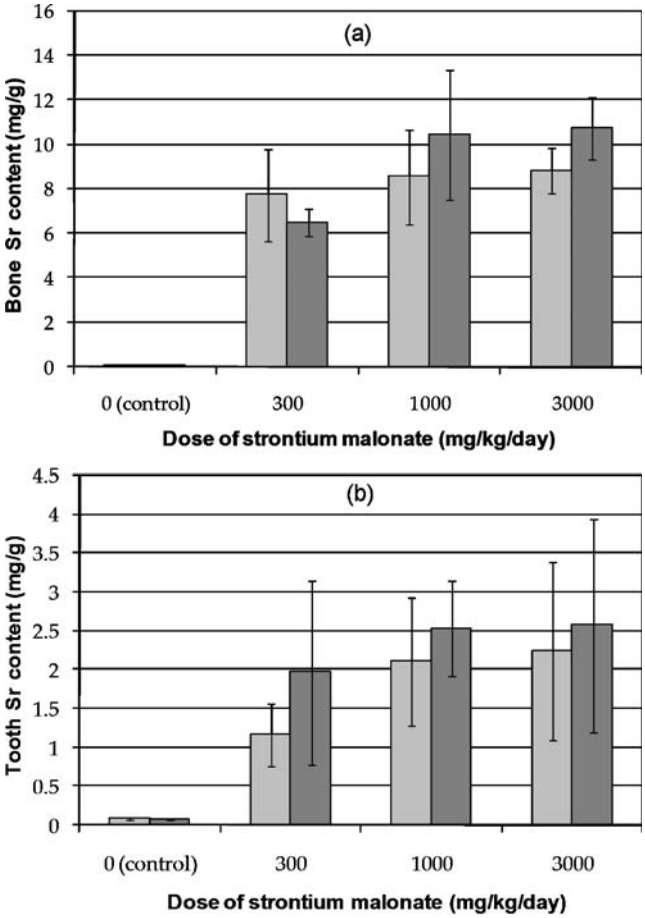

Fig. 1 Bar plot of the strontium content of (**a**) bone and (**b**) teeth of dogs after oral administration of strontium malonate at doses of 0, 300, 1000, and 3000 mg kg^{-1} day^{-1}. *Light grey bars* indicate male, *dark grey bars* indicate female. The *error bars* indicate combined biological uncertainty and instrument uncertainty. All four isotopes of strontium (^{84}Sr, ^{86}Sr, ^{87}Sr, ^{88}Sr) were analysed

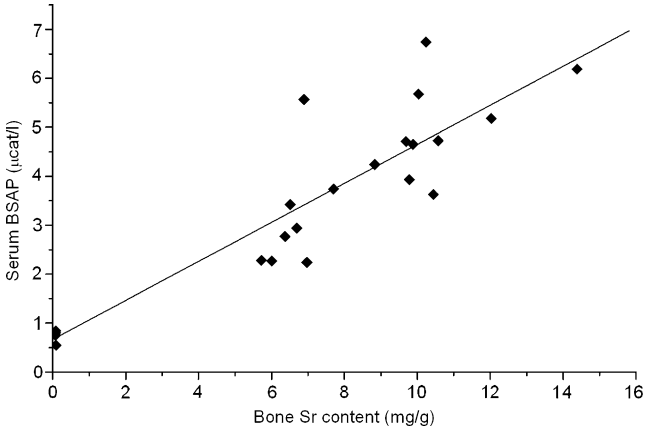

Fig. 2 Correlation of serum BSAP levels with bone strontium content at the end of treatment in the treated groups ($P < 0.001$). The slope of the line is 0.39±0.04 and the intercept is 0.67±0.31

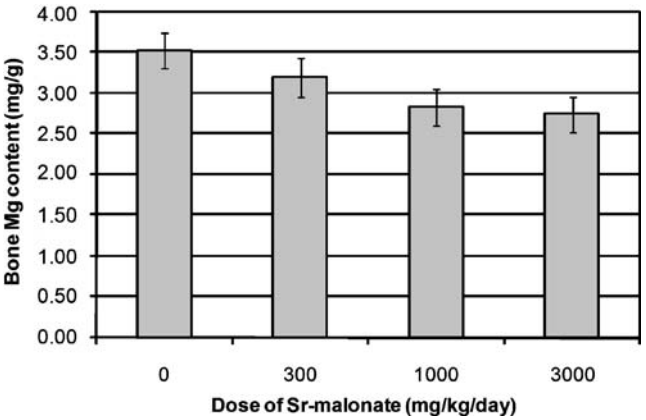

Fig. 3 The magnesium content of bone depicted as a function of dose. The *error bars* represent the standard deviation within the groups. The most abundant isotope, ^{24}Mg, was used for the analysis

been carried out with sufficient accuracy for this correlation to be observed.

Magnesium in bone

Magnesium levels in bone were assessed in all groups (Fig. 3). A dose-dependent decrease was observed from the placebo group to the 1000 mg kg^{-1} day^{-1} dose group, while no further decrease in the highest-dose group was found. No significant gender difference was observed. This indicates that strontium displaces magnesium from bone, when present in large quantities.

Calcium in bone

The calcium content of the femur bone was determined by quantifying three isotopes ^{42}Ca, ^{43}Ca, and ^{44}Ca. Figure 4 shows calcium levels in all groups from the study, and it is apparent that calcium levels are very similar ranging from 249±9 mg g^{-1} Ca in the placebo group to 276±22 mg g^{-1} Ca in the group treated with 300 mg kg^{-1} day^{-1}. Calcium levels showed less variability in the control group, which indicates that strontium may result in a somewhat larger individual variability in the calcium content. The average Sr/Ca ratio in the bones of the control group was 1:3300, while in the treated groups, the ratios were 1:40, 1:28, and 1:26 for doses 300, 1000, and 3000 mg kg^{-1} day^{-1}, respectively. These latter ratios approached the maximum value of 1:10 that was reported by Boivin et al. [30]. On a normal diet, the Sr/Ca ratio in human bone is approx. 1:1000, which is comparable with the ratio found in blood [31].

Zinc and barium in bone

A few additional elements which might affect the balance between calcium and strontium in bone, were also analysed. Zinc and barium were thus identified and determined at levels of 85±15 μg g^{-1} and 2.4±1.4 μg g^{-1}, respectively. The amounts of these two elements were not found to be affected by administration of strontium.

Strontium and calcium in teeth

Strontium levels in the teeth of the treated groups were approximately a factor of four lower than the levels seen in femurs. The strontium content of the control group was 75±14 μg g^{-1}, which is almost identical to the strontium levels in bone seen in the placebo group. In the strontium malonate groups, the strontium level in teeth increased to 1.6±1.0 mg g^{-1}, 2.3±0.7 mg g^{-1}, and 2.2±1.1 mg g^{-1} in the 300, 1000, and 3000 mg kg^{-1} day^{-1} groups, respectively (Fig. 5). This suggests that saturation is observed in the investigated dose range, and that already the 1000 mg kg^{-1} day^{-1} group shows maximum incorporation of strontium. The lower level of strontium incorporated in teeth compared with bone is in accordance with the lower remodelling of the mineralized matrix of teeth. Calcium levels in the teeth were similar in all groups, with relatively small intra-individual variability. The correlation between the strontium content of bone and teeth of treated and untreated dogs was $R=0.523$ ($P < 0.05$). The slope of the correlation line, $a=0.229$, suggests that strontium was incorporated in bone at a rate four to five times higher than the rate of uptake in teeth.

Strontium and calcium in bone marrow

Only 16 bone samples contained sufficient amounts for analysis of marrow. In the control group, the concentrations ranged from 8 μg g^{-1} to 77 μg g^{-1}, while the strontium treated groups showed strontium levels ranging from 0.2 mg g^{-1} to 2.6 mg g^{-1}. This demonstrates that the

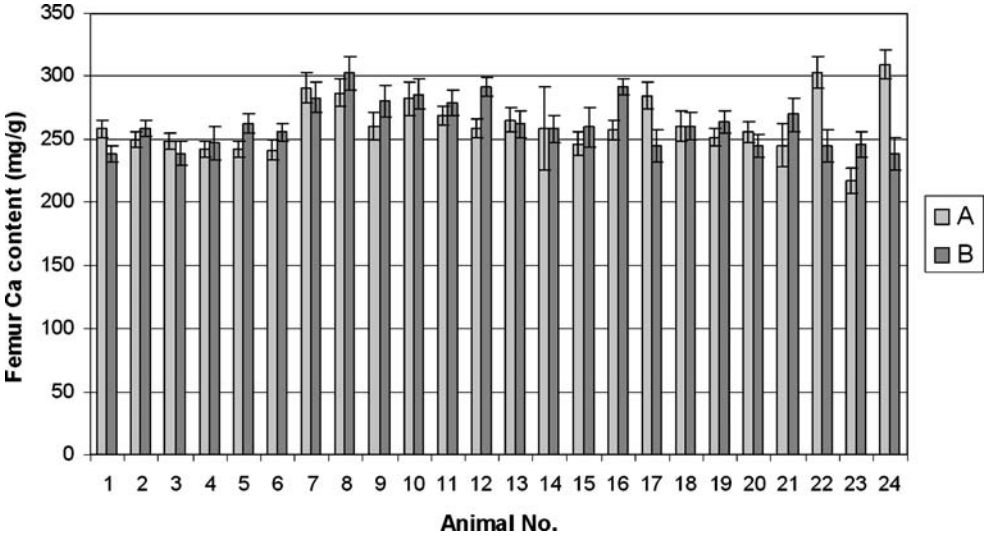

Fig. 4 The calcium content of the femur bones of dogs determined by ICP–MS analysis of ^{42}Ca, ^{43}Ca, and ^{44}Ca. Two subsamples, denoted *A* and *B*, from each dog were analysed. Dogs 1–6, control group; dogs 7–12, Sr dose 300 mg kg day^{-1}; dogs 13–18, Sr dose 1000 mg kg day^{-1}; dogs 19–24, Sr dose 3000 mg kg day^{-1}

strontium malonate treatment induces a significant increase in strontium content in also the non-mineralized tissue of bone, but the magnitude of the effect is difficult to estimate accurately, owing to the incomplete availability of suitable samples. There was no significant indication of increased bone-marrow-strontium content with increased dosing, suggesting that uptake of strontium by this tissue may already be close to saturation at the lowest administered dose (300 mg kg^{-1} day^{-1}). Only a limited number of studies with analysis of strontium in bone marrow are available in the literature [23, 32], and they might not be directly comparable with the current results because the conditions of analysis and the types of sample are very different. The results of the strontium measurements showed that the strontium content of the control group was much higher than that reported by Hasegawa et al. [23], who analysed human-bone marrow and found 0.027 μg g^{-1} (wet weight). However, the contents were determined at a level much lower than the content of 180 μg g^{-1} (dry weight) reported by Gawlik et al. [32], who used neutron-activation analysis (NAA) for the analysis. According to the explanation by Hasegawa et al. [23], the origin of the large difference is related to the presence of amounts of small bone fragments that must be separated from the matrix by spinning the sample in a centrifuge. However, careful microscopy of the samples of bone marrow in the current investigation did not reveal such bone fragments. The calcium content of bone marrow also varied substantially but no significant changes were observed as a result of strontium treatment. The calcium content of marrow was determined as 13±7 mg g^{-1}.

Quality assurance

One of the key problems of chemical analysis is related to discrimination between uncertainties imposed by the instrument and the biological variation. It is expected that the biological variation by far exceeds the uncertainty of measurement but in a relatively well defined matrix, such as the bone matrix, the biological variation was lower (Fig. 2) than the biological variation of other types of sample, e.g. in samples of marrow. Initial investigations revealed that the choice of standards for the construction of the calibration

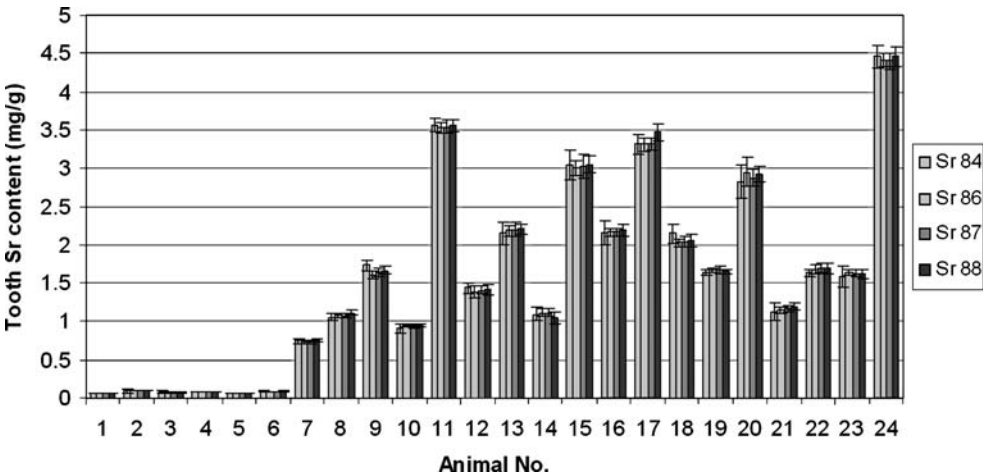

Fig. 5 The strontium content of teeth measured by ICP–MS after four weeks of dosing with strontium malonate. All four isotopes of strontium (^{84}Sr, ^{86}Sr, ^{87}Sr, ^{88}Sr) were analysed. Dogs 1–6, control group; dogs 7–12, Sr dose 300 mg kg day^{-1}; dogs 13–18, Sr dose 1000 mg kg day^{-1}; dogs 19–24, Sr dose 3000 mg kg day^{-1}

line might affect the standard deviation of the results. In addition, the measurements could be performed by applying ordinary linear regression including correlation terms [33–35], by applying weighted linear regression [36], or by functional relationship estimation by maximum likelihood that can be downloaded as an add-in to the MS Excel software from the homepage of the Analytical Methods Committee [37]. A slight and almost unrecognisable curvature to the calibration measurements, depicted as a function of concentration, was found to significantly affect the measured concentration of unknowns. In general, by applying a wide calibration range there was a tendency to obtain concentrations too high, compared with expected values. It was thus found that the optimum range of calibrations was from 0–200 μg L^{-1} for the isotopes ^{84}Sr, ^{86}Sr, ^{87}Sr, and ^{88}Sr. The key results associated with the three methods of analysis were determined as shown in Table 2. Within this range of concentrations a Wald–Wolfowitz test [36, 38] showed that the sequence of signs of residuals was randomly distributed. Since all the results were equal within the limits of the standard deviation, the least laborious method of ordinary-linear regression with correlations was chosen for the analysis. This certified that the results could be obtained at the lowest possible STDEV within the linear range of concentrations.

Before measurement an uncertainty budget was constructed on the basis of the methods stipulated in QUAM [39] and the uncertainties of the calibration line including terms of correlation [40]. The relative uncertainties are presented in Fig. 6, where the major contributions to the uncertainty budget were calculated on the basis of an Ishikawa diagram (not shown). By far, the major contribution to the uncertainty originated from the spread of data around the calibration line, that is, uncertainties related to dilution and weighing were of minor importance to the total uncertainty (Fig. 6). This notion may be illustrated by investigating one particular measurement of strontium in bone, which yielded a result of 76.5±1.3 μg g^{-1}, by applying the full uncertainty budget including correction for triangular distributions and square distributions [39]. However, omission of these corrections for abnormal distributions provided exactly the same result, whereas the result was marginally different, 76.5±1.2 μg g^{-1}, when using only the STDEV of calibrations. The reliability of these results was maintained by applying many standards, samples, and replicates to the analysis. The reliability of the analysis depends on the number of replicates according to the central-limit theorem [41].

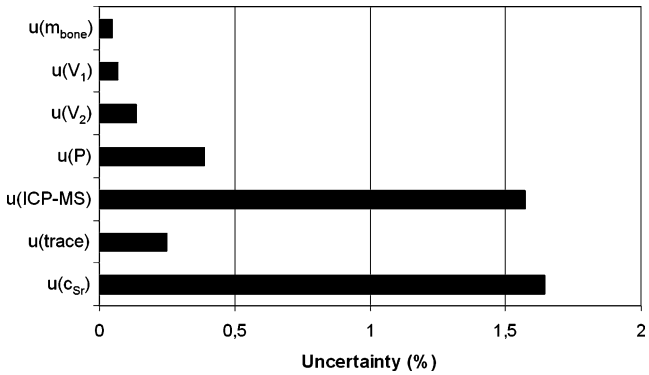

Fig. 6 The uncertainty budget of analysis of strontium in bone. The contributions to the total uncertainty $u(c_{Sr})$ are represented by the symbols: $u(m_{bone})$, uncertainty of the weight of bone; $u(V_1)$ and $u(V_2)$, uncertainty of volume of dilution; $u(P)$, uncertainty of volume of pipette; u(ICP–MS), uncertainty of ICP–MS measurement; and u(trace), uncertainty of traceability

NIST SRM 1486 bone meal contains 264±7 μg g^{-1} strontium, and the reported uncertainty refers to an extended uncertainty [39, 41] that was based on numerous replicates. In Fig. 6 a is shown a Shewhart chart of 45 replicates of the determination of strontium by ICP–MS. All the four isotopes were applied to the analysis, and the average concentration was thus determined as 255.0±6.8 μg g^{-1} (Fig. 7a). A *t*-test showed that this value was close to the certified value but significantly lower (95% level of confidence) than the concentration stipulated for the SRM (t=8.93 > 1.68=$t_{0.05}$(N=45)). It should be noted that 5–7 of the measurements were determined very close to the certified value and 16 replicates were found within the

Table 2 Estimates and uncertainties of parameters from ordinary least squares regression (OLSR), weighted least squares regression (WLSR), and functional relationship estimation by maximum likelihood (FREML) [32]

Regression	^{84}Sr	^{86}Sr	^{87}Sr	^{88}Sr
OLSR				
Slope (cps L mg^{-1})	5.57±0.07	99.6±1.1	71.18±0.49	816±7
Intercept (cps)	−4±7	38±107	12±48	852±731
WLSR				
Slope (cps L mg^{-1})	5.56±0.11	100.1±1.2	71.44±0.83	820±10
Intercept (cps)	−4±7	13±3	7±7	85±53
FREML				
Slope (cps L mg^{-1})	5.56±0.11	100.1±1.2	71.44±0.84	820±10
Intercept (cps)	−4±7	13±3	7±7	85±53

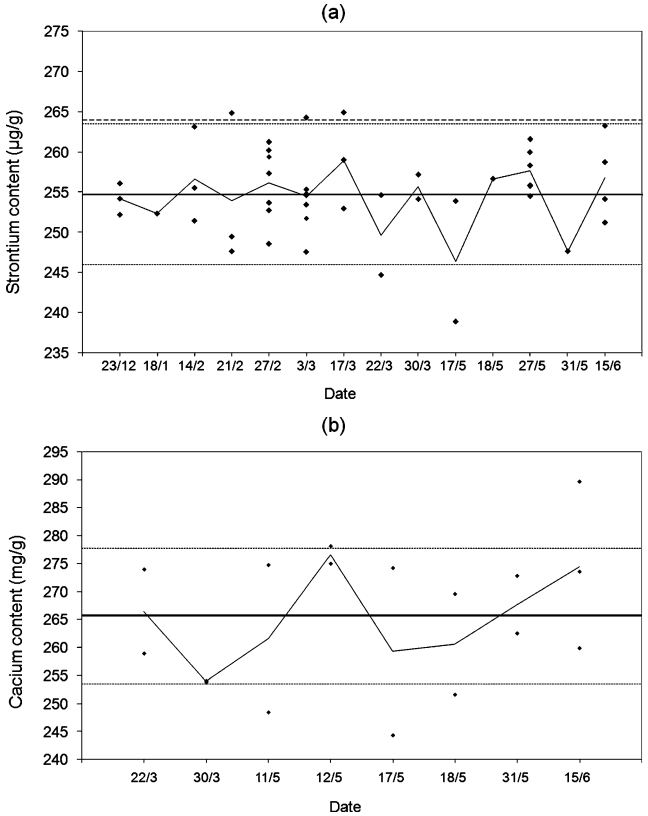

Fig. 7 Shewhart charts of determination of (**a**) strontium and of (**b**) calcium over a long period of time. The *horizontal straight line* indicates the average value of all determinations and the *dotted lines* represent the limits given by the uncertainty. The *thick dotted line* represents the position of the certified value of NIST SRM 1486 bone meal, and the concentrations connected by *thick lines* represents the average value for each day

limits of the certified value. This distribution of data complies with the properties of a normal distribution, and the results of Fig. 7a thus demonstrate the importance of many replicates being applied to the analysis. The recovery was 97%, which could be related to a loss of material during the procedure of digestion. However, this is contradicted by simultaneous determinations of calcium in the NIST reference material, as shown in the Shewhart chart of Fig. 7b, where a perfect match (100% recovery) was obtained between measured values and the expected value (N=17). Similarly, the concentrations of Mg, Zn, and Ba were determined in the reference material, and a satisfactory correspondence was obtained for Mg and Zn also (Table 3).

The validity of the calculated uncertainties may be verified by applying an F-test to the uncertainties of the uncertainty estimated by the uncertainty budget (Fig. 6) and comparing with the uncertainty of the experiment (Fig. 7a and b). The uncertainty of Fig. 6 was estimated as 8.1 µg g^{-1} by calculating the effective number of degrees of freedom by use of the Welch–Sattertwaite equation and applying it to the extended uncertainty [39, 41]. The F-test thus

Table 3 Analysis of NIST SRM 1486 Bone Meal

Element	Result	Certified value
Mg	4.4±0.4	4.66±0.17
Ca	266±10	265.8±2.4
Zn	0.124±0.022	0.147±0.016
Sr	0.255±0.008	0.264±0.007
Ba	0.189±0.008	–

Mean values ± standard uncertainty according to the uncertainty budget, both in units of mg g^{-1}

provided a test value of 1.42 that is not significant at 45 degrees of freedom ($F_{0.05}(45, 45)$=1.64). Therefore, it may be concluded that the uncertainty of the uncertainty budget predicts well the observed uncertainties, which is the requirement for statistical control.

Conclusions

Samples of bones, teeth and bone marrow were analysed by ICP–MS after careful sample preparation. The procedure was validated on the certified reference material NIST SRM 1486 bone meal, which provided a recovery of 97% for strontium and a reliable estimate of the uncertainties thus confirming statistical control. The strontium content was determined at high precision corresponding to an RSD of 1.5% for the strontium isotopes ^{86}Sr, ^{87}Sr, and ^{88}Sr, and slightly lower precision for the less abundant isotope ^{84}Sr.

Strontium malonate showed high bioavailability and was generally well tolerated when administered to dogs by oral gavage over the four-week study period. At the investigated dose levels the pharmacokinetic analysis indicated saturation at the highest dose level (3000 mg kg^{-1} day^{-1}). Strontium malonate induced a significant increase in bone formation apparent as a highly significant increase in the circulating levels of BSAP. Analysis of the mineralized tissues of bone and teeth revealed a significant increase in strontium content.

Strontium was incorporated into both teeth and bone but uptake by teeth was approximately a factor of five lower than that of bone, in accordance with the lower rate of remodelling of dentine compared with bone. The increased strontium content was not correlated with a corresponding decrease in the content of calcium, which remained constant in all groups. Within the of low dose group the calcium content increased slightly but in general the calcium content of bone, marrow, and teeth was found to be virtually unaffected by administration of strontium malonate.

The magnesium content of bone was lower in the group treated with 3000 mg kg^{-1} day^{-1} strontium malonate, which may be interpreted as substitution of magnesium by strontium.

Acknowledgements Financial support from the Director Per Henriksen's Foundation, the Idella Foundation, and from the Carlsberg Foundation is gratefully acknowledged.

Many thanks are due to Flemming E. Hansen for his expert technical assistance in operation of the Elan 5000 ICP–MS.

References

1. Shorr E, Carter A (1952) Bull Hosp Joint Dis 13:59–66
2. McCaslin FE, Janes JM (1959) Proc Staff Meetings of the Mayo Clinic 34:329–334
3. Sorbera LA, Castaner J, Leeson PA, Bayes M (2003) Drug Future 28:328–335
4. Nielsen SP (2004) Bone 35:583–588
5. Marie PJ (2003) Osteoporos Int 14(Suppl 3):S9–S12
6. Canalis E, Hott M, Deloffre P, Tsouderos Y, Marie PJ (1996) Bone 18:517–523
7. Marie PJ, Ammann P, Boivin G, Rey C (2001) Calc Tiss Inter 69:121–129
8. Jensen J-EB, Stang H, Kringsholm B (1997) Bone 20(S4):104–108
9. Boivin G, Meunier PJ (2003) Osteopor Inter 14:S19–S24
10. Dahl SG, Allain P, Marie PJ, Mauras Y, Boivin G, Ammann P, Tsouderos Y, Delmas PD, Christiansen C (2001) Bone 28:446–453
11. Briggman B, Oskarsson A (1977) Acta Crystallogr B 33:1900–1906
12. Christensen A (2005) Strontium malonate–4 week toxicity study in dogs with toxicokinetics, Scantox Study report 59147
13. Helsby CA (1974) Anal Chim Acta 69:259–265
14. Burguera M, Burguera JL, Di Bernardo ML, Alarcon OM, Nieto E, Salinas JR, Burguera E (2002) Tr Elem Electr 19:143–151
15. Scancar J, Milacic R, Benedik M, Bukovec P (2000) Clin Chim Acta 293:187–197
16. Burguera M, Burguera JL, Rondon C, Di Bernardo ML, Gallignani M, Nieto E, Salinas J (1999) Spectrochim Acta B 54:805–818
17. D'haese PC, VanLandeghem GF, Lamberts LV, Bekaert VA, Schrooten I, Debroe ME (1997) Clin Chem 43:121–128
18. Burguera M, Burguera JL, Di Bernardo ML, Rondon C, Carrero P, Nieto E, Salinas R, Burguera E (1999) Quim Anal 18:305–312
19. Roberts NB, Walsh HPJ, Klenerman L, Kelly SA, Helliwell TR (1996) J Anal At Spectrosc 11:133–138
20. Outridge PM, Hughes RJ, Evans RD (1996) At Spectrosc 17:1–8
21. Kang D, Amarasiriwardena D, Goodman AH (2004) Anal Bioanal Chem 378:1608–1615
22. Gy PM (1998) Sampling for analytical purposes. Wiley, Chichester
23. Hasegawa T, Matsuura H, Inagaki K, Haraguchi H (2003) Anal Sci 19:147–150
24. Hsiung CS, Andrade JD, Costa R, Ash KO (1997) Clin Chem 43:2303–2311
25. Goulle JP, Mahieu L, Castermant J, Neveu N, Bonneau L, Laine G, Bouige D, Lacroix C (2005) For Sci Inter 153:39–44
26. Vezzoli G, Baragetti I, Zerbi S, Caumo A, Soldati L, Bellinzoni P, Centemero A, Rubinacci A, Moro G, Bianchi G (1998) Clin Chem 44:586–590
27. Olsen KJ (2005) Four week toxicity study in dogs with toxicokinetics, end of text listings, tables, figures and statistical output, Study NBS T07 GE
28. Olsen KJ (2005) Four week toxicity study in dogs with toxicokinetics, Statistical report of toxicokinetic data, Study NBS T07 GE
29. Marie PJ (2006) Bone 38:S10–S14
30. Boivin G, Deloffre P, Perrat B, Panczer G, Boudeulle M, Mauras Y, Allain P, Tsouderos Y, Meunier PJ (1996) J Bone Miner Res 11:1302–1311
31. Cabrera WE, Schrooten I, De Broe ME, D'Haese PC (1999) J Bone Miner Res 14:661–668
32. Gawlik D, Behne D, Bratter P, Gatschke W, Gessner H, Kraft D (1982) J Clin Chem Clin Biochem 20:499–507
33. Danzer K, Currie LA (1998) Pure Appl Chem 70:993–1014
34. Inczedy J, Lengyel T, Ure AM (1998) International Union of Pure and Applied Chemistry, Compendium of analytical nomenclature, online ed, Blackwell Science; http://www.iupac.org/publications/books/author/inczedy.html
35. Brüggemann L, Morgenstern P, Wennrich R (2005) Accred Qual Assur 10:344–351
36. Miller JN, Miller JC (2005) Statistics and chemometrics for analytical chemistry, 5th edn. Pearson, Edinburgh
37. Analytical Methods Committee (AMC) (2002), Technical Brief no. 10. Fitting a linear functional relationship to data with error on both variables, Royal Society of Chemistry, Cambridge; http://www.rsc.org/Membership/Networking/InterestGroups/Analytical/AMC/TechnicalBriefs.asp
38. Miller JN (1991) Analyst 116:3–14
39. Ellison SLR, Rösslein M, Williams A (eds) (2000) Eurachem/CITAC Guide, Quantifying uncertainty in analytical measurement, 2nd edn
40. Cuadros-Rodriguez L, Gamiz-Cracia L, Almansa-Lopez E, Laso-Sanchez J (2001) Trends Anal Chem 20:195–206
41. International Organization for Standardization (1995) Guide to the expression of uncertainty in measurement (GUM). Geneva, Switzerland

Appendix III

Parameters for ordinary least-squares regression and weighted least-squares regression. X denote standard concentrations and Y is the corresponding instrument response. m is the number of standards, n the number of sample replicates and w is the weight [1, 2].

	Ordinary least-squares regression	Weighted least-squares regression
Mean concentration	$\bar{X} = \frac{1}{m}\sum_i X_i$	$\bar{X}_w = \frac{1}{m}\sum_i w_i X_i$
Mean response	$\bar{Y} = \frac{1}{m}\sum_i Y_i$	$\bar{Y}_w = \frac{1}{m}\sum_i w_i Y_i$
Slope	$a = \frac{\sum_i \left(X_i - \bar{X}\right)\left(Y_i - \bar{Y}\right)}{\sum_i \left(X_i - \bar{X}\right)^2}$	$a_w = \frac{\sum_i w_i X_i Y_i - n\bar{X}_w \bar{Y}_w}{\sum_i w_i X_i^2 - n\bar{X}_w^2}$
Intercept	$b = \bar{Y} - a\bar{X}$	$b_w = \bar{Y}_w - a_w \bar{X}_w$
Standard deviation of residuals	$s_e = \sqrt{\frac{\sum_i \left(Y_i - \hat{Y}_i\right)^2}{m-2}}$	$s_{e,w} = \sqrt{\frac{\sum_i w_i \left(Y_i - \hat{Y}_i\right)^2}{m-2}}$
Uncertainty of slope	$u(\alpha) = \frac{s_e}{\sqrt{\sum_i \left(X_i - \bar{X}\right)^2}}$	
Uncertainty of intercept	$u(b) = s_e \sqrt{\frac{\sum_i X_i^2}{m\sum_i \left(X_i - \bar{X}\right)^2}}$	
Uncertainty of predicted value*	$u(X_p) = \frac{s_e}{\alpha}\sqrt{\frac{1}{m} + \frac{1}{n} + \frac{\left(Y_0 - \bar{Y}\right)^2}{\alpha^2 \sum_i \left(X_i - \bar{X}\right)^2}}$	$u(X_p)_w = \frac{s_{e,w}}{\alpha_w}\sqrt{\frac{1}{w_p} + \frac{1}{m} + \frac{\left(Y_p - \bar{Y}_w\right)^2}{\alpha^2\left(\sum_i w_i X_i^2 - n\bar{X}_w^2\right)}}$

1. J. N. Miller & J. C. Miller, in *Statistics and chemometrics for analytical chemistry, 5. udg,* Paerson Education Limited, Edinburgh, 2005.

2. L. Bruggemann, P. Morgenstern & R. Wennrich. Comparison of regression techniques for linear calibration. *Accreditation and Quality Assurance* (2005) **10**, 344-351.